(2)

BERKELEY RESEARCH ASSOCIATES, INC.

BRA-89-349R

FINAL REPORT: Contract No. N00014-87-C-0490

RESEARCH ON FREE ELECTRON LASERS

to

Office of Naval Research
C/O Naval Ocean Systems Center - Code 843
271 Catalina Blvd.
San Diego, CA 92152-5000

from

William B. Colson
Berkeley Research Associates
P. O. Box 241
Berkeley, CA 94701

DISCLAIMER NOTICE

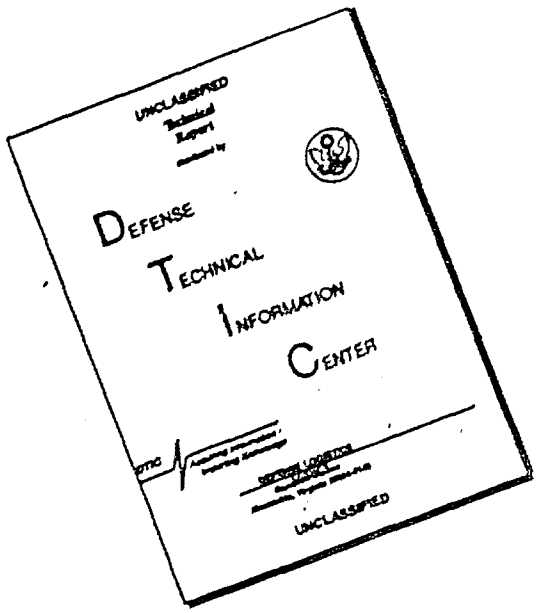

THIS DOCUMENT IS BEST QUALITY AVAILABLE. THE COPY FURNISHED TO DTIC CONTAINED A SIGNIFICANT NUMBER OF PAGES WHICH DO NOT REPRODUCE LEGIBLY.

Berkeley Research Associates, Inc.

BRA-89-349R

FINAL REPORT: Contract No. N00014-87-C-0490

RESEARCH ON FREE ELECTRON LASERS

to

Office of Naval Research

C/O Naval Ocean Systems Center - Code 843

271 Catalina Blvd.

San Diego, CA 92152-5000

from

William B. Colson

Berkeley Research Associates

P. O. Box 241

Berkeley, CA 94701

BRA-89-349R

FINAL REPORT: Contract No. N00014-87-C-0490

RESEARCH ON FREE ELECTRON LASERS

Principal Investigator: William B. Colson

TABLE OF CONTENTS

RESEARCH ON FREE ELECTRON LASERS

W. B. Colson

Berkeley Research Associates, Inc., P.O. Box 241, Berkeley, CA 94701

1. Introduction

The research carried out during this contract has resulted in several review talks and five publications. The work has been done in close collaboration with colleagues at the Los Alamos National Laboratory, Lawrence Livermore National Laboratory, Lawrence Berkeley Laboratory, and other free electron laser (FEL) facilities.

The research includes the derivation of better high-efficiency equations for describing the FEL in the strongly saturated regime. The equations retain much of the simplicity of the old theory, but are accurate for high energy extraction. The dimensionless parameters of the equations are used to describe the LANL and LLNL FEL experiments. In a publication, the importance of the dimensionless current density j is emphasized for describing many diverse FEL physical effects.

The effects of waveguides on the FEL radiation interaction are derived and presented in this report. The ELF FEL amplifier used a waveguide and is used as an example. It was found during the study that the gain spectrum of high-gain amplifiers like ELF can have sharp spikes. The spikes are not related to the use of a waveguide, but are an important result of this contract. A review paper invited by SPIE discusses some the techniques used to simulate FELs of many different kinds.

In the weak-field regime, the derivation of the FEL integral equation is presented with some simple cases solved. In the limit of low current, the integral equation is used to derive relationships describing gain degradation in terms of the FEL lineshape. A major FEL review paper was prepared and published in the Proceedings of the SPIE. Many of the topics covered in research during this period are presented in the review.

In order to use the FEL integral equation to undulator the affect of beam distributions on the FEL interaction, several distribution functions describing realistic electron beams are derived from first principles. Then, the characteristic function for each distribution function is derived. The characteristic function gives a good understanding of the effect of beam quality on the FEL bunching process and gain. Another publication explores the gain degradation of FELs with several sample beam distributions. The integral equation is used to understand the gain spectra observed in the Paladin experiment at 5m undulator length.

A method is developed for using the integral equation to give the evolution of the phase-space distribution function when the beam quality is poor. The integral equation itself does not contain information about the electron beam, but can handle continuous distributions of arbitrary shape. The resulting phase-space distortion is reconstructed using the solution of the complex field evolution. The integral equation and the related phase-space evolution are used to explain the formation of plateau's in the gain evolution of Paladin at 15 m length. This is an important result of the contracting period.

A large review paper is prepared for North-Holland Publishing Co. describing many aspects of FEL theory.

2. FEL Equations for High Efficiency

The FEL equations used previously are the self-consistent pendulum and wave equations. They provide a simple model of the FEL that is valid in strong and weak optical fields for high and low beam current. The assumptions required to derive the simple form of the equations are $\gamma \gg 1$ and $N \gg 1$ where γmc^2 is the electron beam energy, and N is the number of undulator periods. Since the most important aspects of the interaction take place near resonance, the changes in the electron energy, $\Delta\gamma / \gamma$, are small when $N \gg 1$, and the FEL efficiency is low. For high efficiency, in the

tapered undulator or in a short undulator with few periods, the changes in the electron energy are expected to be large. Below is a derivation of the generalized FEL equations where N can be large and the FEL efficiency can large.

The electron motion is determined by the Lorentz force in the combined undulator and radiation fields. For the helical undulator, the field is

$$\vec{B} = B\ (\ \cos(k_0 z)\ ,\ \sin(k_0 z)\ ,\ 0\ )\quad , \tag{1}$$

where $\lambda_0 = 2\pi/k_0$ is the undulator period, and B is the peak field strength. The corresponding electric and magnetic components of the radiation fields are

$$\vec{E} = E\ (\ \cos\psi\ ,\ -\sin\psi\ ,\ 0\ )\qquad ,\qquad \vec{B} = E\ (\ \sin\psi\ ,\ \cos\psi\ ,\ 0\ )\quad , \tag{2}$$

where $\psi = kz-\omega t+\phi$, $\lambda = 2\pi/k = 2\pi c/\omega$ is the optical wavelength, ϕ is the optical phase, and E is the radiation field strength.

The transverse velocity components of an electron in the fields (1) and (2) are found by noting that the right side of the Lorentz force equation is a perfect time derivative over one undulator period where B and E remain substantially constant. The transverse electron velocity, $c\vec{\beta}_\perp$, is

$$\vec{\beta}_\perp = -\frac{K}{\gamma}\ [\ \cos(k_0 z),\ \sin(k_0 z)\ ,\ 0\ ] + \frac{A}{\gamma}\ [\ \sin\psi\ ,\ \cos\psi\ ,\ 0\ ]\quad , \tag{3}$$

where $K = eB\lambda_0/2\pi mc^2$ is the dimensionless undulator vector potential, $A = eE\lambda/2\pi mc^2$ is the dimensionless optical vector potential, and $e = |e|$ is the electron charge magnitude. Typically, the value of K is near unity in most FELs. The constants of integration have been set equal to zero indicating perfect injection into the undulator; imperfect injection is considered later. Using (3), the electron energy change is

$$\dot{\gamma} = \frac{d\gamma}{dt} = \frac{\omega KA}{\gamma}\cos(\zeta+\phi)\quad , \tag{4}$$

where the electron phase is $\zeta = (k+k_0)z-\omega t$, and $\dot{\gamma} = d\gamma/dt$. The combination of $\gamma^{-2} = 1-\vec{\beta}_\perp^2-\beta_z^2$ and (3) gives the exact electron phase motion,

$$\ddot{\zeta} = \frac{KA\ (2\omega\omega_0-2\omega\dot{\zeta}+\omega_0^2-\dot{\zeta}^2)\,(2\omega\omega_0-\omega\dot{\zeta}+\omega_0^2)\cos(\zeta+\phi)}{(\omega+\omega_0)^2\,(1+K^2-KA\sin(\zeta+\phi)+A^2)}\quad , \tag{5}$$

where $\omega_0 = k_0 c$. The bunching mechanism for an initially random beam arizes from

the important relation $\ddot{\zeta} \propto \cos(\zeta+\phi)$. In order for bunching to develop, the electrons must be near resonance where $\dot{\zeta} \approx 0$. Near resonance, the FEL frequency is $\omega \approx \beta_z \omega_0/(1-\beta_z)$, and in the relativistic limit $\omega \gg \omega_0$. Furthermore, it can be shown that $A^{max} \sim (N_S/N)^2$ where N_S is the number of synchrotron oscillations of trapped electrons along the undulator length. Typically, $A^{max} \sim 10^{-4}$ so that $K \gg A$ for even the strongest optical fields. In high efficiency FELs where the undulator is altered to maintain resonance with trapped electrons that lose significant energy to the optical wave, the untrapped electrons can drift far off-resonance. Allowing that $\dot{\zeta}$ is far from resonance, but with the restriction $\dot{\zeta} \ll \omega_0$, the electron motion is accurately described by the simpler equation

$$\dot{\nu} = (1 - 3\nu/4\pi N) |a| \cos(\zeta + \phi) \quad , \tag{6}$$

where $(\dot{..}) = d(..)/d\tau$, $\tau = ct/L$ is the interaction time over the undulator ($\tau = 0 \rightarrow 1$), $\nu = \dot{\zeta}$ is the electron phase velocity, and $|a| = (4\pi N)^2 KA/(1+K^2)$ is the dimensionless optical field amplitude.

In this formulation, electrons trapped near resonance, $\nu \approx 0$, are described accurately, while untrapped electrons far from resonance, $\nu \rightarrow 4\pi N$, are handled less accurately. However, the untrapped electrons are expendable since they become randomly spread in phase as well as uncoupled from the bunching interaction, as can be seen in (6). For electrons near resonance, the bunching rate is determined by the field strength $|a|$. When $|a| \ll \pi$, the optical field is considered weak, and bunching is imperceptible. When $|a| \gg \pi$, the electrons bunch rapidly, and become trapped in closed phase-space orbits. In strong fields, $|a| \geq 4\pi^2$, the trapped electrons oscillate at the dimensionless synchrotron frequency $\nu_S \approx |a|^{1/2}$, and there are $N_S \approx \nu_S/2\pi$ oscillations in time $\Delta\tau = 1$. Integration of (6) can be accomplished numerically on a small computer, or analytically in some specific cases. Because (6) is slowly varying, numerical τ-steps can jump over several undulator periods. When $N \gg 1$, so that the FEL efficiency is not too large, (6) simplifies further to take the form of the pendulum equation.

An FEL that goes far into saturation should be tapered to improve its efficiency. Tapering can be added to the basic FEL equation of motion (6) by adding a phase acceleration, δ. The equation becomes

$$\dot{\nu} = \delta + (1 - 3\nu/4\pi N) |a| \cos(\zeta + \phi) \quad . \tag{7}$$

The amount of taper in the resonant energy is then $\Delta\gamma_r/\gamma_r \approx \delta/4\pi N$.

In order to have a self-consistent theory, the complex, time-varying field envelope, $(E(t),\phi(t))$, is allowed to vary slowly over an optical period ($\dot{E} \ll \omega E$, $\dot{\phi} \ll \pi\omega$). The transverse beam current, $\vec{J}_\perp$, is the sum of all single particle currents, but an average over sample particles, <..>, can be used if weighted by the electron density ρ. The current is then $\vec{J}_\perp = -ec\rho<\vec{\beta}_\perp>$, and the slowly-varying wave equation can be written as

$$\frac{d(Ee^{i\phi})}{dt} = -2\pi ecK\rho<(e^{-i\zeta}/\gamma)> \quad . \tag{8}$$

From the electron dynamics, the dynamic Lorentz factor is given by $\gamma^{-1} \approx (1-v/4\pi N)\,\gamma_0^{-1}$ with the static, resonant Lorentz factor $\gamma_0 = (\omega(1+K^2)/2\omega_0)^{1/2}$. Then, in terms of the electron phase and phase velocity, the wave equation becomes

$$\overset{\circ}{a} = -j<(1 - v/4\pi N)\,e^{-i\zeta}> \quad , \tag{9}$$

where the complex dimensionless field is $a = |a|e^{i\phi}$, and the dimensionless current density is

$$j = 8N(e\pi KL)^2\rho\,/\,\gamma_0^3 mc^2 \quad . \tag{10}$$

The current j determines the coupling between the electron beam and the optical wave, and is the most important dimensionless variable describing an FEL. Without current $j = 0$, or with no bunching <..> = 0, there is no change in the initial optical field, $a(0) = a_0$. When $j \le 1$, the FEL gain is low, and when $j \gg 1$ the FEL gain is high. The combined equations, (6) for each sample electron and (8) for the light wave, are valid for weak fields ($|a| \le \pi$), strong fields ($|a| \gg \pi$), low gain ($j \le \pi$), high gain ($j \gg \pi$), low efficiency ($<\Delta v> \ll 2\pi N$), and high efficiency ($<\Delta v> \approx 2\pi N$). The "filling factor", F="area of the electron beam"/"area of the optical mode", can be added to the dimensionless current, $j \rightarrow jF$ to describe the optical mode coupling. When the FEL is tapered, the wave equation is not altered.

In the linearly polarized undulator, each electron experiences fast, periodic oscillations that are comparable to the radiation wavelength and modify the interaction strength in the fundamental and higher frequency harmonics. To account for this reduced coupling, the dimensionless current j should include the factor $(J_0(\xi)-J_1(\xi))^2$ where $\xi = K^2/2(1+K^2)$. For LANL with $K = 0.55$, the reduction factor is $(J_0-J_1)^2 = 0.9$.

For LLNL ELF experiments and the later Paladin experiments $K = 1$, so that the reduction factor is $(J_0-J_1)^2 = 0.85$.

3. LANL Oscillators and LLNL Amplifiers

The parameters describing FEL experiments at LANL and LLNL are only j and N in the above equations. All other quantities, like $|a|$, ϕ, ζ, and v are dynamical, and depend on j and N. For the LANL FEL oscillator, $N = 40$ while for the LLNL ELF FEL amplifier, $N = 30$. The values of the dimensionless current j are obtained below.

The early LANL FEL [B. E. Newnam, R. W. Warren, R. L. Sheffield, J. C. Goldstein, and C. A. Brau, Nucl. Instr. and Methods in Phys. Res. **A237**,187 (1985)] had a beam current of $I \approx 40$ A with a beam energy of $\gamma mc^2 \approx 21$ MeV ($\gamma \approx 42$). The undulator was $L = 1$ m long with wavelength $\lambda_0 \approx 2.73$ cm, peak field strength $B = 3$ kG, and $N = 37$ periods. The dimensionless current density was $j \approx 3.6$.

The newer LANL FEL [R. W. Warren, D. W. Feldman, B. E. Newnam, S. C. Bender, W. E. Stein, A. H. Lumpkin, R. A. Lohsen, J. C. Goldstein, B. D. McVey, and K. C. Chan, Nucl. Instr. Meth. Phys. Res. A259, 8 (1987)] has an improved beam current of $I \approx 130$ A with the same beam energy (21 MeV). The beam radius is $r_b \approx 0.1$ cm so that the new beam density is $\rho \approx 8\times10^{11}$. The electron pulse length is $l_b \approx 0.5$ cm and is $\sigma_z \approx 12$ slippage distances in length. The beam energy spread is still $\Delta\gamma / \gamma \approx 2\%$. The FEL undulator is the same as in the last LANL FEL. There are $N = 37$ periods of $\lambda_0 = 2.73$ cm wavelength with $K = 0.55$. The resulting resonant wavelength, $\lambda \approx 10$ μm, is the same as in the last LANL experiment. The optical resonator is also the same as in the last experiment, and is described by a Rayleigh length of $Z_0 = 63$ cm and optical mode waist of $w_0 \approx 1.4$ mm. The resonator loss results in a $Q \approx 50$. The dimensionless current describing the new experiment is $j \approx 50$ and is significantly more than before.

The LLNL ELF experiments at $\lambda \approx 8$ mm and 2 mm, used beam current of $I \approx 1000$ A at $\gamma mc^2 \approx 3.5$ MeV energy (the Lorentz factor is $\gamma \approx 7.8$) [A. L. Throop, T. J. Orzechowski, B. R. Anderson, F. W. Chambers, J. C. Clark, W. M. Fawley, R. A. Jong, A. C. Paul, D. Prosnitz, E. T. Scharlemann, R. D. Stever, G. A. Westenskow, and S. M. Yarema, *Experimental Characteristics of a High-Gain Free-Electron Laser Amplified Operating at 8 mm and 2 mm Wavelengths*, presented at AIAA 19th Fluid

Dynamics and Lasers Conf., Honolulu, HA, June 8, 1987]. The electron beam size was elliptical in the transverse directions described by $x_b \approx 0.6$ cm and $y_b \approx 1.2$ cm, and extended over $l_b \approx 300$ cm in length. The emittance was $\varepsilon \approx 0.07$ cm-rad with an effective energy spread of roughly $\Delta\gamma/\gamma \approx 6\%$. The undulator length is $L = 4$ m with period $\lambda_0 = 9.8$ m, and peak field $B = 1700$ G. There are $N = 40$ periods. The fundamental waveguide mode area is $A_{mode} \approx 7.5\ cm^2$ so that the filling factor is $F \approx 0.24$. The FELs dimensionless current is $j \approx 5700$ with an electron density of $\rho \approx 10^{11}$. The amplifier used an input power of $P_{in} \approx 30$ W so that the dimensionless initial field is $a_0 \approx 0.3$ with wavelength $\lambda \approx 2$ mm.

The Paladin experiments first used a $L = 5$ m undulator, then later increased it to $L = 15$ m. The 5 m experiment [D. Prosnitz, T. J. Orzechowski, J. K. Boyd, G. J. Caporaso, F. W. Chambers, Y. P. Chong, H. W. Clay, G. A. Deis, W. M. Fawley, R. A. Jong, B. Kulke, J. L. Miller, V. K. Neil, A. C. Paul, L. L. Reginato, D. Rogers, Jr., E. T. Scharlemann, J. T. Weir, S. Yarema, K. Halbach, and W. B. Colson, "Using the Gain Spectrum to Determine the Beam Distribution in the LLNL 5m Paladin Experiment", presented as a poster at the Ninth International Free Electron Laser Conference, Williamsburg VA (September 1987)] used an electron beam with Lorentz factor $\gamma = 85$ and current $I = 600$ A in a radius of $r_b \approx 0.6$ cm. The undulator length of $L = 5$ m contained $N = 62$ periods of $\lambda_0 = 8$ cm wavelength. The undulator strength was $K = 0.875$, and the laser wavelength was $\lambda = 10.6$ μm. The optical mode waist was $w_0 = 0.6$ cm with a Rayleigh length $Z_0 = 2$ m. The electron beam particle density is $\rho \approx 10^{11}$ so that the dimensionless current is $j \approx 50$. With an input power of 1 MW, the initial dimensionless field is $a_0 \approx 2$.

The 15 m Paladin experiments [D. Prosnitz, T. Orzechowski, et. al., American Physical Society Meeting, Baltimore, MD (April, 1988)] used a beam of $I \approx 600$ A again, but with the energy increased so that $\gamma = 91$. The beam radius was $r_b \approx 0.5$ cm with density $\rho \approx 1.6\times10^{11}$. The longer undulator contained $N = 187$ periods with $K \approx 1$ ($B = 1957$ G) and $\lambda_0 = 8$ cm. The radiation wavelength was $\lambda = 10.6$ μm with a Rayleigh length of $Z_0 = 5$ m and waist size $w_0 = 0.6$ cm. There are two betatron oscillations along such an undulator. The input power could be 14 kW or 5 MW, corresponding to dimensionless fields, $a_0 = 2$ or $a_0 = 38$. The dimensionless current density describing Paladin at 15 m is around $j = 1200$.

4. Parameterizing Physical Effects in FELs

A paper was prepared for the Ninth International Free Electron Laser Conference in Williamsburg, VA, Sept. 14-18, 1987. The paper shows the value of the dimensionless variables j, ζ, ν, and a that have been developed for the theory presented earlier in this report. The reference is W. B. Colson and J. Blau, "Parameterizing Physical Effects in Free Electron Lasers", Nuclear Instruments and Methods in Physics Research **A272**, 386 (1988).

In the paper, the parameters describing the free electron laser (FEL) experiments from 1976 to the present are briefly summarized. The dimensionless current density j is important for determining the relationship between experiments and evaluating many FEL effects. Developing a consistent description of all the diverse FEL systems starts with the electron phase in the combined undulator and optical field forces. Over the entire undulator length, the nonlinear coupling between the electron phase and the electron phase velocity uniquely defines the dimensionless optical field strength. The dimensionless current density j is then the resultant coupling between the averaged electron beam phases, and the dimensionless optical field strength in the wave equation. The gain regime of each FEL can be simply identified by j.

Many FEL effects can be expressed simply in terms of j. The importance of optical guiding is given by $jz_0^3 \geq \pi$ where $z_0 =$ "Rayleigh length"$/L$. The spectral linewidth expected in an FEL oscillator after n passes is given by $\approx (njN^2)^{-1/2}$. The number of plasma oscillations in the FEL beam is given by $(j/NK^2)^{1/2}$. In the high current regime, both saturation (strong optical fields) and inhomogeneous broadening are determined by $(j/2)^{1/3}$. In weak optical fields, FEL dynamics depend only on the parameter j, and the distribution of initial electron phase velocities. The FEL integral equation method provides a way of systematically evaluating the effects of an arbitrary distribution of electron phase velocities.

386 Nuclear Instruments and Methods in Physics Research A272 (1988) 386–391
North-Holland, Amsterdam

PARAMETERIZING PHYSICAL EFFECTS IN FREE ELECTRON LASERS

W.B. COLSON and J. BLAU

Berkeley Research Associates, P.O. Box 241, Berkeley, CA 94701, USA

The dimensionless current density j is important for determining the relationship between different experimental systems as well as evaluating many FEL effects. Multimode operation in the FEL oscillator is expressed in terms of a mapping depending only on j and the resonator Q.

1. Introduction

It is usually desirable to identify a few dimensionless variables that summarize reoccurring combinations of physical parameters in a complex problem like the free electron laser (FEL). Dimensionless variables can further be used to gain insight into relevant physical processes without reference to detailed calculations or simulations [1]. A particular choice of variables is presented here that has proved useful over many years of research on several different FEL oscillator and amplifier experiments.

2. The electron phase ζ

An outline of FEL theory [1] showing how the dimensionless current j develops starts with the electron phase in the combined undulator and optical field forces. The force on a relativistic electron in an undulator field with wavelength λ_0 is

$$\beta_\perp \propto K e^{ik_0 z(t)},$$

where $k_0 = 2\pi/\lambda_0$, $z(t)$ is the electron z position, $K = e\bar{B}\lambda_0/2\pi mc^2$, e is the electron charge magnitude, m is the electron mass, c is the speed of light, and $\bar{B}$ is the rms undulator field. Electron bunching, coherent emission, and high efficiency all require that the electron energy $\gamma(t)mc^2$ and the electron position $z(t)$ evolve in the presence of the copropagating radiation. The Lorentz force gives the rate of energy change

$$\dot{\gamma}(t) \propto \beta_\perp \cdot E \propto K e^{ik_0 z(t)} E e^{i(kz(t) - \omega t + \phi)}$$
$$= KE e^{i\zeta(t)} e^{i\phi},$$

where the optical field strength is E with carrier frequency $\omega = kc = 2\pi c/\lambda$ and phase ϕ. The electron phase,

$$\zeta = (k + k_0) z(t) - \omega t,$$

is a function of the fixed wavenumbers k and k_0 so that the only dynamical variable in $\zeta(t)$ is $z(t)$; in the relativistic limit, $k \gg k_0$, ζ is the electron phase in a section of the beam one optical wavelength long, $\Delta\zeta = (k + k_0)\Delta z \approx k\Delta z$.

3. The electron phase velocity $\nu = \dot{\zeta}$

Evolution of the light and electrons takes place while they both propagate through the long undulator with many periods $N = L/\lambda_0 \gg 1$. The average electron evolves for a time $L/\bar{\beta}_z c$, where $\bar{\beta}_z c$ is the average electron z velocity. In a relativistic beam $\beta_z \approx \bar{\beta}_z \approx 1$ so that the common interaction time is $L/\bar{\beta}_z c \approx L/c$ for all electrons. We chose the dimensionless time $\tau = \bar{\beta}_z ct/L \approx ct/L$, so that a pass through the undulator is described by $\tau = 0 \to 1$. Even the faster light wave, traveling at speed c, evolves for nearly the same time as electrons, $\tau = 0 \to 1 - O(\gamma^{-2}) + \cdots \approx 1$. Other timescales defined by the plasma frequency in a relativisitic beam, or the high-gain exponential growth-rate in the case of large j, can become important in a specific FEL experiment. But, instead of making a commitment to a time-scale that may, or may not, be relevant, we use $\tau = 0 \to 1$, and relate other effects to the evolution time over which they might occur, L/c; the total evolution time is always important.

Using the time τ, the electron phase velocity becomes

$$\nu(\tau) = L[(k + k_0)\beta_z(t) - k] = \dot{\zeta}(\tau),$$

where $\dot{(\cdots)} = d(\cdots)/d\tau$. When $\nu = 0$, the electron experiences resonant optical and undulator field forces which maximize coupling. The resonant FEL wavelength is identified as $\lambda = \lambda_0(1 + K^2)/2\gamma^2$. As with the simple pendulum, the pair of phase-space coordinates $(\zeta(\tau), \nu(\tau))$ provide a natural and useful choice.

0168-9002/88/$03.50 © Elsevier Science Publishers B.V.
(North-Holland Physics Publishing Division)

4. The dimensionless optical field a

Both the electron phase and phase velocity evolve in time governed by the Lorentz force equations of motion. In the limit of large N (implying low efficiency), the phase and phase velocity are coupled by the dimensionless complex optical field $a = |a|e^{i\phi}$ through the pendulum equation,

$$\dot{\nu} = \ddot{\zeta} \propto = |a|\cos(\zeta + \phi), \tag{1}$$

where $|a| = 4Ne\pi KLE/\gamma^2 mc^2$. When $|a| \sim \pi$, there is visible electron bunching in phase space after a single pass through the undulator. When $|a| \ll \pi$, the bunching is imperceptible, and the optical field is weak. When $|a| \gg \pi$, the optical field induces a phase spread over several optical wavelengths and bunching is diminished; this is saturation in strong optical fields. The trapped electrons in strong fields execute synchrotron oscillations about the phase $\pi/2$ with frequency $|a|^{1/2}$ in units of τ; when $|a| = 4\pi^2$ there is one synchrotron oscillation along the undulator. When eq. (1) is extended to include corrections for higher efficiency, the coupling between ζ and ν is still given by the dimensionless field a.

5. The dimensionless current density j

The evolution of the light wave is governed by the transverse optical wave equation driven by the transverse beam current $J_\perp$. An individual electron in the beam contributes a current in proportion to its transverse motion $-ec\beta_\perp e^{ik_0 z}$. The slowly-varying field envelope $a(\tau)$ can only respond to the average current in a small volume element a few wavelengths of light long, and weighted by the electron beam particle density ρ. The wave equation for the dimensionless optical field envelope is then

$$\dot{a} = -j\langle e^{-i\zeta}\rangle, \tag{2}$$

where $\langle \cdots \rangle$ is the average over sample electron phases ζ, and the dimensionless current density is

$$j = 8N(e\pi KL)^2 \rho/\gamma^3 mc^2. \tag{3}$$

It is j that determines the response of the optical wave to bunching in the beam. The dimensionless current j provides the coupling between the electron beam and the light wave so that each gain regime can be simply identified by j; when $j \leq 1$, the FEL gain is low, when $j \gg 1$ the FEL gain is high.

In summary,

- The identification of the electron phase ζ and the dimensionless interaction time τ leads directly to the corresponding electron phase velocity $\nu = \dot{\zeta}$.
- The coupling between the electron phase and phase velocity, the cause of bunching, is given by the dimensionless optical field $a = |a|e^{i\phi}$.
- The response to bunching, the coupling between the bunched electron beam and the light wave, is finally determined by the dimensionless current j.

Each definition is found to be physically meaningful and useful in the evaluation of FEL effects.

6. FEL experiments described by j

Table 1 summarizes many of the relativistic ($\gamma > 5$) FEL experiments from 1976 to the present. The location and date of the experiments are given in the first column; no date is given for the last eight experiments that are planned for the future. The electron beam current I (A), given in amperes, and the electron beam area πr_e^2 determine the electron beam density $\rho = 3 \times 10^9 I(\mathrm{A})/ec\pi r_e^2$. (There are two practical corrections to the value of j listed in table 1 that are not defined in eq. (3): the "filling factor", describing optical mode coupling by the substitution $j \to j(r_e^2/w_0^2)$ where w_0 is the optical mode radius; and Bessel function factors for linearly polarized undulators [1]). Notable in the list is the small range of dimensionless currents j that have been explored so far; exceptions are the low currents of the storage ring devices, and the high currents of the ELF experiments at LLNL. Below are some examples of important FEL effects that can be expressed in terms of j. Only the basic physical concepts are outlined without detailed derivation. The scaling in terms of physical parameters like I, N, K, and γ are also given for each example.

7. Gain determined by j

Two operating regimes with high and low gain are explored in the experiments reported in table 1. The weak-field coupling between the electron beam and light is maximum when the initial phase velocity is at resonance, $\nu(0) = \nu_0 = 0$. The FEL gain that might result from good coupling is defined as $G = a_F^2/a_0^2 - 1$, where a_F is the final field amplitude at $\tau = 1$, and a_0 is the initial field amplitude.

In the low-gain FEL, where $j \leq 1$, the maximum gain is $G = 0.135j$ at $\nu_0 = 2.6$. While the maximum coupling occurs at resonance, the energy lost and gained by the electron beam cancels so there is no net gain; operating off resonance upsets this cancellation and allows useful nonzero gain. There is no significant optical phase shift in the low-gain regime. The natural gain spectrum bandwidth is $\Delta\nu \approx \pi$ about $\nu_0 = 2.6$ with a corresponding range of optical wavelengths $\Delta\lambda/\lambda \approx 1/2N$.

In the high-gain FEL, where $j \gg 1$, the maximum gain is $G = \exp[(j/2)^{1/3}\sqrt{3}]/9$ near resonance $\nu_0 \approx 0$. There is significant optical phase evolution, $\phi(\tau) = (j/2)^{1/3}\tau/2$. In the ELF experiments of table 1, $j = 10^4$ so that $G \approx 10^{12}$ and $\Delta\phi \approx 3\pi$. The natural gain spec-

Table 1
Free electron lasers

FEL	I (A)	γ	N	λ_0 (cm)	K	λ (μm)	w_0 (cm)	j	Comments [a]
[2] Stanford '76	0.07	48	160	3.2	0.72	12	0.3	0.2	First A, RF, H
[3] Stanford '77	2.6	86	160	3.2	0.72	3.4	0.3	6	First O, RF, H
[4] Stanford '80	1.3	85	160	3.3	0.71	3.4	0.14	3.6	O, RF, H
[5] LANL '82	20	40	37	2.7	0.55	11	0.16	1.8	A, RF, L, $\delta = 10\pi$
[6] MSNW/Boeing '83	3	38	91	2.5	0.44	11	0.16	2.8	A, RF, L, $\delta = 33\pi$
[7] TRW/EG&G '83	10	50	75	3.6	0.63	11	0.17	1.6	A, RF, L
[8] LANL '84	40	40	37	2.7	0.54	11	0.15	3.6	O, RF, L
[9] TRW/Stanford '84	2.5	130	153	3.6	0.97	1.6	0.1	3.4	O, RF, L, $\delta = 4\pi$
[10] Orsay ACO '84	0.03	326	17	7.8	1.2	0.65	0.03	0.0003	A, SR, L, $D = 100$
[11] Novosibirsk '84	7	686	22	6.9	2.7	0.62	0.03	0.06	A, SR, L, $D = 280$
[12] Frascati ENEA '85	2.4	40	50	2.4	0.35	11	0.1	0.14	O, M, L
[13] Orsay ACO '85	0.2	432	17	7.8	2	0.63	0.03	0.004	O, SR, L, $D = 100$
[14] UCSB '85	1.25	6.8	160	3.6	0.11	400	1	0.35	O, V, L
[15] INFN LELA '85	0.018	1224	20	12	3.5	0.51	0.04	0.00006	A, SR, L
[16] LLNL ELF '85	500	7.5	30	9.8	2.8	8700	1.5	9000	A, IL, L
[17] LANL '86	130	40	37	2.7	0.56	11	0.14	53	O, RF, L, $\delta = 18\pi$
[18] Stanford Mark III '86	20	87	47	2.3	1.5	3.1	0.07	3.2	O, RF, L
[19] LLNL ELF '86	850	6.9	30	9.8	2.5	8700	1.5	14100	A, IL, L
[20] LLNL ELF Tapered '86	850	6.9	30	9.8	2.4	8700	1.5	14400	A, IL, L, $\delta = 50\pi$
[21] LLNL ELF '87	1000	7.8	40	9.8	1.1	2000	1.5	7200	A, IL, L
[22] Boeing/Spectra '87	100	223	229	2.2	1.3	0.5	0.06	687	O, RF, L, $\delta = 92\pi$
[23] Rocketdyne/Stanford '88	20	75	80	2.5	0.61	3.0	0.08	6.2	O, RF, L
[24] Bell Labs	5	24	50	20	0.93	240	2	2	O, M, H
[25] BNL	22	588	39	6.5	2.3	0.6	0.07	0.25	A, SR, L
[26] United Kingdom	10	118	76	6.5	1.9	11	0.3	8.9	O, RF, L
[27] LANL XUV	100	400	750	1.6	0.79	0.08	1.6	414	O, RF, L
[28] Duke University XUV	270	1958	422	6.4	1.6	0.03	0.06	37	O, SR, L
[29] NBS XUV	2	363	130	2.8	1	0.23	0.04	0.6	O, M, L
[30] LBL/BNL XUV	200	1470	870	2.3	2.6	0.04	0.03	1360	SR, SRA, L
[31] Beijing PRC	15	40	50	3	1	11	0.1	5	O, RF, L

[a] RF – rf linac accelerator, IL – induction linac accelerator, M – microtron accelerator, SR – electron storage ring, V – Van de Graaff electrostatic accelerator, H – helical undulator polarization, L – linear undulator polarization, $\delta = \#$ – tapered undulator FEL, $D = \#$ –klystron undulator FEL, A – FEL amplifier, O – FEL oscillator, SRA – superradiant amplifier in a long, single-pass undulator.

trum bandwidth $\Delta\nu_j \approx \pi j^{1/6}$ about resonance with a corresponding range of optical wavelengths is $\Delta\lambda/\lambda \approx j^{1/6}/2N$ that scales as $\Delta\lambda/\lambda \approx I^{1/6}/(\gamma N)^{1/2}$.

8. Plasma oscillations determined by j

In the high-gain regime described above, interparticle Coulomb forces play no role. The high-gain regime is truly collective, however, since the electrons influence each other through the changing optical field. Coulomb forces can be incorporated in eq. (1) as an additional force depending on the longitudinal position of all other electrons in each optical wavelength [1]. It is then found that plasma oscillations can occur in the beam as it passes through the undulator; the number of plasma oscillations is

$$N_{\mathrm{PLASMA}} \approx \left(\frac{j}{8\pi^3 NK^2}\right)^{1/2} \qquad (4)$$

Even in the LLNL ELF experiments with the highest j, $N_{PLASMA} \approx 0.6$, and gives only a minor effect. The scaling is $N_{PLASMA} \propto N(I/\gamma^3)^{1/2}$.

9. Optical guiding determined by j

FEL optical guiding can occur when the high-current electron beam alters the propagation of the light wave and continually focuses it back into the electron beam. The optical phase evolution in a distance dz along the undulator is $d\phi_j = (jr_e^2/2w_0^2)^{1/3}\, dz/2L$ including the filling factor. Natural diffraction produces a phase shift of the opposite sign, $d\phi_D = -dz\, \lambda/\pi w_0^2$. If the FEL interaction is to offset natural diffraction, we must have $d\phi_j \geq d\phi_D$ so that a large optical wavefront collapses to approximately the electron beam size. Making the rough estimate $w_0 \approx 2r_e$ to simplify the optical guiding condition, the optical mode area that can be propagated without diffraction becomes

$$\pi w_0^2 \approx \frac{4L\lambda}{j^{1/3}}. \tag{5}$$

The mode area becomes smaller as j is increased, and is independent of L since $j \propto L^3$. The scaling in eq. (5) is $w_0 \propto I^{-1/4}$ showing that phase guiding requires a substantial current.

10. Optical linewidth determined by j

The spectral linewidth in the FEL oscillator is normally determined by mode competition among many closely spaced wavelengths in a long overmoded resonator. The initial spontaneous spectrum has a width $\Delta\nu(k) \approx 2\pi$ centered around resonance $\nu(k) = 0$. The gain bandwidth is smaller, $\Delta\nu(k) = \pi$ centered around $\nu(k) = 2.6$. After many passes n, the power at wavelengths near peak gain of $G = 0.135j$ begin to grow substantially compared to wavelengths with less gain, and the spectral linewidth expected is

$$\Delta\nu(k) \approx \frac{2\pi}{(nj)^{1/2}}, \tag{6}$$

assuming negligible losses. After $n = 10^3$ passes, the spectrum of a moderate gain oscillator with $j = 5$ narrows by about 10^2. The spread in wavelengths scales as $\Delta\lambda/\lambda \propto 1/(nN^5I)^{1/2}$.

11. Electron beam quality requirements determined by j

Many experiments use an imperfect electron beam with a range of initial phase velocities $\sigma = \Delta\nu_j$ that are comparable with the FEL's natural gain spectrum bandwidth. The competition between the coherent bunching and random thermalizing can completely alter the properties of the FEL interaction and, of course, reduce the gain. In strong optical fields where the FEL interaction induces a large phase-velocity spread, beam quality is less important.

In the case of low gain and weak fields, $\sigma \leq \pi$ is sufficient to avoid significant gain degradation. The critical spread in energy scales as $\Delta\gamma \propto N^{-1}$ showing that a longer undulator increases the FEL's sensitivity to electron beam quality.

In the case of high gain and weak fields, the exponential growth-rate of the optical field is large so that bunching can compete better against random thermalization. The critical spread in the high-current limit is $\sigma_j \approx j^{1/3}$; for large current, $j \sim 10^4$, σ_j can be almost 10 times the low-gain critical spread. The high-gain critical spread is independent of L, since $j \propto L^3$ and $\sigma_j = \Delta\nu_0 \propto L$, and scales as $\sim I^{1/3}/\gamma$.

12. The onset of saturation determined by j

In the FEL oscillator, the optical field grows to saturation over many passes of amplification; in the FEL amplifier, the optical field grows to saturation in a single pass. In both cases, the gain decreases from its weak-field value when the optical field is strong enough to move some electrons by $\sim\pi$ with respect to other electrons.

In the case of low gain, the onset of saturation occurs when the field amplitude is $a_s \approx \pi$. The change in the bunched beam's phase velocity is determined by the height of the phase-space separatrix $\Delta\nu \approx 4a_s^{1/2} \approx 2\pi$. Since $\Delta\nu = 4\pi N\Delta\gamma/\gamma$, the natural efficiency is $\eta \approx 1/2N$.

In the case of high gain, the onset of saturation occurs when the field amplitude is $a_j \approx 2(j/2)^{1/3}$. The dependence on j in the high gain case results from the altered electron dynamics in eq. (1). For $j = 10^4$, saturation occurs at substantially stronger fields than in the low gain case, $a_j \approx 200\pi \gg \pi$. The corresponding change in the bunched beam's phase velocity is $\Delta\nu_j \approx 2(j/2)^{1/3}$ so that the natural efficiency is $\eta_j \approx (j/2)^{1/3}/2\pi N$. For $j = 10^4$, the efficiency is $\eta_j \approx 5/2N$.

13. Multimodes in the FEL oscillator determined by j and Q

The FEL equations of motion, eqs. (1) and (2), depend only on the initial values a_0, ν_0, $\phi = 0$, and the dimensionless current j; the initial electron phases are randomly spread. In the overmoded FEL oscillator, the optical field is free to take on any value consistent with

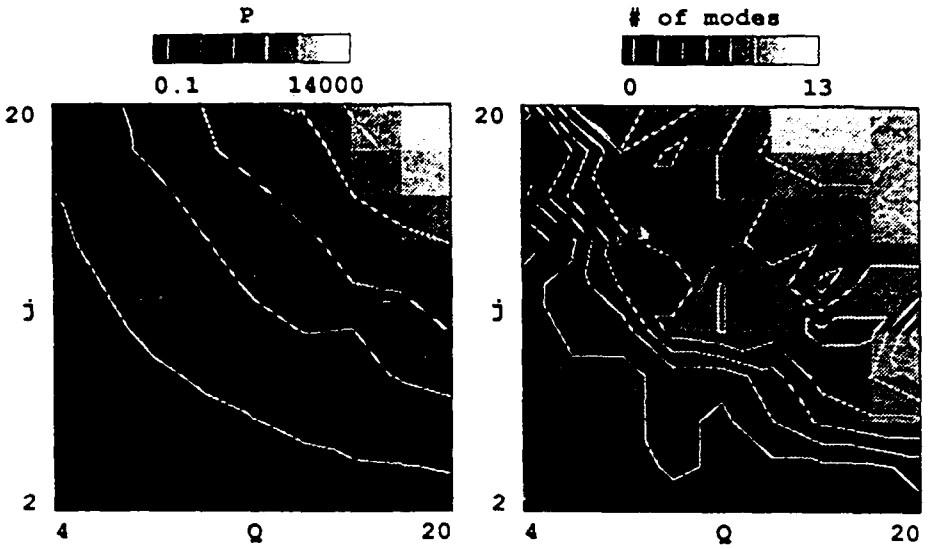

Fig. 1. On the left is the intensity-contour plot of $P(j, Q)$, with larger values of P drawn brighter and a scale at the top. The corresponding plot of the number of modes in the FEL oscillator is shown on the right.

the physics determined by the equations. For modes above threshold, the power will grow to saturation as determined by the resonator losses. To describe losses, the optical power is taken to decay as $\propto e^{-n/Q}$ over many passes n in the absence of gain. After many passes n, saturation decreases the gain/pass to equal the loss/pass, so that the final steady-state power and mode structure can only depend on j and Q.

On the left of fig. 1 is an intensity-contour plot of the final steady-state power $P(j, Q) = a_F^2$. For each point on the (j, Q) surface, a multimode simulation runs for many passes n until steady-state power is reached. Values of j and Q resulting in large P are drawn brighter with an intensity scale shown at the top; contours connect points of equal power. At the lowest values of j and Q, the oscillator is below threshold. As either j or Q is increased, the power steadily increases reaching a peak field strength $a_F \approx 10^2$.

After strong saturation, the trapped electrons execute synchrotron oscillations in the closed-orbit region of phase-space at the synchrotron frequency $a_F^{1/2}$. When the beam current oscillates at this new frequency, sidebands are formed around the carrier frequency. The presence of sidebands increases the optical power, and causes even more sidebands to form.

On the right of fig. 1 is an intensity-contour plot of the number of modes in the final steady-state spectrum of the simulation followed on the left. A value of (j, Q) resulting in more modes is drawn brighter with the scale shown at the top. At only the lowest values of j and Q is single mode operation possible. At the highest values, there are more than 10 modes present. Simulations at selected values of (j, Q) show that when there are more than ~ 4 modes, the FEL spectrum appears chaotic, and continues of evolve. The field strength where multimode behavior starts is seen to be $a_F^{1/2} \approx 2\pi$, just the value needed to start synchrotron oscillations!

Acknowledgements

The author is grateful for support of this work by the Lawrence Livermore National Laboratory, and the U.S. Office of Naval Research.

References

[1] W.B. Colson, in: Free Electron Lasers: Critical Review of Technology, ed. B.E. Newnam, Proc. SPIE 738 (1988) pp. 2–27.

[2] L.R. Elias, W.M. Fairbank, J.M.J. Madey, H.A. Schwettman and T.I. Smith, Phys. Rev. Lett. 36 (1976) 717.

[3] D.A.G. Deacon, L.R. Elias, J.M.J. Madey, G.J. Ramian, H.A. Schwettman and T.I. Smith, Phys. Rev. Lett. 38 (1977) 892.

[4] J.N. Eckstein, J.M.J. Madey, K. Robinson, T.I. Smith, S. Benson, D. Deacon, R. Taber and A. Gaupp, Physics of Quantum Electronics, Vol. 8 (1982) p. 49.

[5] R.W. Warren, B.E. Newnam, J.G. Winston, W.E. Stein, L.M. Young and C.A. Brau, IEEE J. Quantum Electron QE-19 (1983) 391.

[6] J.M. Slater, J.L. Adamski, D.C. Quimby, T.L. Churchill, L.Y. Nelson and R.E. Center, IEEE J. Quantum Electron QE-19 (1983) 374.

[7] J.A. Edighoffer, H. Boehmer, M.Z. Caponi, S. Fornaca, J. Munch, G.R. Neil, B. Saur and C. Shih, IEEE J. Quantum Electron QE-19 (1983) 316.

[8] B.E. Newnam, R.W. Warren, R.L. Sheffield, J.C. Goldstein and C.A. Brau, Nucl. Instr. and Meth. A237 (1985) 187.

[9] J.A. Edighoffer, G.R. Neil, C.E. Hess, T.I. Smith, S.W. Fornaca and H.A. Schwettman, Phys. Rev. Lett. 52 (1984) 344.

[10] P. Elleaume, J.M. Ortega, M. Billardon, C. Bazin, M. Bergher, M. Velghe and Y. Petroff, J. Phys. (Paris) 45 (1984) 989.

[11] G.A. Kornyukhin, G.N. Kulipanov, V.N. Litvinenko, N.A. Mesentsev, A.N. Skrinsky, N.A. Vinokurov and P.D. Voblyi, Nucl. Instr. and Meth. A237 (1985) 281.

[12] U. Bizzarri, F. Ciocci, G. Dattoli, A. De Angelis, G.P. Gallerano, I. Giabbai, G. Giordano, T. Letardi, G. Messina, A. Mola, L. Picardi, A. Renieri, E. Sabia, A. Vignati, E. Fiorentino and A. Marino, Nucl. Instr. and Meth. A250 (1986) 254.

[13] M. Billardon, P. Elleaume, Y. Lapierre, J.M. Ortega, C. Bazin, M. Bergher, J. Marilleau and Y. Petroff, Nucl. Instr. and Meth. A250 (1986) 26.

[14] L.R. Elias, J.Hu and G. Ramain, Nucl. Instr. and Meth. A237 (1985) 203.

[15] R. Barbini, G. Vignola, S. Trillo, R. Boni, S. DeSimone, C. Faini, S. Guiducci, M. Preger, M. Serio, B. Spataro, S. Tazzari, F. Tazzioli, M. Vescovi, A. Cattoni, C. Sanelli, M. Castellano, N. Cavallo, F. Cevenini, M.R. Masullo, P. Patteri, R. Rinzivillo, S. Solimeno and A. Cutolo, J. Phys. (Paris) 44 (1985) C1-1.

[16] T.J. Orzechowski, B. Anderson, W.M. Fawley, D. Prosnitz, E.T. Scharlemann, S. Yarema, D. Hopkins, A.C. Paul, A.M. Sessler and J. Wurtele, Phys. Rev. Lett. 54 (1985) 889.

[17] R.W. Warren, D.W. Feldman, B.E. Newnam, S.C. Bender, W.E. Stein, A.H. Lumpkin, R.A. Lohsen, J.C. Goldstein, B.D. McVey and K.C.D. Chan, Nucl. Instr. and Meth. A259 (1987) 8.

[18] S.V. Benson, J.M.J. Madey, J. Schultz, M. Marc, W. Wadensweiler, G.A. Westenskow and M. Velghe, Nucl. Instr. and Meth. A250 (1986) 39.

[19] T.J. Orzechowski, B.R. Anderson, W.M. Fawley, D. Prosnitz, E.T. Scharlemann, S.M. Yarema, A.M. Sessler, D.B. Hopkins, A.C. Paul and J.S. Wurtele, Nucl. Instr. and Meth. A250 (1986) 144.

[20] T.J. Orzechowski, B.R. Anderson, J.C. Clark, W.M. Fawley, A.C. Paul, D. Prosnitz, E.T. Scharlemann and S.M. Yarema, Phys. Rev. Lett. 57 (1986) 2172.

[21] A.L. Throop, T.J. Orzechowski, B.R. Anderson, F.W. Chambers, J.C. Clark, W.M. Fawley, R.A. Jong, A.C. Paul, D. Prosnitz, E.T. Scharlemann, R.D. Stever, G.A. Westenskow and S.M. Yarema, Experimental Characteristics of a High-Gain Free-Electron Laser Amplifier Operating at 8 mm and 2 mm Wavelengths, presented at AIAA 19th Fluid Dynamics and Lasers Conf., Honolulu, HA, June 8, 1987.

[22] K.E. Robinson, T.L. Churchill, D.C. Quimby, D.M. Shemwell, J.M. Slater, A.S. Valla, A.A. Vetter, J. Adamski, T. Doering, W. Gallagher, R. Kennedy, B. Robinson, D. Shoffstall, E. Tyson, A. Vetter and A. Yeremian, Nucl. Instr. and Meth. A259 (1987) 49.

[23] A. Bhowmik, M.S. Curtin, W.A. McMullin, S.V. Benson, J.M.J. Madey, B.A. Richman and L. Vintro, these Proceedings (9th Int. FEL Conf., Williamsburg, VA, 1987) Nucl. Instr. and Meth. A272 (1988) 10.

[24] E.D. Shaw and C.K.N. Patel, Phys. Quantum Electron. 9 (1982). 671.

[25] A. Luccio, C. Pellegrini, A. van Steenbergen, and L.H. Yu Proc. Int. Conf. LASERS '82 (1983) 198.

[26] W.A. Gillespie, P.F. Martin, M.W. Poole, G. Saxon, R.P. Walker, J.M. Reid, M.G. Kelliher, C.R. Pidgeon, S.D. Smith, W.J. Firth, D.A. Jaroszinski, D.M. Tratt, J.S. Mackay and M.F. Kimmitt, Nucl. Instr. and Meth. A250 (1986) 233.

[27] J.C. Goldstein and B.D. McVey, Nucl. Instr. and Meth. A259 (1987) 203;
B.E. Newnam, J.C. Goldstein, J.S. Fraser and R.K. Cooper, A Linac-Driven XUV Free-Electron Laser, Los Alamos National Laboratory Report, Los Alamos, NM, USA.

[28] J.E. LaSala, D.A.G. Deacon and J.M.J. Madey, Nucl. Instr. and Meth. A250 (1986) 262.

[29] X.K. Maruyama, S. Penner, C.M. Tang and P. Sprangle, Nucl. Instr. and Meth. A259 (1987) 259.

[30] K-J. Kim, J. Bisognano, S. Chattopadhyay, M. Cornacchia, A. Garren, K. Halbach, A. Jackson, H. Lancaster, J. Peterson, M. Zisman, C. Pellegrini and G. Vignola, Storage Ring Design for a Short Wavelength FEL, Lawrence Berkeley Laboratory Report.

[31] Xie Jialin, Director, Institute of High Energy Physics, Beijing, PRC, private communication.

5. Waveguide Effects In the FEL

Some applications, like the medical FELs, could make use of longer wavelengths like $\lambda \approx 100$ μm up to 1mm. The LLNL ELF FEL, the UCSB FEL, and the Hughes FEL, all use waveguides to counter the detrimental effects of free-space diffractions with long wavelengths. Designing an FEL to operate at long wavelengths can lead to the consideration of a waveguide to confine the wavefront from excess diffraction. Free space diffraction can spread the optical wavefront away from the co-propagating electron beam and reduce coupling. FEL coupling is proportional to the filling factor F, so that the dimensionless current density, j, should be replaced with jF when mode coupling is important. The filling factor, F, is the ratio of the electron beam area to the optical mode area whether in a waveguide or free-space.

The natural distance for a light beam of wavelength λ to double its initial beam area, πw_0^2, is the Rayleigh length $\pi w_0^2/\lambda$. Comparing this length to the undulator length L defines the dimensionless Rayleigh length $z_0 = \pi w_0^2/L\lambda$. Without a waveguide, the optical wavelength is determined by the resonance condition, $\lambda = \lambda_0(1+K^2)/2\gamma^2$ where $K = e\bar{B}\lambda_0/2\pi mc^2$ is the undulator parameter, $\lambda_0 = 2\pi/k_0$ is the undulator wavelength, and γmc^2 is the electron beam energy. In a waveguide, the resonance condition can be modified, but remains roughly correction with the FEL is far above the waveguide cut-off frequency. The Rayleigh length becomes $z_0 = 2\pi w_0^2\gamma^2/(1+K^2)N\lambda_0^2$, and expresses how an FEL with a low energy electron beam gives a short Rayleigh length.

For any FEL design, the filling factor should be near $F \approx 0.5$ for optimum coupling. If the electron beam is larger than the optical mode, $F \geq 1$, then much of the electron beam does not see the optical wave and does not bunch. This part of the beam is lost. If $F \ll 1$, the electron beam only amplifies a small portion of the optical wavefront and the coupling is poor. At long wavelengths, the optical mode tends to be much larger than the electron beam so that coupling is small. The filling factor could be increased for an optical wavefront of any size, if the electron beam size is increased. But, as the electrons move off of the undulator axis, approaching the undulator magnets, the field strength $\bar{B}$ increases and deflects electrons back towards the axis causing betatron oscillations. The extra transverse motion decreases the z velocity of the relativistic electrons and changes the resonance condition. The change in the electron phase velocity in a matched beam with radius r_b is

$\Delta\nu_\beta = 4\pi N(Kk_0r_b)^2/(1+K^2)$. Gain degradation begins when the beam radius is large enough to cause $\Delta\nu_\beta \approx \pi$. The limit on the beam radius for good coupling is then $r_b \leq (1+K^2)^{1/2}\lambda_0/4\pi KN^{1/2}$. For $K \approx 1$, we have $r_b \leq 0.01\lambda_0$, or for $K \ll 1$, we have $r_b \leq 0.01\lambda_0/K$.

When natural diffraction spreads the optical wave away the electron beam the filling factor is reduced further; assuming the light remains in the lowest order Gaussian mode with its waist at the center of the undulator, the average filling factor over the undulator length is $\bar{F} = F_0/(1+1/12z_0^2)$, or $\bar{F} = \sigma_e^2/(z_0+1/12z_0)$ where $\sigma_e = r_b(\pi/L\lambda)^{1/2}$ is the dimensionless electron beam radius. Typically, $\sigma_e \approx 1$ in an FEL, but the following arguments are independent of that value and only depend on the Rayleigh length z_0. For $z_0 \to 0$, $\bar{F} \to 0$ and coupling $\to 0$, because the optical wave spreads away from the electron beam at the two ends of the undulator; for $z_0 \to \infty$, $\bar{F} \to 0$ and coupling $\to 0$ again, because the wavefront is too large compared to electron beam. The maximum filling factor, $\bar{F}^{max} = F_0/2$, or $\bar{F}^{max} = \sqrt{3}\sigma_e^2$, occurs at $z_0^{max} = (12)^{-1/2}$. The maximum is relatively broad in z_0 and $\bar{F}^{max}$ drops to half of its peak value, $\sqrt{3}\sigma_e^2/2$, at $z_0 \approx 0.11$ and 0.75.

The restriction on the spread of electron phase velocities, or the beam radius, together with the requirement of good coupling, or large filling factor F, gives a restriction on the Rayleigh length in terms of γ and N. To relate r_b and w_0, assume that the filling factor is not too small, say $F > F_0 \geq 0.1$, so that $w_0 \leq 3r_b$. Then, the dimensionless Rayleigh length is limited by $z_0 \leq \gamma^2/\pi K^2N^2$. Either a low energy beam or a long undulator can limit z_0 to a small value and decrease the filling factor. The limit is relaxed when K is small, because the electron beam can be expanded to support a wide optical wavefront without much diffraction. But, the FEL gain is small with small values of K; recall that $G \propto K^2$. Gain degradation begins to occur when the coupling is reduced by small values of $\bar{F}$. The peak value of $\bar{F}$, $\sqrt{3}\sigma_e^2$, decreases to less than half its value when the limit above restricts $z_0 \leq 0.1$. Therefore, an FEL design requires

$$\gamma \geq KN/2 \qquad (11)$$

so that natural diffraction does not significantly decrease the interaction strength. An FEL with low electron beam energy and a long, strong undulator, requires a waveguide for good coupling strength. The inequality above is then well-satisfied:

$\gamma = 42 \gg KN/2 \approx 10$. If the wavelength of the FEL is pushed up to $\lambda = 100$ μm by decreasing the electron beam energy, then the new Lorentz factor is $\gamma \approx 13$. For the values of K and N, the inequality is not dramatically satisfied, $\gamma \approx 13 \geq KN/2 \approx 10$, and a waveguide can be considered to improve or maintain coupling. At longer wavelengths yet, the waveguide probably becomes necessary.

If an FEL requires a waveguide for good coupling, there is a change in the FEL resonance condition. In a single waveguide mode, the cross-section of the mode can be used in the filling factor to estimate coupling to the mode. The electron beam size should be close to, but smaller than, the radiation cross-section for best coupling. Assuming the electron beam is on-axis, the mode should have a transverse electric field on-axis as well. Higher order modes will average to smaller coupling if the electron beam size is not much smaller than the mode. If the FEL gain is not too large, higher order modes might be below threshold, or out of resonance with the gain spectrum bandwidth. The following analysis can help determine this coupling and resonance.

Waveguide modes are separated into two classes: TE - transverse electric modes where the longitudinal component of the electric field $E_z = 0$ everywhere, and TM - transverse magnetic modes where the longitudinal component of the magnetic field $B_z = 0$ everywhere. The time dependence of the waveguide fields is taken to be $\propto e^{-i\omega t}$ with longitudinal dependence $\propto e^{\pm ikz}$. At the waveguide wall, the TE mode boundary condition is $B_z' = 0$, while the TM mode boundary condition is $E_z = 0$. The waveguide cross-section and boundary conditions specify an eigenvalue problem with a number of eigenvalues Λ_{pq}, where $p,q = 0,1,2,3,....$ are eigenvalues that specify the mode. For a given frequency, the wave equation in the waveguide determines the wavenumber k_{pq} for each value of pq,

$$k_{pq}^2 = \omega^2/c^2 - \Lambda_{pq}^2 \quad . \tag{12}$$

When the frequency is below cut-off, $\omega/c \leq \Lambda_{pq}$, the wavenumber k_{pq} is zero, or imaginary, and mode does not propagate; $\omega_{pq} = c\Lambda_{pq}$ is called the cut-off frequency of the waveguide.

All waveguide modes have the form $E_\perp \propto e^{\pm ik_{pq}z - i\omega t}$. The backward propagating wave, $E_\perp \propto e^{-ik_{pq}z}$, results in an FEL interaction at rather long wavelengths. It can sometimes be of interest, but most applications of the relativistic

FEL interaction seek shorter wavelengths. Therefore, the backward propagating wave is not discussed here, and we concentrate on waveguide modes with form $E_\perp \propto e^{+ik_{pq}z - i\omega t}$. When the polarization of the waveguide mode is chosen to match the electron motion in the periodic undulator field, we have the best coupling. The form of the transverse electron motion is $\beta_\perp \propto e^{ik_0 z}$ where $\lambda_0 = 2\pi/k_0$ is the undulator wavelength. The fourth component of the Lorentz force equation governs the electron energy evolution and bunching. It has the form $\dot{\gamma} \propto \beta_\perp E_\perp \propto e^{i(k_0+k_{pq})z - i\omega t}$, and naturally defines the electron phase $\zeta = (k_0+k_{pq})z - \omega t$ where k_0, k_{pq}, and ω are fixed by the FEL design, and $\zeta(t)$ follows the evolution of $z(t)$. The corresponding phase velocity is $\propto \dot{\zeta}$. Generally, the electron phase and phase velocity evolve over the whole undulator length L so that it is natural to relate the time t to the evolution time $L/c\beta_z \approx L/c$ in the relativistic FEL with electron beam z velocity β_z. The natural definition for the electron phase velocity is then $v = L[(k_0+k_{pq})\beta_z - \omega/c]$. The electron phase velocity $v(t)$ depends on k_0, k_{pq}, ω, and L, which are fixed in an FEL design, and follows the evolution of the electron z velocity $\beta_z(t)$.

The electron motion in the periodic undulator and interaction with the waveguide mode are resonant when $v = 0$. This occurs at the resonant frequency $\omega^* = c(k_0+k_{pq})\beta_z$ where $k_{pq} = (\omega^{*2}/c^2 - \Lambda_{pq}^2)^{1/2}$. The equation can be solved for ω^* in terms of k_0, k_{pq}, and β_z, and the eigenvalue Λ_{pq} depends on the waveguide dimension and shape. For the rectangular waveguide with sides a and b we have

$$\Lambda_{pq} = \pi \left(\frac{p^2}{a^2} + \frac{q^2}{b^2} \right)^{1/2} , \tag{13}$$

where $p,q = 0,1,2,3,....$, but not both $p = q = 0$. For the circular waveguide with radius R,

$$\Lambda_{pq} = \frac{x_{pq}}{R} , \tag{14}$$

where x_{pq} is the qth root of $J_p'(x_{pq}) = 0$. For both waveguides, the cut-off frequency is $\omega_{pq} = c\Lambda_{pq}$. Assuming a circular waveguide with $R = 5$mm, the lowest order mode gives roughly $\Lambda_{01} \approx \pi/R$, and a cut-off frequency $\omega_{01} \approx c\pi/R \approx 30$GHz.

The radiation phase velocity in the waveguide mode is given by $v_\phi = c(1 + c^2\pi^2/2b^2\omega^2 + ...)$ where we take the short waveguide dimension to be

$b = 5$mm. The radiation group velocity is given by $v_g \approx c(1 - c^2\pi^2/2b^2\omega^2 + ...)$. The slippage distance of the field nodes over the electrons is $s \approx (v_p - v_z)L/c$ where $v_z \approx c(1-(1+K^2)/2\gamma^2)$ is the electron z velocity.

Expanding in Λ_{pq} gives the form of the phase velocity $v = v^{(0)} + \Delta v_{pq} + ...$ where $v^{(0)}$ is the old phase velocity definition without waveguide corrections, $v^{(0)} = L[(k_0+\omega/c)\beta_z - \omega/c]$, and Δv_{pq} is the first order waveguide correction in Λ_{pq}. The old, unperturbed resonance condition, $v^{(0)} = 0$ gives the resonant frequency $\omega^* = ck_0/(1-\beta_z) \approx 2\gamma^2 ck_0/(1+K^2)$. A relativistic FEL that is near resonance $\omega \sim \omega^*$ for maximum coupling, has a shift in phase velocities caused by the waveguide,

$$\Delta v_{pq} \approx -\frac{N\lambda_0^2\Lambda_{pq}^2(1+K^2)}{8\pi\gamma^2} \tag{15}$$

where $N = L/\lambda_0$ is the number of undulator periods. The shift in resonance is negative, and diminishes when $\gamma \to \infty$. In a rectangular waveguide,

$$\Delta v_{pq}^R \approx -\frac{\pi N\lambda_0^2(1+K^2)}{3\gamma^2}\left[\frac{p^2}{a^2}+\frac{q^2}{b^2}\right] . \tag{16}$$

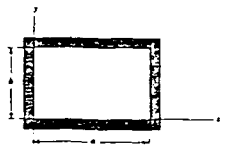

If a circular waveguide is used, the shift is

$$\Delta v_{pq}^C \approx -\frac{N\lambda_0^2(1+K^2)}{8\pi\gamma^2}\left[\frac{x_{pq}}{R}\right]^2 . \tag{17}$$

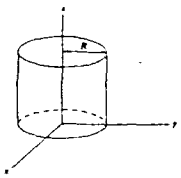

The ELF FEL experiments at LLNL in 1985 provide the first results of an FEL operating in the high-current, high-gain, high-efficiency regime [T. J. Orzechowski, B. Anderson, W. M. Fawley, D. Prosnitz, E. T. Scharlemann, S. Yarema, D. Hopkins, A. C. Paul, A. M. Sessler, and J. Wurtele, Phys. Rev. Lett. **54**, 889 (1985); T. J. Orzechowski, E. T. Scharlemann, B. Anderson, V. K. Neil, W. M. Fawley, D. Prosnitz, S. Yarema, D. Hopkins, A. C. Paul, A. M. Sessler, and J. Wurtele, IEEE J. Quantum Electronics **QE-21**, 831 (1985)]. These experiments used a waveguide because of the long-wavelength of the radiation and the long interaction length. A free radiation field with a mode radius comparable to the radius of the ELF electron beam would have a Rayleigh length of $Z_0 = \pi(2r_e)^2/\lambda \approx 2.4$cm; less than one tenth of the undulator length. Therefore, ELF must use a waveguide to confine the radiation near the electron beam

for further amplification. A rectangular waveguide, 10cm by 3cm, is used with the TE_{01} mode so that the electric field extends along the long dimension of the guide. The undulator field is oriented along the short dimension so that electrons "wiggle" in the long dimension parallel to the radiation electric field.

The phase velocity of the radiation in the mode is given by $v_p \approx c(1+c^2\pi^2/2Y^2\omega^2+....)$ where the short waveguide dimension is $Y = 3$cm. The radiation group velocity is given by $v_g \approx c(1-c^2\pi^2/2Y^2\omega^2+....)$. In ELF, the operating frequency, $\omega = 35$GHz, is far above the cutoff frequency, $\omega_c = c\pi/Y = 5$GHz, so that the phase and group velocities are close to c; $v_p^{ELF} \approx 1.01c$ and $v_g^{ELF} \approx 0.99c$. The slippage of the field nodes over the electrons is $s \approx (v_p - v_z)L/c \approx 0.09L$ where $v_z \approx c(1-(1+K^2)/2\gamma^2)$ is the electron z velocity. For ELF, the slippage distance is then given by $s \approx N\lambda$ as in most FELs. This slippage distance is $s \approx 24$cm, or about 1/12th of the undulator length, and only 1/20th of the electron beam pulse length. In one pass through the amplifier, information is transferred only over this small slippage distance so that sections along the electron and light pulses evolve independently.

The TE_{01} waveguide mode area can be estimated by averaging the field over the waveguide cross section. The effective TE_{01} mode area is roughly given by $A_{01} = 2XY/\pi \approx 19\text{cm}^2$ where $X = 10$cm and $Y = 3$cm. This high gain FEL is amplifying a mode that has $X = 10$cm width using an electron beam of about $r_e \approx 4$mm radius. This mismatch, or "filling factor", $F = \pi r_e^2/A_{01}$, has the small value $F = 0.026$. Since the bunching electron beam only amplifies the light within the electron beam cross section, the small filling factor, or coupling, could be changed as higher order modes are excited during the FEL interaction. In the short direction, the beam-mode mismatch is $r_e = 4$mm compared to $Y = 3$cm, while in the long direction the mismatch is much greater, $r_e = 4$mm compared to $X = 10$cm. After the FEL bunching time plus one or two e-folding distances, the next higher-order symmetric modes in the long dimension could mix with the fundamental TE_{01} to reduce the mode size and increase the filling factor. Therefore, for the later stages of the interaction along the undulator, it could be more appropriate to use a larger filling factor as more representative of the interaction coupling.

6. Gain Spectrum Spikes in FEL Amplifiers

Recently, it has been found that sharp spikes can appear far from resonance in the gain spectrum of high-gain, high-power FEL amplifiers with good beam quality. At the spike, gain is larger than in the rest of the broad, smooth gain spectrum.

The FEL gain spectrum plots gain, G, against a quantity like the laser wavelength, or the electron beam energy. The FEL gain spectra for (i) low gain in weak optical fields, (ii) low gain in strong optical fields, (iii) and high gain in weak optical fields have been understood for some time, and in each case, the curves have simple, smooth shapes. Surprisingly, the next logical case, (iv) high gain in strong optical fields, has not been explored, and is not simple or smooth. The high-gain, strong-field gain spectrum can have sharp spikes located far from resonance superimposed on a simpler, broad and smooth curve. The gain at the peak of a spike can be significantly higher than in the rest of the spectrum.

The figure below shows an example of a gain spectrum for the new case of high gain and strong fields ($j \gg \pi$, $|a| \gg \pi$). The initial field is $|a| = 10$, but the high current density, $j = 3000$, increases the field to saturation $|a| \approx 4(j/2)^{2/3} \approx 500$ near the end of the undulator. Because the FEL reaches saturation, the gain is significantly reduced from the weak-field, high-gain example with the same current. The dimensionless parameters selected here roughly describe the ELF FEL amplifier at LLNL, but with ideal beam quality.

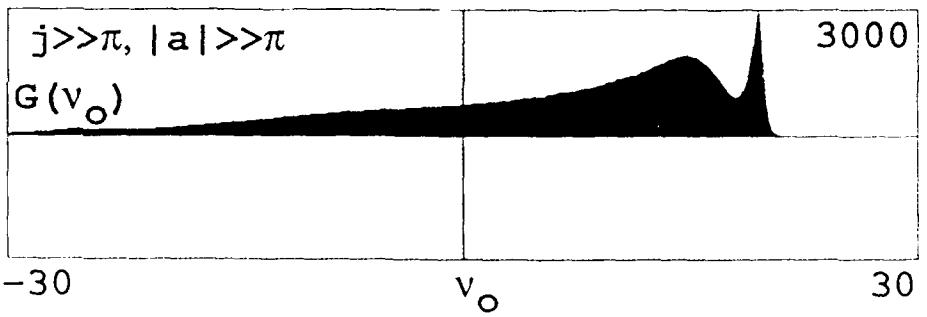

FEL Amplifier Gain Spectrum with a Spike.

The surprising structure in the gain spectrum above is caused by saturation, and the subsequent synchrotron oscillation of trapped electrons. A slight change in v_0 away from the spike causes the saturation peak to occur just beyond, or just before, the end of the undulator.

The existence of gain spectrum spikes means that the maximum gain and efficiency in an FEL amplifier occurs far from resonance over a narrow range of resonance parameters. Any FEL amplifier design would normally seek high beam quality so that high gain could produce saturation in strong fields. The discovery of the sharp resonance for just these conditions means that the benefits of higher beam quality may be underestimated.

The necessary conditions for the gain spectrum spikes are high-gain, saturation, and good beam quality. If the LLNL ELF experiment had 5 times better edge emittance, the spike could have possibility been observed. But, the actual beam emittance "washed out" the spike. The LLNL ELF II or IMP experiments [4] have substantially better beam quality than ELF, and may be able to observe the gain spectrum spikes far from resonance.

7. SPIE Review of FEL Simulations

In this invited review article, the FEL provides a unique physical system for analysis with computer simulations. The only physical constants needed are the electron charge and mass, and the speed of light, in order to accurately represent complex effects such as short optical pulse evolution, high-power saturation, diffraction and optical guiding, electron phase-space evolution, noise, high-gain exponential growth, and high-power multimode instabilities. The theory uses (i) the relativistic Lorentz force for each electron in the combined optical and undulator fields, and (ii) the driven, transverse wave equation for the slowly-varying optical field envelope. Depending on the kind of analysis required, the solution to the resulting equations can be found analytically, solved on a small desk-top computer, or simulated on large main frames. Simulations continue to play an essential role in the design of future FELs as well as in the understanding of current experiments.

The publication reference is W. B. Colson, Proc. SPIE **1045**, 2-9 (1989).

Proc. SPIE **1045**, 2-9 (1989).

Simulations of Free Electron Lasers

W. B. Colson

Berkeley Research Associates, P.O. Box 241, Berkeley, CA 94701

Abstract

Free electron lasers (FELs) provide a unique physical system for analysis with computer simulations. The only physical constants needed are the electron charge and mass, and the speed of light, in order to accurately represent many complex physical effects. Large simulations requiring CRAY computers have successfully supported many large FEL experiments, but most often, the important physical processes can be simulated on small workstations.

Introduction

The free electron laser (FEL) couples the energy in a relativistic electron beam to a co-propagating optical wave with the use of a periodic undulator magnet [1]. In the oscillator configuration, coherent electron bunching develops on each successive pass through the undulator. Over many passes, the optical power stored in the resonator grows to saturation. In the amplifier configuration, coherent electron bunches develop rapidly in the first part of the undulator followed by large growth of the optical field. Due to the simplicity of the fundamental FEL mechanism and experimental conditions, theory and experiment agree over the wide range of parameters explored. Instead of describing a large comprehensive code, a few simple numerical procedures are outlined for small workstations. Two FELs, the oscillator at LANL [2,3,4] and the amplifier at LLNL [5,6,7], are used as examples for simulations that can be performed on small computers.

Electron dynamics in high-efficiency FELs

The Lorentz force equations determine the electron motion in the combined undulator and radiation fields. For the helical undulator, the field is

$$B = B\,(\cos(k_0 z), \sin(k_0 z), 0) \quad , \tag{1}$$

where $\lambda_0 = 2\pi/k_0$ is the undulator period, and B is the peak field strength. The corresponding electric and magnetic components of the radiation fields are

$$\vec{E} = E\ (\cos\psi\ ,\ -\sin\psi\ ,\ 0\ ) \quad , \quad \vec{B} = E\ (\sin\psi\ ,\ \cos\psi\ ,\ 0\ ) \quad , \tag{2}$$

where $\psi = kz - \omega t + \phi$, $\lambda = 2\pi/k = 2\pi c/\omega$ is the optical wavelength, ϕ is the optical phase, and E is the radiation field strength.

The transverse velocity components of an electron in the fields (1) and (2) are found by noting that the right side of the Lorentz force equation is a perfect time derivative over one undulator period where B and E remain substantially constant. The transverse electron velocity, $c\vec{\beta}_\perp$, is

$$\vec{\beta}_\perp = -\frac{K}{\gamma}\ [\ \cos(k_0 z)\ ,\ \sin(k_0 z)\ ,\ 0\ ] + \frac{A}{\gamma}\ [\ \sin\psi\ ,\ \cos\psi\ ,\ 0\ ] \quad , \tag{3}$$

where $K = eB\lambda_0/2\pi mc^2$ is the dimensionless undulator vector potential, $A = eE\lambda/2\pi mc^2$ is the dimensionless optical vector potential, $e = |e|$ is the electron charge magnitude, m is the electron mass, c is the speed of light, and γmc^2 is the electron energy. Typically, $K \approx 1$ in most FELs. The constants of integration have been set equal to zero indicating perfect injection into the undulator; imperfect injection is considered later. Using (3), the electron energy change is

$$\dot{\gamma} = \frac{d\gamma}{dt} = \frac{\omega K A}{\gamma}\ \cos(\zeta+\phi) \quad , \tag{4}$$

where the electron phase is $\zeta = (k+k_0)z - \omega t$, and $\dot{\gamma} = d\gamma/dt$. The combination of $\gamma^{-2} = 1 - \vec{\beta}_\perp^{\,2} - \beta_z^2$ and (3) gives the exact electron phase motion,

$$\ddot{\zeta} = \frac{KA\ (2\omega\omega_0 - 2\omega\dot{\zeta} + \omega_0^2 - \dot{\zeta}^2)\ (2\omega\omega_0 - \omega\dot{\zeta} + \omega_0^2)\cos(\zeta+\phi)}{(\omega+\omega_0)^2\ (1+K^2 - KA\ \sin(\zeta+\phi) + A^2)} \quad , \tag{5}$$

where $\omega_0 = k_0 c$. The bunching mechanism for an initially random beam arizes from the important relation $\ddot{\zeta} \propto \cos(\zeta+\phi)$. In order for bunching to develop, the electrons must be near resonance where $\dot{\zeta} \approx 0$. Near resonance, the FEL frequency is $\omega \approx \beta_z \omega_0/(1-\beta_z)$, and in the relativistic limit $\omega \gg \omega_0$. Furthermore, it can be shown that $A^{max} \sim (N_S/N)^2$ where N_S is the number of synchrotron oscillations of trapped electrons along the undulator length. Typically, $A^{max} \sim 10^{-4}$ so that $K \gg A$ for even the strongest optical fields. In high efficiency FELs where the undulator is altered to maintain resonance with trapped electrons that lose significant energy to the optical wave, the untrapped electrons can drift far off-resonance. Allowing that ζ is far from resonance, but with the restriction $\dot{\zeta} \ll \omega_0$, the electron motion is accurately described by the simpler equation

$$\ddot{\zeta} = (\ 1 - 3\nu/4\pi N\ )\ |a|\ \cos(\ \zeta + \phi\ ) \quad , \tag{6}$$

where $(\overset{\circ}{..}) = d(..)/d\tau$, $\tau = ct/L$ is the interaction time over the undulator ($\tau = 0 \rightarrow 1$), $\nu = \overset{\circ}{\zeta}$ is the electron phase velocity, and $|a| = (4\pi N)^2 KA/(1+K^2)$ is the dimensionless optical field amplitude.

In this formulation, electrons trapped near resonance, $\nu \approx 0$, are described accurately, while untrapped electrons far from resonance, $\nu \rightarrow 4\pi N$, are handled less accurately. However, the untrapped electrons are expendable since they become randomly spread in phase as well as uncoupled from the bunching interaction, as can be seen in (6). For electrons near resonance, the bunching rate is determined by the field strength $|a|$. When $|a| \ll \pi$, the optical field is considered weak, and bunching is imperceptible. When $|a| \gg \pi$, the electrons bunch rapidly, and become trapped in closed phase-space orbits. In strong fields, $|a| \geq 4\pi^2$, the trapped electrons oscillate at the dimensionless synchrotron frequency $\nu_S \approx |a|^{1/2}$, and there are $N_S \approx \nu_S/2\pi$ oscillations in time $\Delta\tau = 1$. Integration of (6) can be accomplished numerically on a small computer, or analytically in some specific cases. Because (6) is slowly varying, numerical τ-steps can jump over several undulator periods. When $N \gg 1$, so that the FEL efficiency is not too large, (6) simplifies even further to take the form of the pendulum equation.

The wave equation in high-efficiency FELs

In order to have a self-consistent theory, the complex, time-varying field envelope, $(E(t), \phi(t))$, is allowed to vary slowly over an optical period ($\dot{E} \ll \omega E$, $\dot{\phi} \ll \pi\omega$). The transverse beam current, $\vec{J}_\perp$, is the sum of all single particle currents, but an average over sample particles, <..>, can be used if weighted by the electron density ρ. The current is then $\vec{J}_\perp = -ec\rho < \vec{\beta}_\perp >$, and the slowly-varying wave equation can be written as

$$\frac{d(Ee^{i\phi})}{dt} = -2\pi ecK\rho < (e^{-i\zeta}/\gamma) > \quad . \tag{7}$$

From the electron dynamics, the dynamic Lorentz factor is given by $\gamma^{-1} \approx (1 - \nu/4\pi N)\,\gamma_0^{-1}$ with the static, resonant Lorentz factor $\gamma_0 = (\omega(1+K^2)/2\omega_0)^{1/2}$. Then, in terms of the electron phase and phase velocity, the wave equation becomes

$$\overset{\circ}{a} = -j < (1 - \nu/4\pi N)\, e^{-i\zeta} > \quad , \tag{8}$$

where the complex dimensionless field is $a = |a| e^{i\phi}$, and the dimensionless current density is

$$j = 8N(e\pi KL)^2 \rho / \gamma_0^3 mc^2 \quad . \tag{9}$$

The current j determines the coupling between the electron beam and the optical wave, and is the most important dimensionless variable describing an FEL. Without current ($j = 0$), or with no bunching ($<...> = 0$), there is no change in the initial optical field.

$a(0) = a_0$. When $j \leq 1$, the FEL gain is low, and when $j \gg 1$ the FEL gain is high. The combined equations, (6) for each sample electron and (8) for the light wave, are valid for weak fields ($|a| \leq \pi$), strong fields ($|a| \gg \pi$), low gain ($j \leq \pi$), high gain ($j \gg \pi$), low efficiency ($<\Delta v> \ll 2\pi N$), and high efficiency ($<\Delta v> \approx 2\pi N$). A practical correction that can be included, $j \rightarrow jF$, is the "filling factor", F ="area of the electron beam"/"area of the optical mode", describing optical mode coupling [8].

Initial conditions

Integration of (6) and (8) starts with an initial value for each ζ and v sampled in the beam, and the field a_0. A large number of electrons enter the undulator randomly spread in phase, $\zeta(0)$. To represent the "fluid" beam, a smaller number of sample electrons are uniformly spread, but with a small additional random phase $\delta\zeta$ to characterize shot noise. If the spread in the initial phase velocities is narrow compared to the gain spectrum bandwidth, the electron beam can be considered perfect and represented by a single value, v_0. In strong optical fields, the FEL interaction induces a large phase-velocity spread that can make an initial spread negligible. But, when the phase-velocity spread exceeds the gain spectrum bandwidth and the optical fields are weak, the distribution of phase velocities, $f(v)$, becomes important and can reduce the FEL performance by degrading bunching. The random spread is determined by a combination of the beam's energy spectrum and emittance, and several types of distribution function shapes can occur. An example is the "exponential" distribution [9] that results from an emittance dominated beam with no external focusing in the undulator,

$$f_\theta(v) = \exp[(v - v_0)/\sigma_\theta]\sigma_\theta^{-1} \quad \text{for} \quad v \leq v_0 \quad , \quad f_\theta(v) = 0 \quad \text{for} \quad v > v_0 \quad . \tag{10}$$

A symmetric radial spread gives the asymmetric exponential distribution where $\sigma_\theta = 4\pi N \gamma^2 \bar{\theta}^2/(1+K^2)$ and $\bar{\theta}$ is the rms angle away from the z axis. A beam with matched contributions from a spread in radial positions, $\bar{r}$, and angles, $\gamma\bar{\theta} = Kk_0\bar{r}$, also gives the exponential distribution.

A difficult case for simulations is the combination of poor beam quality, $\sigma_\theta \geq \pi$, and large current. As the phase-space area occupied by the beam increases, the shot noise contribution from the relatively few sample electrons can cause significant field growth, and large values of j emphasize the error. Poor quality beams must use more sample electrons for accurate results.

Single-mode phase-space simulations

Probably the most useful tool for understanding FEL physics is the single-mode phase-space simulation [10]. Many of the features calculated in more complete

multimode simulations can be seen in this simpler, faster case. As an example of an FEL interaction with poor beam quality, high current, and strong fields, figure 1 shows the final (ζ,v) phase space distribution of a beam with an initial spread of $\sigma_\theta = 3\pi$ in an exponential distribution. The electron beam current is $j = 10^3$ in an initial optical field of $a_0 = 4\pi$. The initial phase velocity, or resonance condition, is at the value $v_0 = 4\pi$ for nearly optimum gain under these conditions. The sharp edge along the top of the distribution results from the sharp edge in the initial exponential distribution at v_0. With a perfect beam and in weak fields, the gain, $G(\tau) = |a(\tau)|^2/a_0^2 - 1$, for this current would be exponential in τ and would reach $G \approx 10^5$, but poor beam quality and strong fields have reduced the final gain to $G \approx 70$. The slight oscillation in the growth rate near $\tau \approx 0.5$ is caused by the shape of the exponential distribution. The reduction of the growth rate near $\tau \approx 1$ is caused by strong field saturation. The optical phase shift, $\Delta\phi \approx \pi/2$, is significant to the interaction.

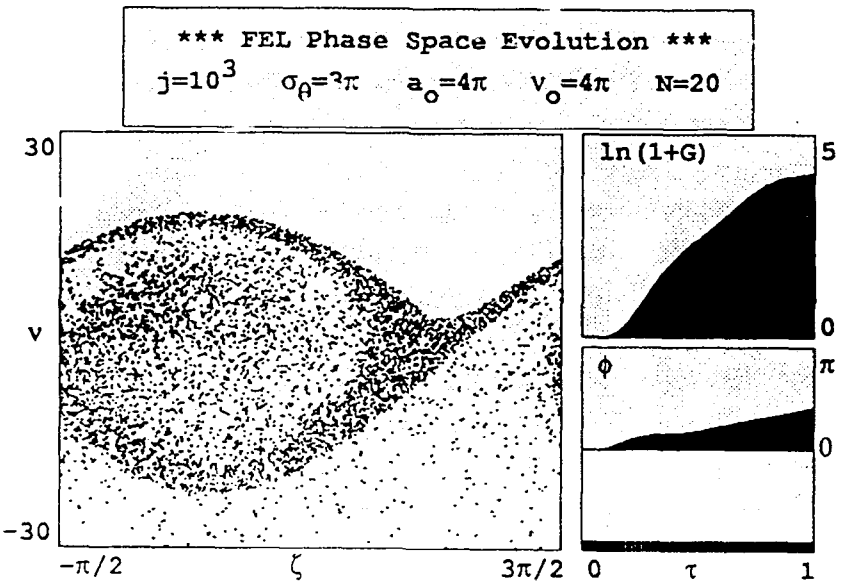

Figure 1. A single-mode phase-space simulation.

Strong fields are identified by "over-bunching", when some electrons over-take others complicating and diminishing coherent bunching. Because the field is strong in figure 1, bunching is clear despite the large initial spread in phase velocity. Electrons are trapped and have rotated by about one synchrotron oscillation around the stable fixed-point $\zeta = \pi/2 - \phi$.

LANL FEL oscillator simulations

In some FELs, a single mode analysis is inadequate. An important example is the LANL FEL oscillator that first demonstrated the effects of the trapped-particle instability [11-15]. To generalize the previous equations to follow multiple modes, we follow multiple field sites along the complex wave envelope $a(z)$ and the electron beam. The extension to spatial modes, $a \rightarrow a(z)$, is completely equivalent to an extension in longitudinal wavenumbers, $a \rightarrow a(k)$. All longitudinal distances are normalized to the slippage distance, $z/N\lambda \rightarrow z$, so that $a \rightarrow a_z$, $\nu \rightarrow \nu_{z-\tau}$, $\zeta \rightarrow \zeta_{z-\tau}$, and $j \rightarrow j_{z-\tau}$. The light, traveling at speed c, remains fixed in z while the slower electrons slip back by $z-\tau$ at time τ. The mode spacing is $\Delta\nu = 2\pi/W$ where W is the number of slippage distances used in the simulation. The site spacing Δz can be made equal to the integration time step $\Delta\tau$, so that electrons slip back one site in the calculational window for each time step.

The LANL FEL is driven by short electron pulses from an RF accelerator. The electron pulse has a length, $\sigma_z = 10$, that is 10 slippage distances long, with a shape of the form $j(z) = j(1-2z^2/\sigma_z^2)$ for $j(z) > 0$, and zero otherwise; the peak current is $j = 10$. In figure 2, the current density, $j(z-\tau)$ (lower-left), is shown at $\tau = 0$ (dark grey), and at $\tau = 1$ (light grey) after slipping back by $\Delta z = 1$ in the window of width $W = 16$. During the simulation, a new electron pulse is injected into the undulator with $N = 37$ periods at the resonant phase velocity, $\nu_0 = 0$. The electrons are uniformly spread with a small random phase $\delta\zeta = 10^{-4}$. The emittance in the experiment is large enough to reduce weak-field gain, and j has been decreased to reflect that degradation. But, the strong-field features of the simulation are not significantly altered by the beam quality, and no spread in ν is included. The shot noise contributions start a small amplitude optical pulse at peak gain. The single-mode gain spectrum, $G(\nu)$ (lower-center), is shown for reference. In the experiment, the rebounding optical pulse is approximately synchronized to arrive at the beginning of the undulator coincident with the series of electron pulses from the RF accelerator [16-18]. The amount of desynchronism, $d = 10^{-3}$ here, is the displacement between the electron and optical pulses at $\tau = 0$ each pass; d is normalized to the slippage distance. The resonator losses are determined by $Q = 20$, so that without gain the optical power would decay as $\propto \exp(-n/Q)$ over n passes. The optical pulse amplitude, $|a(z,n)|$ (left-middle), evolves for $n = 640$ passes until a dynamic steady-state is achieved. The final optical pulse shape, $|a(z)|$ (top-left), shows a spiked structure as a result of the trapped-particle instability. The grey scale above shows the peak field $|a(z,n)| = 210$ in white, and zero field in black with one contour.

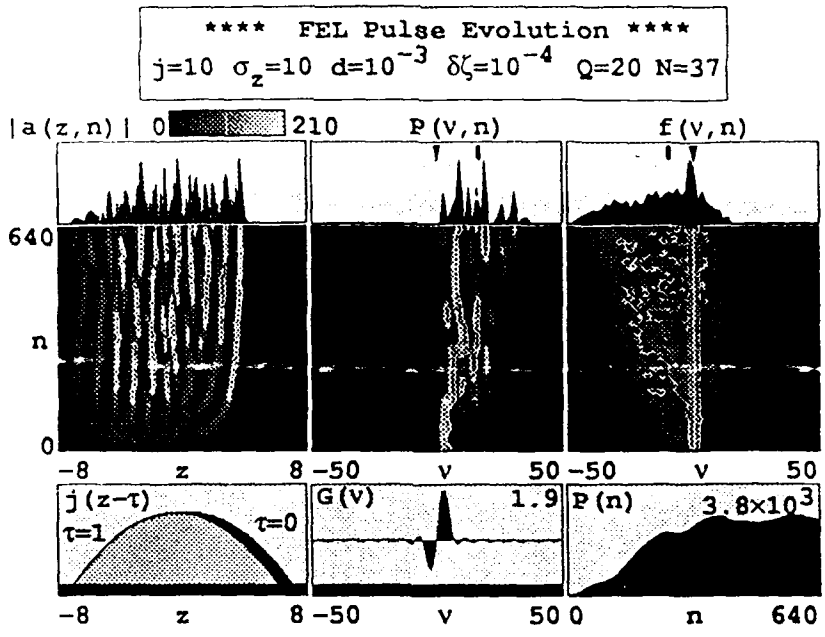

Figure 2. Full pulse simulation of the LANL FEL oscillator.

The instability starts with the motion of trapped electrons in phase-space. As substantial current is trapped by a strong optical field, and oscillates at frequency $\nu_S \approx |a|^{1/2}$, the wave equation can drive multiple sideband frequencies around the fundamental at $\nu_0 \pm \nu_S$. The field strength required to cause one synchrotron oscillation is $|a| \approx 4\pi^2 \approx 40$. In stronger fields, the sidebands can mix further causing a chaotic pulse shape and corresponding chaotic spectrum, as can be seen in figure 2.

The average power per site, $I(n) = \overline{|a(z)|}^2$ (lower-right), has increased from noise to strong-field saturation. The complicated optical pulse shape gives the multimode power spectrum, $P(\nu, n)$ (middle-center) with several sidebands covering a spectral width $\Delta\nu = 8\pi$. The strong fields broaden the electron spectrum, $f(\nu, n)$ (middle-right), and extract energy from the beam. The final pulse shape, power spectrum (top-center), and electron spectrum (top-right) show the final chaotic state of the FEL operation. The details of the result cannot be reproduced when there are slight changes to the initial conditions, so that the agreement between theory and experiment should be confined to their overall features. An important feature in the LANL FEL is the broad, $\Delta\lambda/\lambda = \Delta\nu/2\pi N = 10\%$, optical spectrum caused by the trapped-particle instability [2,3,4].

Periodic "wrapped" windows

When the electron pulse and optical pulse are long compared to the slippage distance, as in the LANL FEL, periodic boundary conditions can be imposed at the ends

of the window W in order to restrict the number of modes and sites followed [13-15]. The end effects of the periodic boundary conditions are considered non-physical and inconsequential. Figure 3 shows the results of the same simulation as in figure 2, but with periodic boundary conditions applied to a smaller window of width $W = 4$. The simulation in figure 2 required 4h running time while that of figure 3 required only 1h. The detailed spectra and evolutions are different because a different number of modes are sampled, but the most useful overall features are the same.

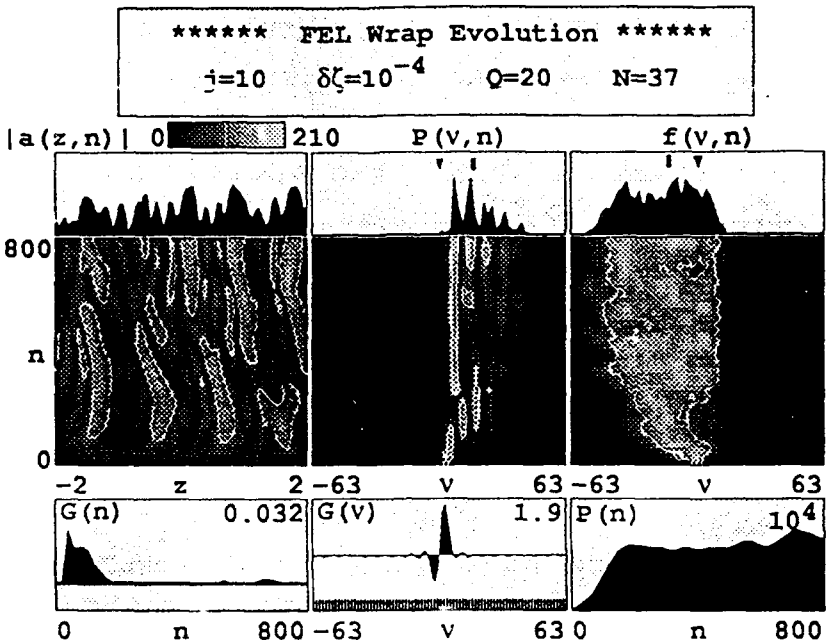

Figure 3. Wrapped-window simulation of the LANL FEL oscillator.

The simulation in figure 3 is intended to represent a small section from the middle of the long pulse in figure 2. The current $j = 10$ is uniform in z, and the variables σ_z and d do not enter the long-pulse problem, but otherwise the simulation in figure 3 is run in the same way as figure 2. The shot noise, $\delta\zeta = 10^{-4}$, is now essential, since without some source of noise, every site z would evolve identically, and no spectral features could develop. However, the resulting steady-state solution is insensitive to the details of the noise source. The chaotic pulse shape, power spectrum, and power evolution $P(n)$ all have features similar to figure 2. The peak field strength, $|a| = 210$, found in spikes is the same for both simulations. The large peak seen in the electron spectrum, $f(\nu, n)$, of figure 2, but not in figure 3, is caused by electrons near the front of the electron pulse that do not interact with significant optical fields.

LLNL FEL amplifier simulations

In the FEL amplifier, a coherent input signal, sufficiently far above the noise level, determines the longitudinal frequency of the optical mode. While longitudinal multimode

operation may become important to some amplifier applications, it is generally less critical than in the FEL oscillator. In a long undulator with high current, there can be significant distortion of the transverse optical mode caused by natural diffraction and the FEL interaction.

A coherent, freely-propagating optical wave of area πw_0^2 will spread due to natural diffraction over the undulator length L. The dimensionless Rayleigh range, $z_0 = \pi w_0^2 / L\lambda$, compares the characteristic spreading distance to the undulator length, and should be near unity to justify ignoring diffraction effects. If z_0 is too large or too small, the FEL coupling can be significantly reduced. A low energy, long wavelength FEL tends to have a small Rayleigh range, z_0, in a long undulator. The mode waist, w_0, cannot be increased arbitrarily to compensate, because of the off-axis undulator fields. Therefore, an FEL design requires

$$\gamma \geq KN/2 \tag{11}$$

so that natural diffraction does not significantly decrease the interaction strength. In the LLNL ELF experiment [19], $\gamma \approx 7$, $K = 2.5$ and $N = 30$ so that the electron beam's Lorentz factor did not satisfy (11) and a waveguide was used. The waveguide alters the propagation speed of the light wave, and the FEL resonance condition. For the LLNL ELF experiment where $\lambda_0 \approx 10$cm and the smallest rectangular waveguide dimension is 3cm, the waveguide shift is $\Delta\nu_{01}^{ELF} \approx -6\pi$ for the lowest-order mode. This shift is observable, but not detrimental to maximum gain. In a single waveguide mode, the cross-section of the mode can be used in the filling factor, F, to estimate coupling to the mode. The electron beam size should be close to, but smaller than, the radiation cross-section for best coupling.

An example of transverse mode distortion in free space is "optical guiding". In the case of large current, $j \gg 1$, the transverse optical mode can be continuously distorted by the electron beam, because of the large optical phase shift associated with the high-current regime. This is an important practical advantage for the high-gain amplifier configuration where natural diffraction would provide a limitation to a long undulator length. When the FEL has large enough current for optical guiding to persist, the FEL interaction must continually compensate for the phase shift associated with free-space diffraction at each step $\Delta\tau$. The critical current density needed for optical guiding,

$$j_G \approx 32\, z_0^{-3} \tag{12}$$

In the LLNL ELF experiment, the electron beam is small enough so that a light wave with a small Rayleigh length, $z_0 \approx 0.1$, could be matched to the beam at the beginning of the undulator. The current density needed for effective guiding would have to exceed $j_G \approx 3.2 \cdot 10^4$. But, the ELF experiment is described by $j \approx 2.5 \cdot 10^4$, and significant

guiding is not possible.

In both the longitudinal and transverse directions, the ELF amplifier tends to work in a single mode, so that the simpler, phase-space simulation may capture the most important features of the experiment. Equations (6) and (8) are valid for high j, high power, and high efficiency as needed to describe the FEL. The fundamental gain mechanism is still electron bunching, but the interaction is collective since all electrons interact through the rapidly growing optical wave. In weak fields, the gain is $G(\tau) = \exp[(j/2)^{1/3}\sqrt{3}\tau]/9$, after a bunching time $\tau_B \approx (2/j)^{1/3}$. During the bunching time, $\tau_B^{ELF} \approx 0.05$, there is no significant gain, but final gain, $G \geq 10^{16}$, is enormous. The weak-field optical phase shift, $\phi(\tau) = (j/2)^{1/3}\tau/2$, can be as much as $\geq 3.5\pi$ for ELF, and is a significant feature of the high-current regime. The weak-field gain spectrum bandwidth is wider than in the low-current regime. If the gain bandwidth is defined by the range of phase velocities over which the gain is reduced by 1/e, then we have $\Delta\nu_0 \approx 4j^{1/6}$. If the gain bandwidth is identified by the range of phase velocities over which the exponential growth rate is reduced by 10%; then we have $\Delta\nu_0 \approx 2\tau_B^{-1} \approx 2j^{1/3}$. For ELF, $\Delta\nu_0 \approx 2j^{1/3} \approx 20\pi$.

Saturation in the high-current regime is caused by the over-bunching of trapped electrons in strong optical fields just as in the low-current case, but at a different field strength. Equation (6) shows that at $a_j \approx 2(j/2)^{2/3}$, the electron phases can be shifted by as much as $\Delta\zeta \approx \pi$ causing the onset of saturation. For $j^{ELF} \approx 2.5\times10^4$, the saturation field, $a_j^{ELF} \approx 350\pi$, can be significantly larger than for the low current case, as has been observed. The natural efficiency in the high current limit is $\eta_j \approx (j/2)^{1/3}/4\pi N$. For ELF with $N = 30$, the natural efficiency is $\eta_j \approx 0.06$. In the high-current, strong-field regime, about half the electrons are bunched near $\zeta \approx \pi/2-\phi$ so that the optical phase evolves as $\dot{\phi} \approx j/a_j$, or $\phi \approx (j/2)^{1/3}\tau/2$ again. Remarkably, the optical phase evolution in the high current regime is roughly the same in both strong and weak optical fields.

Figure 4 shows a simulation of the ELF FEL with high current $j = 2.5\times10^4$, an initial field of $a_0 = 20$, and $N = 30$ undulator periods. The initial electron phases are uniformly spread, but the phase velocities are distributed according to the exponential distribution function in (10) with $\sigma_\theta = 15$. The distribution peak is located at $\nu_0 = 30$ for highest efficiency. Ten thousand sample electrons are shown in their final phase space (ζ,ν) orientation. The bunching and trapping of the beam inside the closed-orbit area are clear. The electron bunch has rotated several times around the stable fixed-point $\zeta^* = \pi/2-\phi(\tau)$, while the optical phase has shifted ζ^* through $\approx 2\pi$. The positions of the electrons indicate the outline of the closed-orbits that have trapped most of the beam. The weak field growth-rate is reduced by $\approx 20\%$ by the large random spread σ_θ. Gain in the first third of the undulator is $G \approx 3\times10^3$, or $G(\text{dB}) = 10\log(G-1) \approx 35\text{dB}$. The peak power at saturation, $a_j^2 \approx 4(j/2)^{4/3} \approx 10^6$, is predicted accurately, and shows the

synchrotron frequency $\nu_S \approx a_j^{1/2} \approx 10\pi$ in the oscillations of $\ln(P(\tau)/P_0)$. The efficiency is 5% in good agreement with the analytical estimate above. The optical phase, $\phi(\tau)$, shifts at about half the predicted rate because of beam quality.

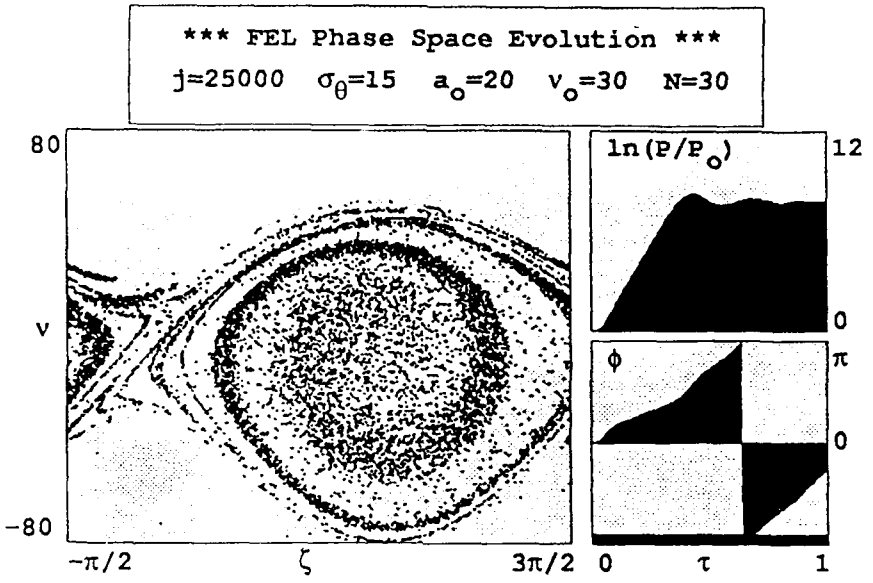

Figure 4. The single-mode phase simulation of LLNL ELF amplifier.

The tapered undulator design [20,21] can increase power beyond the saturation limit seen in figure 4. At normal saturation, the electrons lose energy and drop out of the gain spectrum bandwidth. But, resonance can be maintained by decreasing, or "tapering", the undulator wavelength λ_0 along z, or the undulator field strength B along z, or both. In weak optical fields, the electron's equation of motion in the tapered undulator is of the form $\nu = \delta\tau + \ldots$ where δ is the artificial acceleration. The electron equation can include an additional constant torque due to δ on the right side of (6) as a representation of the effect of tapering. In a sufficiently strong optical field, $|a| > \delta$, some electrons can be "trapped" in the closed orbits of the pendulum phase space centered near the stable fixed-point $\zeta^* \approx \cos^{-1}(-\delta/|a|) - \phi$. In stronger fields, a large fraction of the electrons can be trapped and continue to lose energy to the optical field. If 50% of the electrons are trapped, the efficiency is estimated at $\eta \approx \delta/8\pi N$.

Figure 5 shows the single-mode simulation of the tapered high-current ELF FEL. The current is $j = 2.5\times10^4$, initial field is $a_0 = 20$, $\sigma_\theta = 15$, and $N = 30$ as in figure 4. The exponential electron distribution is position at resonance, $\nu_0 = 0$, for maximum efficiency in this case. The phase acceleration, $\delta = 100\pi$, is applied when the optical field strength is near saturation, $|a(\tau)| = a_j/5$, at $\tau = 0.2$. Approximately half of the ten thousand sample electrons are untrapped, and have been accelerated to $\Delta\nu \approx \delta$ during the

interaction. The electrons near resonance are bunched and continue to drive the wave after being trapped by strong the field. The final phase space positions outline the closed-orbit region, and show how electrons "leak" out of the right side near the unstable fixed-point. The final power $P \approx 6\times10^6$, and efficiency $\eta \approx 30\%$, are 6 times greater than in the untapered FEL in figure 4. Several synchrotron oscillations caused by the trapped electrons can be seen in $P(\tau)$. The optical phase, $\phi(\tau)$, changes at a different rate when tapering begins.

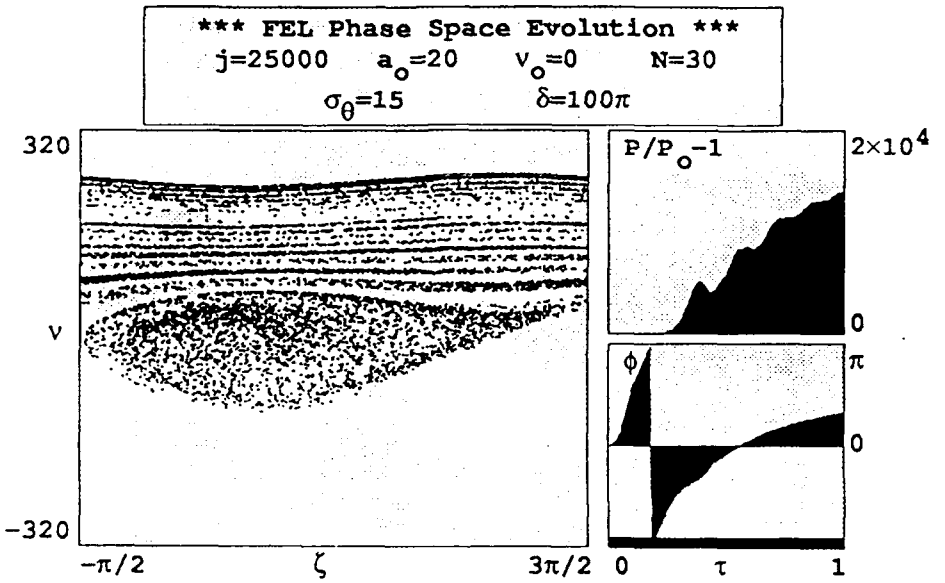

Figure 5. The single-mode phase simulation of LLNL ELF tapered amplifier.

The main features of these simple simulations are seen in the LLNL ELF experiments. Like many FELs that work well, their operation is simple and can be successfully simulated on small computers. The phase-space simulations in figures 4 and 5 took only 16m running time, but could be run accurately in 2m with fewer particles.

Acknowledgments

The author is grateful for support of this work by the Naval Research Laboratory, and the U. S. Office of Naval Research.

References

[1] J. M. J. Madey, J. Appl. Phys. **42**, 1906 (1971); J. M. J. Madey, *Stimulated Emission of Radiation in Periodically Deflected Electron Beam*, U.S. Patent 3,822,410 (1974).

[2] B. E. Newnam, R. W. Warren, R. L. Sheffield, J. C. Goldstein, and C. A. Brau, Nucl. Instr. & Methods in Phys. Res. **A237**, 187 (1985).

[3] J. C. Goldstein, B. E. Newnam, R. W. Warren, and R. L. Sheffield, Nucl. Instr. & Meth. in Phys. Res. **A250**, 4, (1986).

[4] R. W. Warren, D. W. Feldman, B. E. Newnam, S. C. Bender, W. E. Stein, A. H. Lumpkin, R. A. Lohsen, J. C. Goldstein, B. D. McVey, and K. C. D. Chan, Nucl. Instr. & Methods in Phys. Res. **A259**, 8 (1987).

[5] T. J. Orzechowski, B. R. Anderson, W. M. Fawley, D. Prosnitz, E. T. Scharlemann, S. M. Yarema, A. M. Sessler, D. B. Hopkins, A. C. Paul, and J. S. Wurtele, Nucl. Instr. & Methods in Phys. Res. **A250**, 144 (1986).

[6] E. T. Scharlemann, W. M. Fawley, B. R. Anderson, and T. J. Orzechowski, Nucl. Inst. & Meth. in Phys. Res. **A250**, 150 (1986).

[7] T. J. Orzechowski, B. R. Anderson, J. C. Clark, W. M. Fawley, A. C. Paul, D. Prosnitz, E. T. Scharlemann, and S. M. Yarema, Phys. Rev. Lett., **57**, 2172 (1986).

[8] W. B. Colson, *Free Electron Lasers: Critical Review of Technology*, Proc. SPIE **738**, 2-27 (1988).

[9] W. B. Colson and J. Blau, Nucl. Instr. & Methods in Phys. Res. **A259**, 198 (1987).

[10] W. B. Colson, Phys. Lett. **64A**, 190 (1977).

[11] N. M. Kroll, P. L. Morton, and M. N. Rosenbluth, *Physics of Quantum Electronics*, Vol. 7, 89 (1980).

[12] N. M. Kroll, P. L. Morton, and M. N. Rosenbluth, Journal of Quantum Electronics **QE-17**, 1436 (1981).

[13] W. B. Colson and Roger A. Freedman, Optics Communication **46**, 37 (1983).

[14] Roger A. Freedman and W. B. Colson, Optics Communication **52**, 409 (1985).

[15] W. B. Colson, *Free Electron Generators of Coherent Radiation*, SPIE **453**, 289, eds. Brau, Jacobs, Scully (1984).

[16] F. A. Hopf, T. G. Kuper, G. T. Moore and M. O. Scully, *Physics of Quantum Electronics*, Vol. 7, 31 (Addison-Wesley, 1980).

[17] N. Al-Abawi, G.T. Moore and M.O. Scully, Phys. Rev. **A24**, 3143 (1981).

[18] W. B. Colson and A. Renieri, Journal de Physique, Colloque **C1-44**, 11 (1983).

[19] J. S. Wurtele, E. T. Scharlemann and A. M. Sessler, Nucl. Instr. & Methods in Phys. Res. **A250**, 176 (1986).

[20] P. Sprangle, C. Tang, and W. Manheimer, Phys. Rev. Lett., **43**, 1932 (1979).

[21] N. M. Kroll and M. N. Rosenbluth, *Physics of Quantum Electronics*, Vol. 7, 147 (1980).

8. The FEL Integral Equation Derivation

The Paladin experiment with 5 m or 15 m undulator length is described by $j_{5m} = 50$ or $j_{15m} = 1200$. In both cases $j \gg \pi$ and the FEL is in the high-current regime. But in both cases, the electron beam quality leads to gain degradation so that the FEL distribution function becomes important. The integration of the self-consistent FEL equations is valid for any initial electron distribution, but simulations become awkward when the distribution is broad in ν. There can be large sources of error due to artificial shot noise when the number of particles included in the simulation is too small. With a moderate current j and moderately broad spread in $f(\nu)$, there can be as much as 100% error in the calculated gain. The integral equation was developed as a better approach to studying the effects of beam quality. Reference to individual electrons does not occur in the integral equation so that broad distribution functions can be treated and examined without the numerical problems of artificial shot noise. The gain degradation due to beam quality is most important when the optical fields are weak, so that the FEL integral equation can be a useful tool. The derivation of the integral equation is presented here. Some of the simple properties of the integral equation are presented.

The FEL equations (6) and (9) can be simplified for the case of weak fields, and no taper, $\delta = 0$. In weak fields, there would normally be low efficiency so that the factor $\propto \nu/4\pi N$ are negligible compared to unity, and the equations return to their form for low efficiency FELs. For weak optical fields, $|a| \ll \pi$, the electron phase can be expanded in powers of the field, $\zeta = \zeta_0 + \nu_0\tau + \zeta^{(1)} + \ldots$ where the initial electron phase is ζ_0 and the initial electron phase velocity is ν_0. The result to lowest order is

$$\overset{\circ\circ}{\zeta}{}^{(1)} = |a| \cos(\zeta^{(0)} + \phi) = |a| \cos(\zeta_0 + \nu_0\tau + \phi) \qquad (18)$$

$$\dot{a} = -j < e^{-i(\zeta_0+\nu_0\tau+\zeta^{(1)})} > = -j < e^{-i(\zeta_0+\nu_0\tau)}(1 - i\zeta^{(1)}) > = ij < e^{-i(\zeta_0+\nu_0\tau)}\zeta^{(1)} > \quad .$$

The phase average over all the random initial electron phases, $< e^{-i\zeta_0} > = 0$, has been used. Expressed as integrals in complex form, the equations can be solved as

$$\zeta^{(1)}(\tau') = \int_0^{\tau'} d\tau'' \int_0^{\tau''} \frac{d\tau'''}{2} \left\{ a(\tau''') e^{i(\zeta_0+\nu_0\tau''')} + a^*(\tau''') e^{-i(\zeta_0+\nu_0\tau''')} \right\} \quad , \qquad (19)$$

$$a(\tau) = a_0 + ij \int_0^{\tau} d\tau' < e^{-i(\zeta_0+\nu_0\tau')} \zeta^{(1)}(\tau') > \quad ,$$

where the initial field is $a(0) = a_0$ with $\phi(0) = 0$. Substituting the change in the electron

phase $\zeta^{(1)}$ into the wave equation gives the integral equation

$$a(\tau) = a_0 + \frac{ij}{2}\int_0^\tau d\tau' \int_0^{\tau'} d\tau'' \int_0^{\tau''} d\tau''' < e^{-i(\zeta_0+v_0\tau')} e^{i(\zeta_0+v_0\tau'')} a(\tau'') + e^{-i(\zeta_0+v_0\tau')}\, e^{-i(\zeta_0+v_0\tau'')}\, a^*(\tau''') > \quad (20)$$

Use $< e^{-i\zeta_0}\, e^{\zeta_0} >_{\zeta_0} = 1$ and $< e^{-2i\zeta_0} >_{\zeta_0} = 0$ to get

$$a(\tau) = a_0 + \frac{ij}{2}\int_0^\tau d\tau' \int_0^{\tau'} d\tau'' \int_0^{\tau''} d\tau''' < e^{iv_0(\tau''' - \tau')}\, a(\tau''') >_{v_0} \quad , \quad (21)$$

where $<..>_{v_0}$ is a possible average over a v_0-distribution.

To begin examining the integral equation, consider a perfect beam with no v_0-distribution, and at resonance $v_0 = 0$. The leaves the case of either high or low gain at resonance with a perfect beam. The integral equation becomes

$$a(\tau) = a_0 + \frac{ij}{2}\int_0^\tau d\tau' \int_0^{\tau'} d\tau'' \int_0^{\tau''} d\tau'''\, a(\tau''') \quad , \quad (22)$$

and determines the evolution of the complex field $a(\tau)$ in terms of the dimensionless current density j. By taking successive derivatives, the integral equation can be written as a differential equation,

$$\overset{\circ\circ\circ}{a}(\tau) = \frac{ij}{2}\, a(\tau) \quad . \quad (23)$$

Using the form $a = a_0 e^{\alpha\tau}$, the differential equation has the form, $\alpha^3 = ij/2$. The roots of this cubic equation are

$$\alpha_n = (j/2)^{1/3}\, e^{i\pi(4n-3)/6} \qquad n = 1,2,3 \quad \text{roots} \quad . \quad (24)$$

The specific roots give the complex growth rates

$$\alpha_1 = (j/2)^{1/3}\, e^{i\pi/6} \quad , \quad \alpha_2 = -(j/2)^{1/3}\, e^{-i\pi/6} \quad , \quad \alpha_3 = -i(j/2)^{1/3} \quad . \quad (25)$$

The general field is described by

$$a(\tau) = \sum_{n=1}^{3} a_n\, e^{\alpha_n \tau} \quad , \quad (26)$$

where we know the initial field values

$$a(0) = a_0 = |a_0| \quad , \quad \overset{\circ}{a}(0) = 0 \quad , \quad \overset{\circ\circ}{a}(0) = 0 \quad . \quad (27)$$

Substituting the general field into the initial field values, gives the three equations,

$$a_1 + a_2 + a_3 = a_0 \quad , \quad \alpha_1 a_1 + \alpha_2 a_2 + \alpha_3 a_3 = 0 \quad , \quad \alpha_1^2 a_1 + \alpha_2^2 a_2 + \alpha_3^2 a_3 = 0 \quad . \quad (28)$$

Solving for the fields gives

$$a_1 = \frac{\alpha_2\alpha_3 a_0}{(\alpha_1-\alpha_2)(\alpha_1-\alpha_3)} \quad , \quad a_2 = \frac{\alpha_1\alpha_3 a_0}{(\alpha_2-\alpha_1)(\alpha_2-\alpha_3)} \quad , \quad a_3 = \frac{\alpha_1\alpha_2 a_0}{(\alpha_3-\alpha_1)(\alpha_3-\alpha_2)} \quad . \tag{29}$$

Using the complex growth rates gives $a_1 = a_2 = a_3 = a_0/3$, and the complex field evolution is

$$a(\tau) = \frac{a_0}{3}\left[\, e^{(j/2)^{1/3}(i+\sqrt{3})\tau/2} + e^{(j/2)^{1/3}(i-\sqrt{3})\tau/2} + e^{-i(j/2)^{1/3}\tau} \right] \quad . \tag{30}$$

If the current is large $j \gg \pi$, and the gain is high, the field grows exponentially,

$$a(\tau) \approx \frac{a_0}{3}\, e^{(j/2)^{1/3}\sqrt{3}\tau/2}\, e^{i(j/2)^{1/3}\tau/2} \quad . \tag{31}$$

The amplitude and phase of the field evolve as

$$|a(\tau)| = \frac{a_0}{3}\, e^{(j/2)^{1/3}\sqrt{3}\tau/2} \quad , \quad \phi(\tau) = (j/2)^{1/3}\tau/2 \quad . \tag{32}$$

Note that if the single exponential root was used alone with the initial condition $a(0) = a_0$, the resulting field would be incorrect. The initial field divides the field into three solutions at $\tau \ll 1$ regardless of high or low gain. When there is high gain, the fast growing root emerges but has only 1/3 the initial field strength.

If $\tau \ll 1$ near the beginning of the undulator, the field can be expanded to show that

$$a(\tau) \approx a_0\,(\,1 + ij\tau^3/12 + ...) \quad . \tag{33}$$

There is no change in the field until some bunching occurs. The bunching time is $\tau_B = 2/j^{1/3}$.

The FEL gain is defined as $G = (|a|^2 - a_0^2)/a_0^2$. Substituting the field into the gain expression, the gain is

$$G(\tau) = 1 + \frac{1}{9}\left[e^{r\sqrt{3}\tau} + 1 + e^{r(3i+\sqrt{3})\tau/2} + 1 + e^{-r\sqrt{3}\tau} + e^{r(3i-\sqrt{3})\tau/2} + e^{r(-3i+\sqrt{3})\tau/2} + e^{r(-3i-\sqrt{3})\tau/2} + 1 \right] , \tag{34}$$

where $r = (j/2)^{1/3}$. Simplifying the expression gives the gain on resonance for a perfect beam,

$$G(\tau) = \frac{1}{9}\left[\, 2\cosh(r\sqrt{3}\tau) + 4\cos(r3\tau/2)\,\cosh(r\sqrt{3}\tau/2) - 6 \right] \quad . \tag{35}$$

In the limit of high current $j \gg \pi$, $r = (j/2)^{1/3} \gg 1$, the exponential gain becomes

$$G(\tau) \approx \frac{e^{r\sqrt{3}\tau}}{9} = \frac{e^{(j/2)^{1/3}\sqrt{3}\tau}}{9} \quad . \tag{36}$$

The final gain at $\tau = 1$ is

$$G \approx \frac{e^{(j/2)^{1/3}\sqrt{3}}}{9} \quad . \tag{37}$$

The dimensionless e-folding time is $\tau_e = 1/(j/2)^{1/3}\sqrt{3}$, and $G = \exp(\tau/\tau_e)/9$.

Now consider a perfect beam that is not at resonance, $v_0 \neq 0$. The integral equation (21) then becomes

$$a(\tau) = a_0 + \frac{ij}{2} \int_0^\tau d\tau' \int_0^{\tau'} d\tau'' \int_0^{\tau''} d\tau''' \, e^{iv_0(\tau''' - \tau')} \, a(\tau''') \quad . \tag{38}$$

After taking a single derivative and multiplying through by $e^{v_0\tau}$, the integral equation is

$$e^{iv_0\tau} \, \dot{a}(\tau) = \frac{ij}{2} \int_0^\tau d\tau' \int_0^{\tau'} d\tau'' \, e^{iv_0\tau''} \, a(\tau'') \quad . \tag{39}$$

Define the variable $b = e^{iv_0\tau}a$, so that $\dot{b} = e^{iv_0\tau} \, \dot{a} + iv_0 b$. In terms of b, the integral equation becomes

$$\dot{b} - iv_0 b = \frac{ij}{2} \int_0^\tau d\tau' \int_0^{\tau'} d\tau'' \, b(\tau'') \quad . \tag{40}$$

After taking successive derivatives, the integral equation is a cubic differential equation,

$$\dddot{b} - iv_0 \ddot{b} = \frac{ij}{2} b \quad . \tag{41}$$

To find the roots use the form $b = a_0 e^{\alpha\tau}$. The roots are determined by the cubic equation,

$$\alpha^3 - iv_0 \alpha^2 - ij/2 = 0 \tag{42}$$

The form of the solutions of the cubic equation are known and can be expressed as

$$\begin{aligned} \alpha_1 &= s_1 + s_2 + iv_0/3 \quad , \\ \alpha_2 &= -(s_1 + s_2)/2 + iv_0/3 + i\sqrt{3}(s_1 - s_2)/2 \quad , \\ \alpha_3 &= -(s_1 + s_2)/2 + iv_0/3 - i\sqrt{3}(s_1 - s_2)/2 \quad , \end{aligned} \tag{43}$$

where $u = i[j/4-(v_0/3)^3]$, $q = (v_0/3)^2$, $s_1 = (u+(q^3+u^2)^{1/2})^{1/3}$ $s_2 = (u-(q^3+u^2)^{1/2})^{1/3}$. This is an exact solution, but complicated.

In the limit of high current $j \gg \pi$, the cubic solution can be simplified. We get

$$u \approx ij/4 \quad , \quad q \approx (v_0/3)^2 \quad , \quad s_1 \approx (2u)^{1/3} \quad , \text{ and } \quad s_2 \approx q(-1/2u)^{1/3} \quad . \tag{44}$$

The roots then become

$$\begin{aligned} \alpha_1 &\approx (2u)^{1/3} + q(-1/2u)^{1/3} + iv_0/3 \\ \alpha_2 &\approx (-1+i\sqrt{3})(2u)^{1/3}/2 + (-1-i\sqrt{3})\, q(-i/2u)^{1/3}/2 + iv_0/3 \\ \alpha_3 &\approx (-1-i\sqrt{3})(2u)^{1/3}/2 + (-1+i\sqrt{3})\, q(-1/2u)^{1/3}/2 + iv_0/3 \end{aligned} \tag{45}$$

In terms of $r = (j/2)^{1/3}$, use $2u = ir^3$ to write

$$\begin{aligned} \alpha_1 &\approx i^{1/3}(r + q/r) + i\sqrt{q} \\ \alpha_2 &\approx i^{1/3}[(-1+i\sqrt{3})r/2 + (-1-i\sqrt{3})(q/2r)] + i\sqrt{q} \\ \alpha_3 &\approx i^{1/3}[(-1-i\sqrt{3})r/2 + (-1+i\sqrt{3})(q/2r)] + i\sqrt{q} \end{aligned} \tag{46}$$

Using the root $i^{1/3} = -i$, then

$$\alpha_1 \approx 0 + ... \quad , \quad \alpha_2 \approx \sqrt{3}(r - q/r)/2 \quad , \quad \alpha_3 \approx -\sqrt{3}(r - q/r)/2 \quad . \tag{47}$$

The field then grows as

$$a \approx \frac{a_0}{3}\, e^{r\sqrt{3}(1 - (v_0/3r)^2)/2} \quad , \tag{48}$$

and the gain is

$$G(v_0) \approx \frac{1}{9}\, e^{\sqrt{3}r}\, e^{-v_0^2/3\sqrt{3}r} \approx \frac{1}{9}\, e^{\sqrt{3}r}\, (1 - v_0^2/3\sqrt{3}r) \quad . \tag{49}$$

The gain expressed here is symmetric about resonance, and drops off at a value of the phase velocity $\Delta v \approx 2(3\sqrt{3})^{1/2}(j/2)^{1/6} \approx 4.22j^{1/6}$ away from resonance. As an example, consider $j = 100$, then $\Delta v \approx 2\pi$, and is broader than the normal gain spectrum bandwidth, $\Delta v \approx \pi$. For $j = 10^4$, then $\Delta v \approx 4\pi$, and is significantly broader than the low-current gain bandwidth.

In order to recover the usual low gain formula, consider a perfect beam and small current j. The field growth is small for low j, and the field $a(\tau'') \approx a_0$ can be removed from the triple integral. It does not have to be followed self-consistently. The integral

equation then becomes

$$a = a_0 + \frac{ij}{2} a_0 \int_0^\tau d\tau' \int_0^{\tau'} d\tau'' \int_0^{\tau''} d\tau''' \, e^{iv_0(\tau'''-\tau')} \quad . \tag{50}$$

The integral can now be performed directly. The first integral gives

$$\frac{a-a_0}{a_0} = \frac{ij}{2} \int_0^\tau d\tau' \, e^{iv_0\tau'} \int_0^{\tau'} d\tau'' \left[\frac{e^{iv_0\tau''} - 1}{iv_0} \right] \quad . \tag{51}$$

After completing the second and third integral, the result is

$$\frac{\Delta a}{a_0} = \frac{j}{2v_0{}^3} [\, 2 - iv_0\tau - (\, 2 + iv_0\tau)\, e^{-iv_0\tau} \,] \quad , \tag{52}$$

where the change in the field is $\Delta a = a - a_0$. The gain in the low-current case is given by $G = 2\Delta a/a_0$, and is

$$G \approx 2\Delta a/a_0 = j \, [\, 2 - 2\cos(v_0\tau) - (v_0\tau)\, \sin(v_0\tau)] \,/\, v_0{}^3 \quad . \tag{53}$$

This is the usual low-current gain equation that can be derived without the use of the integral equation. The change in the optical phase is

$$\Delta\phi \approx j \, [\, 2\sin(v_0\tau) - (v_0\tau) \, (\, 1 + \cos(v_0\tau))] \,/\, 2v_0{}^3 \quad , \tag{54}$$

and is also in agreement with the usual low-current result.

9. Gain Degradation in Low Gain FELs

The FEL oscillator typically works in the low current regime where the gain per pass is small. In this case, the integral equation can be simplified by removing the self-consistent field $a(q)$ from the integral. The effect of distributions can be then evaluated with a new analytical method. The integral equation is a triple integral in it's original form, but since it is an interated integral, it can be written as a double integral,

$$a(\tau) = a_0 + \frac{ij}{2} \int_0^\tau ds \int_0^s dq \, < e^{-iv_i(s-q)} >_{v_i} (s-q)a(q) \quad , \tag{55}$$

where $<...>_{v_i}$ is an average over the electron beam's distribution of phase velocities v_i. That is

$$<...>_{v_i} = \int_{-\infty}^{\infty} dv_i \; f(v_i)(...) \qquad \text{with} \qquad \int_{-\infty}^{\infty} dv_i \; f(v_i) = 1 \quad .$$

The normalized distribution function $f(v_i)$ can be written in the form $f(v_i - v_0)$ where all

phase velocities are referenced to some value v_0. The distribution function need not be center about v_0, but is just referenced to that phase velocity. Define $\Delta = v_i - v_0$ so that the integral equation can be written as

$$a(\tau) = a_0 + \frac{ij}{2} \int_0^\tau ds \int_0^s dq < e^{-i\Delta(s-q)} >_\Delta e^{-iv_0(s-q)} (s-q) a(q) \quad , \tag{56}$$

where $<...>_\Delta = \int_{-\infty}^{\infty} d\Delta \, f(\Delta)(...)$, and $f(\Delta) = f(v_i - v_0)$. It is best to use v_0 as a reference phase velocity for the perfect electron trajectory through the undulator.

In the limit of low current, $j \leq \pi$, the field $a(q)$ doesn't change significantly, so that $a(q) \approx a_0 + ...$ Then the integral equation can be written as

$$\frac{a(\tau) - a_0}{a_0} = \frac{ij}{2} \int_0^\tau ds \int_0^s dq < e^{-i\Delta(s-q)} >_\Delta e^{-iv_0(s-q)} (s-q) \quad . \tag{57}$$

Inside the integral, the factor $(s-q)$ can be replaced with an operation on the exponential factor,

$$(s-q) e^{-iv_0(s-q)} = i \partial_{v_0} e^{-iv_0(s-q)} \quad . \tag{58}$$

With the substitution above, the integrand can be simplified, and the integral equation becomes

$$\frac{a(\tau) - a_0}{a_0} = -\frac{j}{2} \partial_{v_0} \int_0^\tau ds \int_0^s dq < e^{-i\Delta q} >_\Delta e^{-iv_0 q} \quad . \tag{59}$$

For further development, if we interpret the exponential $e^{-i\Delta q}$ as a power series expansion,

$$e^{-i\Delta q} = \sum_{m=0}^{\infty} \frac{(-i\Delta q)^n}{n!} \quad , \tag{60}$$

then the integrand contains a factor that can be interpreted as

$$(-iq)^n e^{-iv_0 q} = \partial_{v_0}^n e^{-iv_0 q} \quad . \tag{61}$$

With this substitution, the average over the beam distribution no longer depends on time, but contains a derivative. The integral equation can then be written as

$$\frac{a(\tau) - a_0}{a_0} = -\frac{j}{2} < \exp(\Delta \partial_{v_0}) >_\Delta \partial_{v_0} \int_0^\tau ds \int_0^s dq \; e^{-iv_0 q} \quad . \tag{62}$$

The more complicated time integral containing the distribution function has been

replaced by a simple time integral, but with an infinite sum of derivatives to be executed for an exact expression. The simple time integral can be evaluated,

$$\int_0^\tau ds \int_0^s dq\ e^{-i\nu_0 q} = \frac{1-i\nu_0\tau-e^{-i\nu_0\tau}}{\nu_0^2} = \frac{1-\cos(\nu_0\tau)+i(\sin(\nu_0\tau)-\nu_0\tau)}{\nu_0^2} \quad , \tag{63}$$

and the complex integral equation becomes

$$\frac{a(\tau)-a_0}{a_0} = -\frac{j}{2} < \exp(\Delta\partial_{\nu_0}) >_\Delta \partial_{\nu_0}\left[\frac{1-i\nu_0\tau-e^{-i\nu_0\tau}}{\nu_0^2}\right] \quad . \tag{64}$$

The field evolution $a(\tau)$ is now determined by an explicit expression, but depending on the complexity of the distribution function, an infinite series of derivatives is requires. The value of the form of the integral equation is than the derivatives can be taken to successively higher order in the spread Δ. The relation between the successive derivatives and the distribution function is

$$< \exp(\Delta\partial_{\nu_0}) >_\Delta = \int_{-\infty}^{\infty} d\Delta f(\Delta) \exp(\Delta\partial_{\nu_0}) \quad . \tag{65}$$

As an example, consider the normal, or Gaussian, distribution function.

$$f(\Delta) = \frac{e^{-\Delta^2/2\sigma_G^2}}{\sqrt{2\pi}\sigma_G} \quad , \tag{66}$$

where σ_G is the spread in the distribution. Then, the function containing successive derivatives is

$$< \exp(\Delta\partial_{\nu_0}) >_\Delta = \exp(\sigma_G^2\partial_{\nu_0}^2/2) \quad . \tag{67}$$

For the exponential distribution function is another example that results from a symmetric angular spread in the beam. The exponential distribution is

$$f(\Delta) = \frac{e^{\Delta/\sigma_\theta}}{\sigma_\theta} \quad \text{for} \quad \Delta < 0 \quad , \tag{68}$$

where σ_θ is the spread in the exponential distribution. In this case, the resulting derivatives are expressed as

$$< \exp(\Delta\partial_{\nu_0}) >_\Delta = \frac{\exp(\Delta(\sigma_\theta^{-1}+\partial_{\nu_0})}{(1+\sigma_\theta\partial_{\nu_0})}\Big|_{-\infty}^{0} = \frac{1}{1+\sigma_\theta\partial_{\nu_0}} \quad . \tag{69}$$

Combining the two distributions, in the integral equation gives

$$\frac{a(\tau)-a_0}{a_0} = -\frac{j}{2}\left[\frac{\exp(\sigma_G^2\partial_{\nu_0}^2/2)}{1+\sigma_\theta\partial_{\nu_0}}\right]\partial_{\nu_0}\left[\frac{1-i\nu_0\tau-e^{-i\nu_0\tau}}{\nu_0^2}\right] \quad . \tag{70}$$

This is closed form solution for the complex field evolution of the radiation field, $a(\tau)$. It is valid to all orders in σ_G and σ_θ, but assumes weak optical fields and low gain. When there is no spread due to beam quality, the expression is less complicated, and contains only a single derivative of a simple complex function.

The gain in the low-current limit with weak fields is $G \approx 2\mathrm{Re}\, a^{(1)}/a_0$, and is

$$G = -\frac{j}{2}\left[\frac{\exp(\sigma_G^2\partial_{\nu_0}^2/2)}{1+\sigma_\theta\partial_{\nu_0}}\right]\partial_{\nu_0}\left[\frac{\sin^2(\nu_0/2)}{(\nu_0/2)^2}\right] \quad . \tag{71}$$

The factor on the right is recognized as the derivative of the spontaneous emission lineshape. The usual relationship between the gain and the spontaneous lineshape, the Madey theorem, is generalized here to include the detrimental effects of beam quality.

After accepting this relationship between the lineshape and the FEL gain, we can introduce another functional form for the spontaneous spectrum. In a real experiment, the electron trajectories are not perfect and most often lead to some distortions to the idealized lineshape. Consider a Gaussian lineshape instead of the sinusoidal "sinc" shape above:

$$\frac{\sin^2(\nu_0/2)}{(\nu_0/2)^2} = \mathrm{sinc}^2(\nu_0/2\pi) \rightarrow e^{-\nu_0^2/4\pi} \quad . \tag{72}$$

For comparison of the two lineshapes, note that both have the value unity at $\nu_0 = 0$. Furthermore, as $\nu_0 \rightarrow \pm\infty$, both lineshapes go to zero. The full-width-half-maximum (FWHM) of the sinc shape is $\Delta\nu_0 = 5.566$, while the FWHM of the Gaussian shape is $\Delta\nu_0 = 5.903$. The gain is proportional to the slope of the lineshape so that

$$G \propto \partial_{\nu_0} e^{-\nu_0^2/4\pi} = -\nu_0\, e^{-\nu_0^2/4\pi}/2\pi \quad , \tag{73}$$

and the peak of the gain spectrum is given by $\partial_{\nu_0} G = 0$. This is determined by

$$\partial_{\nu_0} G \propto \partial_{\nu_0}^2\, e^{-\nu_0^2/4\pi} = \left[(\nu_0/2\pi)^2 - 1/2\pi\right] e^{-\nu_0^2/4\pi} \quad . \tag{74}$$

So, the gain from the Gaussian lineshape has a peak and minimum at $\nu_0 = \pm\sqrt{2\pi} \approx \pm 2.51$, whereas the gain from the sinc lineshape has a peak and minimum at $\nu_0 = \pm 2.6$. For $\sigma_G = \sigma_\theta = 0$, the gain expression for the Gaussian lineshape is

$$G(\nu_0) = -\frac{j}{2}\,\partial_{\nu_0}\, e^{-\nu_\delta^2/4\pi} = \frac{j\nu_0}{4\pi}\, e^{-\nu_\delta^2/4\pi} \quad . \tag{75}$$

The peak gain at $\nu_0 = \sqrt{2\pi}$ is $G = j/2\sqrt{2\pi e} \approx 0.12j$, whereas the sinc lineshape gives $G \approx 0.135j$. In all, the Gaussian representation works well.

With beam quality included, the gain expression can be expanded to evaluate the lowest order changes to the gain using the Gaussian lineshape. Expanding the gain depression operator gives

$$\frac{\exp(\sigma^2\partial_{\nu_0}^2/2)}{1+\sigma_\theta\partial_{\nu_0}} = 1 - \sigma_\theta\partial_{\nu_0} + (\sigma_\theta^2 + \sigma_G^2/2)\,\partial_{\nu_0}^2 + \ldots . \tag{76}$$

The lowest order terms altering the FEL gain are then

$$G \approx -\frac{j}{2}\,[\,\partial_{\nu_0} - \sigma_\theta\,\partial_{\nu_0}^2 + (\sigma_\theta^2 + \sigma_G^2/2)\,\partial_{\nu_0}^3\,]\, e^{-\nu_\delta^2/4\pi} + \ldots . \tag{77}$$

Evaluating the derivatives gives

$$G \approx \frac{j}{2}\,[\,\nu_0/(2\pi) + \sigma_\theta\,(\nu_0^2-2\pi)/(2\pi)^2 + (\sigma_\theta^2 + \sigma_G^2/2)\nu_0(\nu_0^2-6\pi)/(2\pi)^3\,]\, e^{-\nu_\delta^2/4\pi} \quad . \tag{78}$$

Near resonance the gain above can be expanded. The result near $|\nu_0| \approx 0$ is

$$G_0 \approx \frac{j}{4\pi}\,[\,\nu_0 - \sigma_\theta - 3\nu_0(\sigma_\theta^2 + \sigma_G^2/2)/2\pi + \ldots .\,] \quad . \tag{79}$$

If $\nu_0 \to 0$, the gain no longer goes to zero, as in the case of a perfect beam, but $G \to -j\sigma_\theta/4\pi$. The slope of the gain spectrum at $\nu_0 = 0$ is

$$G'_0 \approx \frac{j}{4\pi}\,[\,1 - 3(\sigma_\theta^2 + \sigma_G^2/2)/2\pi + \ldots .\,] \quad . \tag{80}$$

As either σ_G or σ_θ increase, the slope decreases indicating broader spectrum.

At peak gain, $\nu_0 \approx \sqrt{2\pi}$, the gain may be expanded to find the changes due to beam quality. Let $\nu_0 = \sqrt{2\pi} + x$, where $x \ll \pi$. Then, the gain spectrum becomes

$$G_{2\pi} \approx \frac{j}{2\pi\sqrt{2\pi e}}\,[\,\pi + \sigma_\theta x - (\sigma_\theta^2 + \sigma_G^2/2)\,] \quad . \tag{81}$$

The first term just gives the peak gain at $\nu_0 = \sqrt{2\pi}$ for a perfect beam. The second term shows there is a positive slope to the gain spectrum at $\nu_0 = \sqrt{2\pi}$ when there is an angular spread. This indicates that the actual peak moves to the right when σ_θ increases. The last term term decreases the value of the gain at $\nu_0 = \sqrt{2\pi}$ when either the angular spread σ_θ or energy spread σ_G increases.

10. SPIE FEL Review Paper

During the contracting period, Dr. Brian Newnam (LANL) put together a group of authors to write a series of papers reviewing the status of FEL technology. I was asked to provide a review of FEL theory. The resulting publication reference is W. B. Colson, "Fundamental Free Electron Laser Theory and New Principles for Advanced Devices", *Free Electron Lasers: Critical Review of Technology*, B. E. Newnam, editor, Proc. SPIE **738**, 2-27 (1988).

The paper tries to establish that the fundamentals of FEL theory are now well-established and can provide a sophisticated description of experiments over a wide range of parameters. While new technology is being developed for systems working from 1mm to 10nm wavelengths, the theory remains the same. The paper has 139 cited references. The topics covered the FEL electron dynamics, and the FEL wave equation. Dimensionless variables are introduced to examine the electron phase-space evolution. The electron trajectories through the undulator are derived with the natural undulator focusing causing betatron motion. The study of radiation begins with the Liénard-Wiechert optical fields, spontaneous emission, and the coupling to higher harmonics. The collective high gain regime and gain degradation due to electron beam quality are explored using the integral equation. The relatively minor role of Coulomb forces is demonstrated. The effects of saturation in strong optical fields are derived. Alternative undulator designs like the tapered undulator and the FEL klystron are described. More sophisticated phenomena involving multiple optical modes show the FEL coherence development, and more general longitudinal multimode theory. The multimode theory is then used to describe the short pulse evolution in the FEL, and the trapped particle instability. In the transverse dimension, diffraction is included in a general formalism. The electron dynamics in a Gaussian optical mode are derived and the simple physics of optical self-guiding are studied.

Fundamental free electron laser theory and new principles for advanced devices

W. B. Colson

Berkeley Research Associates, P.O. Box 241, Berkeley, CA 94701

Abstract

The fundamentals of free electron laser theory are now well-established and can provide a sophisticated description of experiments over a wide range of parameters. While new technology is being developed for systems working from 1mm to 10nm wavelengths, the theory remains the same.

Introduction

The free electron laser (FEL) uses a beam of relativistic electrons passing through a long, transverse, periodic magnetic field to amplify a co-propagating optical wave. The first description of the short-wavelength FEL configuration in 1971 [1,2] was followed by successful experiments in 1976 and 1977 [3,4] at Stanford University. While closely related to earlier long-wavelength radiation mechanisms using free electron beams and periodic undulators [5,6], the present FEL has several important advantages over competitive sources. There are now many FEL experiments that have explored a wide range of physical parameters and system configurations. Collections of papers [7-31] and specific review articles [32-38] provide a good overview of the development of the experiments and theory. Several theoretical approaches describe the FEL with the first analyses using quantum concepts [1], and quantum electrodynamics [39,40]. Later, classical methods were shown to be accurate and complete [41-46]. The quasi-Bloch equations have enhanced the laser physics perspective [47], while plasma dispersion relations [48,49] and computer simulations [50,51] have emphasized the role of collective effects.

Maxwell's wave equation driven by a beam of single-particle electron currents provides a clear, intuitive description of both the electron and wave dynamics [43,52,53]. Most FEL theoretical work now uses this approach. Theory and experiment have been tested over a wide range of parameters and show excellent agreement. The success of the theory is largely due to the simplicity of the fundamental FEL mechanism and experimental conditions. In the interaction volume, there are only free electrons, a static magnetic field, and light. Furthermore, the laser's long-range coherence means that only a modest number of modes are needed for an accurate representation. No material constants, or empirical data are used in the theory; classical results depend only on the electron charge, mass, and the speed of light. In this chapter, a simple description of the electron dynamics and the slowly-varying wave equation is systematically generalized to develop a more detailed, comprehensive theory.

In the FEL oscillator configuration resonator mirrors are positioned beyond the ends of the undulator to store short wavelength radiation. See Figure 1. The optical power builds up from spontaneous emission noise over many repeated passes of the light through the resonator. Gain per pass, or amplification, only occurs when the light and electrons are traveling in the same direction. In the amplifier configuration, the resonator mirrors are not used for optical feedback so that high gain in a single pass is desirable. The electron beam current is typically larger than in the oscillator case so that significant energy can be converted to radiation at the end of the undulator.

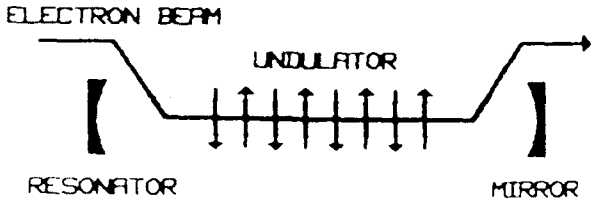

Figure 1. FEL oscillator schematic.

The undulator provides a periodic, transverse, magnetic field that slightly deflects electrons from side-to-side as they travel along the optical mode axis. The undulator extends over an interaction length L with wavelength λ_0 in the range of 2cm to 10cm. The peak magnetic field strength B in a period is from 2kG to 5kG, and the length of the undulator can extend for a few meters up to several tens of meters. The number of periods in the undulator N is nominally around 100, but could be as few as 10 or as much as 1000. The energy of the electrons γmc^2 entering the undulator can be mildly relativistic ($\gamma \sim 1$) or ultra relativistic ($\gamma \gg 1$) ranging from about 1MeV up to a few GeV with peak currents from less than 1A up to

several kA in a beam that is typically from 1mm to 1cm in diameter. Consider a typical current and energy, say I = 100A and γmc^2 = 50MeV; the FEL power source is then an impressive 5GW. Since the power source is inherently large, even with small efficiency, the fraction of electron beam energy converted to radiation, can result in a powerful laser.

For a relativistic electron in a weak undulator, the optical wavelength λ is given by

$$\lambda = \frac{\lambda_0}{2\gamma^2} \quad . \tag{1}$$

This simple relationship between the electron energy, the undulator, and the optical wavelength shows two of the most important attributes of the FEL: continuous tunability and design flexibility. The FEL can be designed to work in new wavelength ranges where there are now no powerful sources of light. New and important regions of the electromagnetic spectrum where FELs can operate are $10^3\mu m \rightarrow 20\mu m$ and $200nm \rightarrow 20nm$. The design flexibility of the undulator is another attribute of the FEL. Not only can the undulator wavelength, field strength, and polarization be selected to suit a particular application, but the properties of the undulator can be changed along its length to attain specific interaction qualities. In the tapered undulator operating at high power, the electrons lose energy and fall out of resonance with the light as shown in (1). In order to compensate, the undulator wavelength λ_0 can be decreased to maintain resonance, extend the interaction over a longer undulator length, and improve efficiency. FELs can be made in a variety of configurations with different electron beam sources. The different configurations present many varied theoretical problems.

FEL electron dynamics

In order to describe the FEL electron dynamics, the classical Lorentz force equations are solved for an electron in the undulator with a superimposed electromagnetic wave. Circular polarization is used to simplify the mathematics of the analysis. The helical undulator field is represented by

$$\vec{B} = (B_x, B_y, B_z) = B\ (\cos(k_0 z), \sin(k_0 z), 0) \quad . \tag{2}$$

The radiation signal with the polarization that couples best to this undulator has the transverse electric and magnetic fields

$$\vec{E_s} = E(\cos(kz-\omega t+\phi), -\sin(kz-\omega t+\phi), 0), \quad \vec{B_s} = E(\sin(kz-\omega t+\phi), \cos(kz-\omega t+\phi), 0) . \tag{3}$$

The optical wave is traveling along the z axis with wavelength $\lambda = 2\pi/k = 2\pi c/\omega$, field strength E, and phase ϕ. In normal FEL operation, the predominant radiation in the undulator will have a narrow distribution of frequencies and angles as in (3).

The Lorentz force equations of motion are solved for one electron in the presence of the fields (2) and (3). The transverse velocity components $\vec{\beta}_\perp = (v_x, v_y, 0)/c$ may be integrated trivially over an undulator period by noting that the force is a perfect time derivative. The result is

$$\gamma\vec{\beta}_\perp = -K(\cos(k_0 z), \sin(k_0 z), 0) + K_s(\sin(kz-\omega t+\phi), \cos(kz-\omega t+\phi), 0) \tag{4}$$

where $K = e\bar{B}\lambda_0/2\pi mc^2$, $\bar{B} = B$ is the rms undulator field strength, $k_0 = 2\pi/\lambda_0$, $K_s = e\bar{E}\lambda/2\pi mc^2$ is the dimensionless optical vector potential, and $\bar{E} = E$ is the rms optical field. If the undulator and light were linearly polarized, $\bar{B} = B/\sqrt{2}$ and $\bar{E} = E/\sqrt{2}$. The constants of integration have been set equal to zero for now so that the orbits are perfect sinusoids; this is the condition of perfect injection of an electron into the FEL. Substitute $\vec{\beta}_\perp$ above into the fourth component of the Lorentz force to describe the change in the electron energy

$$\dot{\gamma}(t) = \frac{KK_s\omega}{\gamma}\cos[(k+k_0)z(t)-\omega t+\phi] \quad . \tag{5}$$

where $\dot{\gamma} = d\gamma/dt$. The phase $(k+k_0)z(t) - \omega t+\phi$ determines whether an electron's energy increases or decreases in time. As the electron energy changes, the z velocity is found by substituting $\vec{\beta}_\perp$ into the electron energy $\gamma^{-2} = 1 - \vec{\beta}^2$. This gives

$$\beta_z(t) = \left(1 - \frac{1 + K^2 - 2KK_s\sin[(k+k_0)z(t)-\omega t+\phi] + K_s^2}{\gamma^2(t)}\right)^{1/2} \quad . \tag{6}$$

The energy and z velocity equations (5) and (6) with $\beta_z(t) = v_z(t)/c$ are sufficient to solve for the electron motion. Reference to $\gamma^2(t)$ can be removed to describe the electron motion in terms of parallel components only,

$$\dot{\beta}_z(t) = \frac{KK_s(1-\beta_z^2(t))(k_0 c + \omega(1-\beta_z(t)))\cos[(k+k_0)z(t)-\omega t+\phi]}{1 + K^2 - 2KK_s\sin[(k+k_0)z(t)-\omega t+\phi] + K_s^2} \quad . \tag{7}$$

Other than assuming perfect injection, no other assumptions have been made, and (7) is exact. The consequences of imperfect injection will be discussed later. The system of Lorentz force equations has now been reduced to a single non-linear, second-order, ordinary differential equation in $z(t)$. With some additional information, a much simpler form can be found.

In a typical FEL undulator $K \sim 1$. Then, (6) shows that only relativistic electrons, $\gamma \gg 1$, can travel along the whole axis of the undulator; less energetic electrons would be turned around in the first undulator period. The maximum value of K_s is at saturation where electrons can be trapped by strong optical fields and execute synchrotron oscillations: $K_s^{max} \sim N_S^2/N^2$ where N_S is the number of synchrotron oscillations along the undulator. Typically, $K_s^{max} \leq 10^{-4}$, so that $K \gg K_s$ even in the strongest possible optical fields. From (7) we see that the changes in the electron's relativistic z velocity component are small. The unperturbed motion is $z(t) \approx z_0 + \beta_0 ct$ where $\beta_0 = (1-(1+K^2)/\gamma^2)^{1/2} \approx 1-(1+K^2)/2\gamma^2$. The most significant optical feedback occurs when the electron phase $(k+k_0)z(t) - \omega t$ evolves slowly. This occurs when $\beta_0 \approx k/(k+k_0)$ making the undulator and optical forces resonant. The radiation wavelength determined by the resonance condition is $\lambda = \lambda_0(1-\beta_0)/\beta_0 \approx \lambda_0(1+K^2)/2\gamma^2$ as in (1).

In order to solve for $z(t)$ with these simplifying conditions assume that $N \gg 1$ and $\gamma \gg 1$. Then, (7) takes the form of the simple pendulum equation,

$$\overset{\circ\circ}{\zeta} = \overset{\circ}{\nu} = |a| \cos(\zeta + \phi) \quad , \tag{8}$$

where $\overset{\circ}{(..)} = d(..)/d\tau$, the dimensionless time is $\tau = ct/L$, the electron phase is $\zeta = (k+k_0)z - \omega t$, the electron phase velocity is $\nu = L[(k+k_0)\beta_z - k]$, and the dimensionless optical field is $a = |a| e^{i\phi}$ with $|a| = (4\pi N)^2 K K_s/(1+K^2) = 4\pi N e K L E/\gamma^2 mc^2$. The exact solutions are incomplete elliptic integrals of the first kind; however, it is fruitful to derive physical results from (8) directly. The important feature of (5)-(6), (7), or (8) is that the equations have been made slowly varying over an undulator period. Further integration can be accomplished numerically on a small computer, or analytically with some specific assumptions. The integration steps can jump over one or a few undulator periods, and need not integrate the motion within each undulator wavelength as would be needed in (4). Along the whole length of the undulator $\tau = 0 \rightarrow 1$, the electron phase and phase velocity (ζ, ν) can change significantly in strong optical fields when $|a| \geq \pi$. In the high gain limit, the field amplitude $|a|$ and phase ϕ change significantly along the undulator, but not within an undulator period. The pendulum equation (8) is valid in both weak and strong optical fields with high or low gain, and has been used to solve many FEL problems [54-61]. In high efficiency FELs [62], the energy change of the electrons is large enough so that many authors [63-67] use the more accurate equations (5) and (6) with $\gamma \gg 1$.

The FEL wave equation

It is important that both the electron and optical equations vary slowly. Near resonance an electron passing through one wavelength of the undulator has approximately one wavelength of light pass over it. The optical field amplitude and phase in that wavelength must also vary slowly so that resonance can be maintained. To describe the evolution of the complex optical field, we use the transverse wave equation with a source current $\vec{J}_\perp$. Insert the fields (3) into the wave equation, and use $\dot{E} \ll \omega E$ and $\dot{\phi} \ll \omega\phi$ to drop all second derivatives and terms with two derivatives. Projecting the wave equation with only single derivatives onto the two unit vectors, $\hat{\varepsilon}_1$ and $\hat{\varepsilon}_2$, we have

$$\dot{E} = -2\pi \vec{J}_\perp \cdot \hat{\varepsilon}_1 \quad , \quad \text{and} \quad E\,\dot{\phi} = 2\pi \vec{J}_\perp \cdot \hat{\varepsilon}_2 \quad . \tag{9}$$

where $\hat{\varepsilon}_1 = (\cos\Psi, -\sin\Psi, 0)$, $\hat{\varepsilon}_2 = (\sin\Psi, \cos\Psi, 0)$, and $\Psi = kz - \omega t + \phi$.

The current from a single electron is $\vec{J}_{\perp i} = -ec\vec{\beta}_\perp \delta^{(3)}(\vec{x} - \vec{r}_i)$ where $\vec{r}_i$ is the trajectory of the ith electron. Using (4) with $K_s \ll K$, the current determined by the transverse motion in the undulator and the electron phase becomes

$$\vec{J}_{\perp i} \cdot \hat{\varepsilon}_1 = \frac{eKc}{\gamma} \cos(\zeta+\phi)\, \delta^{(3)}(\vec{x} - \vec{r}_i) \quad \text{and} \quad \vec{J}_{\perp i} \cdot \hat{\varepsilon}_2 = \frac{eKc}{\gamma} \sin(\zeta+\phi)\, \delta^{(3)}(\vec{x} - \vec{r}_i) \quad . \tag{10}$$

The total electron current is the sum over all single electron currents. Since the left-hand side of the wave equation changes slowly over several optical wavelengths, it can only respond to an average current in a small volume element a few optical wavelengths long. The electron pulse shape from any accelerator is much longer than this volume element, and is not distorted by the microscopic bunching of electrons on the optical wavelength scale. The electron density ρ remains fixed on a macroscopic scale, and the wave equation can be expressed as [43]

$$\dot{E} = -2\pi eKc\rho \langle \cos(\zeta+\phi)/\gamma \rangle \quad , \quad \text{and} \quad E\,\dot{\phi} = 2\pi eKc\rho \langle \sin(\zeta+\phi)/\gamma \rangle \tag{11}$$

where $\langle .. \rangle$ represents an average over sample electrons in the beam weighted by the particle density ρ. We chose to label electrons by their initial conditions $\nu(0) = \nu_0$ and $\zeta(0) = \zeta_0$. So many electrons ($\sim 10^8$) are spread randomly over the initial phases $\zeta_0 = (k+k_0)z_0 \approx kz_0$ that the current looks uniformly spread, and the averages $\langle .. \rangle$ are initially zero. When the interaction starts, the bunching of phases due to optical feedback gives non-zero averages, and the field evolves. When $N \gg 1$ and $\gamma \gg 1$, as in the pendulum equation, the wave equation can be put into the simple form [68]

$$\overset{\circ}{a} = -j \langle e^{-i\zeta} \rangle \quad , \tag{12}$$

where the dimensionless electron current density is $j = 8N(e\pi KL)^2 \rho/\gamma^3 mc^2$. The pendulum and wave equation together, (8) and (12), are valid in weak or strong optical fields with either high or low gain. In a high efficiency FEL where the changes in the electron energy are large, the wave equation (11) combined with (5)-(6) is more accurate.

Dimensionless variables

It is desirable to find dimensionless variables to summarize combinations of physical variables and reduce the complexity of the notation. More importantly, dimensionless variables can give insight into the physical processes involved before any calculation begins. The starting point is the electron phase $\zeta = (k+k_0)z(t) - \omega t$. Since $k = \omega/c$ and k_0 are fixed by the experimental design, ζ follows changes in the electron's longitudinal coordinate $z(t)$. As seen in (7) or (8), the electron motion is periodic in ζ with the corresponding physical "bunching length" along the beam given by $\lambda/(1+\lambda/\lambda_0) \approx \lambda$ for $\gamma \gg 1$. The optical phase ϕ is followed separately from ζ so that ζ depends only on the electron dynamics.

The dimensionless time along the undulator is τ so that the evolution of all quantities is over $\tau = 0 \rightarrow 1$. In the pendulum equation (8), the electron phase ζ and phase velocity v are coupled by the dimensionless optical field strength $|a|$ which determines the rate of bunching along the undulator. If $|a| \gg \pi$, the optical field is strong and bunching occurs quickly; perhaps before the end of the undulator causing saturation. If $|a| \leq \pi$, the optical field is weak. The wave equation (12) drives the complex field $a = |a|e^{i\phi}$ in proportion to the electron phase average $< e^{-i\zeta} >$ with the coupling given by dimensionless current density j. It will be shown later that if $j \leq 1$, the gain is low, and if $j \gg 1$, the gain is high.

Briefly described in Table 1 are some of the relativistic ($\gamma > 5$) FEL experiments. The radius of the optical mode w_0 is used in the estimate of j as will be explained later. For most experiments, the optical power and electron-beam efficiency at saturation can be estimated from the data shown using expressions presented later. The last eight experiments are on-going, or planned for the future.

Table 1. Free Electron Lasers

FEL	I (Amps)	γ	N	λ_0 (cm)	K	λ (μm)	w_0 (cm)	j	Comments
[3] Stanford '76	0.07	48	160	3.2	0.72	11	0.3	0.2	First A,RF,H
[4] Stanford '77	2.6	86	160	3.2	0.72	3.4	0.3	6	First O,RF,H
[69] Stanford '80	1.3	85	160	3.3	0.71	3.4	0.14	3.6	O,RF,H
[70] LANL '82	20	40	37	2.7	0.55	11	0.16	1.8	A,RF,L,δ=10π
[71] MSNW/Boeing '83	3	38	91	2.5	0.44	11	0.16	2.8	A,L,δ=33π
[72] TRW/EG&G '83	10	50	75	3.6	0.63	11	0.17	1.6	A,RF,L
[73] LANL '84	40	40	37	2.7	0.54	11	0.15	3.6	O,RF,L
[74] TRW/Stanford '84	2.5	130	153	3.6	0.97	1.6	0.1	3.4	O,RF,L,δ=4π
[75] Orsay ACO '84	0.03	326	17	7.8	1.2	0.65	0.03	0.0005	A,SR,L,D=100
[76] Novosibirsk '84	7	686	22	6.9	2.7	0.62	0.03	0.06	A,SR,L,D=280
[77] Frascati ENEA '85	2.4	40	50	2.4	0.35	11	0.1	0.14	O,M,L
[78] Orsay ACO '85	0.2	432	17	7.8	2	0.63	0.03	0.004	O,SR,L,D=100
[79] UCSB '85	1.25	6.8	160	3.6	0.11	400	1	0.35	O,V,L
[80] INFN LELA '85	0.018	1224	20	12	3.5	0.51	0.04	0.00006	A,SR,L
[81] LLNL ELF '85	500	7.5	30	9.8	2.8	8700	1.5	9000	A,IL,L
[82] LANL '86	130	40	37	2.7	0.56	11	0.14	53	O,RF,L,δ=18π
[83] Stanford Mark III '86	20	87	47	2.3	1.5	3.1	0.07	3.2	O,RF,L
[84] LLNL ELF '86	850	6.9	30	9.8	2.5	8700	1.5	14100	A,IL,L
[85] LLNL ELF Tapered '86	850	6.9	30	9.8	2.4	8700	1.5	14400	A,IL,L,δ=50π
[86] LLNL ELF '87	1000	7.8	40	9.8	1.1	2000	1.5	7200	A,IL,L
[87] Boeing/Spectra '87	100	223	229	2.2	1.3	0.5	0.06	687	O,RF,L,δ=92π
[88] Bell Labs	5	24	50	20	0.93	240	2	2	O,M,H
[89] BNL	22	588	39	6.5	2.3	0.6	0.07	0.25	A,SR,L
[90] United Kingdom	10	118	76	6.5	1.9	11	0.3	8.9	O,RF,L
[91] LANL XUV	100	400	750	1.6	0.79	0.08	1.6	414	O,RF,L
[92] Stanford XUV	270	1958	422	6.4	1.6	0.03	0.06	37	O,SR,L
[93] NBS XUV	2	363	130	2.8	1	0.23	0.04	0.6	O,M,L
[94] LBL/BNL XUV	200	1470	870	2.3	2.6	0.04	0.03	1360	SR,SRA,L
[95] Boeing PBC	15	40	80	3	1	11	0.1	5	O,RF,L

RF - RF Linac Accelerator, IL - Induction Linac Accelerator, M - Microtron Accelerator, SR - Electron Storage Ring, V - Van De Graaff Electrostatic Accelerator, H - Helical Undulator Polarization, L - Linear Undulator Polarization, δ # - Tapered Undulator FEL, D # - Klystron Undulator FEL, A - FEL Amplifier, O - FEL Oscillator SRA - Super Radiant Amplifier in a Long, Single-Pass Undulator

Electron phase-space evolution

The evolution of sample electrons in one section of the periodic (ζ,ν) phase-space has proven useful in understanding many FEL problems. In weak fields with low current ($|a|$ and j are both small), (8) and (12) can be easily solved self-consistently to obtain [55]

$$\nu(\tau) = \nu_0 + \frac{a_0}{\nu_0}\,[\,\sin(\zeta_0+\nu_0\tau) - \sin(\zeta_0)\,] + \ldots \quad , \quad \zeta(\tau) = \zeta_0 + \nu_0\tau - \frac{a_0}{\nu_0^2}\,[\,\cos(\zeta_0+\nu_0\tau) - \cos(\zeta_0) + \nu_0\tau\sin(\zeta_0)\,] + \ldots \qquad (13)$$

$$|a(\tau)| = a_0 + \frac{ja_0}{2\nu_0^3}\,[\,2 - 2\cos(\nu_0\tau) - \nu_0\tau\sin(\nu_0\tau)\,] + \ldots \quad , \quad \phi(\tau) = \frac{j}{2\nu_0^3}\,[\,2\sin(\nu_0\tau) - \nu_0\tau\,(1+\cos(\nu_0\tau))\,] + \ldots \quad .$$

where the initial field is $a(0) = a_0$, and the initial electron phase-space coordinates are $\zeta(0) = \zeta_0$ and $\nu(0) = \nu_0$. The phase-space evolution in Figure 2 is generated by solving (8) and (12) numerically with $j = 1$, $a_0 = 2$, and $\nu_0 = 2$, but is also described analytically in (13). At $\tau = 0$, a uniform "fluid" of sample electrons starts at ν_0. As the electrons evolve, they become darker, and are finally black at $\tau = 1$. The continuous distribution of electrons initially forms a "line" across the (ζ,ν) phase-space at $\nu_0 = 2$. As this section of the electron beam moves along the undulator, $\tau = 0 \rightarrow 1$, the line of electrons distorts and is plotted darker until the final positions are shown in black. As a guide to the phase space paths, the separatrix is shown given by $\nu_s^2 = 2|a|[\,1 - \sin(\zeta_s + \phi)\,]$ passing through the critical points $(-\pi/2,0)$ and $(3\pi/2,0)$. The peak-to-peak height of the separatrix is $4|a|^{1/2}$ and the horizontal position is determined by the optical phase ϕ. Motion along the ν axis corresponds to an increase in electron energy since $\Delta\nu = 4\pi N\Delta\gamma/\gamma$. Roughly half the electrons are initially positioned such that work is done on them; they gain energy and move ahead of the average flow. The other half lose energy to the radiation field, and move back causing spatial "bunching". The wave equation (12) shows that when electrons over-populate the phase π, then the optical amplitude is driven, and there is gain, $G(\tau) = |a(\tau)|^2/a_0^2 - 1$. If the bunching over-populates phase $\pi/2$, then the optical phase is driven, and there is little or no gain. In the low gain case $G(\tau) \approx 2|a(\tau)|/a_0 - 1$, the third equation in (13) gives an analytic expression for the gain. Plotted at the right in Figure 2 is $G(\tau)$ and the optical phase $\phi(\tau)$. Initially, there is no gain or phase shift from the uniformly spread electron beam. As bunching develops and drifts near the phase π, the gain and optical phase increase. The density of electrons at phase ζ is given by the phase distribution function [35]

$$f(\zeta,\tau) = \rho\left\{\,1 + \frac{a_0}{\nu_0^2}\,[\,\sin(\zeta-\nu_0\tau) - \sin(\zeta) + \nu_0\tau\cos(\zeta-\nu_0\tau)\,] + \ldots\right\} \qquad (14)$$

which can be calculated from (13). It is characteristic of the low gain case that the optical phase shift is small so that the changes in the position of the separatrix in Figure 2 are imperceptible.

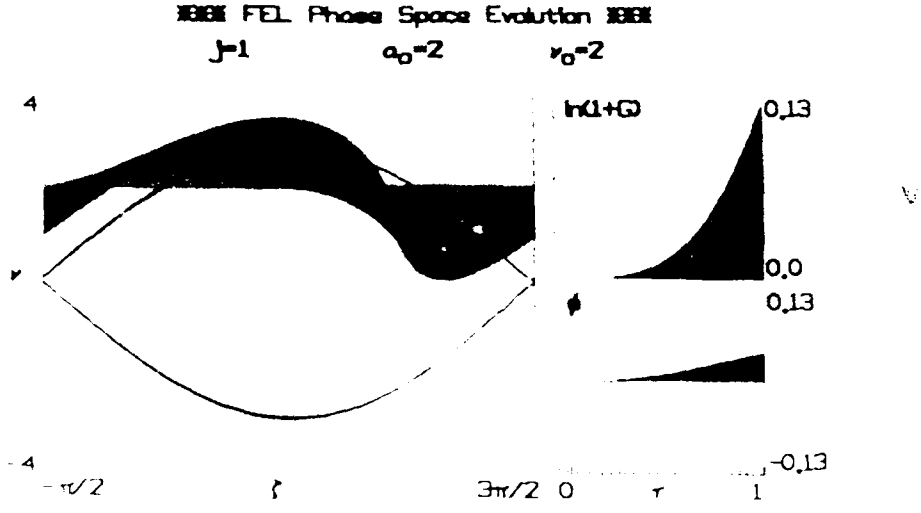

Figure 2. Electron phase-space evolution.

The initial gain spectrum $G(\nu_0)$ at $\tau = 1$ is anti-symmetric in ν_0 with a peak gain of $G = 0.135j$ at $\nu_0 = 2.6$. At [illegible] gain, while at values of $\nu_0 < 0$ there is net adsorption of the optical power. Note that a change [illegible] 2π can change the interaction from amplification to adsorption. This requires only a small change in [illegible] when $N \gg 1$. The width of the positive gain spectrum is about $\Delta\nu_0 = \pi$. We now go

on beyond the fundamental physics of the FEL interaction and extend the same theoretical approach to include a range of diverse effects.

Electron trajectories through the undulator

The FEL gain depends on the detailed trajectories of electrons through the undulator [96-99]. Since $K_z \ll K$ in (4), the undulator field alone determines the path of an electron and its eventual coupling to the optical field. The transverse amplitude of a perfect helical trajectory, $K\lambda_0/2\pi\gamma \approx 0.1$mm, is much smaller than the typical beam size, 1mm to 1cm. A small, imperfect injection angle θ away from the perfect injection angle ($-K/\gamma$ in (4)) causes the electron to drift in the transverse direction. A co-propagating optical wave of area πw_0^2 will also spread in the transverse dimension due to natural diffraction. The length over which the transverse optical area doubles, the Rayleigh range $\pi w_0^2/\lambda$ [100], should be comparable to the undulator length $L = N\lambda_0$. It will be shown later [100] that for small j, the maximum gain occurs when the transverse optical mode has radius $\sim \sqrt{L\lambda/\pi}$. If we require that an electron does not drift out of the optical mode as they travel together through the undulator, then we have $\theta \leq 1/(\pi\gamma N^{1/2})$ using the resonance condition.

An electron traveling at a small angle θ away from the z axis also has a reduced z velocity $\beta_z \approx \beta_0(1-\theta^2/2+...)$ that reduces its phase velocity by $\Delta v \approx -2\pi N\gamma^2\theta^2/(1+K^2)$. If we require that a random spread in the injection angle does not spread the phase velocity by more the gain bandwidth, then we recover the same requirement $\theta \leq 1/(\pi\gamma N^{1/2})$ as above from a different physical argument.

In a linearly polarized undulator $\vec{B} = B(0, \sin(k_0 z), 0)$, perfect trajectories have a more complicated motion than in the helical case where β_z is constant without the optical interaction; recall (7) with $K_z = 0$. Solving for trajectories with a perturbation expansion in powers of K/γ, we find the z motion has the form $z(t) \approx \beta_0 ct + \Delta z(t) + ...$, and is not constant through each undulator period. The small longitudinal oscillations cause the electron phase ζ to oscillate every undulator period [101] by

$$\Delta\zeta(t) \approx k\,\Delta z(t) \approx -\xi \sin(2\omega_0 t) \quad , \tag{15}$$

where $\xi = K^2/2(1+K^2)$, and $\omega_0 = \beta_0 k_0 c t \approx k_0 c t$ is the oscillation frequency of the electrons in the undulator. For $K \geq 1$, the fast, periodic oscillations are comparable to the optical wavelength and modify the interaction strength in the fundamental and higher frequency harmonics. The electrons are taken far off-resonance through $\Delta v(t) \approx -4\pi N\xi\cos(2\omega_0 t)$ in each undulator period, but since the motion is not random, the interaction continues; the interaction strength is reduced as the electrons spend some time out of resonance.

Imperfect trajectories in both the linear and helical undulator will also cause fast oscillations that reduce coupling to the fundamental frequency, and cause emission and gain in higher harmonics. In the helical case, injection at an angle gives the oscillating phase,

$$\Delta\zeta(t) \approx k\,\Delta z(t) \approx \frac{2K\gamma\theta}{1+K^2}\sin(\omega_0 t) \quad . \tag{16}$$

When $\gamma\theta$ and K are comparable to unity, the amplitude of $\Delta\zeta(t)$ is large enough to significantly alter the interaction [102].

Even with perfect initial injection, the electron trajectories can be altered by field errors in the undulator itself [103,104]. Consider the ith period of an undulator described by $\vec{B}_i = (0, B\sin(k_0 z) + \Delta B_i, 0)$ with a small error ΔB_i. We only examine the trajectory at the end of each undulator period and ignore the y motion for simplicity. At the end of the ith period, the deflection integrates to $\Delta x_i \approx \pi\Delta K_i\lambda_0/\gamma$ where $\Delta K_i = e\,\Delta B_i\lambda_0/2\pi mc^2$. Typically, the deflection is $\Delta x_i \approx 0.01$mm if the undulator period has a 1% field tolerance. Over many periods, the electron performs a random walk in x with varying step size and direction. If we take the same amount of error in each period, $\Delta K_i = \Delta K$, then the typical transverse deflection after N periods is $\Delta x \approx \pi\sqrt{N}\,\Delta K\lambda_0/\gamma \approx 0.1$mm. Requiring that the transverse excursions do not take the electron out of the optical mode, the field error must only satisfy $\Delta K < 1/\pi^2$. Typically, $\Delta K/K \approx 10^{-2}$ so that random errors are not the worst problem for building an undulator; systematic errors over several undulator periods can be much more damaging.

Natural undulator focusing, betatron motion

Electrons injected into an undulator with an small angular spread over a small cross section may have some of the [illegible] discussed above. When the electron beam is larger in cross section or has a larger angular spread, the field [illegible] out of the undulator axis must be included to calculate trajectories. Fortunately, these fields tend to focus the [illegible] the undulator axis causing "betatron" oscillations in the transverse direction [96-99,103-105]. The [illegible] above are only accurate near the undulator axis at $x = y = 0$. A more complete expression of the [illegible] undulator field is

$$\vec{B} = B(0, \sin(k_0 z)\cosh(k_0 y), \cos(k_0 z)\sinh(k_0 y)) \tag{17}$$

[illegible] field, in the y direction, but not in the x direction. Off axis, closer to the magnetic [illegible] permanent magnet sections or coils, the average field magnitude increases as $B_{rms} = B(1 + \tfrac{1}{2}(k_0 y)^2 + ...)$, and

focuses electrons back toward the undulator axis. Under the proper conditions, the whole beam is confined so that $k_0 y \ll 1$ at all points along the undulator.

The x component of the motion is exactly integrable, and can be substituted into the y and z components. Averaging over an integral number of undulator periods λ_0, allows us to concentrate on and solve for the larger scale betatron motion.

$$\bar{\beta}_y \approx -\frac{K^2\omega_0}{2\gamma^2}\sinh(2k_0 y) \quad , \quad \text{and} \quad \bar{\beta}_z = \beta_0 = \text{constant} \quad , \tag{18}$$

assuming $(K/\gamma)^2 \ll 1$. If the natural focusing is successful so that $k_0 y \ll 1$, then the y motion is given by

$$\ddot{y}(\tau) = -\omega_\beta^2\, y(\tau) \quad , \tag{19}$$

where the dimensionless betatron frequency is $\omega_\beta = Kk_0L/\gamma = 2\pi NK/\gamma$. Typically, with $\gamma \approx 10^2$, $N \approx 10^2$, and $K \approx 1$, we have $\omega_\beta \approx 2\pi$, or one betatron oscillation along the undulator length.

The general solution to the betatron motion is

$$y(\tau) = y_0 \cos(\omega_\beta \tau) + \frac{L\theta_y}{\omega_\beta}\sin(\omega_\beta \tau) \quad , \tag{20}$$

where $y(0) = y_0$ and $\dot{y}(0) = L\,\theta_y$ are the initial conditions, and θ_y is the initial injection angle away from the z axis along the y axis. Both injection on-axis at an angle or injection off-axis at no angle will result in betatron motion. The longitudinal z motion accompanying the transverse betatron oscillations can be derived from $\gamma^{-2} = 1-\bar{\beta}^2$ since $\dot{\gamma} = 0$. In the relativistic limit and near resonance, we can express the modification to the phase velocity as

$$\Delta v_\beta \approx \frac{2\pi N}{1+K^2}\left(K^2k_0^2y_0^2 + \gamma^2\theta_y^2\right) \quad . \tag{21}$$

Note that Δv_β is a constant of motion for the harmonic oscillations in (20) so that an electron's phase velocity does not change as it undergoes betatron focusing. If we require that the initial spread in positions $\bar{y}_0$ does not cause a spread in phase velocities greater than the gain bandwidth, then $k_0\bar{y}_0 \le 1/N^{1/2} \approx 0.1$ for $K \approx 1$.

In an FEL experiment, it is desirable to make the two contributions in (21) comparable because of the properties of electron beam emittance. The electron beam quality that the accelerator and transport system present to the front of the undulator can be described by "emittance", $\varepsilon_y = \pi\bar{y}_0\theta_y$ where $\bar{y}_0$ is the rms initial position of electrons in the beam along y and θ_y is the rms initial angle of electrons in the beam along the y axis. Both $\bar{y}_0$ and θ_y can be changed by focusing fields at the entrance of the undulator, but ε is fixed. A wide beam, with electrons spread randomly over a large range of initial positions y_0, starts the FEL interaction with a broad range in phase velocity, even if the beam is monoenergetic. Likewise, if a small beam is focussed sharply at the undulator entrance, the range of initial angles may degrade the electron bunching. Matching the two contributions to the phase velocity spread requires that $Kk_0\bar{y}_0 \approx \gamma\theta_y$. If we match the contributions, and require that emittance does not spread the electrons beyond the gain bandwidth, then we have $\varepsilon_y \le \lambda_0/4\gamma NK$. Typically (assuming $K = 1$, $N = \gamma = 10^2$, $\lambda_0 = 3$cm), the FEL requires emittance in the range of 1mm-mradian.

The example above provides no focusing of the beam in the x direction. In an experiment, external focusing magnets are often used to confine the beam in both directions even with the aid of betatron focusing. Additional focusing in the x direction can be obtained by shaping the magnetic material providing the field source [105]. The gap between the magnets on either side of the electron beam diminishes so that the rms magnetic field increases in the x direction just as in the y direction. With a parabolic shape to the magnetic pole faces, the focusing can made equal in both x and y, and more importantly maintains the electrons resonance condition along the undulator.

Lienard-Wiechert optical fields

The properties of the electron trajectories in the undulator determine the character of the spontaneous emission spectrum and ultimately the FEL gain. The Lienard-Wiechert potentials [106,107] describe the radiation fields created by the electron's transverse accelerations in the undulator. The Lienard-Wiechert "acceleration field" is proportional to the acceleration $\dot{\beta}_\perp$, and falls off with distance as $1/R$; for most FELs, the instantaneous Coulomb fields are of less importance. Ideal electron trajectories without harmonic content (K is not too large) are inserted into the expressions for the radiation fields. At large distances from the undulator, near the undulator axis, $\gamma\theta \ll 1$, the Lienard-Wiechert electric fields from a helical (H) and linear (L) undulator are

$$E_H' = \frac{4eK\gamma^3k_0}{R}\left(\sin(\omega_u t'), -\cos(\omega_u t'), 0\right) \quad , \quad \text{and} \quad E_L' = \frac{4eK\gamma^3k_0}{R}\left(\sin(\omega_u t'), 0, 0\right) \quad , \tag{22}$$

where the retarded time t' is given by $t' = t - R(t')/c$, $R = |x^* - r^*|$, $r^*(t)$ is the trajectory of a single electron. The frequency of the electron's oscillation in the periodic undulator is $\omega_0 = k_0c$, but the retarded time alters the oscillation frequency of the emitted radiation as seen in the lab. The determination of the radiation polarization from the undulator

polarization is clear. The strength of the radiation field is proportional to the electron acceleration through K, and decays with distance R as expected.

The retarded time describes the relativistic Doppler shift of the radiation and the dependence of the emission frequency on the angle θ. Far away from the undulator, the retarded time t' is given by $t' \simeq t - \hat{n}\cdot\vec{r}(t')/c$ where $\hat{n}$ is the unit vector in the direction of observation. The largest component of the electron trajectory is $\vec{r} \simeq (0, 0, \beta_0 ct)$ with smaller corrections down by factors of K/γ. Solving for the retarded time, we find the fields (22) have the Doppler shifted frequency of the oscillating electrons in the undulator. The retarded time is $t' \simeq 2\gamma^2 t/(1+K^2+\gamma^2\theta^2)$, and the resulting radiation frequency observed is

$$\omega \simeq \frac{2\gamma^2 \omega_0}{1 + K^2 + \gamma^2\theta^2} \quad . \tag{23}$$

This relation gives the frequency of radiation off-axis as well as that already derived on axis. At increasing angle off of the undulator axis, the radiation frequency decreases dramatically as $\theta \rightarrow 1/\gamma$. For a typical electron energy $\gamma \simeq 10^2 \gg 1$, only a small angle $\theta \simeq 10^{-2}$radians is needed to change the FEL frequency by as much as 50%.

Spontaneous emission

The electron trajectories calculated previously remain accurate during spontaneous emission because the radiation loss is small. Even with simple, idealized electron trajectories, the radiation's frequency and angular distributions are complicated since we have just seen that the frequency of emission changes with angle. There are many reasons to understand the spontaneous emission process even though the FEL gain mechanism relies on stimulated emission. Spontaneous emission is necessary for FEL oscillator start-up, or a detailed description of the development of coherence. In the super-radiant amplifier, spontaneous emission in the beginning of the undulator is amplified by the co-propagating, high-current electron beam. In any FEL, the spontaneous spectrum and angular distribution can be useful as a diagnostic tool for the electron beam trajectories and the undulator quality. Harmonics, both coherent and incoherent, are also important to FEL operation.

The relativistic Larmor formula [106] gives the total power emitted from one electron, but with no spectral information. With an ideal helical trajectory, the Larmor formula is easily evaluated, $P = (8\pi r_0^2/3)(2\gamma^2 B^2 c/8\pi)$, and gives a useful physical interpretation of the FEL radiation process. The first factor is recognized as the non-relativistic Thomson scattering cross section, where $r_0 = e^2/mc^2$ is the classical electron radius. The second factor is the energy flux in the approaching helical undulator field as "seen" in the frame of the relativistic electrons. The back-scattering of the virtual photons from the undulator field is the fundamental process of spontaneous emission in the FEL. In the electron's frame, the approaching periodic undulator field is indistinguishable from a powerful, coherent electromagnetic wave; this is the Weizsacker-Williams approximation of the scattering process [106]. Furthermore, we know that the energy of the photons emitted is $\hbar\omega$ and the emission time is L/c; so the transition rate, or emission probability for one electron passing through the undulator is $W_T = (P/\hbar\omega)(L/c) = \pi\alpha N K^2$ where $\alpha = e^2/\hbar c \simeq 1/137$ is the fine structure constant. Typically, $W_T \simeq 1$, so that each electron emits only about one spontaneous photon while passing through the undulator.

We can understand more details of the process by examining the dynamics of the relativistic radiation cone. Radiation from a relativistic particle is confined to a forward cone of angular width $\sim 1/\gamma$. The electron trajectories above give the maximum deflection angle $\sim K/\gamma$ in each undulator period. If transverse motion in the undulator has a large amplitude, the forward radiation cone will periodically deflect out of a detector on-axis at infinity ("the search-light effect" [106]). The requirement for the cone to stay in the detector is $K \leq 1$. If $K \geq 1$, then radiation from several harmonics will appear in addition to the fundamental. However, since we do not use $K \gg 1$ for FELs, the radiation process should be distinguished from broad-band synchrotron radiation and bremsstrahlung.

The complete frequency and angular spectrum can be calculated without much difficulty using ideal trajectories [101-103,108-112]. The intensity distribution $d^2I/d\Omega d\omega$ is the energy radiated into the solid angle $d\Omega$ per unit frequency interval $d\omega$, from one electron. Figure 3 shows the radiated intensity for a linearly polarized undulator with $K = 1$ and $N = 5$. Intensity contours are plotted as a function of $\gamma\theta$ and frequency $\omega/2\gamma^2\omega_0$ with brighter points (white) in the plane indicating peak emission of $[8(e\gamma N)^2/c] \times 0.047$, while black areas indicate no emission; two white contours are superimposed on the intensity plot. The scale at the top can be used to evaluate the intermediate grey emission intensities. The angle θ moves away from the z axis along the x axis. The spectral width of each emission line is determined by the number of periods N and occurs in a narrow range of wavelengths satisfying $\Delta\nu \leq 2\pi$. We have taken $N = 5$ in this example so as to make the regions of emission more clear in the figure; normally, $N \sim 100$ and the regions of emission are much more narrow and well-separated. The frequency at the line center of each harmonic is shifted towards lower frequencies with increasing angle. A number of harmonics are present on and off axis. The number of peaks in each harmonic over the full angular range is equal to the harmonic number in the linear undulator; in the helical case there is no harmonic emission on axis.

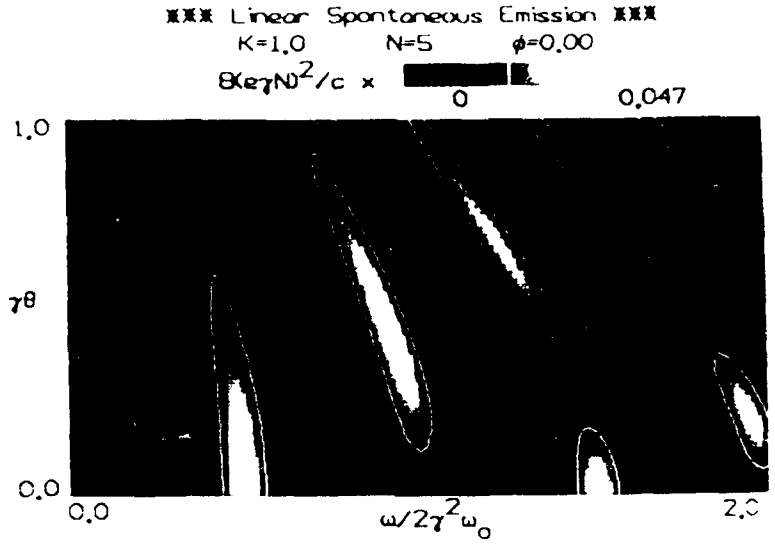

Figure 3. Spontaneous emission from a linearly polarized undulator.

The harmonic emission in either the linear or helical undulator is caused by the fast oscillation of the electron phase ζ in each undulator period as described in (15) and (16). The phase oscillations in both (15) and (16) are negligible when $K \ll 1$, and there is no harmonic emission. The fast oscillation frequency $2\omega_0$ in (15) shows why the emission from the linear undulator above has only even harmonics on axis, and the dependence on θ in (16) shows why the helical undulator only emits harmonics off axis.

Coupling to higher harmonics

Spontaneous emission in the harmonics indicates that gain may also be possible in the harmonics. Several experiments have already observed harmonic emission from an FEL [76,113,114], and harmonic gain has also been measured [115]. Use of harmonics could significantly extend the FEL tunable range to shorter wavelengths; it may also be possible for the FEL oscillator to operate in multiple harmonics simultaneously. The self-consistent, nonlinear wave and electron equations, (8) and (12), can be generalized to describe FEL operation in a single harmonic [101,111]. The fast oscillating phases in (15) and (16) are responsible for harmonic emission, but we actually want to describe the slow evolution about these periodic oscillations and recover a slowly-varying theory. The new dimensionless current densities found below contain the coupling factors that describe the averaged effects of the fast, periodic motion. When used in the combined pendulum and wave equations, (8) and (12) are again valid in both strong and weak fields with high or low gain. We average over one undulator wavelength to get the slowly evolving z velocity, $\bar{\beta}_z$ and define the dimensionless phase velocity as $v(t) = L\,[(k+k_0)\bar{\beta}_z(t) - k\,]$. Integration of $v(t)$ gives the electron phase $\zeta(t) = (k+k_0)\bar{z}(t) - \omega t$ as usual. The averaged equations of motion then define a modified dimensionless current in the linear undulator case,

$$j_L = \frac{8Nh(e\pi K[\,J_{(h-1)/2}(h\xi) - J_{(h+1)/2}(h\xi)\,]L)^2\rho}{\gamma^3 mc^2} \qquad \text{for} \quad h = 1, 3, 5, \ldots \tag{24}$$

where $\xi = K^2/2(1+K^2)$, and h is the harmonic number; $h = 1$ is the fundamental. The cylindrical Bessel functions J_h express a weighted coupling between electrons and light due to the time electrons spend in periodic longitudinal motion while transferring energy to the optical wave. Note that the linear undulator has reduced coupling in the fundamental ($h = 1$) proportional to $[J_0(\xi) - J_1(\xi)]$; for $K \approx 1$, this is only about a 20% reduction. The harmonic coupling diminishes as h increases, but does so slowly if $K \geq 1$.

In the helical undulator, imperfect injection can also cause emission and gain in higher harmonics. The new coupling is calculated in the same manner as discussed above and the modified dimensionless current density is

$$j_H = \frac{8Nh(\pi eKJ_{h-1}(h\chi)L)^2\rho}{\gamma^3 mc^2} \qquad \text{for} \quad h = 1, 2, 3, \ldots \tag{25}$$

where $\chi = K^2/2(1+K^2)$. There is FEL gain even if the electron beam, undulator, or light beam are not perfectly aligned

There is also gain off axis that could be used to tune the FEL wavelength as shown in (23) without changing the FEL electron beam energy. However, confining the electron beam with the optical mode provides an important constraint that limits the tunable range.

Collective high gain

When the dimensionless current density is large $j \gg 1$, the fundamental gain mechanism in the FEL changes in character [46,55,56,61]. The high gain regime is becoming increasing important as accelerators are specifically designed and optimized for the FEL interaction, but presently Table 1 shows that only LLNL has reached $j \approx 10^4$. Maximizing j can depend on several factors. Undulator technology appears to yield $\lambda_0 \sim 3$cm, and the optimization of gain ($j \propto K^2$) without severe harmonic emission establishes that $K \sim 1$; most experiments in Table 1 show only a little variation in these parameters. The electron beam density is determined by the current and the size of the beam, $\rho = 3\times10^9 I(\mathrm{A})/ec\pi r_e^2$ where r_e is the electron beam radius, and the current I(A) is given in Amperes. A typical beam density is $\rho = 10^{12}\mathrm{cm}^{-3}$ for I = 100A and r_e = 1mm radius. If we assume the electron beam size is comparable to the optical mode size $\sqrt{L\lambda/\pi}$, then the dimensionless current depends only on $j \propto IN^3\lambda^{1/2}$. The penalty for increasing the undulator length indefinitely is that the sensitivity to emittance and beam quality increase with N (recall that the gain bandwidth decreases as $1/N$); the penalty for increasing the current indefinitely is that the beam quality from the accelerator begins to decrease. Finally, we see that gain at short wavelengths is more difficult because relativistic electrons traveling nearer the speed of light are more difficult to bunch.

The basic equations (8) and (12) are valid in the high gain regime so we can explore the phase space evolution numerically. In Figure 4, the continuous "fluid" of electrons starts on resonance at $\nu_0 = 0$ in a weak field $a_0 = 0.2$ with j = 50. The electrons are drawn darker as they evolve just as in Figure 2. At the beginning of the undulator near $\tau = 0$ there is no optical gain or phase shift as shown on the right. Because the beam is on resonance, the electrons start bunching at relative phase $\zeta+\phi = \pi/2$, and drive the optical field phase ϕ in (12), but not the amplitude $|a|$. Unlike the evolution seen in Figure 2, the optical phase starts to evolve before the gain. It is when the optical phase increases enough to shift the relative phase $\zeta+\phi$ towards π that gain begins. This is so important that the maximum gain occurs on resonance in the high gain regime, where both the electron bunching and the optical phase evolve the fastest. The height of the separatrix ($\propto |a|^{1/2}$) increases dramatically because of the high gain, $G \approx 19$; the optical phase $\phi(\tau)$ moves the critical points in the separatrix to the left by about $\pi/2$. In the low current case of Figure 2, the optical phase change was negligible, but it is crucial here. The interaction is collective since all electrons interact with each other through the growing optical wave amplitude and phase.

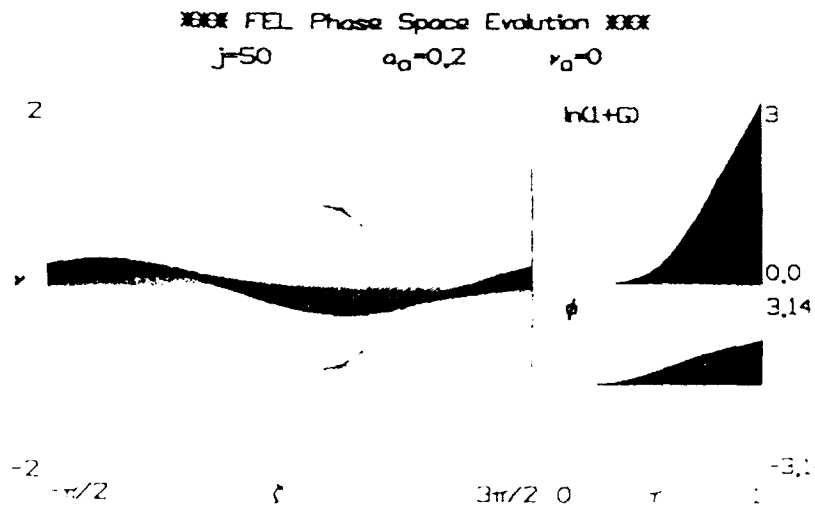

Figure 4. FEL phase-space evolution in the high gain case.

The pendulum and wave equations, (8) and (12), can also be solved analytically in the high gain regime with weak optical field. Strong optical fields cause non-linear behavior, but would also diminish the potentially high gain. In weak field, $|a(\tau)| \ll \pi$, the phase of the ith electron can be expressed as $\zeta = \zeta_0 + \nu_i\tau + \zeta^{(1)}$ where $\zeta^{(1)}$ is the first-order perturbation in $a(\tau)$. Combining the electron and wave equations, and integrating over all initial phases $\int d\zeta_0$, we obtain an integro-differential equation governing the evolution of the optical field [116,117]

$$\overset{\circ}{a}(\tau) = \frac{ij}{2}\int_0^\tau d\tau'\,\tau'\,F(\tau')\,e^{-iv_0\tau'}\,a(\tau-\tau') \quad , \tag{26}$$

where $F(\tau') = \int dq\, f(q) e^{-iq\tau'}$ is the characteristic function of the distribution $f(q)$, $f(q)$ is the distribution of initial electron phase velocities $v_i = v_0 + q$ about v_0, and $\int dq\, f(q) = 1$. All reference to the electron phases has been removed, but there remains an average over the distribution of initial electron phase velocities.

To solve (26), consider a perfect beam at resonance $v_0 = 0$ so $f(q) = \delta(q)$ and $F(\tau') = 1$. Taking successive derivatives, (26) simplifies to $\overset{\circ\circ\circ}{a}(\tau) = ija(\tau)/2$. If the current density is small $j \to 0$, or the evolution time is small $\tau \ll 1$, we have the result $a(\tau) = a_0(1+ij\tau^3/12+...)$ showing the initial growth in the optical phase and no corresponding growth in the optical amplitude. The general solution has three roots describing complex exponential changes of the field. In the high-current limit, $j \gg 1$, the fastest growing root dominates and describes exponential gain $G(\tau) \approx \exp[(j/2)^{1/3}\sqrt{3}\tau]/9$. There is little change in the field during the bunching time, $\Delta\tau \leq (2/j)^{1/3}$, that precedes exponential growth. During this time, the electrons move from their initially uniform phase distribution to bunch near the phase $\zeta+\phi = \pi/2$. As soon as bunching forms, the high current immediately causes exponential field growth and high gain. The large accompanying optical phase shift, $\phi(\tau) = (j/2)^{1/3}\tau/2$, is the distinguishing feature of the high gain regime. Note that FELs with $j \sim 10^4$ have enormous gain $G \sim 10^{12}$ so that saturation is almost assured.

In order to better understand the change from low gain to high gain, Figure 5 shows the surface of gain spectra $\ln(1+G(v_0, j))$ as a function of dimensionless current from $j \ll 1$ to $j = 50$. In the low current region, the gain spectrum is anti-symmetric about resonance $v_0 = 0$ and is given by the third equation in (13), $G = [2-2\cos(v_0)-v_0\sin(v_0\tau)]/v_0^3$. The low-current gain bandwidth is about $\Delta v_0 \approx \pi$. As the current is increased, the gain spectrum distorts to become more symmetric about resonance and the peak gain available increases. The peak of the gain spectrum moves toward resonance, and the spectrum has a long tail for $v_0 < 0$. The high gain bandwidth becomes larger with increasing current and is given by $\Delta v_0 \sim 4j^{1/6}$.

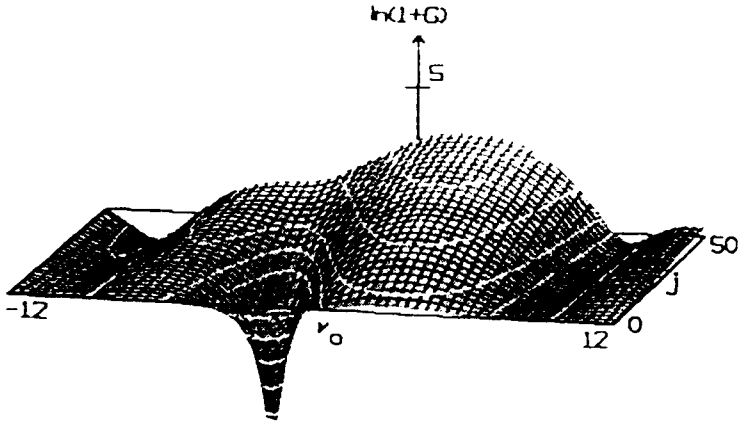

Figure 5. The gain spectrum $G(v_0, j)$ dependence on j.

Gain degradation due to electron beam quality

Most FEL experiments use electron beams that do not fully satisfy the criteria for a perfect beam, and operate with a spread in phase velocities that is about equal to or even greater than the gain bandwidth. Optimizing an FEL design leads to considering $j \propto IN^3\lambda^{1/2}$, but λ is usually determined by the application; the tendency for shorter wavelengths to decrease j makes the burden of optimization even greater on the remaining quantities I and N. Strategy for increasing $j \propto IN^3$ is limited, because increasing I tends to decrease beam quality from the accelerator, and increasing N tends to increase the sensitivity to the beam quality by narrowing the gain bandwidth. Consequently, FELs are often designed to operate in the "warm-beam" regime where there is some, but not too much, gain degradation resulting from the effort to maximize I and N. In strong optical fields $|a| \geq \pi$, where electrons are spread in phase velocity by the FEL interaction itself, the initial spread usually becomes less important in comparison. Therefore, the important warm-beam regime can be explored in the weak-field limit with the integro-differential equation (26). The characteristic function $F(\tau)$ in (26) describes gain degradation through the distribution of initial electron phase velocities $f(q)$ about v_0 [116,117]. Note that $F(\tau)$ and $f(q)$ only depend on the electron's initial conditions with the subsequent dynamics described exactly.

In general, the electron's initial phase velocity ν_0+q will have a random contribution q from a random element of its energy $4\pi N\Delta\gamma/\gamma$, angle $2\pi N\gamma^2\theta^2/(1+K^2)$, and transverse position $2\pi NK^2k_0^2y_0^2/(1+K^2)$ at the beginning of the undulator. For example, a Gaussian energy distribution gives a Gaussian distribution in phase velocity $f_G(q)=\exp[-q^2/2\sigma_G^2]/\sqrt{2\pi}\sigma_G$ about ν_0 where $\sigma_G=4\pi N\Delta\gamma/\gamma$ is the standard deviation. However, because of the quadratic dependence of the phase velocity on entrance angle and position, the phase velocity distribution $f(q)$ is not the same distribution as is the spread in angle or position. In an undulator with small betatron focusing, $\omega_\beta=2\pi NK/\gamma\ll 2\pi$, a Gaussian spread in angles, symmetric in x and y, gives the exponential distribution $f_\theta(q)=\exp(q/\sigma_\theta)/\sigma_\theta$ for $q\le 0$; and $f_\theta(q)=0$ for $q>0$, where $\sigma_\theta=4\pi N\gamma^2\bar{\theta}^2/(1+K^2)$ and θ is the rms angle away from the z axis. An angular spread tends to give an asymmetric distribution in $f(q)$ because small random angles in any direction away from the z axis will only slow down the electrons from ν_0.

In a typical undulator with $K\sim 1$, there would be betatron focusing. Ignoring the lack of focusing in the x direction for simplicity, we can use (20) to find the distribution function $f(q)$ for an electron with rms initial positions $\bar{y}_0$ and angles $\bar{\theta}_y$ along the y axis. With a initial Gaussian distribution in y_0 and θ_y the resulting distribution in phase velocities is

$$f_{\beta_y}(q)=\frac{\exp[\,q\,(\sigma_{\theta y}+\sigma_y)/2\sigma_{\theta y}\sigma_y\,]}{\sqrt{\sigma_{\theta y}\sigma_y}}\,I_0\left[\frac{-q\,|\sigma_{\theta y}-\sigma_y\,|}{2\sigma_{\theta y}\sigma_y}\right]\quad,\quad\text{for}\quad q\le 0\;; \tag{27}$$

and $f_{\beta_y}(q)=0$ for $q>0$, $\sigma_{\theta y}=4\pi N\gamma^2\bar{\theta}_y^2/(1+K^2)$, $\sigma_y=4\pi NK^2k_0^2\bar{y}_0^2/(1+K^2)$, and $I_0(Z)=J_0(iZ)$ is the Bessel function of imaginary argument. When the beam is matched so that $\sigma_{\beta_y}=\sigma_{\theta y}=\sigma_y$, then we recover the exponential distribution $f^m_{\beta_y}(q)=\exp(q/\sigma_{\beta_y})/\sigma_{\beta_y}$ for $q\le 0$; $f^m_{\beta_y}(q)=0$ for $q>0$.

When the distribution function $f(q)$ is found, the characteristic function $F(\tau)=\int dq\,f(q)e^{-iq\tau}$ can be determined and used in (26) to evaluate the evolution of the FEL optical field $a(\tau)$. For the distributions given above, we find the Gaussian spread in energy gives $F_G(\tau)=\exp(-\sigma_G^2\tau^2/2)$, the Gaussian spread in angles away from the z axis gives $F_\theta(\tau)=(1-i\sigma_\theta\tau)^{-1}$, and the betatron focussed beam in the y dimension gives $F_{\beta_y}(\tau)=[(1-i\sigma_{\theta_y}\tau)(1-i\sigma_y\tau)]^{-1/2}$ from (27). The matched beam in (27) has $\sigma_{\beta_y}=\sigma_{\theta_y}=\sigma_y$ so that $F^m_{\beta_y}(\tau)=(1-i\sigma_{\beta_y}\tau)^{-1}$. When a beam is perfect, $\sigma=0$, then $F(\tau)=1$. As the optical field $a(\tau)$ in (26) starts to grow because $j>0$, the integrand containing $a(\tau')$ also grows to further increase the growth rate. In the high current case $j\gg 1$ with $\nu_0=0$, this optical feedback leads to exponential growth of the field. When the beam is not perfect, $\sigma>0$, then the magnitude of the characteristic function $|F(\tau')|$ decays in the integrand of (26) to describe the decay in beam's ability to bunch for a particular distribution $f(q)$. The characteristic time for decay is σ^{-1} so that a poor quality beam with $\sigma\gg\pi$ decays quickly in its ability to bunch. The characteristic function $F(\tau)$ carries with it detailed information describing just how each distribution function $f(q)$ would diminish the FEL's ability to bunch electrons. It can be easily shown that if $f(q)$ is symmetric, then $F(\tau)$ is real, and $f(q)$ is asymmetric, then $F(\tau)$ is complex.

Figure 6 shows the decay of the FEL gain spectrum $\ln(1+G(\nu_0,\sigma_G))$ for a Gaussian spread $f_G(q)$ of increasing width $\sigma_G=0\rightarrow 8$, and low current $j=1$. For all distributions, the characteristic spread that causes decay in the peak gain is $\sigma^*\sim\pi$ as seen in Figure 6. At $\sigma_G=8$, only about one tenth the original gain is available. As σ increases, there are some common features to all types of distributions: the peak gain decreases steadily, the initial phase velocity that gives peak gain increases away from resonance, and the gain bandwidth becomes broader in ν_0. But, the detailed structure of the $G(\nu_0,\sigma)$ surface, and the amount of degradation at any point (ν_0,σ) can be dramatically different for different distributions $f(q)$; as a practical matter, some distributions are clearly better than others giving us a new dimension for FEL design optimization.

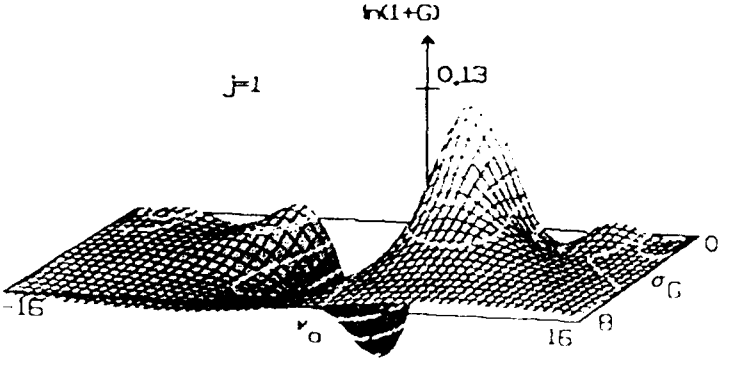

Figure 6. Gain spectrum $G(\nu_0,\sigma_G)$ degradation.

In the high current case $j\gg 1$, the FEL actually becomes more resistant to gain degradation because of the exponential growth in the field $a(\tau)$. The integrand of (26) is only significantly modified by the characteristic function when

$|F(\tau')|$'s rate of decay, the decay of the beam's ability to bunch, is comparable to the optical field's growth rate $(j/2)^{1/3}/2$ in the high-current limit. This comparison gives the characteristic spread $\sigma_j \approx j^{1/3}$ where the beam quality begins to degrade gain in the high-current limit. Since $\sigma_j \propto N$ and $j^{1/3} \propto N$, the resulting relationship does not depend on the undulator length, but on a comparison of growth rates along τ. For $j \sim 10^4$, the increase in the critical spread $\sigma_j \approx 20 \gg \sigma^* \approx \pi$ can be significant. Furthermore, recall that for large j there can be extremely large gain along the undulator, so that even if a beam has $\sigma \geq \sigma_j$ resulting in a large amount of gain degradation, there can be significant and useful gain remaining. The different gains attainable from different distributions becomes greater when the current is large $j \gg 1$, because the potentially high growth rate makes the integrand in (26) sensitive to small differences in the decay of $F(\tau')$. As more experiments begin to operate in the warm beam regime with larger j, the present agreement between FEL theory and experiment might be strained as the distribution function from the accelerator and transport system are not determined accurately enough.

Coulomb forces

As the dimensionless current $j \propto \rho$ is increased, bunching of electrons is resisted by the inter-electron Coulomb potential. We can calculate the Coulomb force on an electron due to the periodic density variation in the bunched beam [56,63,101]. To incorporate the electrostatic force in the electron's equation of motion, evaluate the longitudinal electric field E_z from all other electrons using Poisson's equation. With the same approximations as led to (8), the new pendulum equation has an additional term that depends on the averaged phases of the electrons in the beam,

$$\overset{\circ\circ}{\zeta} = \overset{\circ}{\nu} = |a|\cos(\zeta+\phi) + \frac{j}{4N\xi}\left(\sin(\zeta)\langle\cos(\zeta)\rangle - \cos(\zeta)\langle\sin(\zeta)\rangle\right) \quad , \tag{28}$$

where $\xi = K^2/2(1+K^2)$. The coefficient of the longitudinal Coulomb force can be written as $j/4N\xi = \pi\omega_p^2(1+K^2)$ where $\omega_p = (4\pi e^2\rho/\gamma^3 m)^{1/2}(L/c)$ is the "relativistic plasma frequency" times the "FEL interaction time" L/c. When the beam is uniform, the new term is zero, but non-zero Coulomb forces develop as the optical wave causes bunching. Even without the optical wave, plasma oscillations can grow from any noise source and have the dimensionless frequency $\approx (j/2N)^{1/2}$ when $K \approx 1$. This new frequency of oscillation can alter the resonance condition and the FEL optical wavelength [46,56] in the high current limit. In order to get one plasma oscillation during the FEL interaction time, it is required that $j \geq 2(2\pi)^2 N \sim 10^4$ for $K \approx 1$. We see that Coulomb forces are negligible except for large j and extremely high gains. Typically, there is only a small fraction of a plasma oscillation during $\tau = 0 \rightarrow 1$. Even when $j \sim 10^4$, the relativistic plasma oscillation plays only a minor role in the electron and wave dynamics where there are already dramatic collective effects due to high optical gain.

Strong optical fields, saturation

The Maxwell-Lorentz theory described in (8) and (12) is valid for strong optical fields where $|a| \geq \pi$. The dimensionless field strength is given by several physical variables, $|a| \propto KN^2E/\gamma^2$. The actual optical power density $P = E^2c/8\pi$ that results in strong fields depends on undulator properties, length and strength L and K, and the electron beam energy γmc^2, because they all contribute to the light's ability to change the electron phase ζ. A more energetic electron beam requires more optical power or a longer, stronger undulator, to achieve the same degree of bunching as a less energetic beam. The strong field regime is attained when the electron phase can actually be trapped in the closed orbit region of phase space. The fraction of the electron beam energy converted to light, the FEL's efficiency, is larger than in weak fields, but gain decreases indicating the onset of saturation. The field strengths that give zero growth rate along the FEL amplifier, or steady-state operation in the FEL oscillator are typically far beyond the onset of saturation, and are well into the strong field regime. We first concentrate on the onset of saturation, and how the FEL interaction is modified from the weak field regime.

In weak fields $|a| \leq \pi$, changes in the electron phase $\zeta(\tau)$ remain small so that no electrons overtake, or fall behind, any other electrons in the beam. The result is a smooth distribution in phase as shown in Figures 2 and 4, and calculated in (14). The amount of bunching, or spatial distortion in the beam, can be imperceptibly slight even though the gain, the rate of change of the distortion, may be large. When $|a| \approx \pi$ some electrons with the proper initial conditions can overtake, or fall behind, other electrons in the beam, complicating the distribution in phase $f(\zeta)$. A perfect beam, where all electrons start at a single phase velocity v_0, will have infinite discontinuities in the phase distribution function in strong fields [118]. In reality, the infinite discontinuities would be smoothed by the random imperfections in the phase velocity present in any experiment. The electron bunch is moved too far along the phase axis of phase space, when the field is too strong. Looking at the pendulum equation (8), we see that a bunch, once formed, at the proper relative phase for gain $\zeta + \phi \approx \pi$, would soon evolve by $\Delta\zeta(\tau) \sim |a| \approx \pi$ to the relative phase for absorption $\zeta + \phi \approx 0$.

A bunch formed at the relative phase $\zeta + \phi \approx \pi$ is on a downward path in phase space along the phase velocity axis. It is at this relative phase that electrons lose energy most rapidly and drive the optical wave most efficiently. The energy that can be lost by the bunch is determined by the height of the separatrix path $4|a|^{1/2}$ from peak-to-peak. The change in the phase velocity is $\Delta\nu(\tau) \approx 4|a|^{1/2} \approx 2\pi$ when $|a| \approx \pi$ at saturation. This change in the bunch's phase velocity corresponds to a change in the bunch's energy by $\Delta\nu \approx 4\pi N \Delta\gamma/\gamma \approx 2\pi$. In strong fields, the change in phase velocity is large enough to move the electron bunch across the gain spectrum by as much as the gain bandwidth; the bunch moves from an energy where the

interaction gives gain to an energy where the interaction gives absorption. The fraction of the beam energy that can be extracted by the optical wave as saturation begins is the "natural" efficiency $\eta^* \simeq 1/2N$. A long undulator with $N \gg 1$ may have a larger gain since $j \propto N^3$, but the natural efficiency is reduced. The real efficiency of either an FEL amplifier or oscillator can be much larger than the natural efficiency, since η^* describes just the beginning of saturation, and the corresponding small decrease in gain due to the strong optical fields.

Figure 7 shows the result of solving (8) and (12) numerically with 2000 sample electrons in a strong optical field $a_0 = 20$ and for low current $j = 1$. Initially, the electrons were started with a random Gaussian spread corresponding to $\sigma = 1$ about the phase velocity $\nu_0 = 5$. This phase velocity gives nearly maximum gain at this field strength. The small random spread does not significantly modify the gain in this strong field, but is just included to provide an example of what a spread in phase space looks like. The final phase-space positions of the 2000 electrons are drawn in (ζ,ν) with the optical gain and phase evolution in τ shown at the right. The gain and phase begin to grow rapidly near the beginning of the undulator because of the strong fields and the rapid development of bunching. The best bunching is formed part of the way through the undulator at about $\tau \simeq 1/2$, then the bunch evolves further, past the relative phase $\zeta + \phi = \pi$ around to $\zeta + \phi = 0$. As this occurs, the gain first levels off and then even decreases. The over-bunched electron beam drives the optical wave, but continues to evolve in phase so that energy is actually extracted from the light wave at the end of the undulator, and flows back into the electron beam. The final gain $G \simeq 0.03j$ is significantly reduced from the theoretically possible $G = 0.13j$ in weak optical fields.

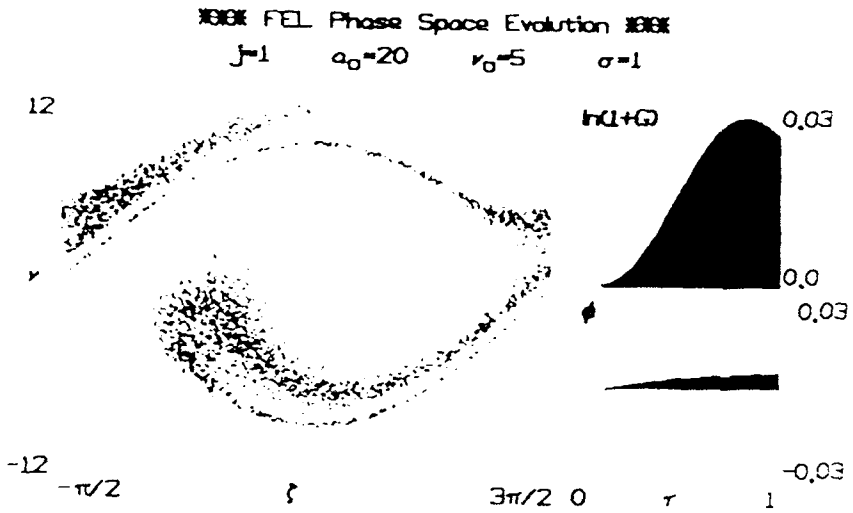

Figure 7. Electron phase-space evolution in a strong optical field.

Not only does the peak gain decrease in strong optical fields, but the gain spectrum $G(\nu_0)$ changes its shape as well. Figure 8 shows the behavior of the FEL gain spectrum as a surface $G(\nu_0, a_0)$. The gain is calculated numerically at each point (ν_0, a_0) with low current $j = 1$. In weak fields $a_0 \leq \pi$, the gain spectrum is anti-symmetric about resonance $\nu_0 = 0$ with a peak value $G = 0.13j$ at the phase velocity $\nu_0 = 2.6$. The peak absorption, or loss, is $G = -0.13j$ at the phase velocity $\nu_0 = -2.6$. The gain bandwidth in weak fields is roughly $\Delta\nu_0 \simeq \pi$. As the initial field strength a_0 increases to 20, the peak gain decreases to about 25% of the weak field value. The phase velocity that gives peak gain increases away from resonance as the field strength a_0 increases. As the gain spectrum decreases and distorts, it also becomes broader in ν_0. The spectral width, from peak gain to peak absorption, roughly follows the full width of the separatrix $4|a|^{1/2}$ as can be seen in Figure 8. This gives yet another, equivalent view of the onset of the saturation process. When the separatrix height $2|a|^{1/2}$ becomes greater than the phase velocity for peak gain in weak fields, $\nu_0 = 2.6$, then an increasingly larger fraction of the beam becomes trapped in the closed orbit region of phase space. The field strength for the onset of particle trapping in strong fields is roughly $a_0 = \pi$ as found before. The gain bandwidth roughly increases with the height of the separatrix above resonance, and is given by $\Delta\nu_0 \simeq 2|a|^{1/2}$ in the strong field regime.

In the FEL oscillator, where the gain is low to moderate, the optical field grows over many passes as new electron pulses from the accelerator continue to amplify it. After each pass, the optical field is a little stronger, and the gain describing the interaction is a little further along the a_0 axis in Figure 8. We expect the relatively narrow optical spectrum to evolve over many passes, and follow the peak gain in Figure 8 as the power grows [68]. Typically, an FEL oscillator will require several hundred passes to evolve from the weak field regime to the strong field regime near saturation. As it does so,

the optical wavelength is observed to shift to longer wavelengths, corresponding to a larger initial phase velocity, just as shown in Figure 8 [69,73]. Note that the general features of diminishing gain due to beam quality in Figure 6 are similar to those due to saturation in Figure 8. This is not a coincidence since the strong field interaction induces a spread in phase velocities about equal to the height of the separatrix $2|a|^{1/2}$. If we were to plot the gain surface shown in Figure 8 as a function of the induced spread $\sigma_a = 2|a|^{1/2}$, Figures 6 and 8 would almost be identical.

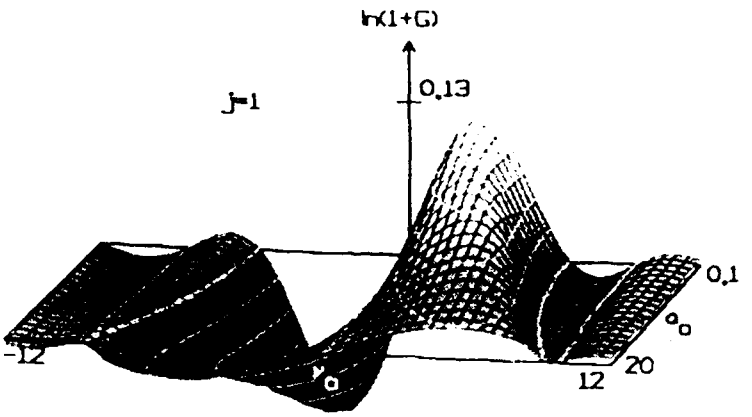

Figure 8. Gain spectrum $G(\nu_0, a_0)$ in strong optical fields.

In the high current regime $j \gg 1$, saturation begins at a different field strength, but the essential physics of saturation is the same as has been discussed in the low current case. In the high gain regime, the optical field magnitude grows as $a(\tau) = a_0 \exp[(j/2)^{1/3}\sqrt{3}\,\tau/2]/3$. The pendulum equation (8) shows that at the field strength $a_j \approx 2(j/2)^{2/3}$ the electron phases can be shifted by as much as $\Delta\zeta(\tau) \approx \pi$ causing the onset of saturation. For $j \sim 10^4$, the saturation field $a_j \approx 200\pi$ can be significantly larger then the low current case as has been observed [85]. The efficiency in the high current limit is also greater than in the low current case. The saturation field a_j causes a change in the electron phase velocity $\Delta\nu_j \approx 2(j/2)^{1/3}$ that corresponds to a change in energy $\Delta\nu \approx 4\pi N \Delta\gamma/\gamma$. The natural efficiency in the high current limit is $\eta_j \approx (j/2)^{1/3}/2\pi N$. For $j \sim 10^4$ and $N \sim 10^2$, the efficiency is typically $\eta_j \approx 0.03$. For the LLNL ELF experiment described in Table 1, $\eta_j \approx 0.09$.

Alternate undulator designs

It was appreciated some time ago that special undulator designs could enhance certain characteristics of the FEL interaction for specific applications [2]. The undulator period and field strength can be varied along the undulator to alter the detailed interaction properties. The analogy in a conventional atomic laser would be to change the properties of the electron binding-potential during the radiative emission time $L/c \approx 10^{-8}$s. This aspect of the FELs design flexibility is one of its most attractive advantages. To illustrate, we consider two designs, the "tapered" undulator and the two-stage "klystron" undulator, that can be characterized by simple modifications to the pendulum equation (8). The goal is to present a clear, simple picture while remaining conceptually accurate. More general designs are possible and will be the subject of continuing research in the future.

At the onset of normal FEL saturation, strong optical fields trap electrons in closed phase-space orbits causing them to lose energy and decrease the interaction strength, or gain. As the energy of the beam decreases by $\Delta\gamma/\gamma < 0$ and shifts across the gain bandwidth, the corresponding change in the beam's phase velocity is $\Delta\nu \approx 4\pi N \Delta\gamma/\gamma \approx -2\pi$. In order to extend this saturation limit, the undulator properties can be altered along z to restore resonance and the interaction strength [52,53]. A change in the resonant phase velocity can be accomplished by "tapering" the undulator wavelength λ_0 along z, or "tapering" the undulator field strength B along z, or both. Each method is conceptually equivalent to providing a longitudinal accelerating field E_z along z to restore the energy of the electrons directly. In weak optical fields, the electron's equation of motion in the tapered undulator is of the form $\nu = \delta\tau + \ldots$ where δ is the artificial acceleration given by $\delta \approx -2\pi N \Delta\lambda_0/\lambda_0$ when the undulator wavelength is decreased, $\Delta\lambda_0 < 0$, or by $\delta = -4\pi N K^2 \Delta B/B(1+K^2)$ when the undulator field strength is decreased, $\Delta B < 0$. With tapering included, the pendulum equation and wave equation have the form

$$\ddot{\zeta} = \dot{\nu} = \delta + |a| \cos(\zeta + \phi) \quad , \quad \dot{a} = -j \langle e^{-i\zeta} \rangle \quad . \tag{29}$$

The self-consistent equations (29) are valid in weak and strong optical fields with either high or low gain, but are not valid when the efficiency is expected to be large. When high efficiency is anticipated, so that the electron energy and undulator

properties change significantly, the more accurate equations of motion (5) and (7) can be used. In the limit of $N \gg 1$, the artificial acceleration can be significant with only a small change in the undulator properties. Then, the dimensionless optical field and current densities are to be evaluated with the un-tapered values of K, λ_0, and L.

When the optical field amplitude is large enough so that $a_0 \geq \delta$, some electrons can be "trapped" in the closed orbits of the pendulum phase space centered near the relative phase $\zeta+\phi \approx \cos^{-1}(-\delta/a_0)$. In stronger fields $a_0 \gg \delta$ with low-to-modest current so that $\phi \approx 0$, roughly 50% of the electrons are trapped near resonance around $\zeta \approx \pi$ and continue to lose energy to the optical field. Tapering is only significant if the artificial acceleration exceeds the height of the separatrix in phase space, $\delta \geq 2a_0^{1/2}$ and the natural deceleration of electrons without taper $\delta \geq 2\pi$. The electrons that are not initially trapped, are accelerated away from resonance and eventually contribute less to the interaction. In this view, tapering is effective because electrons near the gain phase $\zeta \approx \pi$ are trapped, while electrons near the absorption phase $\zeta \approx 0$ are taken away from resonance and eventually stop interacting; the imbalance leads to net gain. While the tapered undulator works better in strong fields, it does not work as well in weak fields as the un-tapered undulator. For moderate tapers in weak fields, the gain reduction is small and simply shifts the position of peak gain to $\nu_0 \approx 2.6-\delta/2$; larger tapers decrease the gain more significantly and distort the gain spectrum [119]. A typical value of δ is given by an undulator with 20% taper in wavelength over $N = 100$ periods, $\delta \approx 40\pi$. For 50% trapping, the efficiency of the tapered undulator is estimated at $\eta \approx \delta/8\pi N \approx 5\%$, and is increased by 10 over the natural efficiency $\eta^* = 1/2N$. An actual FEL system can operate at a power and efficiency greater than these estimates since we have only anticipated where saturation begins. When the current is large $j \gg 1$ we have already seen that the saturation field strength is increased and grows exponentially. As a result, the fraction of the beam trapped can be nearly 100%; an impressive efficiency of 40% has already been observed [85]. Some examples of tapered undulators and their approximate δ are given in Table 1.

While the tapered undulator is designed to enhanced the FEL in strong optical fields, the two-stage optical "klystron" is a design for improved gain in weak optical fields [120-122]. The FEL klystron consists of two undulator sections separated by a drift, or dispersive section. The drift and dispersive mechanisms are the same mathematically, but practically, it is the dispersive section that gives a substantial increase in the FEL gain for a given interaction length. The optical fields in the first undulator section , the "modulator", prepare electrons to bunch as they go through the dispersive section, and then to radiate coherently in the second undulator section, the "radiator". In the dispersive section, the electron-optical interaction is effectively turned off because the electrons are far from resonance. The net change in ζ is then proportional to the modulated value of ν upon exiting the first klystron section $\Delta\zeta = D\nu$, where D is the dimensionless time of the drift, or is a measure of the strength of the dispersive section [122]. The self-consistent equations describing the FEL klystron can be written compactly as

$$\overset{\circ\circ}{\zeta} = \overset{\circ}{\nu} = |a|\cos(\zeta+\phi) \quad , \quad \overset{\circ}{a} = -j\langle e^{-i\zeta}\rangle \quad , \quad \text{for } 0 \leq \tau < 0.5 \text{ , and } 0.5 < \tau \leq 1 \quad , \tag{30}$$

$$\text{and} \quad \Delta\zeta = \nu D \quad , \quad \Delta\nu = 0 \quad , \quad \text{at} \quad \tau = 0.5 \quad .$$

The dispersive interaction is applied instantaneously at $\tau = 0.5$ since we know the analytic solution resulting from the drift. Again, the combined equations (30) are valid in weak and strong optical fields with both high and low current. When (30) is solved analytically in weak optical fields with low current (a_0 and j are both small), and in a strong klystron dispersive section $D \gg 1$, there are many high peaks that appear in the gain spectrum. Near the peak gain, the gain and optical phase shift are

$$G(\nu_0) \approx \frac{jD}{4}\sin(\nu_0 D) \quad , \quad \text{and} \quad \phi(\nu_0) \approx \frac{jD}{8}\cos(\nu_0 D) \quad . \tag{31}$$

The peak gain available in the FEL klystron is $jD/4$ at phase velocity $\nu_0 = \pi/2D$. Typical dispersive sections are designed to give $D \approx 100$ [120]. When the dimensionless current density is low, say $j \approx 10^{-2}$, the klystron design can give $G \approx jD/4 \approx 25\%$ gain where the normal undulator would have much less gain, $G \approx 0.1j \approx 0.1\%$. There are several successful experiments using the FEL klystron concept as shown in Table 1.

Coherence development

The FEL equations presented so far have been restricted to a single mode of the optical field. Because of the relativistic nature of the FEL interaction, modal decompositions in the transverse and longitudinal directions along the beam have different characteristic scale lengths. The natural scale in the longitudinal dimension is determined by the gain bandwidth, $1/2N$, corresponding to the electron-optical slippage distance $N\lambda$; this is the distance that light passes over electrons as the electrons travel through the undulator. At resonance, exactly one wavelength of light passes over an electron as the electron passes through an undulator wavelength; over the whole undulator, N wavelengths of light pass over the resonant electron. The slippage distance $N\lambda$ is the characteristic length over which electrons and light can exchange information during one pass. In the low-gain FEL oscillator, the optical signal develops from spontaneous emission with an initial coherence length of $N\lambda$. Over many passes in the resonator, mode competition can narrow the spectrum significantly and increase the coherence length. In the transverse dimension, the important scale is roughly the radius of the optical beam $(L\lambda/\pi)^{1/2}$ that will double in area due to natural diffraction as it passes through the undulator length L. In the high-gain

amplifier configuration, the transverse mode can be distorted and focussed back into the electron beam in order to extend the interaction over many diffraction lengths. First, we concentrate on the longitudinal modes.

We have assumed a perfectly coherent light wave in the longitudinal direction, and it would useful to understand how this coherence develops from spontaneous emission. In the low-gain oscillator, the modes evolve independently, and can be followed with the theory developed already. Each longitudinal mode, or wavelength $\lambda = 2\pi/k$, is identified by a phase velocity $v(k) = [(k+k_0)\beta_z - k]$; the undulator wavelength and initial electron beam energy from the accelerator are fixed during the evolution over many passes. The FEL gain spectrum $G(\nu)$ with its anti-symmetric shape peaking at $\nu = 2.6$ is determined by the undulator. The spontaneous emission lineshape $s(\nu) \propto [\sin(\nu/2)/(\nu/2)]^2$ is symmetric in shape with a width $\Delta\nu \approx 2\pi$. Figure 9 shows the shapes of the gain and spontaneous emission spectra. On each pass, the power in each mode changes due to the spontaneous emission, the gain, and the loss or output coupling at the resonator mirrors. On the n th pass, the change in the optical power is [40]

$$\Delta P_n(\nu) = s(\nu) + P_n(\nu)[\,G(\nu) - 1/Q\,] \tag{32}$$

where $P_n(\nu)$ is the optical power in mode ν, $s(\nu)$ is the spontaneous emission into mode ν on each pass, $G(\nu)$ is the gain spectrum, and $1/Q$ is the loss on each pass for all modes independent of ν. Only the optical power spectrum $P_n(\nu)$ evolves on each pass.

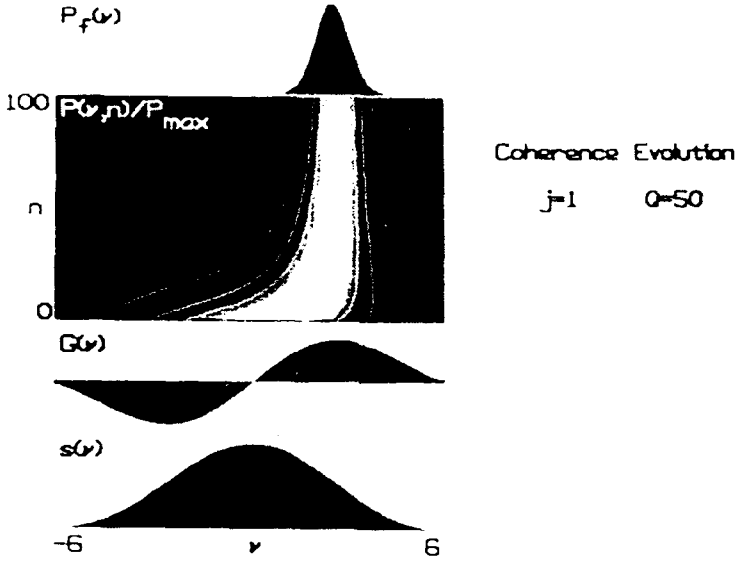

Figure 9. Coherence development and line narrowing in the FEL.

Over many passes, $n = 0 \rightarrow 100$, Figure 9 shows how the normalized optical spectrum $P(\nu,n)/P_{max}$ evolves from spontaneous emission into a narrower spectrum. The peak gain is $G = 0.135j$ with $j = 1$, and the loss is determined by $Q = 50$. The final spectrum is centered around the phase velocity $\nu = 2.6$ at peak gain, and has about 4 times the coherence length of the spontaneous spectrum. As the spectrum continues to narrow, the development of each mode can be expressed as a function of the second derivative of the gain spectrum expanded in a Taylor series about its maximum. A simple expression gives the FEL optical spectrum width after n passes with current j,

$$\Delta\nu \approx 2\pi(nj)^{-1/2} \quad . \tag{33}$$

The physical width of the spectrum is $\Delta\lambda/\lambda \approx (nj)^{-1/2}$. Eventually, at long evolution times, the spectral width is limited by practical noise sources like vibrating optical components. The original Stanford FEL [69] used an accelerator with $n = 10^4$ micropulses in each macropulse burst; the optical spectrum could have narrowed by a factor of 200, but was limited by short pulse effects as described below.

Longitudinal Multimode Theory

More general FEL problems can couple the modes in the longitudinal direction so that a more complete theory is required [47,55,57,91,123-133]. To generalize the optical field in the longitudinal dimension, we follow multiple positions along the complex wave envelope $a(z)$. The extension to spatial modes $a \rightarrow a(z)$ is completely equivalent to an extension in longitudinal wavenumbers $a \rightarrow a(k)$. We normalize all longitudinal distances to the slippage distance so that $z/N\lambda \rightarrow z$. The full extension of the theory uses $a \rightarrow a(z)$, $\nu \rightarrow \nu(z)$, and $\zeta \rightarrow \zeta(z)$; the number of sites N_w needed in a particular

problem is determined by the amount of detail to be followed in the optical spectrum. The optical field sites span a window of width W that is an integral number of slippage distances long; modes that are properly represented in the window are given by

$$\nu_l = \nu_0 - (2\pi/W)(l - N_W/2) \qquad \text{where} \quad l = 0, 1, 2, ..., N_W - 1 \quad , \tag{34}$$

where l is an integer, $W = N_W \Delta z$ and Δz is the spacing between sites. The mode spacing is given by $\Delta\nu = 2\pi/W$, where the window W is typically only a few, to several, slippage distances long; in most cases, $W = 1 \rightarrow 4$ is adequate to characterize FEL phenomena. When the electron pulse and optical pulse are long compared to $N\lambda$, periodic boundary conditions can be imposed at the ends of the window W in order to restrict the number of modes and sites followed [130-133]. The end effects of the periodic boundary conditions are considered non-physical and inconsequential.

The generalized equations for electrons and light are

$$\overset{\circ\circ}{\zeta}_{z+\tau} = |a_z| \cos(\zeta_{z+\tau} + \phi_z) \quad , \quad \overset{\circ}{a}_z = -j_{z+\tau} < \exp(-i\zeta_{z+\tau}) >_{z+\tau} \quad , \tag{35}$$

where the longitudinal field sites z are normalized to the slippage distance $N\lambda$ in the window W, and refer to a position in the optical field envelope. The light, traveling at speed c, remains fixed in z while the slower electrons slip back in the calculational window. A position in the electron pulse is located at site $z+\tau$ at time τ, and slips back by $N\lambda$ in the time $\tau = 0 \rightarrow 1$. The dimensionless current density $j_{z+\tau}$ is a macroscopic variable, and does not distort due to the microscopic bunching on a much smaller scale. When the electrons pass through the undulator, those at a site z interact with a range of sites in the optical wave envelope; in this way, the electron beam and light wave exchange information, and the electrons pass information from one optical field site to another. Often, the site spacing Δz is made equal to the integration time step $\Delta\tau$, so that electrons slip back one site in the calculational window on each time step. In weak optical fields with low gain, the step can be as large as $\Delta\tau = \Delta z = 0.1$; but in strong optical fields or high gain, $\Delta\tau = \Delta z = 0.01$, or smaller, is sometimes necessary. A number of electrons must be followed at each site z as well; the electron phase and phase velocity must be calculated each time step at each site. In weak fields as few as 20 sample electrons at each site is adequate, but in strong fields, a few hundred may be necessary.

Short pulse evolution in the FEL

Many FEL oscillators are driven by short, picosecond long, electron pulses from an RF accelerator. When the electron pulse length is comparable to the slippage distance $N\lambda \approx 1$mm, the modal structure of the pulse current is comparable to the gain bandwidth, and exotic short-pulse effects dominate the FEL interaction [123-129]. Short-pulse behavior is intimately tied to the time development of gain along the undulator. At the lower-left in Figure 10, the current density of a short pulse $j(z+\tau)$ is shown at $\tau = 0$ (black), and at $\tau = 1$ (white) in the calculational window of width $W = 5$. The pulse shape is taken to be parabolic with the form $j(z) = j(1-2z^2/\sigma_z^2)$ for $j(z)>0$, zero otherwise; the pulse is two slippage lengths long, $\sigma_z = 2$, with a peak current of $j = 8$. The optical pulse amplitude $|a(z,n)|$ is shown at the left evolving over $n = 200$ passes through the resonator. The grey scale shows the peak field $|a(z,n)| = 70$ in white, and zero field in black with two contours. On each pass, at $\tau = 0$, the optical wave is not driven because the new electron pulse from the accelerator is not bunched. At a later time $\tau \leq 1$ when bunching develops, the electron pulse slips back, and drives the trailing edge of the light pulse. The light pulse is distorted on each pass because gain is preferentially deposited on the trailing edge of the pulse. Consequently, the center of the light pulse appears to be traveling slower than c even though in vacuum; the effect is called "lethargy" [124]. Exotic short-pulse effects in the FEL have been experimentally and theoretically explored almost as early as the fundamental theory. The agreement between theory and experiment describing this phenomena is probably the best confirmation of our understanding of the FEL.

The rebounding optical pulse, stored in a resonator of length S, arrives at the beginning of the undulator, $\tau = 0$, at intervals $2S/c$; the series of electron pulses from the RF accelerator must be synchronized to arrive at $\tau = 0$ coincident with the light. Define d, the "de-synchronism", as the displacement between the electron and optical pulses at $\tau = 0$ each pass; d is normalized to the slippage distance, as usual, and when $d = 0$, exact synchronism, the electron pulse interval is exactly $2S/c$. At exact synchronism, the lethargic light pulse drifts away from the electron pulse over many passes so that the steady-state FEL power is zero. To compensate for lethargy, the path S must be reduced by $d = -2\Delta S/N\lambda \approx 0.001 \rightarrow 0.05$. In Figure 10 with $d = 0.01$, the advancing of the light pulse is seen in the first 100 passes. Simulations start from an initial seed pulse with small amplitude and arbitrary shape. The gain and resonator loss at the mirrors, determined by $Q = 10$ as in (32), combine to reshape the pulse until steady-state is achieved. The total power, $P(n) = \int dz\, |a(z)|^2$ shown at the lower-right, has increased from the seed pulse to strong-field saturation. The complicated optical pulse shape gives the multimode power spectrum $P(\nu, n)$ shown evolving in the middle. For reference, the single mode gain spectrum $G(\nu)$ is plotted at the bottom-center for $j = 8$. Mode competition keeps the fundamental optical spectrum near peak gain in weak fields, but strong field saturation will move peak gain to larger values of ν as shown in Figure 8. At saturation, the trapped electrons oscillate in the closed orbits of phase space on each pass. Over many passes, the frequency of the trapped particles mixes with the fundamental wavelength to produce sidebands, as will be explored in a later section. At the right is the evolution of the electron phase velocity distribution $f(\nu, n)$ taken at the end of the undulator $\tau = 1$ on each pass; the final spread in phase

velocity becomes broad as the field strength increases. The spread induced by the strong optical fields is roughly given by the peak-to-peak height of the separatrix $4\,|a\,|^{1/2}$.

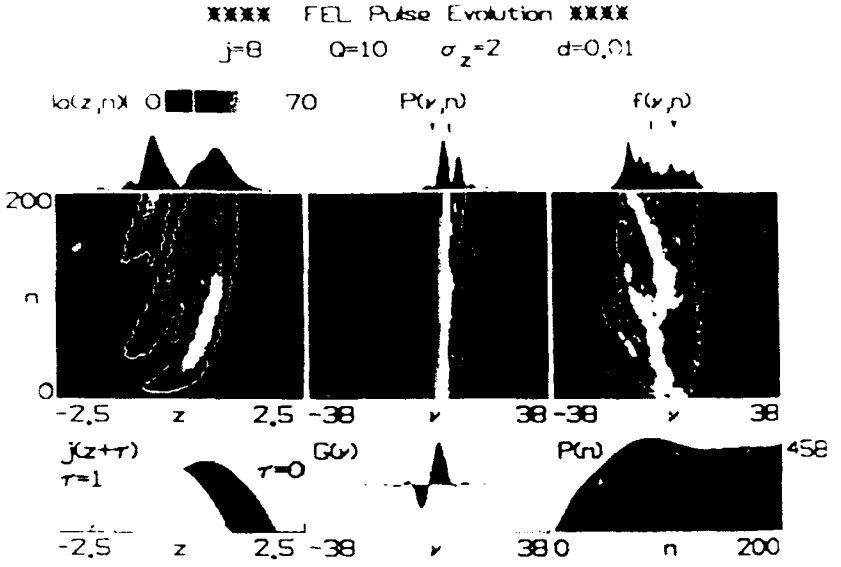

Figure 10. The evolution of short pulses in the FEL.

The general features of short-pulse behavior have now been observed in many simulations and several experiments. At small de-synchronism $d \geq 0$, the power is usually large enough to cause the trapped-particle instability, a broad optical spectrum, and a broad electron distribution. The optical pulse is short and centered on the electron pulse as in Figure 10; it can be modulated with sharp spikes due to the instability. When j and Q are large, the spectrum can be chaotic and much wider than the normal gain bandwidth. At large de-synchronism, the steady-state power is smaller due to the reduced coupling, and the trapped-particle instability cannot occur. The final optical power spectrum and electron distribution are narrow due to the weak optical fields; the center of the optical pulse may actually be ahead of the electron pulse. The microscopic optical pulse length and structure can be altered significantly as the de-synchronism is adjusted. The operating range in d is typically $\Delta d \approx 0.05$, so that the resonator length must be adjusted within a surprisingly small range $\Delta S \approx -10\mu$m.

Transverse mode theory and diffraction

Having extended the single-mode FEL theory in the longitudinal dimension, we now explore an extension in the transverse dimension. The simple wave equation (12) becomes the parabolic wave equation introducing the natural process of diffraction that changes the optical wavefront along the undulator even without the FEL interaction. The theoretical approach is general enough to include betatron motion, arbitrary undulator designs, optical mirror arrangements, and driving currents with no assumptions about x-y symmetry in the transverse dimension. The optical field is given spatial dependence in the transverse and longitudinal dimensions $a(x,y,z,t)$ instead of using a modal decomposition [134].

Anticipating the development of longitudinal coherence, the complex optical field envelop is taken to be slowly varying in z and t with polarization determined by the undulator. The transverse coordinates are normalized to the characteristic mode size $(L\lambda/\pi)^{1/2}$, so that $x(\pi/L\lambda)^{1/2} \rightarrow x$ and $y(\pi/L\lambda)^{1/2} \rightarrow y$. In the longitudinal dimension, we normalize to the slippage distance $N\lambda$, and use the substitution $(z-ct)/N\lambda \rightarrow z$. Introducing the dimensionless time $\tau = ct/L$, the wave equation takes on the form of the parabolic wave equation

$$\left[\frac{i}{4} \nabla_\perp^2 + \frac{\partial}{\partial \tau} \right] a(x,y,z,\tau) = - < j e^{-i\theta} >_{(x,y,z+\tau,\tau)} \tag{36}$$

where $\nabla_\perp^2 = \partial_x^2 + \partial_y^2$. The incremental solution to (36) over distance $\Delta\tau$ is

$$a(x,y,z,\tau+\Delta\tau) = e^{\frac{i}{4}\Delta\tau \nabla_\perp^2} a(x,y,z,\tau) - \Delta\tau < j e^{-i\theta} >_{(x,y,z+\tau,\tau)} + O(j\Delta\tau^2) \tag{37}$$

This solution is exact for any $\Delta\tau$ when there is no current, but when $j > 0$, a small time step $\Delta\tau \ll 1$ is required to accurately integrate the linear term in (37) and the accompanying pendulum equation. To evaluate the diffraction operator

$\exp(i\Delta\tau\nabla_\perp^2/4)$, we work in Fourier space where the operator is diagonal and may be efficiently implemented numerically [134]. The optical wavefronts $a(x,y)$ can now be correctly propagated forward in time, and the beam current will amplify the wave where $j(x,y)$ is non-zero. When the transverse size of the electron beam and the wavefronts are much larger than $(L\lambda/\pi)^{1/2}$, the operator $\exp(i\Delta\tau\nabla_\perp^2/4) \approx 1$ over the propagation distance $\Delta\tau = 1$, and diffraction can be neglected. The self-consistent evolution of the electron current is governed by the Lorentz force equation for each electron in the beam. The pendulum equation has the same form as before with $\zeta \to \zeta(x,y,z+\tau,\tau)$ and $v \to v(x,y,z+\tau,\tau)$. The theory is now fully self-consistent in 4 dimensions (x,y,z,τ); a simulation would introduce arrays of sites in (x,y) at each longitudinal site z in (35). The 3D electron array in (x,y,z) moves with respect to the 3D optical array at every step $\Delta\tau$ because of slippage.

The solution to (37) in free space ($j = 0$) is called a "Gaussian" beam after its shape in the transverse dimension,

$$a_G(r,\tau) = \frac{a_0}{w(\tau)} \exp[-r^2/w^2(\tau)z_0] \exp[i\phi(\tau)] \quad , \quad \text{and} \quad \phi(\tau) = -\tan^{-1}[(\tau-\tau_w)/z_0] + \frac{r^2(\tau-\tau_w)}{z_0^2 + (\tau-\tau_w)^2} \quad , \qquad (38)$$

where $r = (x^2+y^2)^{1/2}$, $w^2(\tau) = 1+(\tau-\tau_w)^2/z_0^2$, and the dimensionless optical wave amplitude is $a_0 = 4\pi NeKLE/\gamma^2 mc^2$ as usual, where E is the physical electric field amplitude at the center ($r=0$) of the mode's waist positioned at τ_w. The dimensionless Rayleigh length is $z_0 = \pi w_0^2/L\lambda$ where w_0 is the physical radius of the mode waist; z_0 is the physical Rayleigh length $(\pi w_0^2/\lambda)$ compared to the undulator length L. As $z_0 \to \infty$, so that $w \to 1$, $\phi \to 0$, we have plane waves of infinite extent. The radius of the wavefront is $z_0^{1/2}$ at the waist $\tau = \tau_w$, and spreads due to diffraction as τ moves away from τ_w; the area of the beam doubles as it propagates a distance $\Delta\tau = z_0$.

Electron dynamics in a Gaussian optical mode

In the low gain FEL oscillator configuration, the optical mode is primarily determined by the resonator and diffraction. The radius of curvature, R_c, of resonator mirrors that are separated by S gives a dimensionless Rayleigh length $z_0 = (2SR_c - S^2)^{1/2}/2L$; typically, R_c is comparable to the undulator length L so that $z_0 \sim 1$. To illustrate some of the effects of the Gaussian beam on the electron dynamics, consider the pendulum equation in the weak optical field (38) $a_0 \ll 1$ with low current and a large Rayleigh length $z_0 \gg 1$.

$$\ddot{\zeta} = \dot{v} = a_0 \exp[-r^2/z_0] \cos[\ \zeta_0 + (1-r^2/z_0)/2z_0 + (v_0 - (1-r^2/z_0)/z_0)\tau + \ldots\ ] + \ldots \quad , \qquad (39)$$

where we have taken $\tau_w = 0.5$ so that the mode waist is optimally centered along the undulator. The field strength seen by electrons diminishes off the mode axis, and the initial electron phase is altered; since the electrons are initially spread randomly, the new phase is inconsequential. However, the phase velocity of the electrons is shifted by the diffracting optical field; $v_0 \to v_0 - (1-r^2/z_0)/z_0$. The phase velocity for maximum gain is now $v_0^{max} = 2.6 + (1-r^2/z_0)/z_0$, and the resonant optical wavelength is shifted by $\Delta\lambda/\lambda = (1-r^2/z_0)/2\pi N z_0$. When the electrons approach the mode waist $z_0^{1/2}$, the shift goes to zero, but at the center of the mode $r=0$, the shift can be as large as the gain bandwidth when $z_0 \approx 1$ [100].

If the Rayleigh length is much larger than the undulator length, the optical mode is too wide, and the field amplitude that bunches electrons diminishes. If the Rayleigh length is much smaller than the undulator length, the optical phase shift can upset bunching and diminish gain. Solving the pendulum equation numerically in the field (38) with $r = 0$, the optimum Rayleigh length has been found to be $z_0 \sim 0.3$ in weak optical fields [100].

FEL optical self-guiding

In the case of large current $j \gg 1$, the transverse optical mode can be significantly distorted by the electron beam. It has been shown theoretically that the large optical phase shift associated with the high-current regime actually focuses the light back into the electron beam [135-137]. This is an important practical advantage for the high-gain amplifier configuration where natural diffraction would provide a limitation to a long undulator length. The effect is called "optical guiding", and allows the electron beam and light to continue interacting over many Rayleigh lengths.

In order to understand optical guiding, consider a small electron beam in the middle of a co-propagating optical wave. In free space, the optical phase at the center of a wavefront evolves as $\Delta\phi = -\Delta\tau/z_0$ for a small step $\Delta\tau$. The FEL interaction also modifies the wavefront as described in (36). If we average (36) over the transverse Gaussian mode area πz_0 for a small step $\Delta\tau$, we can approximately recover the simple form (12) with the new dimensionless current $j \to jF$ where the "filling factor" $F = \pi\sigma_r^2/\pi z_0$ is the ratio of the electron beam area to the optical mode area [1]. The quantity $jF \propto \rho F$ does not depend on the electron beam area, but only on the current within the optical mode. In the high-current regime where $jF \gg 1$, the optical phase evolves as $\Delta\phi = -(jF/2)^{1/3}\Delta\tau/2$. We see that FEL interaction induces a phase shift that is opposite in sign of natural diffraction, and therefore focuses the light back into beam along τ.

In order for optical guiding to persist, the FEL interaction must continually compensate for the phase shift associated with free space diffraction at each step $\Delta\tau$; that is, $(jF/2)^{1/3}\Delta\tau/2 \approx z_0$. The critical current density needed for optical guiding is $jF \approx 8/\sigma_r^2$. An FEL utilizing a small electron beam and a small optical wavefront (with a correspondingly short Rayleigh length), requires a larger current density for guiding. When the initial optical wavefront is matched into the electron beam, we would expect that the filling factor F is not too small; we use $\sigma_r^2 \approx z_0/2$ to write a

simpler relation estimating the critical current density needed for optical guiding,

$$j^* \simeq 32\, z_0^{-3} \quad . \tag{40}$$

If the normalized Rayleigh length is small, say $z_0 = \pi w_0^2 / L\lambda = 0.2$, natural diffraction would spread the light over a large transverse area after the interaction length $\Delta\tau = 1$. Optical guiding can compensate in a typical high-current case where $j \simeq 10^4 > j^* \simeq 4\times 10^3$. Note that the relations $j^* \simeq 16 z_0^{-2}\sigma_\perp^{-2}$ and $j^* \simeq 32\, z_0^{-3}$ do not depend on the length of the undulator L, but express a comparison between the rates of natural diffraction and FEL focusing along τ.

Figure 11 shows a simulation that solves (36), together with the pendulum equation, numerically to illustrate FEL optical focusing. The electron pulse is taken to be long, so that no z dependence is followed; in the transverse dimension, the electron beam is symmetric in x-y with the parabolic shape $j(r) = j(1-r^2/2\sigma_x^2)$ for $j > 0$, and $\sigma_x = 0.4$. The peak density is $j = 200$, and the initial phase velocity of the beam is $\nu_0 = 0$ for maximum gain in the high-current case. A Gaussian optical mode is focused near the beginning of the undulator at $\tau_w = 0.01$ with a Rayleigh length $z_0 = 0.2$, and an initial field strength $a_0 = 10$ at the center of the mode. The field amplitude $|a(x,\tau)|$ grows along τ, and reaches a peak value $|a(0,1)| \simeq 33$ (white) at the end of the undulator; points of zero field amplitude are shown as black. The scale at the top-right indicates the field amplitudes plotted in grey, and several contours following points of constant amplitude are superimposed. Without the FEL interaction, the mode would smoothly spread in z because of natural diffraction, but the contours show how the wavefront is focused back into the electron beam.

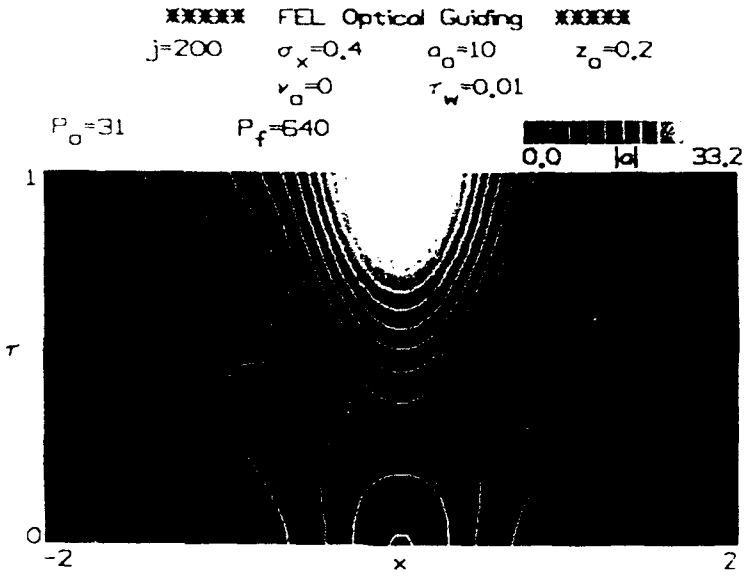

Figure 11. Optical guiding in the FEL.

The trapped-particle instability

The extensions explored so far have considered effects in the longitudinal and transverse dimensions up to the onset of saturation. Typically, the FEL amplifier or oscillator can go beyond the onset of saturation, and may well encounter the trapped-particle instability [130-133,138,139]. In the simulation of short pulses, we noticed that the optical spectrum developed sidebands at saturation. In order to study the effect without the complications of a short pulse, periodic boundary conditions may be taken at the ends of the computational window W. Physically, this corresponds to studying a long pulse, or a CW beam, where translational invariance can be used to examine only one of many repeated sections in the optical mode. Relation (34) determines the mode spacing and spectral width that can be represented. The periodic boundary condition is applied to each variable $\zeta(z-W/2) = \zeta(z+W/2)$, $\nu(z-W/2) = \nu(z+W/2)$, and $a(z-W/2) = a(z+W/2)$.

The origin of the instability starts with the motion of trapped electrons in phase-space [138]. When the FEL reaches high-power saturation, the height of the separatrix is large, and many electrons are trapped in the closed orbits of phase-space. If the current density is not too large, further evolution of the optical field is slowed due to the reduced gain at saturation. The electrons trapped in the center of the phase-space, near the critical point at phase $\zeta^* = \pi/2$, execute [illegible]. The motion of the trapped electrons near phase ζ^* is described by

$$\zeta(\tau) \approx \zeta^* + \frac{v_0}{v_S} \sin(v_S \tau) \tag{41}$$

for the initial position (ζ^*, v_0). The synchrotron, or trapped-particle, oscillation frequency is $v_S = (a_0 \sin(\zeta^*))^{1/2} \approx a_0^{1/2}$. When substantial current is trapped, and oscillates at frequency v_S, the wave equation drives multiple frequencies around the fundamental. The sidebands appear at $v_0 \pm v_S$, and are shifted away from the fundamental wavelength by $\Delta\lambda/\lambda = v_S/2\pi N$. The fractional shift is simply interpretated as the ratio of the "number of synchrotron oscillations along the undulator" to the number of undulator periods. The field strength required to cause one oscillation of the trapped electrons is $a_0 \approx 4\pi^2 \approx 40$. The corresponding peak-to-peak height of the separatrix is $4a_0^{1/2} \approx 25$, so that most beam quality effects are minimized.

Figure 12 shows the result of a simulation with periodic boundary conditions in a window of width $W = 2$, corresponding to two slippage distances along the beam. The long electron beam is described by current $j = 8$ at all points in the window, and interacts with the optical field window for $n = 200$ passes. Each pass, the electrons start uniformly spread in phase at each site z, and at phase velocity $v_0 = 3$. The resonator loss on each pass is determined by $Q = 6$ as in (32). Without some source of noise, every site z would evolve identically, and no spectral features could develop. We start the real part of the optical field with a random component of standard deviation $\delta a = 1$ in a normal distribution about the average value $a_0 = 1$. The resulting steady-state solution is insensitive to the noise source; many alternate noise sources have been tried, with the same final result. The simulation results do not depend on a_0, δa, or even v_0. (If $v_0 = -2.6$ were used, so that there is initially absorption, the small frequency components at $v = 2.6$, due to the noise, would grow over many passes until the same final result as Figure 12 is attained; the only difference would be the larger number of passes required to reach steady-state). The electrons and light slip past each other in the calculational window W, just as in the short pulse simulation of Figure 10.

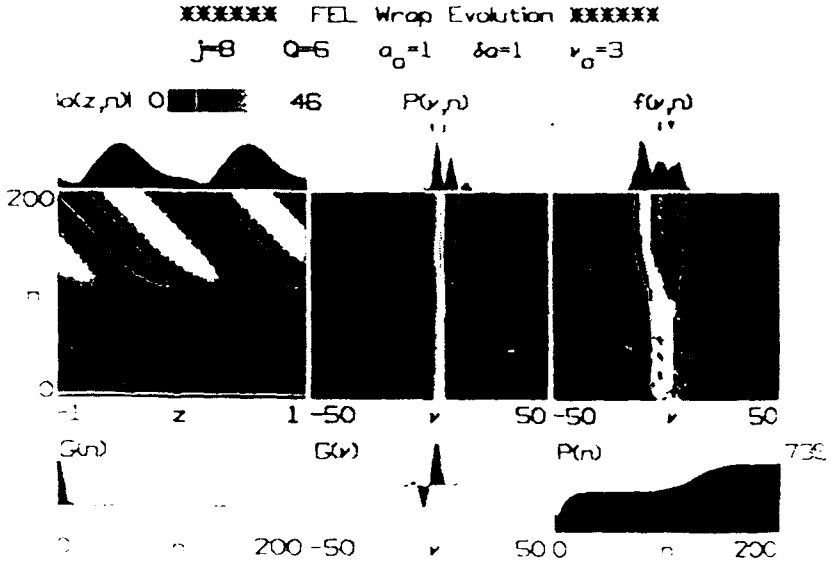

Figure 12. The trapped-particle instability with periodic boundary conditions.

In Figure 12, the power grows to normal saturation rapidly, in about 20 passes. At normal, single-mode saturation, the $G(n)$ (shown at the bottom-left) drops, and the optical power $P(n)$ (shown at the bottom-right) is constant for about 100 passes. During this time, the optical field amplitude $|a(z,n)|$ evolves (shown at the left) and develops a modulation equal to one slippage distance; the calculational window is two slippage lengths long. The grey scale shows the peak field amplitude $|a(z,n)| = 46$ in white, and zero field in black with two contours. The onset of the trapped-particle instability begins when the optical power is sufficient to cause one synchrotron oscillation of the trapped electrons on each pass. As the electrons slip back past the optical field sites and execute one synchrotron oscillation, they modulate the wave envelop. The power spectrum $P(\nu,n)$ shows the sideband frequency associated with the modulation of the field envelop. The peak field of $|a| = 26$ is reached after $n = 200$ passes, and a dynamic steady-state is achieved. The modulation peaks continues to move [illegible] the sideband at a steady rate over many passes n; the total power and power spectrum remain constant. When the trapped-particle instability saturates at about 180 passes, the extra power in the sideband increases the total power in the [illegible] the electron's phase velocity distribution $f(\nu,n)$ is shown at the right; the extra spread and energy [illegible] the instability grows.

The general features of trapped-particle instability in the FEL oscillator depend only on the dimensionless current j and the loss factor Q. Increasing either j or Q makes the trapped-particle instability more severe. Numerically, some source of noise is essential, but the details are not important. In steady-state, there are just a few synchrotron oscillations of the trapped electrons in each pass. Over many passes, the optical wave "sees" many repeated synchrotron oscillations at the same frequency, and the sidebands grow to saturation. Most of the normal values of j and Q give rise to the instability as has been observed experimentally in the LANL FEL [82]. In fact, it is not easy to make j and Q small enough so that just a single sideband occurs as shown in Figure 12. A slight increase in either j or Q will produce more sidebands at multiples of ν_S away from the fundamental; then a chaotic spectrum with many lines develops. The chaotic spectrum [132] does not reach a steady-state, and is several times wider than the normal gain bandwidth.

The FEL amplifier with high current density $j \gg 1$ can reach high power in a single pass. The growth rates are large enough that electrons can be trapped early in the undulator, and begin executing synchrotron oscillations. There can be several to tens of synchrotron oscillations along the undulator, but these are the only oscillations experienced by the optical field. Even with far fewer synchrotron cycles than in the oscillator case, the large current density j can give significant sideband gain once trapping occurs. The sources of noise are much more important in the FEL amplifier than in the FEL oscillator. Suppression of input noise at the sideband frequency could be an important method for avoiding the trapped-particle instability in amplifiers.

Acknowledgments

The author is grateful for support of this work by the Lawrence Livermore National Laboratory, the U.S. Office of Naval Research, and the Los Alamos National Laboratory.

References

[1] J. M. J. Madey, J. Appl. Phys. **42**, 1906 (1971).
[2] J. M. J. Madey, *Stimulated Emission of Radiation in Periodically Deflected Electron Beam*, U.S. Patent 3,822,410 (1974).
[3] L. R. Elias, W. M. Fairbank, J. M. J. Madey, H. A. Schwettman, T. I. Smith, Phys. Rev. Lett. **36**, 717 (1976).
[4] D. A. G. Deacon, L. R. Elias, J. M. J. Madey, G. J. Ramian, H. A. Schwettman and T. I. Smith, Phys. Rev. Lett. **38**, 892 (1977).
[5] R. M. Phillips, I. R. E. Trans. Electron Devices, **7**, 231 (1960).
[6] H. Motz and M. Nakamura, Ann. of Phys. **7**, 84 (1959).
[7] Proceedings of the First Free Electron Laser Conference, Telluride, CO, eds. S. F. Jacobs, M. Sargent, III, and M. O. Scully, *Physics of Quantum Electronics*, Vol. **5** (Addison-Wesley, 1978).
[8] Proceedings of the Second International Free Electron Laser Conference, Telluride, CO, eds. S. F. Jacobs, H. S. Pilloff, M. Sargent, III, M. O. Scully, and R. Spitzer, *Physics of Quantum Electronics*, Vol. **7** (Addison-Wesley, 1980).
[9] Proceedings of the Third International Free Electron Laser Conference, Sun Valley, ID, eds. S. F. Jacobs, H. S. Pilloff, M. Sargent, III, M. O. Scully, and R. Spitzer, *Physics of Quantum Electronics*, Vol. **8** & **9** (Addison-Wesley, 1982).
[10] Proceedings of the Fourth International Free Electron Laser Conference, Bendor Island, France, eds. M. Billardon and D. A. G. Deacon, *Bendor Free Electron Laser Conference*, Journal de Physique, Colloq. **C1-44** (Feb. 1983).
[11] Proceedings of the Fifth International Free Electron Laser Conference, Orcas Island WA, eds. C. A. Brau, S. F. Jacobs, and M. O. Scully, *Free Electron Generators of Coherent Radiation*, SPIE (Int. Soc. Opt. Eng.) **453** (1984).
[12] Proceedings of the Sixth International Free Electron Laser Conference, Castelgondolfo, Italy, eds. J. M. J. Madey and A. Renieri, *Free Electron Lasers*, Nucl. Instr. & Methods in Phys. Res. **A237** (North-Holland Publishing, Amsterdam, 1985).
[13] Proceedings of the Seventh International Free Electron Laser Conference, Tahoe City, CA, eds. E. T. Scharlemann and D. Prosnitz, *Free Electron Lasers*, Nucl. Instr. & Methods in Phys. Res. **A250** (North-Holland Publishing, Amsterdam, 1986).
[14] Proceedings of the Eighth International Free Electron Laser Conference, Glasgow UK, ed. M. Poole, *Free Electron Lasers*, Nucl. Instr. & Methods in Phys. Res. **A259** (North-Holland Publishing, Amsterdam, 1987).
[15] International Conference on LASERS '79, Orlando, FL (Dec. 1979).
[16] International Conference on LASERS '80, New Orleans, LA (Dec. 1980).
[17] International Conference on LASERS '81, New Orleans, LA (Dec. 1981).
[18] International Conference on LASERS '82, New Orleans, LA (Dec. 1982).
[19] International Conference on LASERS '83, San Francisco, CA (Dec. 1983).
[20] International Conference on LASERS '84, San Francisco, CA, (Nov. 1984).
[21] International Conference on LASERS '85, Las Vegas, NV (Dec. 1985).
[22] International Conference on LASERS '86, Orlando, FL (Nov. 1986).
[23] Special Issue of IEEE Journal of Quantum Electronics, QE-17, No. 8 (Aug. 1981).
[24] Special Issue of IEEE Journal of Quantum Electronics, QE-19, No. 3 (Mar. 1983).
[25] Special Issue of IEEE Journal of Quantum Electronics, QE-21, No. 7 (Jul. 1985).

[26] Special Issue of IEEE Journal of Quantum Electronics, QE-23, No. 9 (Sept. 1987).
[27] Nucl. Instr. & Methods in Phys. Res., eds. R. Bonifacio, F. Casagrande, C. Pellegrini, A239, (North-Holland Publishing, Amsterdam, 1985).
[28] *Free Electron Generation of Extreme Ultraviolet Coherent Radiation*, eds. J. M. J. Madey and C. Pellegrini, AIP Conference Proceedings, New York (1984).
[29] Proceedings of the Workshop on Applications of Free Electron Lasers, eds. D. A. G. Deacon and A. De Angelis, Applications of Free Electron Lasers (North-Holland, Amsterdam, 1985).
[30] W. B. Colson, Nucl. Instr. & Methods in Phys. Res. A237, 1 (1985).
[31] *Short Wavelength Coherent Radiation: Generation and Applications*, eds. D. T. Attwood, J. Bokor, Optical Science and Engineering Series 7, AIP Conference Proceedings No. 147, New York (1986).
[32] H. Motz, Contemp. Phys. 20, 547 (1979).
[33] D. Prosnitz, "Free electron lasers." CRC Handbook of Laser Science and Technology 1, ed. M. J. Weber, p. 425, Boca Raton (CRC Press, 1982).
[34] P. Sprangle and T. Coffey, Physics Today, 44 (1984).
[35] W. B. Colson and A. M. Sessler, Ann. Rev. Nucl. Part. Sci. 35,25 (1985).
[36] G. Dattoli, A. Renieri, Experimental and Theoretical Aspects of the Free Electron Laser, in Laser Handbook 4, ed. M. L. Stitch and M. S. Bass (North-Holland, Amsterdam, 1985).
[37] A. M. Sessler and D. Vaughan, American Scientist, 75, 35 (1987).
[38] T. C. Marshall, *Free Electron Lasers* (MacMillan, New York, 1985).
[39] W. B. Colson, Phys. Lett. A59, 187 (1976).
[40] P. Bosco, W. B. Colson, and Roger A. Freedman, IEEE Journal of Quantum Electronics, QE-19, 272 (1983).
[41] F. A. Hopf, P. Meystre, M. O.Scully, W. H. Louisell, Phys. Rev. Lett. 37, 1342 (1976).
[42] W.B. Colson, Phys. Lett. 64A, 190 (1977).
[43] W.B. Colson and S. K. Ride, Phys. Lett. 76A, 379 (1980).
[44] A.Bambini, A. Renieri, and S. Stenholm, Phys. Rev., 19A, 2013 (1979).
[45] V. N. Baier and A. I. Milstein, Phys. Lett., 65A, 310 (1978).
[46] N. M. Kroll and W. A. McMullin, Phys. Rev., 17A, 300 (1978).
[47] H. Al-Abawi, F. A. Hopf, G. T. Moore, and M. O. Scully, Opt. Commun., 30, 235 (1979).
[48] P. Sprangle, C. Tang, and W. Manheimer, Phys. Rev. Lett., 43, 1932 (1979).
[49] D. B. McDermott and T. C. Marshall, *Physics of Quantum Electronics*, Jacobs et al., Eds. Reading, MA, Addison-Wesley, Chap. 18 (1980).
[50] T. Kwan, J. M. Dawson, and A. T. Lin, Phys. Fluids, 20, 581 (1977).
[51] A. T. Lin and J. M. Dawson, Phys. Rev. Lett., 42, 1670 (1979).
[52] N. M. Kroll, P. L. Morton, and M. N. Rosenbluth, *Physics of Quantum Electronics*, 7, 89 (1980).
[53] N.M. Kroll, P.L. Morton, and M.N. Rosenbluth, Journal of Quantum Electronics QE-17, 1436 (1981).
[54] W. B. Colson, *Physics of Quantum Electronics*, 5, 157 (1980).
[55] W. B. Colson and S. K. Ride, *Physics of Quantum Electronics*, 7, 377 (1980).
[56] C.-C. Shih, A. Yariv, IEEE Journal of Quantum Electronics QE-17, 1387 (1981).
[57] G. Dattoli, A. Marino, A. Renieri and F. Romanelli, IEEE Journal of Quantum Electronics, QE-17, 1371 (1981).
[58] W. B. Colson, *Free Electron Laser Wave and Particle Dynamics*, in the International Summer School of Quantum Electronics, A.Renieri and S. Martellucci, Eds. New York, Plenum (1981).
[59] W. B. Colson, *Physics of Quantum Electronics*, 8, 457 (1982).
[60] C.-M. Tang, and P. Sprangle, J. Appl. Phys. 53, 831 (1982).
[61] R. Bonifacio, C. Pellegrini, L. M. Narducci, Opt. Commun. 50, 373 (1984).
[62] D. Prosnitz and A. M. Sessler, *Physics of Quantum Electronics* 9, 651 (1982).
[63] E. T. Scharlemann, W. M. Fawley, B. R. Anderson and T. J. Orzechowski, Nucl. Instr. & Methods in Phys. Res. A250, 150 (1986).
[64] J. S. Wurtele, E. T. Scharlemann and A. M. Sessler, Nucl. Instr. & Methods in Phys. Res. A250, 176 (1986).
[65] B. D. McVey, Nucl. Instr. & Methods in Phys. Res. A250, 449 (1986).
[66] D. C. Quimby, Nucl. Instr. & Methods in Phys. Res. A250, 456 (1986).
[67] T. J. Orzechowski, E. T. Scharlemann and D. B. Hopkins, Phys. Rev. B35, 2184 (1987).
[68] W. B. Colson and R. A. Freedman, Phys. Rev. A27, 1399 (1983).
[69] J. N. Eckstein, J. M. J. Madey, K. Robinson, T. I. Smith, S. Benson, D. Deacon, R. Taber, and A. Gaupp, *Physics of Quantum Electronics* 8, 49 (1982).
[70] R. W. Warren, B. E. Newnam, J. G. Winston, W. E. Stein, L. M. Young, and C. A. Brau, IEEE Journal of Quantum Electronics QE-19, 391 (1983).
[71] J. M. Slater, J. L. Adamski, D. C. Quimby, T. L. Churchill, L. Y. Nelson, and R. E. Center, IEEE Journal of Quantum Electronics QE-19, 374 (1983).
[72] T. A. Eneglotter, H. Boehmer, M. Z. Caponi, S. Fornaca, J. Munch, G. R. Neil, B. Saur, and C. Shih IEEE Journal of

Quantum Electronics, QE-19, 316 (1983).
[73] B. E. Newnam, R. W. Warren, R. L. Sheffield, J. C. Goldstein, and C. A. Brau, Nucl. Instr. & Methods in Phys. Res. A237, 187 (1985).
[74] J. A. Edighoffer, G. R. Neil, C. E. Hess, T. I. Smith, S. W. Fornaca, and H. A. Schwettman, Phys. Rev. Lett., 52, 344 (1984).
[75] P. Elleaume, J. M. Ortega, M. Billardon, C. Bazin, M. Bergher, M. Velghe, and Y. Petroff, Journal de Physique, 45, 989 (1984).
[76] G. A. Komyukhin, G. N. Kulipanov, V. N. Litvinenko, N. A. Mesentsev, A. N. Skrinsky, N. A. Vinokurov and P. D. Voblyi, Nucl. Instr. & Methods in Phys. Res. A237, 281 (1985).
[77] U. Bizzarri, F. Ciocci, G. Dattoli, A. De Angelis, G. P. Gallerano, I. Giabbai, G. Giordano, T. Letardi, G. Messina, A. Mola, L. Picardi, A. Renieri, E. Sabia, A. Vignati, E. Fiorentino, and A. Marino, Nucl. Instr. & Methods in Phys. Res. A250, 254 (1986).
[78] M. Billardon, P. Elleaume, Y. Lapierre, J. M. Ortega, C. Bazin, M. Bergher, J. Marilleau, and Y. Petroff, Nucl. Instr. & Methods in Phys. Res. A250, 26 (1986).
[79] L. R. Elias, J. Hu and G. Ramain, Nucl. Instr. & Methods in Phys. Res. A237, 203 (1985).
[80] R. Barbini, G.Vignola, S. Trillo, R. Boni, S. DeSimone, S. Faini, S. Guiducci, M. Preger, M. Serio, B. Spataro, S. Tazzari, F. Tazzioli, M. Vescovi, A. Cattoni, C. Sanelli, M. Castellano, N. Cavallo, F. Cevenini, M. R. Masullo, P. Patteri, R. Rinzivillo, S. Solimeno, and A. Cutolo, Journal de Physique, 44, C1-1 (1985).
[81] T. J. Orzechowski, B. Anderson, W. M. Fawley, D. Prosnitz, E. T. Scharlemann, S. Yarema, D. Hopkins, A. C. Paul, A. M. Sessler, and J. Wurtele, Phys. Rev. Lett. 54, 889 (1985).
[82] R. W. Warren, D. W. Feldman, B. E. Newnam, S. C. Bender, W. E. Stein, A. H. Lumpkin, R. A. Lohsen, J. C. Goldstein, B. D. McVey, and K. C. D. Chan, Nucl. Instr. & Methods in Phys. Res. A259, 8 (1987).
[83] S. V. Benson, J. M. J. Madey, J. Schultz, M. Marc, W. Wadensweiler, G. A. Westenskow, and M. Velghe, Nucl. Instr. & Methods in Phys. Res. A250, 39 (1986).
[84] T. J. Orzechowski, B. R. Anderson, W. M. Fawley, D. Prosnitz, E. T. Scharlemann, S. M. Yarema, A. M. Sessler, D. B. Hopkins, A. C. Paul, and J. S. Wurtele, Nucl. Instr. & Methods in Phys. Res. A250, 144 (1986).
[85] T. J. Orzechowski, B. R. Anderson, J. C. Clark, W. M. Fawley, A. C. Paul, D. Prosnitz, E. T. Scharlemann, and S. M. Yarema, Phys. Rev. Lett., 57, 2172 (1986).
[86] A. L. Throop, T. J. Orzechowski, B. R. Anderson, F. W. Chambers, J. C. Clark, W. M. Fawley, R. A. Jong, A. C. Paul, D. Prosnitz, E. T. Scharlemann, R. D. Stever, G. A. Westenskow, and S. M. Yarema, "Experimental Characteristics of a High-Gain Free-Electron Laser Amplifier Operating at 8 mm and 2 mm Wavelengths," presented at AIAA 19th Fluid Dynamics & Lasers Conf., Honolulu, HA, June 8, 1987.
[87] K. E. Robinson, T. L. Churchill, D. C. Quimby, D. M. Shemwell, J. M. Slater, A. S. Valla, A. A. Vetter, J. Adamski, T. Doering, W. Gallagher, R. Kennedy, B. Robinson, D. Shoffstall, E. Tyson, A. Vetter, and A. Yeremian, Nucl. Instr. & Methods in Phys. Res. A259, 49 (1987).
[88] E. D. Shaw and C. K. N. Patel, Physics Quantum Electron., 9, 671 (1982).
[89] A. Luccio, C. Pellegrini, A. van Steenbergen, and L. H. Yu, Proc. Int. Conf. LASERS '82, 198 (1983).
[90] W. A. Gillespie, P. F. Martin, M. W. Poole, G. Saxon, R. P. Walker, J. M. Reid, M. G. Kelliher, C. R. Pidgeon, S. D. Smith, W. J. Firth, D. A. Jaroszinski, D. M. Tratt, J. S. Mackay, and M. F. Kimmitt, Nucl. Instr. & Methods in Phys. Res. A250, 233 (1986).
[91] J. C. Goldstein and B. D. McVey, Nucl. Instr. & Methods in Phys. Res. A259, 203 (1987); B. E. Newnam, J. C. Goldstein, J. S. Fraser, R. K. Cooper, "A Linac-Driven XUV Free-Electron Laser," Los Alamos National Laboratory Report, Los Alamos, NM.
[92] J. E. LaSala, D. A. G. Deacon, and J. M. J. Madey, Nucl. Instr. & Methods in Phys. Res. A250, 262 (1986).
[93] X. K. Maruyama, S. Penner, C. M. Tang, and P. Sprangle, Nucl. Instr. & Methods in Phys. Res. A259, 259 (1987).
[94] K-J. Kim, J. Bisognano, S. Chattopadhyay, M. Cornacchia, A. Garren, K. Halbach, A. Jackson, H. Lancaster, J. Peterson, M. Zisman, C. Pellegrini and G. Vignola, "Storage Ring Design for a Short Wavelength FEL," Lawrence Berkeley Laboratory Report.
[95] Xie Jialin, Director, Institute of High Energy Physics, Beijing PRC, private communication.
[96] J. P. Blewett, R. Chasman, J. Appl. Phys. 48, 2692 (1977).
[97] V. K. Neil, SRI Int. Report JSR-79-10, Dec. 1979.
[98] P. Diament, Phys. Rev. Lett. A23, 2537 (1981).
[99] K. Halbach, Journal de Physique 44, C1-211 (1983).
[100] W. B. Colson and P. Elleaume, Appl. Phys. B29, 101 (1982).
[101] W. B. Colson, IEEE Journal of Quantum Electronics QE-17, 1417 (1981).
[102] W. B. Colson, G. Dattoli, and F. Ciocci, Phys. Rev. A31, 828 (1985).
[103] B. M. Kincaid, Nucl. Instr. & Methods in Phys. Res. A246, 109 (1986).
[104] K. E. Robinson, D. C. Quimby, and J. M. Slater, IEEE Journal of Quantum Electronics, QE-23, 1497 (1987).
[105] E. T. Scharlemann, J. Appl. Phys. 58, 2154 (1985).

[106] J. D. Jackson, *Classical Electrodynamics*, (Wiley, New York, 1975).
[107] L. R. Elias and J. C. Gallardo, Phys. Rev. **A24**, 3276 (1981).
[108] G A. Schott, *Electromagnetic Radiation* (Cambridge University, London, 1912).
[109] B. M. Kincaid, J. Appl. Phys. **48**, 2684 (1977).
[110] R. Coisson, IEEE Journal of Quantum Electronics **QE-17**, 1409 (1981).
[111] W. B. Colson, Phys. Rev. **A24**, 639 (1981).
[112] M. V. Fedorov and S. Stenholm, Optics Commun. **49**, 355 (1984).
[113] M. Billardon, P. Elleaume, J. M. Ortega, C. Bazin, M. Bergher, M. Velghe, Y. Petroff, D. A. G. Deacon, K. E. Robinson, and J. M. J. Madey, Phys. Rev. Lett. **51**, 1652 (1983).
[114] R. W. Warren, B. E. Newnam, W. E. Stein, J. G. Winston, R. L. Sheffield, M. T. Lynch, J. C. Goldstein, M. C. Whitehead, O. R. Norris, G. Luedemann, T. O. Gibson, and G. M. Humphrey, Proceedings of the Sixth International Conference on Lasers and Applications, San Francisco (Dec. 12-16, 1983).
[115] M. Biagini, R. Boni, S. De Simone, S. Guiducci, M. Preger, M. Serio, S. Tazzari, F. Tazzioli, S. Trillo, M. Vescovi, M Ambrosio, G. C. Barbarino, M. Castellano, N. Cavallo, F. Cevenini, M. R. Masullo, P. Patteri, R. Rinzivillo, and S. Solimeno, Proc. Soc Photo-Opt. Instrum. Eng. SPIE **453**, 275 (1984).
[116] W. B. Colson, J. C. Gallardo, and P. M. Bosco, Phys. Rev. **A34**, 4837 (1986).
[117] W. B. Colson and J. Blau, Nucl. Instr. & Methods in Phys. Res. **A259**, 198 (1987).
[118] W. H. Louisell, J. Lam, D. A. Copeland, and W. B. Colson, Phys. Rev. **A19**, 188 (1979).
[119] P. Bosco and W. B. Colson, Phys. Rev. **A28**, 319 (1983).
[120] P. Elleaume, *Physics of Quantum Electronics*, **8**, 119 (1982).
[121] P. Elleaume, Journal de Physique, **44**, Colloque C1, 333 (1983).
[122] W. B. Colson and I. Boscolo, Phys. Rev. **A31**, 2353 (1985).
[123] J. C. Goldstein and W. B. Colson, Proc. of the Int. Conf. on LASERS '81, p. 93, ed. C.B. Collins (STS Press, McLean, VA, 1981).
[124] H. Al-Abawi, J. K. McIver, G. T. Moore, and M. O. Scully, *Physics of Quantum Electronics*, **8**, 415 (1982).
[125] G. Dattoli, A. Marino, and A. Renieri, *Physics of Quantum Electronics*, **8**, 515 (1982).
[126] J. C. Goldstein and W. B. Colson, Proc. Int. Conf. LASERS '82, p. 218, ed. R. C. Powell, (STS Press, McLean, VA, 1982).
[127] S. Benson and J. M. Madey, *Free Electron Generators of Coherent Radiation*, eds. C. A. Brau, S. F. Jacobs and M. O. Scully, SPIE **453**, 55 (1983).
[128] M. N. Rosenbluth, H. V. Wong, B. N. Moore, *Free Electron Generators of Coherent Radiation*, eds. C. A. Brau, S. F. Jacobs and M. O. Scully, SPIE **453**, 25 (1983).
[129] W. B. Colson and A. Renieri, Journal de Physique, Colloq. **C1-44**, 11 (1983).
[130] W. B. Colson and Roger A. Freedman, Optics Commun. **46**, 37 (1983).
[131] R. A. Freedman and W. B. Colson, Optics Commun. **52**, 409 (1985).
[132] W. B. Colson, Free Electron Generators of Coherent Radiation, SPIE **453**, 289, eds. Brau, Jacobs, Scully (1984).
[133] D. C. Quimby, J. M. Slater, and J. P. Wilcoxon, IEEE Journal of Quantum Electronics **QE-21**, 979 (1985).
[134] W. B. Colson and J. L. Richardson, Phys. Rev. Lett. **50**, 1050 (1983).
[135] G. T. Moore, Opt. Commun. **52**, 46 (1984).
[136] E. T. Scharlemann, A. M. Sessler, and J. S. Wurtele, Phys. Rev. Lett. **54**, 1925 (1985).
[137] C. M. Tang and P. A. Sprangle, IEEE Journal of Quantum Electronics **QE-21**, 970 (1985).
[138] N. M. Kroll and M. N. Rosenbluth, *Physics of Quantum Electronics* **7**, 147 (1980).
[139] W. B. Colson, Nucl. Instr. & Methods in Phys. Res. **A250**, 168 (1986).

11. Distribution Functions Describing FEL Beams

The integral equation developed in an earlier section can be used to study the effects of beam quality in high current FELs, like LLNL Paladin FEL. In order to use the integral equation to examine the effects of beam quality, several different distribution types are developed. The distributions in the electron phase velocity are derived in terms of the velocity spread and angular spreads in the beam. Only the z component of the electron velocity occurs in the definition of the phase velocity, $v = L[(k+k_0)\beta_z - k]$.

The integral equation can be written as

$$\overset{\circ}{a}(\tau) = \frac{ij}{2}\int_0^\tau ds \;\; s\, F(s)\, e^{-iv_0 s}\, a(\tau - s) \quad , \tag{82}$$

where $a(\tau)$ is the complex optical field, $a(0) = a_0$ is the initial optical field, j is the dimensionless current density, and

$$F(s) = \int_{-\infty}^{\infty} dq\; e^{-iqs}\; f(q) \quad , \tag{83}$$

is the characteristic function of the electron distribution function $f(q)$. The characteristic function is just the Fourier transform of the electron distribution function $f(q)$, and $f(q)$ is the distribution of the initial electron phase velocities $v_i = v_0 + q$ about v_0. The distribution function is normalized, $\int dq f(q) = 1$.

The characteristic function is the important factor that carries the affect of the electron distribution function to the FEL optical field. When the distribution is narrow, $f(q) \approx \delta(0)$, the characteristic function has the value $F(s) \approx 1$ so that the field evolution depends only on the dimensionless current j and the initial phase velocity v_0. The initial field growth rate is zero, because the initial value of the integrand of (82) is $\approx s e^{-iv_0 s} a_0 \approx 0$. Later in time, the integrand becomes $sF(s)e^{-iv_0 s} a(\tau - s)$ and is proportional to the field strength. Recalling the derivation of the integral equation, note that the integrand measures the development of bunching in the electron beam as a result of the presence of the field $a(\tau - s)$. As bunching develops, the field growth rate $\overset{\circ}{a}(\tau)$ increases leading to further growth. When the distribution function is broader, we will see that the magnitude of the complex characteristic function decays in s along the undulator length. The detailed features of the decay retard the development of bunching and the increase in the growth rate due to bunching. Ultimately, it is the

shape of the electron distribution function that determines the decay in the beams ability to bunch.

The imaginary part of the characteristic function is a measure of the asymmetry in the distribution function. The imaginary part is

$$F_I(\tau) = \frac{F_I - F_I^*}{2} = \frac{1}{2}\int_{-\infty}^{\infty} dq\ (\ e^{-iqs}\ f(q) - e^{iqs}\ f^*(q)\ )\quad . \tag{84}$$

Since $f(q)$ is a probabilistic function, it is real, $f = f^*$. So

$$F_I(\tau) = \frac{1}{2}\int_{-\infty}^{\infty} dq\ e^{-iq}\tau\ [\ f(q) - f(-q)\ ]\ . \tag{85}$$

If the distribution function is symmetric, $f(q) = f(-q)$, then the characteristic function, $F(\tau)$, is real. If the distribution function is asymmetric so that $f(q) \neq f(-q)$, then the characteristic function is complex.

When the distribution is directly a function of the electron energy or β_z, the v-distribution has the same form as the β_z-distribution. The spread can alsc be related to the energy spread, $\sigma_G = 4\pi N\Delta\gamma/\gamma$. An example is the *Gaussian*, or *normal*, distribution,

$$f(v_i) = \frac{e^{-(v_i - v_0)^2/2\sigma_G^2}}{\sqrt{2\pi}\sigma_G}\quad , \tag{86}$$

where $\sigma_G = Lk\Delta\beta_z$ relates the characteristic velocity spread $\Delta\beta_z$ to σ_G.

The Gaussian distribution function shape can be written as

$$f(v_i) = \frac{e^{-(v_i - v_0)^2/2\sigma_G^2}}{\sqrt{2\pi}\sigma_G} \quad \Rightarrow \quad f(q) = \frac{e^{-q^2/2\sigma_G^2}}{\sqrt{2\pi}\sigma_G}\quad , \tag{87}$$

The corresponding characteristic function is

$$F(\tau) = \int_{-\infty}^{\infty} dq\ e^{-iq\tau}\ f(q) = \int_{-\infty}^{\infty} dq\ e^{-iq\tau}\ \frac{e^{-q^2/2\sigma_G^2}}{\sqrt{2\pi}\sigma_G}\quad , \tag{88}$$

or

$$F(\tau) = e^{-\sigma_G^2\tau^2/2}\quad . \tag{89}$$

The characteristic function is real, because the Gaussian shape is symmetric. The magnitude of $F(\tau)$ decays exponentially with a characteristic time σ_G^{-1}. Bunching

in the integrand of the integral equation decays rapidly as the spread σ_G is increased. For large $\sigma_G \gg 1$, the growth rate of the optical field is severly reduced by beam quality.

A similar simple shape is the *Cauchy*, or *Lorentzian* distribution,

$$f(\nu_i) = \frac{1}{\pi\sigma_L} \frac{1}{(1+(\nu_i-\nu_0)^2/\sigma_L^2)} \quad . \tag{90}$$

The characteristic function is evaluated from

$$F(\tau) = \int_{-\infty}^{\infty} dq\ e^{-iq\tau} \left[\frac{1}{\pi\sigma_L} \frac{1}{1+q^2/\sigma_L^2} \right] \quad , \tag{90}$$

and is

$$F(\tau) = e^{-\sigma_L \tau} \quad . \tag{91}$$

The characteristic function is again real, because the Lorentzian is symmetric. The decay is exponential with a characteristic time σ_L^{-1}, but the form of the decay in the integrand of the integral equation is different than in the Gaussian case.

An angular spread in the beam gives a more subtle relation to the ν-distribution, because the electron's z velocity is quadratically dependent on the angle of propagation with respect to the undulator. At present, we do not consider betatron motion, so that this analysis is only appropriate to weak undulators with K small. For small angles θ with respect to the undulator axis, the electron's z velocity is reduced by

$$\beta_z = \beta_0 \cos\theta \approx \beta_0 \left(1 - \theta^2/2 \right) \quad . \tag{92}$$

The corresponding change in the phase velocity is

$$\nu(\theta) = L[(k+k_0)\beta_0 - k - (k+k_0)\beta_0\theta^2/2] = \nu(0) - N\lambda_0 k\theta^2/2 \approx \nu(0) - 2\pi N\gamma^2\theta^2/(1+K^2) \quad . \tag{93}$$

A misalignment of any sign, ± θ, gives the same decrease in the electron's z velocity.

When the angular spread in the x and y directions are unequal, the ν-distribution is considerably more complicated. Take the probably of an electron in the beam entering the undulator with angle θ_x in the x direction, and θ_y in the y direction, to be given by

$$p(\theta) = \frac{e^{-\theta_x^2/2\Delta_x^2}}{\sqrt{2\pi}\,\Delta_x} \frac{e^{-\theta_y^2/2\Delta_y^2}}{\sqrt{2\pi}\,\Delta_y} \quad \text{where} \quad \theta^2 = \theta_x^2 + \theta_y^2 \quad , \tag{94}$$

where the spread in the x direction is Δ_x and the spread in the y direction is Δ_y. The angle away from the undulator axis is $\theta^2 = \theta_x^2 + \theta_y^2$. The formal expression of the distribution function is

$$f(\nu_i) = \sum_{\theta_x's} \sum_{\theta_y's} \delta(\nu_i+\nu_0 + 2\pi N\gamma^2(\theta_x^2 + \theta_y^2)/(1 + K^2)) \frac{e^{-\theta_x^2/2\Delta_x^2} e^{-\theta_y^2/2\Delta_y^2}}{2\pi\Delta_x\Delta_y} \quad . \tag{95}$$

The delta-function is evaluated by

$$\delta(.) = \delta(\theta_x-\theta_{xr})(1+K^2)/4\pi N\gamma^2\theta_{xr} \quad , \tag{96}$$

where the roots are

$$\theta_{xr} = \pm \left[(\nu_0-\nu_i)(1+K^2)/2\pi N\gamma^2-\theta_y^2 \right]^{1/2} \quad , \tag{97}$$

and

$$\theta_{ymax}^2 = (\nu_0-\nu_i)(1+K^2)/2\pi N\gamma^2 \quad , \tag{98}$$

so that θ_{xr} is real. Inserting the root and evaluating the delta-function leaves only one sum over θ_y's,

$$f(\nu_i) = 2\sum_{\theta_y's} \frac{e^{-(\nu_0-\nu_i)(1+K^2)/4\pi N\gamma^2\Delta_x^2} e^{\theta_y^2/2\Delta_x^2} e^{-\theta_y^2/2\Delta_y^2}}{4\pi N\gamma^2\sqrt{(\nu_0-\nu_i)(1+K^2)/2\pi N\gamma^2-\theta_y^2}} \frac{(1+K^2)}{2\pi\Delta_x\Delta_y} \quad . \tag{99}$$

To simplify the expression define

$$\sigma_{\theta x} = \frac{4\pi N\gamma^2\Delta_x^2}{1+K^2} \quad , \text{and} \quad \sigma_{\theta y} = \frac{4\pi N\gamma^2\Delta_y^2}{1+K^2} \quad . \tag{100}$$

After some manipulation, the remaining integral has the form

$$f(\nu_i) = \frac{e^{-(\nu_0-\nu_i)/\sigma_{\theta x}}}{\pi\sqrt{\sigma_{\theta x}\sigma_{\theta y}}} \int_0^2 dx \frac{e^{-x(\nu_0-\nu_i)(\sigma_{\theta x}-\sigma_{\theta y})/2\sigma_{\theta x}\sigma_{\theta y}}}{\sqrt{x(2-x)}} \quad . \tag{101}$$

The integral can be found in Gradshteyn and Ryzhik, p. 315, and the final ν-distribution is

$$f(\nu_i) = \frac{e^{-(\nu_0-\nu_i)(\sigma_{\theta x}+\sigma_{\theta y})/2\sigma_{\theta x}\sigma_{\theta y}}}{\sqrt{\sigma_{\theta x}\sigma_{\theta y}}} J_0\left[\frac{i(\nu_C-\nu_i)|\sigma_{\theta x}-\sigma_{\theta y}|}{2\sigma_{\theta x}\sigma_{\theta y}} \right] \tag{102}$$

for $\nu_i < \nu_0$, and zero otherwise. Since $J_0(x) = J_0(-x)$, the argument of the Bessel function can be written as $(\sigma_{\theta x} - \sigma_{\theta y}) \rightarrow |\sigma_{\theta x} - \sigma_{\theta y}|$.

In the case that $\sigma_{\theta x} = \sigma_{\theta y}$, $J_0(0) = 1$, and the electron v-distribution becomes the *exponential* distribution,

$$f(v_i) = \frac{e^{-(v_0 - v_i)/\sigma_\theta}}{\sigma_\theta} \quad , \tag{103}$$

where $\sigma_\theta = \sigma_{\theta x} = \sigma_{\theta y} = 4\pi N \gamma^2 \Delta_x^2/(1+K^2)$. We will derive the exponential distribution later from the more basic approach.

The distribution function for the asymmetric angular spread can be written as

$$f(q) = \frac{e^{q\left[\frac{\sigma_{\theta x}+\sigma_{\theta y}}{2\sigma_{\theta x}\sigma_{\theta y}}\right]}}{\sqrt{\sigma_{\theta x}\sigma_{\theta y}}} J_0\left[\frac{iq\,|\sigma_{\theta x}-\sigma_{\theta y}|}{2\sigma_{\theta x}\sigma_{\theta y}}\right] \quad , \tag{104}$$

for $q < 0$, and zero for $q > 0$. The corresponding characteristic function is given by

$$F(\tau) = \int_{-\infty}^{0} dq\; e^{-iq\tau} \frac{e^{qA_+}}{\sqrt{\sigma_{\theta x}\sigma_{\theta y}}} J_0(iqA_-) \qquad \text{where} \qquad A_\pm = \frac{|\sigma_{\theta x} \pm \sigma_{\theta y}|}{2\sigma_{\theta x}\sigma_{\theta y}} \tag{105}$$

The integral can be found on p. 707 of Gradshteyn and Ryzhik, and gives

$$F(\tau) = \frac{1}{\sqrt{\sigma_{\theta x}\sigma_{\theta y}}\sqrt{(A_+ - i\tau)^2 - A_-^2}} \quad . \tag{106}$$

Using the definitions of $\sigma_{\theta x}$ and $\sigma_{\theta y}$ the characteristic function is found to be

$$F(\tau) = \frac{1}{\sqrt{1 - i\sigma_{\theta x}\tau}\,\sqrt{1 - i\sigma_{\theta y}\tau}} \quad . \tag{107}$$

The asymmetric *exponential* electron distribution function from a symmetric spread can be written as

$$f(v_i) = \frac{e^{-(v_0 - v_i)/\sigma_\theta}}{\sigma_\theta} \qquad \Rightarrow \qquad f(q) = \frac{e^{q/\sigma_\theta}}{\sigma_\theta} \quad , \tag{108}$$

for $q < 0$, and zero for $q > 0$, and σ_θ is given above. The characteristic function is given by

$$F(\tau) = \int_{-\infty}^{0} dq\; e^{iq\tau} \left[\frac{e^{q/\sigma_\theta}}{\sigma_\theta}\right] \quad , \tag{109}$$

and is

$$F(\tau) = \frac{1}{(1 - i\sigma_\theta\tau)} \quad . \tag{110}$$

The characteristic function of the exponential distribution is again complex, because $f(q)$ is asymmetric. The amplitude decays more slowly than the Gaussian or Lorentzian cases.

These examples are derived from realistic physical conditions, but mainly form a set of distinct shapes that serve as candidates for studying the affect of shape on the FEL interaction properties. An experiment is usually not able to predict the shape of the electron distribution function so that precise correspondence is not the goal. The main interest is to establish the importance of shape.

12. FEL Theory In Weak Optical Fields

The integral equation was used to evaluate the effect of gain degradation with several distribution functions. The characteristic function for each of the distribution functions was calculated as in the last section of this report, and then used in the integral equation. The publication reference is W. B. Colson and J. Blau, "Free Electron Laser Theory in Weak Optical Fields", Nuclear Instruments and Methods in Physics Research **A256**, 198 (1987).

The gain degradation from various electron beam distributions determines important design criteria for the accelerator-laser interface. The theory presented in this publication uses a convenient, yet powerful, method of including an arbitrary electron distribution function in a self-consistent integral equation for the complex optical field. The method has advantages over a plasma stability analysis or a numerical particle simulation.

The FEL integral equation is proving to be a useful theoretical tool for evaluating gain degradation with electron beams of poor quality. Furthermore, the electron distribution function shape can have a significant effect on the amount of gain degradation in an FEL system. There are important opportunities here to optimize the coupling between the FEL and its electron source. It may also be possible to make further improvements in the performance of an FEL by altering the electron distribution from the electron source as it travels to the FEL undulator; wake field effects caused by the electron pulse interacting with the metallic walls of the transport channel can change the distribution.

198 Nuclear Instruments and Methods in Physics Research A259 (1987) 198–202
North-Holland, Amsterdam

Section VI. Theoretical topics

FREE ELECTRON LASER THEORY IN WEAK OPTICAL FIELDS

W.B. COLSON

Berkeley Research Associates, P.O. Box 241, Berkeley, CA 94701, USA

J. BLAU

Physics Department, University of California, San Diego, CA, USA

In weak optical fields, free electron laser dynamics can be expressed in the form of an integral equation. The integral equation is used to evaluate the gain degradation from various electron beam distributions and determine important design criteria for the accelerator–laser interface.

1. Introduction

The free electron laser (FEL) uses a relativistic electron beam to amplify a co-propagating electromagnetic wave passing through a periodic undulator [1]. In either the high-gain amplifier or the more modest-gain oscillator, maintaining coherence of the electron bunches over a significant interaction length imposes important restrictions on the electron beam quality. Electron accelerator and storage ring technologies usually present a trade-off between beam current and beam quality that make it essential to accurately evaluate the role of beam quality in the high gain regime. It is particularly important for FELs designed to operate at XUV or X-ray wavelengths [2]. The theory presented here uses a convenient, yet powerful, method of including an arbitrary electron distribution function in a self-consistent integral equation for the complex optical field [3]. The method has advantages over a plasma stability analysis or a numerical particle simulation [4–11].

2. Beam quality in some typical experiments

In order to better understand the detrimental effects of poor beam quality consider some simple examples. Coherent bunching of the electron phases is the key element to any FEL gain mechanism. The electron phase with respect to the combined optical and undulator fields is

$$\psi = (k + k_u)z - \omega t,$$

where $\lambda = 2\pi/k = 2\pi c/\omega$ is the optical wavelength, $\lambda_u = 2\pi/k_u$ is the undulator wavelength, and $z(t)$ is an electron position. The electron's phase velocity is

$$\dot{\psi} = (k + k_u)\beta_z c - \omega,$$

where the dimensionless time is $\tau = ct/L$, $L = N\lambda_0$ is the undulator length, and $\beta_z c$ is the electron z velocity. Two electrons with different z velocities owing to an initial energy difference $\Delta\gamma mc^2$, will have a phase spread $4\pi N\Delta\gamma/\gamma$ at the end of the undulator. The natural dimensionless quantity with which to measure an energy spread is therefore $\sigma = 4\pi N\Delta\gamma/\gamma$. When $\sigma \approx \pi$, the phase spread is $\approx \pi$, and coherent bunching begins to be degraded.

An angular spread is also possible due to the finite emittance of an electron beam. An electron of energy γmc^2 entering the undulator with a small injection angle has its z velocity reduced. The natural dimensionless quantity with which to measure an angular spread is

$$\sigma_\theta = 4\pi N\gamma^2\Delta\theta_i^2/(1 + K^2),$$

where $K = e\bar{B}\lambda_0/2\pi mc^2$ with $\bar{B}$ as the rms undulator field strength, e is the electron charge magnitude, and $\Delta\theta_i$ is the width of the actual spread. When $\sigma_\theta \approx \pi$, the resulting phase spread $\approx \pi$, so that coherent bunching begins to be degraded as with the energy spread. These dimensionless quantities allow us to compare different types of beam distributions on the same basis.

In the Maxwell–Lorentz FEL theory [3], the high-gain regime can be described using the dimensionless current density

$$j = 8N(e\pi KL)^2\rho/\gamma^3 mc^2,$$

where ρ is the electron particle density. If $j \lesssim 1$, the FEL operates in the low-gain regime with the peak gain $G \approx 0.135j$, the gain spectrum is centered at an initial phase velocity $\nu_i = \nu(0) = 2.6$ with a characteristic width $\delta\nu_i \approx 1$. If $j \gg 1$, the FEL operates in the high-gain regime with the peak gain $G = \exp[\sqrt{3}(j/2)^{2/3}\sqrt{3}]/9$, the gain spectrum is centered at the resonant phase velocity

Table 1
Comparison of some FEL experiments and their respective beam qualities

	J	σ	σ_θ	N
Stanford (1980)	2	$\approx 10^{-1}$	$\approx 10^{-1}$	160
LLNL ELF induction linac (1985)	25000	2	23	30
LANL linac (1986)	60	10	1	36
Boeing/Spectra linac (1986)	800	29	22	230
LANL XUV linac	2000	10	2	750
Stanford XUV storage ring	500	2	$\approx 10^{-2}$	237

$\nu_i \approx 0$ with a characteristic width $\delta\nu_i = 4J^{1/6}$.

Table 1 compares some experiments and their respective beam qualities. As can be seen, many experiments are now well into the high gain regime, but also suffer some gain degradation due to beam quality.

3. The FEL integral equation

To accurately evaluate the effects of electron beam quality in either the high or low gain regimes, we use the FEL integral equation [3]. The complex electric field envelope, $E = |E|e^{i\phi}$, of the light wave is governed by the slowly-varying wave equation and electron Lorentz force equation [12]:

$$\frac{\mathrm{d}a}{\mathrm{d}\tau} = -J\langle e^{-i\zeta}\rangle,$$

$$\frac{\mathrm{d}^2\zeta}{\mathrm{d}\tau^2} = \frac{\mathrm{d}\nu}{\mathrm{d}\tau} = |a|\cos(\zeta + \phi). \tag{1}$$

where $a = 4N\pi eKLE/\gamma^2 mc^2$ is the dimensionless optical field strength, and $\langle\cdots\rangle$ represents a normalized average over all electrons in the beam. Electrons are labeled by their initial phase-space coordinates $\zeta(0)$ and $\nu_i = \nu(0)$. In weak optical fields, $|a| \ll \pi$, the reference to the individual electron phases can be explicitly removed by combining the equations in (1) to obtain

$$a(\tau) = a_0 + \frac{J}{2}\int_0^\tau \mathrm{d}s \int_0^s \mathrm{d}q\, \langle \exp(-i\nu_i(s-q))\rangle \times (s-q)a(q) \tag{2}$$

where the initial optical field is $a(0) = |a(0)| = a_0$ and $\phi(0) = 0$. The average $\langle\cdots\rangle$ is now only over the initial phase-velocity distribution, $\int \mathrm{d}\nu_i f(\nu_i) = 1$, with $f(\nu_i) \geq 0$.

4. Electron distribution functions

Gaussian:

$$f_G(\nu_i) = \frac{\exp\left[-(\nu_i - \nu_0)^2/2\sigma_G^2\right]}{\sqrt{2\pi}\,\sigma_G} \quad \text{for all } \nu_i, \tag{3}$$

Lorentzian:

$$f_L(\nu_i) = \frac{1}{\pi\sigma_L\left(1 + (\nu_i - \nu_0)^2/\sigma_L^2\right)} \quad \text{for all } \nu_i, \tag{4}$$

where σ_G, $\sigma_L = 4\pi N\Delta\gamma/\gamma$ for an energy spread. The Lorentzian has a fwhm of $2\sigma_L$ with a peak value $1/\pi\sigma_L$ located at ν_0; The Gaussian has a fwhm of 2.35 σ_G with a peak value $1/\sqrt{2\pi}\,\sigma_G$ also located at ν_0. The two distributions are comparable in shape for the same spread, but we will find that their resultant gain degradation can be quite different.

A distribution due to an angular spread is asymmetric, because electrons can only be slowed down by traveling at a random angle with respect to the z axis. Each distribution is found from

$$f(\nu_i) = \sum_i \delta\left(\nu_i - \nu_0 + 2\pi N\gamma^2\theta_i^2/(1+K^2)\right)p(\theta_i),$$

where $p(\theta_i)$ is the probability that an electron in the beam is propagating at angle θ_i. If the angular spread is symmetric in x–y, a "circular spread", the distribution function becomes the exponential distribution

$$f_\theta(\nu_i) = \begin{cases} \dfrac{\exp\left[-(\nu_0 - \nu_i)/\sigma_\theta\right]}{\sigma_\theta} & \text{for } \nu_i < \nu_0, \\ 0 & \text{otherwise,} \end{cases} \tag{5}$$

where σ_θ is the characteristic angle away from the z axis. For a spread of angles in a plane, a "linear spread", the distribution function is

$$f_{\theta_x}(\nu_i) = \begin{cases} \dfrac{\exp\left[-(\nu_0 - \nu_i)/\sigma_{\theta_x}\right]}{\sqrt{\pi(\nu_0 - \nu_i)\sigma_{\theta_x}}} & \text{for } \nu_i < \nu_0, \\ 0 & \text{otherwise.} \end{cases} \tag{6}$$

where σ_{θ_x} is the characteristic angular spread in the x-direction. The distributions (3) through (6) are four examples of different electron distribution functions resulting from energy spreads and angular spreads.

In order to introduce the distribution functions into the integral equation, we note that eq. (2) can be written in the form

$$a(\tau) = a_0 + \frac{J}{2}\int_0^\tau \mathrm{d}s \int_0^s \mathrm{d}q\, qF(q)\, e^{-i\nu_0 q}a(s-q), \tag{7}$$

where

$$F(\tau) = \int_{-\infty}^{\infty} \mathrm{d}\nu_i f(\nu_i) e^{-i\nu_i\tau}.$$

properties. For the distributions (3) through (6) above we have

Gaussian:

$$F_G(\tau) = \exp\left(-\sigma_\theta^2 \tau^2/2\right),$$

Lorentzian:

$$F_L(\tau) = \exp(-\sigma_L \tau),$$

circular:

$$F_\theta(\tau) = 1/(1 - i\sigma_\theta \tau),$$

and linear:

$$F_{\theta_x}(\tau) = 1/\sqrt{1 - i\sigma_{\theta_x}\tau}\,. \tag{8}$$

Each of these factors describes the characteristic decay in the integrand of eq. (7) while the current density j increases the size of the integrand as the optical field $a(\tau)$ grows. Note that the imaginary part of $F(\tau)$ is a measure of the asymmetry in the distribution function. If $f(\nu_i)$ is symmetric, then $F(\tau)$ is purely real. If $f(\nu_i)$ is antisymmetric, then $F(\tau)$ is complex.

5. Gain degradation with modest current

In both fig. 1 and fig. 2 there are four surfaces plotted. Each shows $\ln(1 + G(\nu_0, \sigma))$ with spreads $\sigma = \sigma_G$, σ_L, σ_θ or σ_{θ_x} (the Gaussian, Lorentzian, circular, or linear distributions are used). For a given current j, each surface starts with the same gain spectrum $G(\nu_0, \sigma = 0)$, but as the amount of spread σ increases, there are features common to all the types of the distributions examined:

- the peak gain decreases steadily,
- the ν_0-position of peak gain increases away from resonance ($\nu_0 = 0$),
- the gain spectrum width around peak gain becomes broader in ν_0.

These qualitative features are common to nearly all of the distributions examined, but the details of the degradation can be dramatically different.

Both figs. 1a and 1b are symmetric distributions, the Gaussian and Lorentzian, in an FEL with $j = 10^2$; this

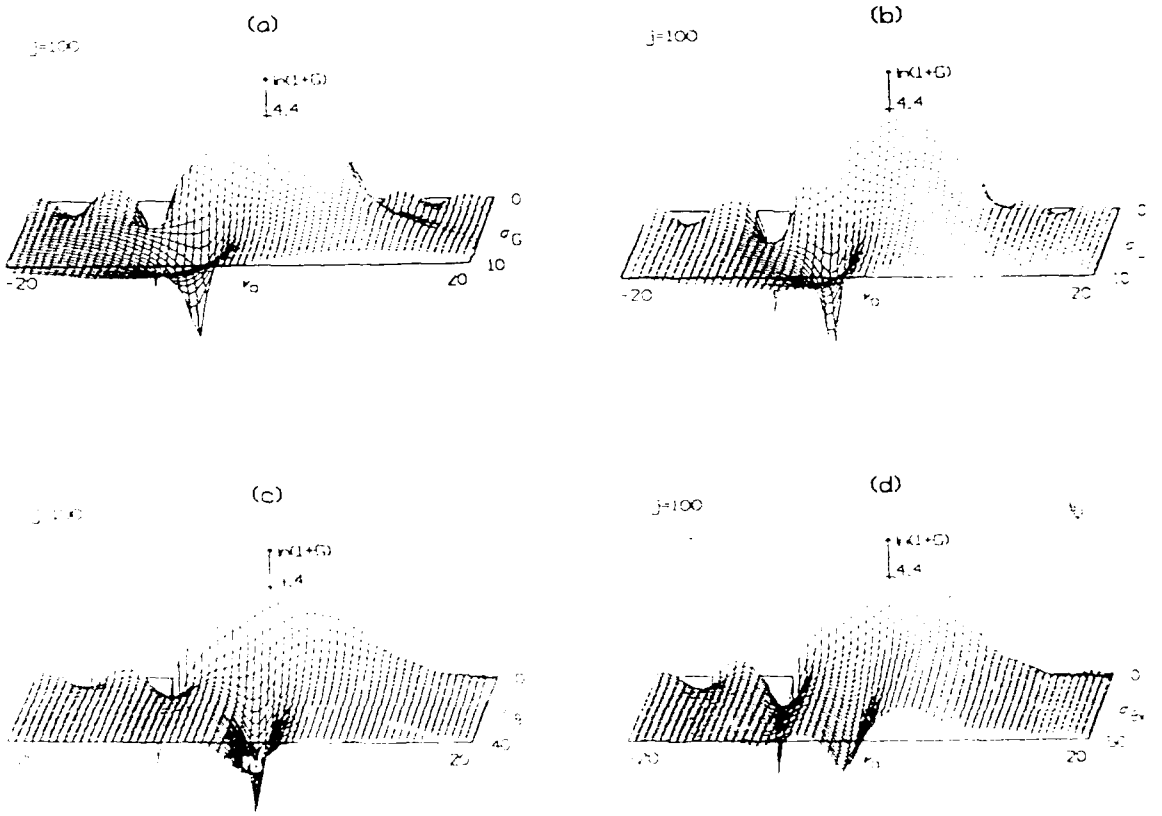

current is characteristic of a moderately high-gain FEL oscillator. For $\sigma_G = \sigma_L = 0$, the peak gain is $\ln(1 + G) \approx 4.4$, or $G \approx 80$, and is positioned just above $\nu_0 \approx 0$; the gain spectrum width is about $\delta\nu_0 \approx 4j^{1/6} \approx 9$. Near $\nu_0 \approx -10$ and $\sigma = 0$, there is large loss, or negative gain, so that $\ln(1 + G) \ll 0$. Note that logically, $G \geq -1$, and that when $\ln(1 + G) \to -\infty$, nearly all of the light is absorbed. Surprisingly, at $\nu_0 \approx -5$, $\sigma_G \approx 8$ in fig. 1a, and at $\nu_0 \approx -2$, $\sigma_L \approx 8$ in fig. 1b there is also large loss. In this parameter region, it is possible to decrease the beam quality, (that is, increase σ) and increase the FEL gain. To our knowledge, this is previously unknown in FELs. Increasing the Lorentzian spread σ_L causes the gain peak to move less far from resonance than does the Gaussian spread σ_G.

Figs. 1c and 1d show asymmetric distributions due to the circular and linear angular spreads, σ_θ and $\sigma_{\theta x}$. At large spreads these distributions both have large absorption "troughs" that are somewhat independent of ν_0. The linear spread appears to be less susceptible to degradation than the circular spread.

6. Gain degradation with high current

Fig. 2 represents an FEL with large current, $j = 10^4$, characteristic of a single-pass FEL amplifier. The peak gain near resonance for $\sigma = 0$ is now up to $\ln(1 + G) \approx 27$ or $G \approx 8 \times 10^{11}$. The general trends outlined for fig. 1 are still valid, but details have changed because of the higher current density j. The linear angular spread appears more resistant to gain degradation than the circular spread. In these cases, an FEL could withstand factors of 10^2 less beam quality depending on the specific beam distribution shape. Note also, that it is possible to find regions on the gain surface where increasing the energy spread can actually increase the gain.

The FEL integral equation is proving to be a useful theoretical tool for evaluating gain degradation with electron beams of poor quality. Furthermore, the electron distribution function shape can have a significant effect on the amount of gain degradation in an FEL system. There are important opportunities here to opti-

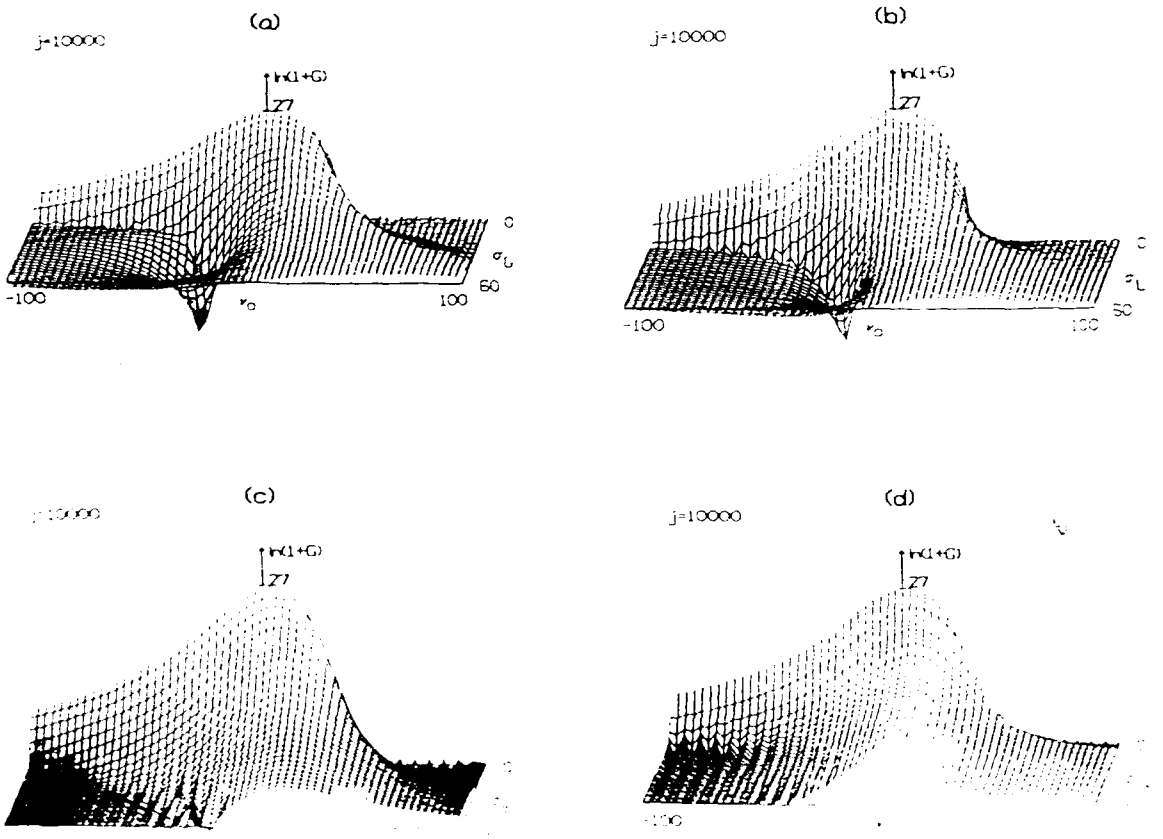

mize the coupling between the FEL and its electron source. It may also be possible to make further improvement in the performance of an FEL by altering the electron distribution from the electron source as it travels to the FEL undulator; wake field effects caused by the electron pulse interacting with the metallic walls of the transport channel can change the distribution.

Acknowledgement

The authors are grateful for support of this research by the U.S. Office of Naval Research the Los Alamos National Laboratory, and the Lawrence Livermore National Laboratory.

References

[1] W.B. Colson and A.M. Sessler, Ann. Rev. Nucl. Part. Si. 35 (1985) 25.

[2] Free-Electron Generators of Extreme Ultraviolet Coherent Radiation, Brookhaven National Laboratory (1983) eds., J.M.M. Madey and C. Pellegrini (AIP, New York, 1984)

[3] W.B. Colson, J.C. Gallardo and P.M. Bosco, Phys. Rev. A34 (1986) 4875.

[4] N.M. Kroll and W.A. McMullin, Phys. Rev. A17 (1978) 300.

[5] V.K. Neil, JASON Technical Report JSR-79-10 (1979).

[6] W.B. Colson and S.K. Ride, Physics of Quantum Electronics, vol. 7, eds., S. Jacobs, H. Pilloff, M. Sargent, M.O. Scully and R. Spitzer (Addison-Wesley, Reading, Mass. 1980) p. 377.

[7] G.T. Moore, Opt. Commun. 54 (1985) 121.

[8] L.K. Grover, J. Feinstein and R.H. Pantell, IEEE J. Quantum Electron. QE-21 (1985) 470.

[9] P. Sprangle and Robert A. Smith, Phys. Rev. A21 (1980) 293.

[10] G. Dattoli and A. Renieri, in: Experimental and Theoretical Aspects of the Free Electron Laser, Vol. 4 of Laser Handbook, M.L. Stich and M.S. Bass (North-Holland, Amsterdam, 1985).

[11] E. Jerby and A. Gover, IEEE J. Quantum Electron. QE-21 (1985) 1041.

[12] W.B. Colson, IEEE, J. Quantum Electron. QE-17 (1981) 1417.

13. Analysis of Paladin at L = 5m Length

Some of the most important work of the contract came as a consequence of reviewing the 5m Paladin experimental observations. It was noticed that the measured gain spectrum was 5 times wider than the natural undulator spectrum. The Paladin experiment provides a unique opportunity to observe how the FEL gain spectrum can be determined by the electron beam velocity distribution instead of the natural undulator spectrum. The natural gain, or undulator, spectrum has a width, $\approx 1/2N$, that is determined only by the number of undulator periods, $N = 62$, over an interaction length of $L = N\lambda_0 = 5$ m. More of the Paladin parameters are discussed in an earlier section of this report.

For reference, the figure below shows the natural gain spectrum for a perfect beam with $j = 50$. There is no significant loss region, and the peak gain is $G = 21$ near resonance.

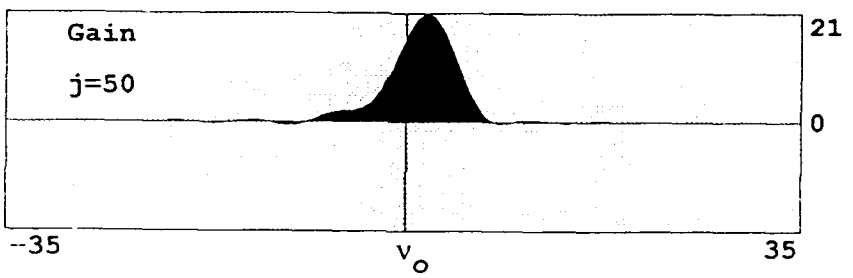

Gain spectrum with j = 50 and an ideal beam.

For more realistic beam distributions we consider candidates from a Gaussian spread where $\sigma_G = 4\pi N\langle\delta\gamma\rangle / \gamma$, a symmetric angular spread where $\sigma_\theta = 4\pi N\gamma^2\langle\delta\theta^2\rangle / (1+K^2)$ and $\delta\theta$ is the characteristic angle of an electron in the beam. For Paladin the observed brightness establishes that $\sigma_G \approx 10$, or $\sigma_\theta \approx 10$, but the shaped is distribution is left unknown.

The weak-field gain spectrum was measured at 10.6μm optical wavelength by varying the undulator field strength B over a small range to change the resonance condition. The gain spectrum was observed to be roughly antisymmetric in shape with a peak gain (and absorption) of $G \approx 0.5$, and a width ≈ 5 times that of the natural undulator spectrum. The shape, overall width, and peak value of the measured gain

spectrum are dramatically altered from the idealized gain spectrum, and in this case, are determined primarily by the distribution of electron velocities along the undulator axis. The FEL integral equation is used to estimate some of the detailed features of the electron beam distribution from the 5m Paladin gain spectrum measurement. The gain spectrum shape and width yield unique information about the actual emittance, energy spread, undulator focusing, and beam positioning in the experiment.

Below are the gain spectra for $j = 50$ and $\sigma_G = 10$, and $\sigma_\theta = 10$.

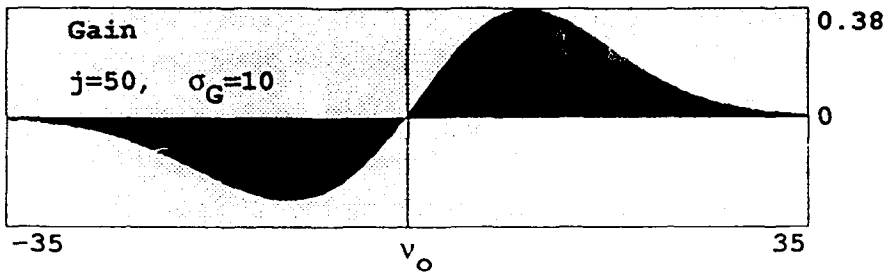

Gaussian spread.

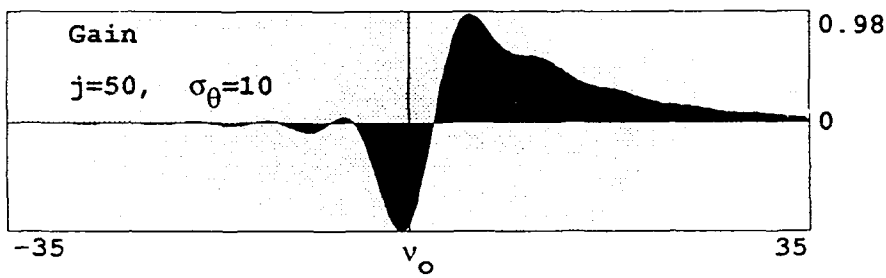

Exponential distribution from a symmetric angular spread.

The gain spectrum information was compared with the experimental gain spectra, but there is so much shot-to-shot variation in the current and beam energy that the gain spectrum shape was difficult to determine. The gain evolution along the undulator, described below, became a much better method of finding the best distribution function shape.

14. Phase-Space Evolution in Paladin

The integral equation (82) can be used to solve for the evolution of the complex optical field, $a(\tau)$. When the history of the field evolution is known, the pendulum equation (7) can be used to recreate the phase-space motion of some sample electrons. In the examples here, the tapering factor δ is set equal to zero because it was not incorporated in the integral equation initially, and the factor $(1-3\nu/4\pi N) \rightarrow 1$

because the integral equation assumes weak fields. The integral equation is solved numerically and the complex field $a(\tau)$ is saved at each τ-step. From the known quantity $a(\tau) = |a(\tau)|\exp(i\phi(\tau))$, we determine $\nu(\tau)$ and $\zeta(\tau)$ by numerically integrating

$$\ddot{\zeta}(\tau) = \dot{\nu}(\tau) = |a(\tau)|\cos(\zeta + \phi(\tau)) . \qquad (111)$$

The integral equation solution is valid for any weak optical field so that a_0 is chosen to illustrate the electron motion most clearly. The initial field value is selected so that the maximum electron phase change $\Delta\zeta$ is about π, but no electrons over-take or fall-behind any other electrons.

The figure below illustrates the phase-space evolution as determined by the integral equation. The parameters are chosen to characterize Paladin with a $L = 15$ m undulator. The dimensionless current is $j = 1200$ and the spread in the ν-distribution is $\sigma_G = 50$ with a Gaussian shape. The gain, $\ln(1+G(\tau))$, is plotted against τ, the undulator length. The beginning of the undulator is $\tau = 0$ while the end of the undulator is $\tau = 1$. After a small bunching time $\tau_B \approx 0.05$, the gain is exponential and reaches the final value $G \approx 35$ %. The optical phase grows linearly in τ and reaches the final value $\Delta\phi \approx 0.04$. The phase space plot in (ζ,ν) shows the final position of several sample electrons, but the distribution is actually continuous. The sample electron are initially spaced uniformly in ζ and ν and the larger, darker sample electrons represent more real electrons at the peak of the Gaussian distribution. The center of the initial distribution is above resonance at $\nu_0 = 50$ for maximum gain under these conditions. Most of the sample electrons remain close to their initial positions, but those near resonance are distorted slightly because of bunching. The separatrix path, $\nu_s^2 = 2|a|[1+\sin(\zeta_s+\phi)]$, shows the only region in this weak field, $a_0 = 2$, that is affected by the interaction. Only a few of the electrons participate in the interaction when the beam quality is poor. The result for these Paladin parameters is a great deal of gain degradation because of beam quality.

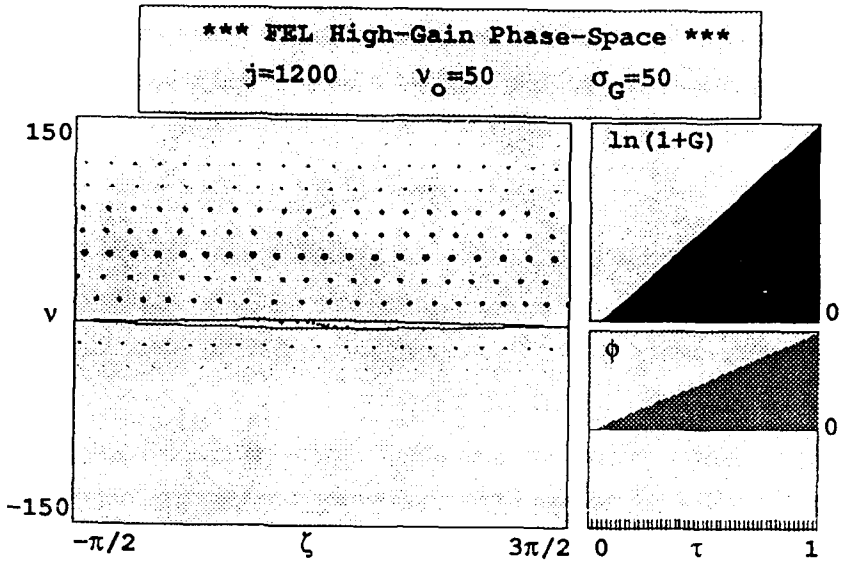

For comparison, the integral equation is solved below to find the phase-space evolution for a nearly perfect beam with $\sigma_G = 1$ and $j = 1200$. The peak gain in this case is at the initial phase velocity $\nu_0 = 0$, and the initial weak field is chosen as $a_0 = 0.1$. After some bunching time $\tau_B \approx 0.25$, the gain grows exponentially to a final value of $G = 1.6 \times 105$, while the phase shift is $\Delta\phi \gtrsim \pi$. In this case, the whole beam is represented by sample electrons all starting at $\nu_0 = 0$. The bunching in the beam is clear, and more importantly, it is clear that the whole beam participates in the gain process.

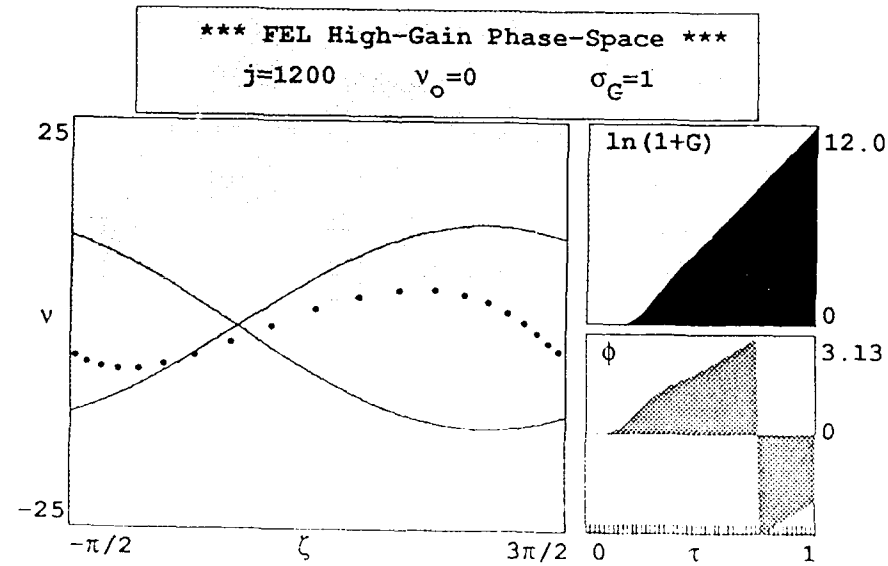

15. Paladin at L = 15 m

One of the highlights of the beam quality research is to identify characteristics of the Paladin 15 m experiments that are unique to the distribution function shape. The distribution function shape in a complicated accelerator and transport system like Paladin is hard to predict. But, an emittance filter was used to decrease the current and improve the beam quality entering the undulator. T. Scharlemann performed a detailed study of the filter and transport system, and concluded that the distribution function shape looked something like the exponential distribution given above.

Below is the phase-space evolution found by solving the integral equation with the exponential distribution of width $\sigma_\theta = 50$, and $j = 1200$. The beam is started at $\nu_0 = 12$ for maximum gain under these conditions. The maximum gain is found experimentally by searching through undulator field strengths K.

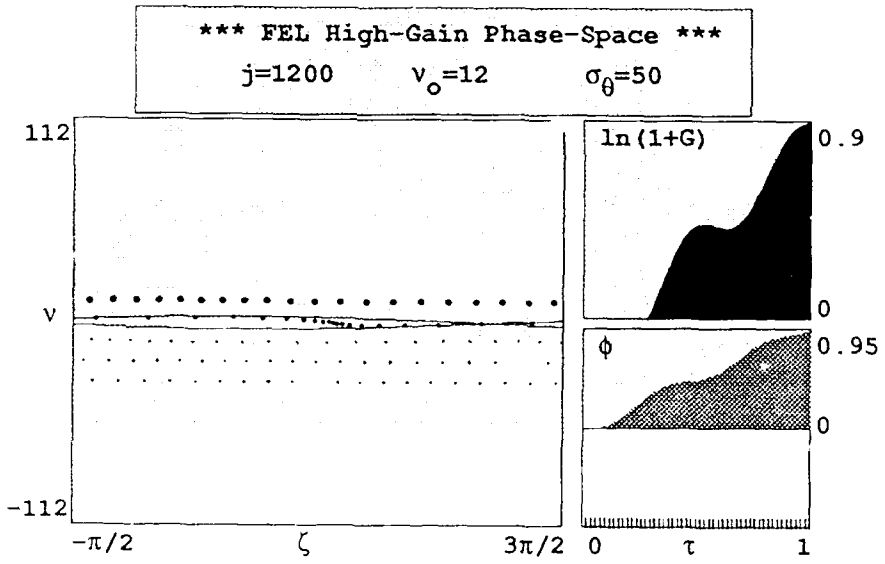

The range explored changes the observed gain primarily because the resonance condition is changed rather than a significant change in j. The large, dark dots represent the peak in the exponential distribution and the small dots represent the tail towards smaller values of ν. As usual, only a small part of the beam contributes to gain and most electrons are not significantly affected by the interaction.

A surprising and distinguishing feature of the evolution above is the gain evolution, $G(\tau)$. The other distribution functions presented above and the others that have been examined do not have the dramatic plateau of zero or even negative gain about half way along the undulator at $\tau = 0.5$. The optical phase evolution $\phi(\tau)$ also shows the plateau feature, but less dramatically.

The gain along the Paladin 15 m undulator was measured, and presented at the April '88 American Physical Society Meeting [D. Prosnitz, T. Orzechowski, et. al., APS Meeting, Baltimore MD (April 1988). The results on the next page also show the prominent plateau in the middle of the interaction length. While not conclusive, it appears that the shape of the distribution function in the Paladin experiment has resulted in not only a decrease in the gain from an ideal beam, but a change in the time-evolution of the interaction strength or growth rate. It is remarkable that the Paladin distribution function can "wait" until half way through the undulator and then turn off" the FEL interaction. Even if the Paladin plateau is not caused by the exponential distribution (as the evidence suggests), it has been shown that the exponential distribution function shape can produce a plateau in the gain evolution, $G(\tau)$.

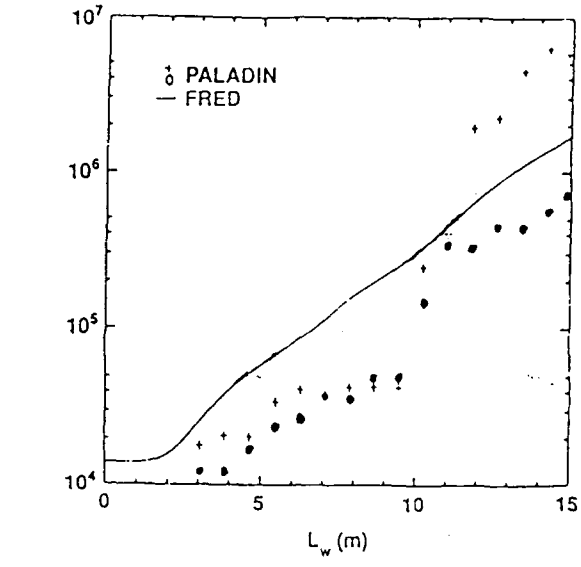

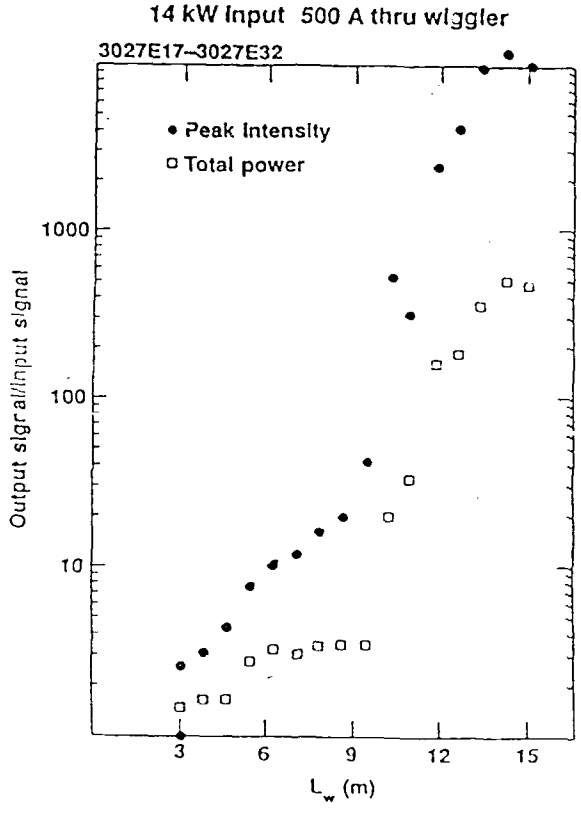

D. Prosnitz, T. Orzechowski, et. al., American Physical Society Meeting, Baltimore MD (April 1983).

16. North-Holland FEL Review Paper

During the contracting period, a review paper describing the theory of FELs was completed. The paper will Chapter 3 of an FEL Handbook published by North-Holland and is titled "Classical Free Electron Laser Theory". The topics covered in the chapter are dimensionless variables and experiments, electron trajectories in the undulator, spontaneous emission, the FEL optical wave equation, FEL electron dynamics, the low-current, low-gain FEL, the collective, high-current, high-gain FEL, FEL coupling to higher frequency harmonics, gain degradation due to beam quality, strong optical fields and saturation, the FEL klystron and tapered undulator designs, FEL Lagrangian and Hamiltonian, mode competition and coherence development, longitudinal multimode theory, the FEL trapped-particle instability, short optical pulses in FEL oscillators, FELs using waveguides, FELs using a Gaussian optical mode, and general transverse mode theory and diffraction.

CLASSICAL FREE ELECTRON LASER THEORY

W. B. Colson

Chapter 3
in
"Free Electron Laser Handbook"
W. B. Colson, C. Pellegrini and A. Renieri (*editors*)
North-Holland Laser Handbook Series

1. Introduction

The initial concept for the free electron laser (FEL) was introduced in 1971 [1]. Later, successful experiments demonstrating the FEL amplifier in 1976 [2] and the FEL oscillator in 1977 [3] showed how a relativistic electron beam could be coupled to the optical power in an open resonator cavity [4] with the use of a periodic undulator magnet. See figure 1. The electron beam energy γmc^2 ranges from a few MeV ($\gamma \sim 5$) to a few GeV ($\gamma \sim 5000$) with peak current from about 1A up to several kA in a beam diameter of 1mm to 1cm. A current of $I = 100$A in a beam with radius $r_b = 1$mm and 50MeV energy provides a high power density, more than 100 GW/cm^2, to the optical field. At such large power densities, an important attribute of the FEL configuration is that the interaction volume contains only free electrons, light, and a static magnetic field. Even for small efficiency, the FEL can yield large peak power. However, since the electron beam from an accelerator is usually pulsed, the average power can be much smaller.

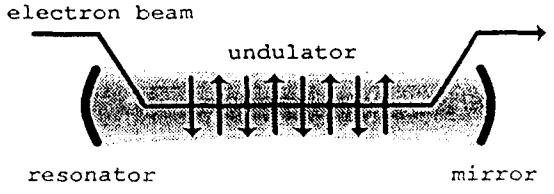

Figure. 1. The FEL schematic.

In the oscillator configuration, coherent electron bunching develops on each successive pass through the undulator. Over many passes, the optical power stored in the resonator grows to saturation. The current density used in the FEL oscillator is usually modest, from one to a few hundred Amperes. In the amplifier configuration, coherent electron bunches develop rapidly in the first part of the undulator followed by large growth of the optical field. Relative to the oscillator, a large current of about 1kA is necessary.

A coherent, freely-propagating optical wave of area πw_0^2 will spread due to natural diffraction over the undulator length L_u. The Rayleigh range, $\pi w_0^2 / \lambda$, is the distance over which light of wavelength, λ, doubles in transverse area. If the optical mode area becomes much larger than the electron beam, the FEL coupling is reduced. So, it is important that the Rayleigh range

than the electron beam, the FEL coupling is reduced. So, it is important that the Rayleigh range is comparable to the interaction length L_u, and that the optical mode waist w_0 is not too much larger than the electron beam radius, r_b. A optical wave with waist of $w_0 = 2$mm and wavelength, $\lambda = 1\mu$m, has a Rayleigh range of about 10m, longer than the typical undulator length. This condition can be altered when the radiation wavelength is large enough to require a waveguide, or when the FEL beam current is large enough to continuously distort, or "guide", the radiation wavefront as it travels along the undulator.

The role of the undulator is to periodically deflect the electrons in the transverse direction as they travel along the optical mode axis. This motion allows energy to flow between the electron beam and light wave over an interaction length $L_u = N_u \lambda_u$ where N_u is the number of undulator periods. The undulator wavelength λ_u is from 2cm to 10cm, and the peak magnetic field strength B_u is from 2kG to 7kG. Extending over twenty to several hundred periods, the undulator is from 1m to 20m in length. An important quantity characterizing many FEL properties is the "undulator parameter" $K = e\bar{B}_u \lambda_u / 2\pi mc^2$ where $\bar{B}_u$ is the rms field strength over each period, m is the electron mass, $e = |e|$ is the electron charge magnitude, and c is the speed of light in vacuum. In most FELs $K \approx 1$. The relativistic Lorentz contraction of the undulator period λ_u, and the Doppler shifted optical wavelength $2\gamma\lambda$ seen by electrons with a large Lorentz factor, $\gamma \gg 1$, combine to give the resonance condition $\lambda = \lambda_u / \gamma^2$ between the forces of the two periodic fields. An FEL with a 100MeV electron beam, $\gamma = 200$, and $\lambda_u = 5$cm gives visible light at $\lambda = 0.6\mu$m wavelength. By changing the electron beam energy, the FEL can be continuously tuned over a wide range. More importantly, the FEL can be used from $\lambda \geq 5$cm wavelength down to $\lambda \leq 5$nm without a fundamental change in the interaction physics. The FEL can be designed to work in new wavelength ranges where there are few powerful sources of radiation, 500μm $\rightarrow$ 20μm and 300nm $\rightarrow$ 20nm.

Another FEL attribute is the flexibility in the design of the undulator. The properties of the undulator can be changed along the undulator length to attain special interaction properties. One example is the tapered undulator that allows efficient operation above the FEL's natural high-power saturation limit; the undulator wavelength λ_u is decreased to maintain resonance at fixed optical wavelength after the electron beam has bunched and lost significant energy. A second example is the FEL klystron which consists of two undulator sections separated by a dispersive section; weak optical fields in the first section prepare electrons for bunching in the dispersive section and coherent radiation in the last section, so that net gain can be substantially increased in a fixed interaction length.

FELs have now been made in a variety of configurations with different electron beam sources and undulators. Experiments have explored a wide range of physical parameters such as the optical wavelength, power, electron beam energy, and single-pass gain. Conference proceedings and collections of papers in journals provide a good overview of FEL theory and

experiments [5-34]. Review articles and books [35-41] can give a better focused picture of the field. Over many years, several theoretical approaches have been used to describe the FEL. The first analyses used quantum mechanics [1], and quantum electrodynamics [42-48], but classical methods have been shown to be accurate [49-54]. The FEL has been analyzed from the laser physics perspective [55-59], while plasma dispersion relations [60-62] and plasma computer simulations [63,64] have emphasized the role of interparticle Coulomb forces and collective effects. The physics of particle accelerators has been used to improve the efficiency of FELs [65,66].

The picture of single-particle currents driving Maxwell's wave equation is a mixture of these views and provides a clear, intuitive description of both the electron and wave dynamics. Due to the simplicity of the fundamental FEL mechanism and experimental conditions, theory and experiment agree over the wide range of parameters explored. This chapter outlines classical FEL theory from a single theoretical approach. Both numerical and analytical procedures are described.

2. Dimensionless parameters and experiments

A few dimensionless variables can summarize recurring combinations of physical parameters in a complex problem like the FEL. Some dimensionless variables are identified here, and will be used throughout the chapter to gain insight into relevant physical processes without reference to detailed calculations or simulations.

The force on a relativistic electron in an undulator with period λ_u gives the transverse velocity $c\beta_\perp \propto cKe^{ik_u z(t)}$ where $k_u = 2\pi/\lambda_u$ is the undulator wavenumber, and $z(t)$ is the electron z position. Electron bunching, coherent emission, and high efficiency all require that an electron's energy $\gamma(t)mc^2$ and its microscopic position $z(t)$ are coupled by the co-propagating radiation with electric field strength E, carrier frequency $\omega = kc = 2\pi c/\lambda$ and phase ϕ. The Lorentz force gives the rate of energy change for an electron $\dot{\gamma}(t) = d\gamma/dt \propto \vec{\beta}_\perp \cdot \vec{E}$. The small transverse deflections caused by the undulator field allow co-propagating light with the correct polarization to alter the electron's energy, $\dot{\gamma} \propto Ke^{ik_u z(t)} \cdot Ee^{i(kz(t) - \omega t + \phi)} = KEe^{i\zeta(t)} e^{i\phi}$. The electron phase that emerges, $\zeta = (k + k_u) z(t) - \omega t$, has fixed wavenumbers k and k_u so that the only dynamical variable in $\zeta(t)$ is $z(t)$. In the relativistic limit where $k \gg k_u$, the electron phase ζ follows the electron position in a section of the beam one optical wavelength long, $\Delta\zeta = k\Delta z$.

The FEL interaction takes place while light and electrons travel through the long undulator. In the relativistic limit, the interaction time is close to L_u/c for both. Defining the dimensionless time $\tau = ct/L_u$, a pass through the undulator is described by $\tau = 0 \rightarrow 1$. Then, the electron phase velocity becomes $v(\tau) = L_u [(k + k_u)\beta_z(t) - k] = \mathring{\zeta}(\tau)$ where $\mathring{(..)} = d(..)/d\tau$, and $c\beta_z$ is the electron z velocity. When $v = 0$, the electron experiences resonant optical and undulator field forces which maximize coupling; the resonant FEL wavelength is $\lambda = \lambda_u (1 + K^2)/2\gamma^2$. Near resonance, the

electron phase velocity can also be written as $v(\tau) = L_u [k_u - k(1+K^2)/2\gamma^2]$; a change in electron energy $\Delta\gamma mc^2$ changes the phase velocity by $\Delta v = 4\pi N_u \Delta\gamma/\gamma$. FEL coupling decreases off resonance when $|\Delta v| \geq \pi$, and the range of good coupling defines the FEL natural gain bandwidth, $|\Delta\gamma/\gamma| = 1/2N_u$.

When $N_u \gg 1$, the change in an electron's energy is small. The electron phase and phase velocity are coupled by the dimensionless complex optical field $a = |a| e^{i\phi}$ through the simple pendulum equation [50,51,67,68]. The field amplitude is $|a| = 4\pi N_u e K L_u E/\gamma^2 mc^2$. When $|a| \ll \pi$, the electron bunching after a single pass through the undulator is imperceptible, and the optical field is weak, but when $|a| \sim \pi$, bunching becomes clear. When $|a| \gg \pi$, the electrons bunch rapidly in the undulator, and start to become trapped in closed phase-space orbits. The trapped electrons then swing to a phase that causes absorption from the optical wave. The decrease in gain marks the beginning of saturation in strong optical fields. The coupling between ζ and v is given by the dimensionless field a and determines the electron bunching rate on the optical wavelength scale.

The light wave is driven by the transverse beam current $\vec{J}_\perp$ which is the sum of individual electron currents $-ec\beta_\perp e^{ik_u z(t)}$. The slowly-varying field envelope $a(\tau)$ is governed by the average of the electron phases $\langle e^{-i\zeta} \rangle$ weighted by the dimensionless current density $j = 8N_u (e\pi K L_u)^2 n_e/\gamma^3 mc^2$ where the actual beam particle density is n_e. The electron beam current I(A), given in Amperes, and the electron beam area πr_b^2 determine the electron beam density $n_e = 3\times 10^9 I(\mathrm{A})/ec\pi r_b^2$. Two practical corrections can be included in the value of j: (i) the "filling factor", $F = \pi r_b^2/\pi w_0^2$, describing optical mode coupling by the substitution $j \rightarrow jF$, and (ii) Bessel function factors of order unity depending only on K and the undulator polarization [69]. The dimensionless current j determines the response of the optical wave to bunching in the beam, and provides the coupling between the electron beam and the light wave. Each gain regime is given by the value of j. When $j \leq 1$, the FEL gain is low, and when $j \gg 1$ the FEL gain is high. Each definition above, ζ and v describing the electrons, $a = |a| e^{i\phi}$ describing the light wave, and j describing the whole FEL, is physically meaningful and useful in the evaluation of many FEL effects.

Table 1 summarizes the relativistic ($\gamma > 5$) FEL experiments. The reference, location and date of the experiments are given in the first column; no date is given for the last experiments that are planned for the future.

Table 1. Free Electron Lasers

FEL	I (Amps)	γ	N_u	λ_u (cm)	K	λ (μm)	w_0 (cm)	j	Comments
[2] Stanford '76	0.07	48	160	3.2	0.72	11	0.3	0.2	First A,RF,H
[3] Stanford '77	2.6	86	160	3.2	0.72	3.4	0.3	6	First O,RF,H
[70] Stanford '80	1.3	85	160	3.3	0.71	3.4	0.14	3.6	O,RF,H
[71] Orsay ACO '83	0.03	326	17	7.8	1.2	0.65	0.03	0.0005	A,SR,L,D=3
[72] LANL '83	20	40	37	2.7	0.55	11	0.16	1.8	A,RF,L,δ=10π
[73] MSNW/Boeing '83	3	38	91	2.5	0.44	11	0.16	2.8	A,RF,L,δ=33π
[74] TRW/EG&G '83	10	50	75	3.6	0.63	11	0.17	1.6	A,RF,L
[75] LANL '84	40	40	37	2.7	0.54	11	0.15	3.6	O,RF,L
[76] TRW/Stanford '84	2.5	130	153	3.6	0.97	1.6	0.1	3.4	O,RF,L,δ=4π
[77] Novosibirsk '84	7	686	22	6.9	2.7	0.62	0.03	0.06	A,SR,L,D=4
[78] Frascati ENEA '85	2.4	40	50	2.4	0.35	11	0.1	0.14	O,M,L
[79] Orsay ACO '85	0.2	432	17	7.8	2	0.63	0.03	0.004	O,SR,L,D=3
[80] UCSB '85	1.25	6.8	160	3.6	0.11	400	1	0.35	O,V,L
[81] INFN LELA '85	0.018	1224	20	12	3.5	0.51	0.04	0.00006	A,SR,L
[82] LLNL ELF '85	500	7.5	30	9.8	2.8	8700	1.5	9000	A,IL,L
[83] LANL '8	130	40	37	2.7	0.56	11	0.14	53	O,RF,L,δ=18π
[84] Stanford Mark III '86	20	87	47	2.3	1.5	3.1	0.07	3.2	O,RF,L
[85] LLNL ELF '86	850	6.9	30	9.8	2.5	8700	1.5	14100	A,IL,L
[86] LLNL ELF Tapered '86	850	6.9	30	9.8	2.4	8700	1.5	14400	A,IL,L,δ=50π
[87] LLNL ELF '87	1000	7..	40	9.8	1.1	2000	1.5	7200	A,IL,L
[88] Boeing/Spectra '87	100	223	229	2.2	1.3	0.5	0.06	687	O,RF,L,δ=92π
[89] Rocketdyne/Stanford '88	20	75	80	2.5	0.61	3.0	0.08	6.2	O,RF,L
[90] FOM Holland	70	30	38	6.5	0.98	70	0.4	22	O,RF,L
[91] BNL	22	588	39	6.5	2.3	0.6	0.07	0.25	A,SR,L
[92] LANL XUV	100	400	750	1.6	0.79	0.08	1.6	414	O,RF,L
[93] Duke University XUV	270	1958	422	6.4	1.6	0.03	0.06	37	O,SR,L
[94] NBS XUV	2	363	130	2.8	1	0.23	0.04	0.6	O,M,L
[95] Beijing PRC	15	40	50	3	1	11	0.1	5	O,RF,L

RF - RF Linac Accelerator, IL - Induction Linac Accelerator, M - Microtron Accelerator,
SR - Electron Storage Ring, V - Van De Graaff Electrostatic Accelerator,
H - Helical Undulator Polarization, L - Linear Undulator Polarization,
δ=# - Tapered Undulator FEL, D=# - Klystron Undulator FEL, A - FEL Amplifier,
O - FEL Oscillator, SRA - Super-Radiant Amplifier in a Long, Single-Pass Undulator

3. Electron trajectories in the undulator

The details of the electron trajectories in the undulator ultimately determine the character of the FEL interaction. It the electron's "wiggling" motion in the undulator that provides coupling to the transverse optical field. This feedback process creates the electron bunching that is responsible for the coherent radiation at the end of the undulator. We start the FEL analysis by examining the trajectories in the undulator field alone, without the presence of light. The importance of a deviation from the ideal trajectory is assessed using the electron phase ζ, or the electron phase velocity $v = \dot{\zeta}$. Good coupling also requires that the electron beam remain inside the transverse optical mode. If the Rayleigh length, $\pi w_0^2/\lambda$, is much smaller than the undulator length, L_u, the mode area becomes larger than the electron beam, and reduces FEL coupling in two ways: the optical field strength that bunches electrons is smaller, and only a small part of the wavefront is amplified by electrons. A Rayleigh length roughly equal to the undulator length, gives a mode area $= \lambda L_u$.

The undulator field seen by electrons originates from permanent magnet structures, or current carrying coils, placed about one or two centimeter away from the beam center [96]. In cylindrical coordinates (r,θ,z), the "helical" undulator with circular polarization has a field given by [97,98]

$$B_r^H = 2B_u \left[I_0(k_u r) - \frac{I_1(k_u r)}{k_u r} \right] \sin(\theta - k_u z) \quad , \quad B_\theta^H = \left[\frac{2B_u}{k_u r} \right] I_1(k_u r) \cos(\theta - k_u z) \, , \qquad (1)$$

$$B_z^H = -2B_u \, I_1(k_u r) \cos(\theta - k_u r) \quad .$$

The perfect electron trajectories at $r = 0$ are helical paths along the z axis. Off the undulator axis, it is the mainly the transverse field components in (1) that modify the electron's path over many undulator periods. Near the axis, the fields may be expanded, $k_u r \ll 1$, to find that the average transverse field increases off axis,

$$\bar{B}_\perp^H = B_u \, (1 + k_u^2 r^2 / 4 + ...) \quad . \qquad (2)$$

The higher field density focuses electrons back toward the axis where the ideal helical field in rectangular coordinates is

$$\vec{B}_H = [B_x, B_y, B_z] = B_u \, [\cos(k_u z), \sin(k_u z), 0] \quad . \qquad (3)$$

at $x = y = 0$. The magnitude of the ideal helical field is constant along the z axis, $\bar{B}_\perp^H = B_u$, making the mathematics of many calculations simpler.

A linearly polarized undulator has a field of the form [99]

$$\vec{B}_L = B_u \, [0, \sin(k_u z)\cosh(k_u y), \cos(k_u z)\sinh(k_u y)] \, . \qquad (4)$$

The perfect electron trajectories at $(x,y) = (0,0)$ are sinusoidal in the x z plane with no motion in the y direction. Away from the undulator axis, the average transverse field strength increases in the y direction only,

$$\bar{B}_\perp^L = \frac{B_u}{\sqrt{2}} (1 + k_u^2 y^2 / 2 + ...) \qquad (5)$$

This undulator provides focusing in the y direction, but not the x direction; in practice, the experimenter uses other forms of magnetic focusing, such as a quadrupole lens [99] in combination with the natural focusing. The ideal field on-axis is

$$B_L = B_u \, [0, \sin(k_u z), 0] \quad . \qquad (6)$$

The magnitude of the ideal linear field is not constant along z, but the average field seen by electrons is $\bar{B}_\perp^L = B_u/\sqrt{2}$. Since the average transverse acceleration is smaller than in the helical case, the linear undulator has half the coupling, or gain. The complication of building a helical field with the same strength as the linear undulator has made the linear undulator the preferred choice; see table 1.

Natural focusing in the wiggle plane of the linear undulator can be added by machining a slight parabolic curve in the normally flat magnet pole faces [99]. The curved surface gives a smaller gap between the magnetic poles off axis, and increases the field strength off axis. The parabolic shape results in equal focusing in each radial dimension to maintain a circular electron beam cross section. The field from parabolic pole design with equal x-y focusing is

$$B_x^P = B_u \sinh(k_u x/\sqrt{2}) \sinh(k_u y/\sqrt{2}) \cos(k_u z) \quad , \quad B_y^P = B_u \cosh(k_u x/\sqrt{2}) \cosh(k_u y/\sqrt{2}) \cos(k_u z) \, , \qquad (7)$$

$$B_z^P = -2B_u \cosh(k_u x/\sqrt{2}) \sinh(k_u y/\sqrt{2}) \sin(k_u z)$$

The perfect electron trajectories on the axis are again sinusoidal in the x-z plane, but away from the axis the transverse field increases in both the x and y direction equally,

$$\bar{B}_\perp^P = \frac{B_u}{\sqrt{2}} (1 + k_u^2 (x^2 + y^2) /4 + ...) \quad . \qquad (8)$$

The ideal field on axis from the parabolic undulator is the same as the linear case (6).

Electron beams injected into the undulator of an FEL have a small radius and angular spread determined by the beam quality from the accelerator. The off-axis focusing fields cause electrons to execute transverse "betatron" oscillations. In general, the beam quality and the focusing need not be the same in each transverse direction x and y. As a simplified example, consider a beam injected into the linearly polarized undulator field (4); the beam is taken to have perfect quality in the x direction where there is no focusing, but not perfect in the y direction where there is focusing. An electron's trajectory is determined by the relativistic Lorentz force

equations of motion [100] without the presence of radiation. The x component equation is exactly integrable and the constants of integration are set equal to zero indicating a perfect beam with perfect injection in this direction. Substituting the equation for β_x into the y and z components gives

$$\dot{\beta}_x = -\frac{\sqrt{2}K}{\gamma}\cos(k_u z)\cosh(k_u y) \quad , \quad \dot{\beta}_y = -\frac{c K^2 k_u}{\gamma^2}\cos^2(k_u z)\sinh(2k_u y) \quad , \qquad (9)$$

$$\dot{\beta}_z = \frac{c K^2 k_u}{\gamma^2}\sin(2k_u z)\cosh^2(k_u y) \quad ,$$

where $c\vec{\beta} = c(\beta_x, \beta_y, \beta_z)$ is the electron velocity, and $\gamma^{-2} = 1 - \vec{\beta}^2$.

Even with perfect injection of a perfect beam $k_u y \to 0$, the exact solution to (9) involves elliptic integrals. But, the kind of motion of interest is when $K \sim \gamma \gg 1$ so that $K/\gamma \ll 1$; when $K \sim \gamma$ the undulator field is strong enough to begin to trap electrons in a single undulator period and prevent propagation along z. To order $(K/\gamma)^2$, the perfect trajectories that continue along the undulator are

$$z(\tau) = -\frac{K\lambda_u}{\sqrt{2}\pi\gamma}\sin(2\pi N_u \tau) + \ldots . \quad , \quad \dot{\beta}_y(0) = y(0) = 0 \quad , \quad z(\tau) = \bar{\beta}_z L_u \tau - \frac{K^2\lambda_u}{8\pi\gamma^2}\sin(4\pi N_u \tau) + \ldots . \quad , \qquad (10)$$

where $c\bar{\beta}_z = c(1-(1+K^2)/2\gamma^2 + \ldots .) = c$ is the average z velocity in each undulator period, and $\tau = c\bar{\beta}_z t/L_u = ct/L_u$. The typical amplitude of transverse wiggling motion, $K\lambda_u/\sqrt{2}\pi\gamma = 0.1$mm for $K = 1$, $\lambda_u = 5$cm, and $\gamma = 100$, is smaller than the typical beam size of $r_b = 1$mm. The fast z motion oscillates twice each undulator period, and is responsible for emission into the odd harmonics as shown later.

A more realistic beam is not perfect, but is of sufficient quality so that $k_u y \ll 1$. Typically, there are only a few betatron oscillations over a large number of undulator periods N_u. Averaging over a small, integral number of undulator periods λ_u allows us to concentrate on and solve for the larger scale betatron motion. Averaging the y motion in (9) gives

$$\ddot{\bar{y}}(\tau) = -\omega_\beta^2 \bar{y}(\tau) = -\frac{\partial V_\beta(y)}{\partial y} \quad , \text{ where } \quad V_\beta(y) = \frac{1}{2}\omega_\beta^2 y^2 \quad . \qquad (11)$$

where $(\ddot{..}) = d^2(..)/d\tau^2$, and the dimensionless betatron frequency in the harmonic potential, $V_\beta(y)$, is $\omega_\beta = Kk_u L_u/\gamma = 2\pi N_u K/\gamma$ for the linearly polarized undulator. A typical undulator with $K = 1$, $N_u = 100$, and $\gamma = 100$, has one betatron oscillation and $\omega_\beta = 2\pi$.

The harmonic betatron oscillations defined by (11) have the constant of motion $H_\beta = [\omega_\beta^2 y^2(\tau) + \dot{y}^2(\tau)]/2 = [\omega_\beta^2 y_0^2 + \dot{y}^2(0)]/2$ where y_0 is the initial electron transverse position, $\dot{y}(0) = L_u\theta_y$, and θ_y is the initial injection angle. When an electron is injected off-axis by y_0, or at an angle θ_y, its average z velocity is decreased by $\Delta\bar{\beta}_z = -H_\beta/L_u$ relative to an electron injected perfectly. Any change in the electron's average z velocity causes a corresponding change in the electron's phase velocity given by $\Delta\bar{v}_\beta = kL_u\Delta\bar{\beta}_z$. An imperfectly injected electron has a decrease in phase velocity given by

$$\Delta\bar{v}_\beta = -\frac{kH_\beta}{L_u} = -\frac{2\pi N_u}{1+K^2}(K^2 k_u^2 y_0^2 + \gamma^2\theta_y^2) \qquad (12$$

The effect of the both types of errors, y_0 and θ_y, can be compared using their resultant change in phase velocity (12). A longer undulator with a large number of periods is more sensitive to beam quality because the gain bandwidth is narrower. A beam with a random spread in y_0 and θ_y will begin to decrease the FEL's ability to trunch electrons, and decrease gain, when the changes in phase velocity $\Delta\bar{v}_\beta$ becomes of order π.

The quality of an electron beam from an accelerator and transport system can be described by "emittance", $\varepsilon_y = \bar{y}_0\bar{\theta}_y$ where $\bar{y}_0$ is the rms initial position spread of electrons along y, and $\bar{\theta}_y$ is the rms initial angular spread of electrons in the y direction. Either the rms position spread $\bar{y}_0$ or the rms angular spread $\bar{\theta}_y$ can be changed by external focusing fields at the entrance of the undulator, but their product ε_y is fixed. When the beam is guided into the natural undulator potential $V_\beta(y)$, it is desirable to "match" the angular and position spreads so that the beam does not focus or expand as it travels along z. The matching condition requires that $Kk_u\bar{y}_0 = \gamma\bar{\theta}_y$, and gives smooth propagation of the beam along the undulator axis with the minimum spread in FEL phase velocities. A matched beam with emittance ε_y gives a phase velocity spread $\Delta\bar{v}_\beta = 2\pi N_u Kk\,\varepsilon_y/\gamma$. If we require that the phase velocity spread not exceed the natural gain bandwidth, then the FEL emittance is limited to $\varepsilon_y^{max} \sim \gamma\lambda/2\pi N_u K$. A typical FEL requires emittance in the range of 1mm-mradian. The relation shows important trends in FEL design; the emittance requirements are more severe when the FEL wavelength λ is short, and when the number of undulator periods N_u is large.

For the helical or parabolic undulators, it was shown above that the transverse off-axis field increases at half the rate of the linear undulator. The result is a betatron frequency that is reduced by $\sqrt{2}$; $\omega_\beta^{H,P} = \omega_\beta^L/\sqrt{2} = Kk_u L_u/\sqrt{2}\gamma$. The advantage of the helical and parabolic undulators is that there is focusing in both the x and y directions.

4. Spontaneous emission

The electrons passing through the FEL undulator experience small transverse accelerations and radiate in the forward direction along the direction of the beam. The electron trajectories remain unperturbed because the spontaneous radiation loss is small. Because of the relativistic nature of the radiation process, the frequency and angular distributions are complicated. Spontaneous emission is necessary for the start-up of the FEL oscillator and the super-radiant

high-gain amplifier. The characteristics of the FEL spontaneous radiation can be useful as a diagnostic tool for the electron beam trajectories and undulator quality.

The relativistic Larmor formula [100] gives the total power $P_e = 2e^2\gamma^4\dot{\beta}_\perp^2/3c$ emitted from one electron. In the helical undulator the transverse acceleration is $\dot{\beta}_\perp = Kk_u c/\gamma$, so that $P_e = (8\pi r_e^2/3)(2\gamma^2 B_u^2 c/8\pi)$, where $r_e = e^2/mc^2$ is the classical electron radius. The first factor is recognized as the non-relativistic Thomson scattering cross section, and the second factor is the energy flux in the approaching helical undulator as viewed in the frame of the relativistic electrons. The back-scattering of the virtual photons from the undulator field is the fundamental process of spontaneous emission in the Weizsäcker-Williams approximation. The radiation from a relativistic electron is emitted into a forward cone of instantaneous angular width $\sim\gamma^{-1}$. In the undulator, an electron is given a deflection $\beta_\perp = K/\gamma$ in each period. When $K \le 1$, the forward cone stays in a detector on-axis at infinity, so that the detector can resolve the Doppler shifted frequency $\omega = kc = 2\gamma^2 k_u c/(1+K^2)$. But, when $K \ge 1$, the forward cone periodically deflects out of the detector at infinity causing emission into higher frequency harmonics. When $K \gg 1$, there are many harmonics, and the undulator becomes known as a "wiggler" [101]. When $K \sim \gamma$, the electron trajectories do not propagate along the undulator, and the forward cone emits into the detector on-axis at infinity only once; the radiation process then resembles broad-band synchrotron radiation and magnetic bremsstrahlung.

The Liénard-Wiechert fields describe the radiation from the electron trajectories [100]; the fields naturally divide into the "velocity field" that represents the small instantaneous Coulomb interaction between electrons in the beam, and the larger "acceleration field" proportional to $\dot{\beta}_\perp$ and falling off with distance as R^{-1} [102,103]. For small K, observed at a large distance R on the undulator axis, the Liénard-Wiechert electric fields from an electron in a linear (L) and helical (H) undulator are

$$\vec{E}^{\,L}_{LW} = \frac{4eK\gamma^3 k_u}{R}\,[\cos(k_u ct'), 0, 0] \quad , \quad \vec{E}^{\,H}_{LW} \approx \frac{4eK\gamma^3 k_u}{R}\,[\cos(k_u ct'), -\sin(k_u ct'), 0] \quad ; \quad (13)$$

the Liénard-Wiechert magnetic fields are given by $\vec{B}^{\,L,H}_{LW} = \hat{z}\times\vec{E}^{\,L,H}_{LW}$. Far away from the undulator, the retarded time t' is given by $t' = t - z(t')/c$ where $z(t)$ is the electron trajectory. The polarization of the light is determined by the undulator polarization, while the radiation field strength is proportional to K, and decays with the observation distance R. In the undulator, the electron's oscillation frequency is $k_u c$, but the retarded time alters the radiation frequency seen in the lab. The largest component of the electron trajectory is $z(t) \approx \bar{\beta}_z ct$ with smaller corrections down by factors of K/γ. Solving for the retarded time gives $t' \approx 2\gamma^2 t$ when $K \ll 1$ so that the observed radiation frequency is $\omega = 2\gamma^2 k_u c$.

The energy of an emitted photon is $\hbar\omega$, and the emission time is L_u/c. The Larmor formula then gives the number of transitions (emissions) from one electron in one pass through the undulator, $W_t = (P_e/\hbar\omega)(L_u/c) = 2N_u\alpha K^2$ where $\alpha = e^2/\hbar c = 1/137$ is the fine structure constant. The transition number can also be written as $W_t = (B_u^2/4\pi\hbar k_u c)(\pi r_e^2 L_u)$. The first factor is the energy density of the undulator field, $B_u^2/4\pi$, divided by the virtual photon energy in the field, $\hbar k_u c$; it is therefore the density of virtual photons in the undulator. The second factor is the volume swept out by a classical electron traveling through the undulator. In this view, spontaneous emission results from a relativistic classical electron traveling along z and "kicking" virtual photons out of the undulator into real photons. For a typical FEL, $W_t \approx 1$ so that an electron emits about one spontaneous photon each pass into the γ^{-1} cone. Only a fraction of these photons are within the solid angle, $\pi\theta_c^2 \approx 1/N_u\gamma^2$, defined by the coherent optical mode with a Rayleigh length comparable to the undulator length. The number of photons emitted into the coherent mode by an electron during one pass is given by the simple relation

$$W_c \approx \alpha K^2 \quad . \quad (14)$$

A strong undulator emits more light, as expected, but for the typical undulator with $K \approx 1$, only a small fraction of the electrons in the beam, $\approx 1/137$, contribute a photon to the optical field each pass. Neither W_t nor W_c depends on the electron energy γmc^2, because a classical electron kicks the same number of virtual quanta out from the undulator field regardless of energy; the final photon energy $\hbar kc = 2\gamma^2\hbar k_u c$ does increase for higher energy electrons. The number of transitions W_c into a coherent mode is independent of L_u, because the coherent mode associated with the undulator length becomes narrower in proportion to the increased number of transitions W_t.

The quantum nature of the FEL spontaneous emission process is usually not evident because of the high density of electrons in the beam. However, there are important limits to the classical approximation [104]. The purpose of any laser is to create a classical optical field with a well-defined phase and amplitude, so that the validity of the classical approximation is more than just a convenience. Electron recoil resulting from the emission of an energetic photon, changes the electron's energy; if the change moves the electron across the gain bandwidth, $\Delta\gamma/\gamma = 1/2N_u$, then its ability to emit again is significantly decreased. Electron recoil is not important when $\hbar kc \ll \gamma mc^2/2N_u$, or when $\gamma\lambda \gg 4\pi N_u\lambda_C$ where $\lambda_C = \hbar/mc = 3.86\times10^{-13}$cm is the Compton wavelength. In a typical FEL with $\gamma = 100$, $\lambda = 1\mu$m, and $N_u = 100$, this inequality holds by $\sim 10^5$. In fact, unlike an atomic laser, an electron in the FEL can emit $\sim 10^8$ photons before its interaction dynamics are changed significantly.

A classical field is made up of many quanta so that zero-point fluctuations in the optical field are small, and the light can be described as an electromagnetic wave. The longitudinal length corresponding to the gain bandwidth $\sim N_u\lambda$, and the coherent transverse mode area λL_u define a volume element $V_c \sim N_u^2\lambda^2\lambda_u$ in which to count quanta [104]. In a typical FEL, the coherence volume element is $V_c \sim 1\text{mm}^3$, and the electron density is $n_e = 10^{12}\text{cm}^{-3}$. The number of

electrons in V_c is then about 10^9, so that the shot noise fluctuations from one volume element to the next are small, $\sim 3\times10^{-5}$. The number of quanta emitted into V_c is $10^9 W_c \sim 10^7$ in a single pass; again the fluctuations are small. In the FEL oscillator where amplification of the wave takes place over several thousand passes, there are enough quanta after the first pass to approximate a classical optical field. In the FEL super-radiant amplifier, a classical field is formed from noise in the first fraction of the undulator length, and then amplified. Since the volume element $V_c \propto \lambda^2$ decreases rapidly with the optical wavelength, an FEL designed to operate at short x-ray wavelengths, like $\lambda = 1$nm, can be affected by quantum statistics and shot noise. A more complete analysis of FEL quantum theory is found in the chapter by G. Dattoli and A. Renieri.

The classical description of the radiation pattern and the frequency spectrum from FEL spontaneous emission [69,105-113] is found in the chapter by P. Elleaume. Several plots show the radiation intensity as a function of frequency ω and the angle of emission θ. The spectral shape of each emission line is determined by the factor $\sin^2(v_h/2)/(v_h/2)^2$ where $v_h = L_u[hk_u - k(1+K^2+\gamma^2\theta^2)/2\gamma^2]$ for each harmonic $h = 1,2,3,\ldots$. In an undulator with a large number of periods N_u, the line is narrower. Significant emission occurs only in a narrow range of wavelengths satisfying $|v_h| \le \pi$, or $\Delta\omega/\omega \le 1/2N_u$. The resonant frequency at the line-center of each harmonic is shifted towards longer wavelengths with increasing observation angle,

$$\omega = \frac{2\gamma^2 h\, k_u\, c}{1+K^2+\gamma^2\theta^2} \quad . \tag{15}$$

There is a large frequency shift when θ covers the narrow range, 0 to γ^{-1}, but emission diminishes outside the relativistic radiation cone of angular width $\approx \gamma^{-1}$.

The detailed properties of the emitted radiation depend crucially on the size of the parameter K and the polarization of the undulator. A linearly polarized undulator produces linearly polarized light, and the helical undulator produces circularly polarized light. When the undulator is weak $K \ll 1$, only the fundamental frequency radiates. For $K \le 1$, only small harmonic numbers contribute to the emission, while for $K \ge 1$, the power in the fundamental increases, and the first few harmonics rise to comparable intensity. In the helical undulator, emission in higher harmonics above the fundamental frequency can only occur off-axis at $\theta > 0$. The electron trajectories in the linear undulator have the fast oscillatory z motion, derived in (10), which causes emission on-axis into the odd harmonics $h = 1,3,5,7,\ldots$; the number of peaks in these odd harmonics over the angular range $\theta = 0 \to \gamma^{-1}$ is equal to the harmonic number h. Compared to the synchrotron radiation from a bending magnet, the undulator radiates N_u^2 times the energy into a small solid angle and frequency interval.

5. The FEL optical wave equation

In both the FEL oscillator and even the super-radiant amplifier, spontaneous emission rapidly establishes a classical light wave for further amplification by stimulated emission. Since the bandwidth of the spontaneous light is comparable to the number of undulator periods through which electrons have passed, there is usually some degree of coherence in this classical wave. The classical model for stimulated emission and absorption is a plane electromagnetic wave driving an array of charged particles on springs [114]. In this model, the radiation field loses, or gains, energy as work is done on, or by, the oscillating particle. The relative phase between the particle's oscillations and the driving force determines whether stimulated emission or absorption occurs. Borenstein and Lamb [115] used a similar procedure to describe coherent optical beats classically. In an FEL, the electromagnetic radiation provides a driving force on electrons oscillating through the undulator [51,68,69,111].

An electron traveling through the linear undulator $\vec{B}_L$ in (6) radiates Liénard-Wiechert fields with the polarization shown in (13), $\vec{E}^{\,L}_{LW}$ and $\vec{B}^{\,L}_{LW}$. The coherent components of these fields spread more slowly than R^{-1} and are properly described by the Rayleigh length. As the radiation from multiple electron passes is stored in the resonant cavity it takes on a well-defined classical form. Since the resonator cavity is long compared to the optical wavelength, boundary conditions in the longitudinal direction are not important. We follow a complex field envelope $(E(z,t), \phi(z,t))$ with the radiation electric and magnetic fields of the form

$$\vec{E}_R(\vec{x},t) = E(z,t)[\cos(kz-\omega t+\phi(z,t)),\, 0,\, 0] \quad , \quad \vec{B}_R(\vec{x},t) = E(z,t)[0,\, \cos(kz-\omega t+\phi(z,t)),\, 0] \quad , \tag{16}$$

where $E(z,t)$ is the wave amplitude, the carrier frequency is $\omega = kc$, and the phase is $\phi(z,t)$. The field envelope is taken to vary slowly in time during an optical period ($E' \ll \omega E$, $\phi' \ll \omega\phi$), and in space over an optical wavelength ($E' \ll kE$, $\phi' \ll k\phi$). If this were not the case, the FEL would have a broadband spectrum. Within the "slowly-varying amplitude and phase approximation", these fields can be derived from the vector potential $\vec{A}(\vec{x},t) = (E(z,t)/k)\,[\sin(kz-\omega t+\phi(z,t)),\, 0,\, 0]$. When the amplitude E and phase ϕ are held fixed, (16) describes a plane wave traveling in the z direction. Using the fields in (16), the optical wave equation becomes

$$\left[\nabla^2 - \frac{1}{c^2}\frac{\partial^2}{\partial t^2}\right]\vec{A}(\vec{x},t) = 2\left[\frac{\partial E}{\partial z} + \frac{1}{c}\frac{\partial E}{\partial t}\right][\cos(\psi),\, 0,\, 0] + \tag{17}$$

$$+ 2E\left[\frac{\partial \phi}{\partial z} + \frac{1}{c}\frac{\partial \phi}{\partial t}\right][-\sin(\psi),\, 0,\, 0] = -\frac{4\pi}{c}\vec{J}_\perp(\vec{x},t)$$

where $\psi = kz - \omega t + \phi$. If there is no current $\vec{J}_\perp = 0$, the solution to (17) is $E = E(z-ct)$ and $\phi = \phi(z-ct)$.

The total beam current is the sum of all single particle currents, and for a single particle in the beam $\vec{J}_{\perp_i} = -ec\vec{\beta}_\perp \delta^{(3)}(\vec{x}-\vec{r}_i)$ where $\vec{r}_i$ is the trajectory of the i^{th} electron. In the relativistic limit, the electron's transverse motion is almost entirely determined by the undulator field, so that we can accurately use $\vec{\beta}_\perp = -(\sqrt{2}K/\gamma)[\cos(k_u z),0,0]$ from (9) with $y = \dot{y} = 0$. The "fast" factors "cos(ψ)", "sin(ψ)" on the left side of (17), and "cos($k_u z$)" on the right side of (17) each oscillate once as an electron passes through an undulator period. To separate (17) into slowly-varying and fast-varying factors, multiply by "cos(ψ)", and then by "sin(ψ)". At a fixed time, average ($\overline{\cdots}$) the two resulting equations over a volume element dV_c that is much smaller than the coherence volume V_c, but much larger than an optical wavelength λ. The wave equation is then

$$\left(\frac{\partial}{\partial z}+\frac{1}{c}\frac{\partial}{\partial t}\right)Ee^{i\phi} = -2\sqrt{2}\pi eK\sum_i\overline{\left[\frac{e^{-i((k+k_u)z-\omega t)}}{\gamma}+\frac{e^{-i((k-k_u)z-\omega t)}}{\gamma}\right]}\delta^{(3)}(\vec{x}-\vec{r}_i)\ . \qquad (18)$$

The second-order partial differential wave equation has now been reduced to two first-order differential equations for the complex field envelope.

Recall that an electron in a linear undulator experiences fast oscillating z motion as described in (10). This fast motion is periodic whereas the more interesting bunching occurs on a slower time-scale. In order to concentrate on the slow evolution $\bar{z}$ in (18) caused by the FEL interaction, we separate the fast periodic z motion from the electron phase ζ. The first term in the current of (18) has the phase $(k+k_u)z-\omega t = \zeta - \xi\sin(2k_u z)$, where $\xi = K^2/2(1+K^2)$ and $\zeta = (k+k_u)\bar{z}-\omega t$. The electron phase ζ contains only the slowly-varying part of the z motion $\bar{z}$. Similarly, the second term in the current of (18) has the phase $(k-k_u)z-\omega t = \zeta - 2k_u z - \xi\sin(2k_u z)$. As the electrons pass through the volume element dV_c that is several wavelengths of light long, they pass through an equal number of undulator periods. Therefore, the average ($\overline{\cdots}$) over one cycle of the fast periodic motion in the current of (18) is an average over one undulator period. The remaining average ($\overline{\cdots}$) in (18) gives

$$\left(\frac{\partial}{\partial z}+\frac{1}{c}\frac{\partial}{\partial t}\right)Ee^{i\phi} = -2\sqrt{2}\pi eK\,(J_0(\xi)-J_1(\xi))\sum_i\frac{e^{-i\zeta}}{\gamma}\delta^{(3)}(\vec{x}-\vec{r}_i)\ , \qquad (19)$$

where J_0 and J_1 are Bessel functions of the first kind. The Bessel function factors express that reduced coupling caused by the fast periodic z motion in each undulator period [111]. The corresponding fast phase-velocity motion is $\Delta v = -4\pi N_u \xi\cos(4\pi N_u \tau)$. In a typical FEL with $K = 1$, an electron whose averaged slow motion is near resonance, $v \approx 0$, periodically deflects far off resonance by $\pm N_u\pi$ twice while passing through each undulator wavelength.

On the macroscopic scale dV_c the FEL interaction does not alter the electron pulse shape. In a properly designed FEL, no process can distort the electron pulse on this scale, because the smaller scale microscopic electron bunching would be destroyed. There are typically $\sim 10^8$ electrons in the volume element dV_c that are identified by their initial phase-space coordinates $(\zeta(0),v(0))$. Since the field envelope $E(z,t)$ is slowly varying over dV_c, only one slice of the phase space one wavelength of light long, is sampled. Consistent with previous assumptions, all other wavelengths of light in dV_c must evolve in the same way. Similarly, the electrons are sampled in order to achieve an accurate representation of the initial phase space that is occupied. In this way, the sum over all electrons is replaced with an average over sampled electrons and weighted by the macroscopic particle density $n_e(z)$ at the site z. Indicating the appropriate phase-space average by $\langle\ldots\rangle$ at site z, the wave equation becomes

$$\left(\frac{\partial}{\partial z}+\frac{1}{c}\frac{\partial}{\partial t}\right)Ee^{i\phi} = -2\sqrt{2}\pi eK\,(J_0(\xi)-J_1(\xi))\,n_e(z-\bar{\beta}_z ct)\,\langle\exp(-i\zeta)\rangle_{(z-\bar{\beta}_z ct)}\ , \qquad (20)$$

where $n_e(z-\bar{\beta}_z ct)$ is the density of the traveling electron pulse. Both sides of (20) are now slowly-varying in space and time. Evaluation of the operator on the left can be made with the coordinate transformation, $z = \bar{z} + ct$ so that $(\partial_z + c^{-1}\partial_t) \to c^{-1}\partial_{\bar{t}}$. The new coordinate $\bar{z}$ stays with a point on the field envelope traveling at speed c. The slower electrons then drift back at a speed $c(1-\bar{\beta}_z)$.

In the special case where the electron pulse is long all field sites along z evolve in the same way. The electron pulse has no spatial dependence, $n_e(\bar{z}) \to n_e$, and no longitudinal optical modes are followed. The wave equation is then independent of z or $\bar{z}$. A further simplification occurs when $N_u \gg 1$ so that the changes in γ are small even at saturation. The wave equation in the linear undulator then becomes

$$\dot{a} = -j\langle e^{-i\zeta}\rangle\ , \qquad (21)$$

where the complex dimensionless field envelope is

$$a = \frac{4\pi N_u eK\,(J_0(\xi)-J_1(\xi))\,L_u\bar{E}e^{i\phi}}{\gamma^2 mc^2}\ ,\quad j = \frac{8N_u(e\pi K\,(J_0(\xi)-J_1(\xi))\,L_u)^2 n_e}{\gamma^3 mc^2}\ ,$$

and the rms optical field strength is $\bar{E} = E/\sqrt{2}$. In the helical undulator case, the fast z motion does not occur when the trajectory is ideal [111], and the prescription $K(J_0(\xi)-J_1(\xi)) \to K$ in a and j of (21) gives the correct form of the wave equation.

In the absence of current, $j = 0$, the FEL optical wave envelope does not evolve and remains at its initial value. Similarly, when there is current, but no bunching $\langle\ldots\rangle = 0$, there is also no change in the optical field. In the next section, we develop the electron equations of motion that determine the bunching in the phase $\zeta(\tau)$ in response to the presence of the optical field $a(\tau)$. This will complete a "feedback" loop that is the FEL gain mechanism.

6. FEL electron dynamics

The Lorentz force equations [100] govern the electron evolution in phase-space as they move through the classical fields $\vec{E}'_R$, $\vec{B}'_R$ in (16), and $\vec{B}'_L$ in (6). The transverse components may be integrated over one undulator period by noting that the right side is a perfect time derivative when B and E are approximately constant. The result is

$$\gamma \vec{\beta}_\perp = -\sqrt{2}\,K\,[\cos(k_u z),0,0] + \sqrt{2}\,K_R\,[\sin(\psi),0,0] \quad , \tag{22}$$

where $K_R = eE\lambda/2\pi mc^2$ is the dimensionless optical vector potential, and $\psi = kz - \omega t + \phi$. The constants of integration have been set equal to zero indicating perfect injection into the undulator. The consequences of imperfect injection will be discussed later. Using (22), the fourth component describing the electron energy change is

$$\gamma(t) = \frac{d\gamma}{dt} = \frac{2\omega}{\gamma}\,(KK_R\cos(k_u z)\cos(\psi) - K_R^2\sin(\psi)\cos(\psi)) \quad . \tag{23}$$

The electron microscopic position in $z(t)$ determines whether an electron losses or gains energy from the optical wave. As the electron energy changes, the z velocity is found by substituting $\vec{\beta}_\perp$ from (22) into $\gamma^{-2} = 1 - \vec{\beta}_\perp^2 - \beta_z^2$. Then, we obtain

$$\beta_z(t) = \left\{ 1 - \frac{1 + 2K^2\cos^2(k_u z) + 4KK_R\cos(k_u z)\sin(\psi) + 2K_R^2\sin^2(\psi)}{\gamma^2} \right\}^{1/2} \quad . \tag{24}$$

The energy and z-velocity equations (23) and (24) can be used to solve for the electron motion, but again the fast periodic z oscillations unnecessarily complicate the more interesting slow evolution of bunching.

We have already seen that a typical FEL has $K \sim 1$, and that $\gamma \gg 1$. In fact, if K/γ is not small, the electrons are not energetic enough to travel through the undulator and would be turned around in the first period. Furthermore, the maximum value of K_R occurs in strong field saturation where electrons become trapped in phase-space and execute synchrotron oscillations. It can be shown that $K_R^{max} \sim (N_S/N_u)^2$ where N_S is the number of synchrotron oscillations along the undulator length, see section 16. Typically, $K_R^{max} \sim 10^{-4}$ so that $K \gg K_R$ even the strongest optical fields. In (23) and (24), the terms that change $\gamma(t)$ and $\beta_z(t)$ contain both fast and slow factors. As in the wave equation, we fix the time and average over a volume element dV_c that is several wavelengths of light long; while an electron passes back through dV_c, it simultaneously passes over several undulator wavelengths, one for optical wavelength in dV_c. The averaged electron equations of motion are then

$$\frac{d\gamma}{dt} = \frac{\omega K\,(J_0(\xi) - J_1(\xi))\,K_R}{\gamma}\cos(\zeta + \phi) \quad , \quad \beta_z(t) = 1 - \frac{1+K^2}{2\gamma^2} \quad . \tag{25}$$

The equations in (25) are accurate in strong optical fields, and in the high efficiency FEL where there can be significant changes in the electron energy [65,66,116 122]

When $N_u \gg 1$, so that the FEL efficiency is not too large, γ can be eliminated from (25) as a dynamical variable. This reveals a much simpler form of the electron dynamics, the pendulum equation [50,51,68,69,111,123-127],

$$\overset{\circ\circ}{\zeta} = \overset{\circ}{v} \approx |a|\cos(\zeta + \phi) \quad , \tag{26}$$

where $|a| = (4\pi N_u)^2 K\,(J_0(\xi) - J_1(\xi))K_R/(1+K^2)$ in agreement with the definition below (21). The appropriate equations for the helical FEL are obtained by the prescription $K\,(J_0(\xi) - J_1(\xi)) \to K$ in the field $|a|$. The electron equations in either (25) or (26) have been made slowly varying over each undulator period and correctly follow the development of electron bunching. Further integration can be accomplished numerically on a small computer, or analytically with some specific assumptions. Because the equations are slowly varying, numerical time-steps can jump over several undulator periods; it is not necessary to integrate the fast periodic motion within each undulator period as expressed in (23) and (24).

The combination of the Maxwell's wave equation for the light and the relativistic Lorentz force equation for the electrons forms the powerful Maxwell-Lorentz theory of the FEL. In the simplest form the wave equation (21) and the pendulum equation (26), are valid in both weak and strong optical fields with high or low gain. They are not accurate for the high efficiency FEL where there are significant changes in the electron energy γmc^2. In the definition of the dimensionless field strength $|a|$, γ is taken to be the initial electron energy and is not followed self-consistently. The field $|a|$ expresses how more relativistic electrons with a larger Lorentz factor γ require a stronger optical field E to accomplish the same bunching. When an electron loses energy, the value of $|a|$ increases so that the coupling between ζ and $v = \overset{\circ}{\zeta}$ increases. We will see later that the height of the closed-orbit region of phase space is proportional to $|a|^{1/2}$, or $\gamma^{-3/2}$. When more than 10% of the electron beam energy is converted to radiation, the FEL dynamics can be altered so that the more complete wave equation (20) and electron equation (25) may be used. Only one FEL system in table 1, ELF at LLNL, has demonstrated greater than 5% efficiency.

7. The low-current, low-gain FEL

In the Maxwell-Lorentz theory, each electron used in the wave equation beam average $\langle\ldots\rangle$ is labeled by its initial conditions in phase space, $\zeta_0 = \zeta(0)$ and $v_0 = v(0)$, at the beginning of the undulator $\tau = 0$. No redundant label is used in (26); it is to be understood that there are as many separate electron equations as there are sample electrons in $\langle\ldots\rangle$. For each electron, resonance is measured by v_0 as the difference between "the frequency at which electrons pass over wavelengths of the periodic undulator" and "the frequency at which wavelengths of light pass

over the electrons". When $v_0 = 0$, these two frequencies are equal, and the electron is at resonance. If the optical field changes are small, the case of low j, the electrons follow fixed phase-space paths as does the simple pendulum. The phase-space paths in (ζ, v) are given by $v(\zeta) = \pm [2H_0 + 2|a|\sin(\zeta+\phi)]^{1/2}$ where the constant of motion $2H_0 = v_0^2 - 2|a|\sin(\zeta_0+\phi)$ determines the specific path for an electron. An electron starting on any given path remains on that path.

In the limit of low gain, there are stationary solutions to the pendulum equation where the electron phase and phase velocity remain constant in time. If electrons are initially at the resonant phase velocity $v_0 = 0$ and positioned at one of the initial phases $\zeta_0 = \pi/2 \pm \pi p$ where $p = 0, 1, 2, 3, \ldots$, then $\dot{v} = v = 0$ and the electrons do not evolve. These are "critical fixed points" in the phase space, and the initial coordinates (ζ_0, v_0) are constants of the motion. In the helical undulator, electrons travel along helical paths through the undulator magnetic field and the optical radiation fields with no change in energy. No work is done on the electrons, because the transverse motion in the undulator $\vec{\beta}_\perp$ and the optical electric field $\vec{E}_R$ are always orthogonal. In the linear undulator, the fast z motion is superimposed, but still no work is done on the electrons. The phase-space points $v_0 = 0$ and $\zeta_0 = \pi/2 \pm 2\pi p$ are "stable fixed points" surrounded by circular harmonic orbits; the mechanical simple pendulum would be at the bottom of its arc. The phase-space points $v_0 = 0$ and $\zeta_0 = 3\pi/2 \pm 2\pi p$ are "unstable fixed points" where orbits approach and recede from four directions; the mechanical simple pendulum would be at the top of its arc. Electrons near these points evolve slowly in time. Electrons that have a large phase velocity v in relatively weak fields, $|v| \geq 2|a|^{1/2}$, are in open orbits far away from resonance; the mechanical simple pendulum would have enough angular momentum to swing completely around its arc in a weak gravitational field.

In a realistic FEL beam, the electrons are randomly spread over many ($\sim 10^3$ to $\sim 10^8$) optical wavelengths and there are many ($\sim 10^7$) electrons within each optical wavelength. The spatial distribution of such a large number of electrons looks almost uniform to the optical wave envelope. Often, the initial phases ζ_0 of a few sample electrons are taken to be uniformly spread over each 2π range of phase space to represent the real beam. When there is long range coherence in the optical wave, one 2π section of the periodic pendulum phase space is adequate to represent many others that are nearby. One 2π section of the pendulum phase space represents a section in the electron beam that is about one wavelength of light long and traveling with the beam.

If an electron is not at a fixed point, the light wave alters its phase and phase velocity. When the optical field is considered weak, $|a| \ll \pi$, there is not much change in the electron phase velocity during the evolution through the undulator $\tau = 0 \rightarrow 1$. When the dimensionless current is small, $j \ll 1$, there is little change in the optical field amplitude or phase. In weak fields with low current, the solution to the pendulum equation (26) is

$$\zeta(\tau) = \zeta_0 + v_0\tau - \frac{a_0}{v_0^2}\left[\cos(\zeta_0 + v_0\tau) - \cos(\zeta_0) + v_0\tau\sin(\zeta_0)\right] +$$

$$v(\tau) = v_0 + \frac{a_0}{v_0}\left[\sin(\zeta_0 + v_0\tau) - \sin(\zeta_0)\right] + \tag{27}$$

$$+ \frac{a_0^2}{v_0^3}\left[-\frac{1}{4}\left(\cos(2\zeta_0 + 2v_0\tau) - \cos(2\zeta_0)\right) + \cos(v_0\tau) - 1 - v_0\tau\sin(\zeta_0)\cos(\zeta_0 + v_0\tau)\right] +$$

where the initial optical field is $|a(0)| = a_0$ and $\phi(0) = 0$. Recall that $k\Delta z = \Delta\zeta$ and $4\pi N_\lambda \Delta\gamma/\gamma = \Delta v$ relate the above dynamics to the position of the electron in the beam and the electron energy. The changes are periodic in ζ_0, and deviations from the initial coordinates are proportional to the dimensionless optical field strength. About half the electrons have an initial phase ζ_0 that causes them to increase their phase velocity, while the other half are positioned to decrease their phase velocity during the interaction.

The phase-space evolution shown in figure 2 is generated by solving the wave equation (21) and the pendulum equation (26) numerically with $j = 1$, $a_0 = \pi$, and $v_0 = 2.6$, but is also described analytically by (27) since the current is low. The value $a_0 = \pi$ is at the upper limit of the weak-field regime to make the dynamics more visible. Strong fields are identified by over-bunching,

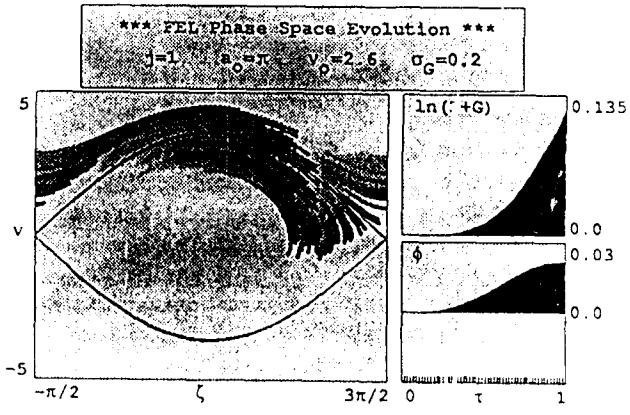

Figure 2. The electron phase space evolution with low current and weak fields.

when some electrons over-take others complicating and diminishing coherent bunching. At $\tau = 0$,

a uniform "load" of several hundred sample electrons starts at v_0. They are given a small, and inconsequential, random spread in phase velocity with a characteristic width $\sigma_v = 0.2$ to more simulate a realistic beam. As the electrons evolve, they become darker and are finally black at $\tau = 1$. As a guide to all the phase space paths, the "separatrix" is shown and given by $v_s^2 = 2|a|[1 - \sin(\zeta_s + \phi)]$. The separatrix separates the open and closed phase-space paths and passes through the critical points $(-\pi/2,0)$ and $(3\pi/2,0)$. The peak-to-peak height of the separatrix is $4|a|^{1/2}$, while the horizontal position is determined by the optical phase ϕ. Some of the electrons are initially positioned such that work is done on them; they gain energy and move ahead of the average flow at the top of the phase-space picture. Other electrons lose energy to the radiation field, and move back behind the average flow causing spatial "bunching". At $\tau = 1$, there is clear bunching near the phase π. Bunching near this phase drives the optical wave amplitude as seen in (21). *Plotted at the right in figure 2 is the gain in optical energy*, $G(\tau)$, and the change in the optical field phase, $\phi(\tau)$. Initially, there is no gain or phase shift from the uniformly spread electron beam, but as bunching develops, the gain and optical phase increase as derived below.

Primarily, the electron beam in figure 2 is spread in energy by the FEL interaction. This can be expressed analytically for an electron beam that is initially monoenergetic, and uniformly spread in phase ζ_0. Integrating over the uniform phases gives the density of electrons with phase velocity v. Using only the first-order terms in $v(\tau)$ of (27), the phase-velocity distribution function is

$$f(v,\tau) = \frac{n_e}{\pi}\left[(v - v_0)^2 - \frac{2a_0^2}{v_0^2}\left[1 - \cos(v_0\tau)\right]\right]^{-1/2} \quad , \qquad (28)$$

in weak optical fields with the restriction $|v_0| \leq \pi$. At $\tau = 0$ the beam is monoenergetic and is represented by a δ function at v_0. For small times, the δ-function splits into two sharply peaked spikes around v_0 representing the electrons that have gained and lost energy from the optical wave. At later times, the increasing distribution width is $\Delta v = a_0\tau$ centered around v_0, with a decreasing value at v_0 given by $f(v,\tau) = (n_e/\pi)(a_0\tau)^{-1/2}$. At later times, the two peaks continue move apart in proportion to the field a_0. Even though a narrow electron distribution is widened by the FEL interaction, the beam is not "thermalized". There is no increase in entropy, because the phase-space area is only distorted, not increased. *To lowest order in* a_0, *there is no net change* in the beam energy, because just as many electrons lose energy as gain. The higher-order terms in (27), proportional to a_0^2, shift and skew the phase velocity distribution function so that there can be a net change in the energy of the beam.

Energy conservation can be used to calculate the low-current FEL gain $G(\tau)$. The radiation energy, $2\bar{E}^2 \Delta V_c / 8\pi$, in a section of the light beam with volume ΔV_c, is amplified by the energy

[illegible] from $n_e F \Delta V_c$ electrons, where $F = (r_b/w_0)^2$ is the "filling factor" [illegible] been assumed in the expansion (27), the optical mode is not [illegible] by the FEL interaction. Assuming the electrons are initially uniformly [illegible] phase ζ_0 and monoenergetic with phase velocity v_0, the average energy [illegible] $\gamma mc^2(\langle v \rangle - v_0)/4\pi N_u$. The phase average eliminates the first order [illegible] order contribution allows gain, $G = 2j(v_0 - \langle v \rangle)/a_0^2$ where the filling factor F [illegible] in the current density $jF \to j$ for brevity. The gain develops [illegible]

$$G(\tau) = j\left[\frac{2 - 2\cos(v_0\tau) - v_0\tau\sin(v_0\tau)}{v_0^3}\right] \quad , \qquad [illegible]$$

where the dimensionless current density j, defined below (21), occurs naturally [illegible] the wave equation. The result (29) closely follows the gain development of the simulation shown in *figure 2*, because the gain is low and the field is weak. Note that FEL gain in this [illegible] is not exponential, and at small times or near resonance, $G(\tau) \approx j v_0\tau^4/12$ [illegible]. Far off resonance, $|v_0| \gg \pi$, the gain oscillates many times along the undulator resulting in a small [illegible] gain. Since the use of energy conservation only calculates the change in the optical field energy $\propto \bar{E}^2$, no information is obtained about the possible evolution of the optical field phase $\phi(\tau)$.

In figure 2, the electrons that increase their phase velocity, or energy, move ahead in the beam to a larger phase relative to the average electron. The electrons that decrease their phase velocity, or energy, fall behind in the beam to a smaller relative phase. This leads to bunching in the beam and coherent radiation from the wave equation. The density of electrons at phase ζ is given by the phase distribution function calculated from (27) to lowest order in a_0,

$$f(\zeta,\tau) = \frac{n_e}{2\pi}\left\{1 + \frac{a_0}{v_0^2}\left[\sin(\zeta - v_0\tau) - \sin(\zeta) + v_0\tau\cos(\zeta - v_0\tau)\right]\right\} \quad . \qquad [illegible]$$

When the beam is far off-resonance, $|v_0| \gg a_0^{1/2}$, so that the [illegible] orbit region of phase space, there is only a small amount of [illegible] radiation. At $\tau = 0$, the distribution is flat and uniformly spread, but at small times, a [illegible] density modulation develops. At resonance, $v_0 = 0$, where the bunching rate [illegible] small times $\tau \ll 1$, the distribution (30) can written as $f(\zeta,\tau) = n_e(1 + a_0\tau^2 \ldots)$ [illegible]. The bunching increases as τ^2, and develops peaks at the phases $\zeta = \pm 2\pi n + \pi/2$ where $n = 0, 1, 2, 3, \ldots$. When the field strength reaches $a_0 = \pi$, there is nearly 100% modulation of the beam. This begins the strong field regime *where* over-bunching can destroy the coherent modulation and reduce gain. If the FEL is slightly off resonance, as in figure 2, the modulations grow rapidly but also shift along the phase axis. If the FEL starts above resonance, $v_0 > 0$, the forming bunch drifts ahead of a resonant electron. If the FEL starts below resonance, $v_0 < 0$, the bunch drifts behind a resonant electron. As shown in (27), electrons bunching near the phase [illegible]

[illegible] the higher energy spike of the phase velocity distribution (v_0), FEL absorption with a phase shift near $\zeta = \pi$ over-populate the lower energy spike, FEL gain.

[illegible] FEL interaction changes both components of the optical field. Using the [illegible] the electron phase evolution, the wave equation (21) can be solved [illegible] and j.

$$a(\tau) = a_0\left(1 + \frac{j}{2}\left\{\frac{2\cos(v_0\tau) - 2 + v_0\tau\sin(v_0\tau)}{v_0^3}\right\} + \ldots\right), \quad \phi(\tau) = j\left\{\frac{2\sin(v_0\tau) - v_0\tau(1+\cos(v_0\tau))}{2v_0^3}\right\} + \ldots \qquad (31)$$

When the electrons start near $v_0 = \pi$, they bunch and drift to over-populate the phase $\zeta = \pi$ in the wave equation (21); as shown in (31), the optical wave amplitude is driven, and there is FEL gain, $G(\tau) = |a(\tau)|^2/a_0^2 - 1$. When the electrons start near $v_0 = -\pi$, they bunch and drift to over-populate the phase $\zeta = 0$ in the wave equation; in the solution (31), the optical wave amplitude decreases, and there is FEL absorption. When the electrons start near resonance $v_0 = 0$, they bunch, but do not drift, so as to over-populate the phase $\zeta = \pi/2$ in the wave equation; the solution (31) shows that the optical phase is driven, and there is little or no gain. In the low-gain case, $G(\tau) = 2|a(\tau)|/a_0 - 1$, and the first equation in (31) gives the same analytic expression for the gain as derived from energy conservation in (29). It is characteristic of the low-gain FEL that the optical phase change is small. At resonance and small times, the phase evolution is given by $\phi = j\tau^3/12 + \ldots$. The plot of $\phi(\tau)$ in figure 2 is close to the analytic result in (31); small differences arise from the finite field or current values.

As seen in the wave equation, or from energy conservation, the initial FEL phase velocity is crucial in the determination of final gain. In fact, in the weak-field low-current case, the gain per unit current G/j, and the phase shift per unit current ϕ/j, depend only on v_0. Shown in figure 3 is the final gain spectrum $G(v_0)$ and the final optical phase shift $\phi(v_0)$ at $\tau = 1$ plotted against the initial phase velocity v_0. The v_0-axis can be considered a function of the electron beam energy $\Delta\gamma = \gamma\Delta v_0/4\pi N_u$ centered about the resonant energy $\gamma = (\lambda_u(1+K^2)/2\lambda)^{1/2}$, or a function of the optical wavelength $\Delta\lambda = \lambda\Delta v_0/2\pi N_u$ centered about the resonant wavelength $\lambda = \lambda_u(1+K^2)/2\gamma^2$. The points are calculated from a simulation, but agree with the analytic results in (31) for a weak optical field and low current j. The gain spectrum is anti-symmetric in v_0 with a peak gain of $G = 0.135j$ at $v_0 = 2.6$. At resonance, $v_0 = 0$, there is no gain at any time, while at values of $v_0 < 0$ there is net adsorption of the optical power. A change in resonance by $\Delta v_0 = 2\pi$ can shift the FEL interaction from amplification to adsorption, and gain spectrum bandwidth is $\Delta v_0 = \pi$. The optical phase shift is symmetric in v_0 with a peak value $\Delta\phi = 0.083j$ at $v_0 = 0$. At the phase velocity for maximum gain $v_0 = 2.6$, the phase shift is only $\Delta\phi = 0.02j$.

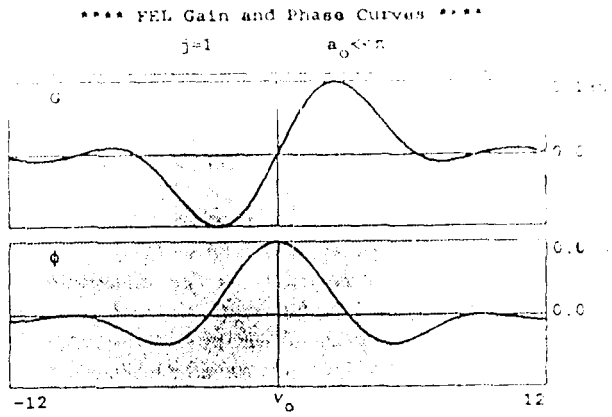

Figure 3. The weak-field gain spectrum $G(v_0)$ and optical phase shift $\phi(v_0)$ for low current.

8. The collective high-current, high-gain FEL

As the dimensionless current density is increased so that $j \gg 1$, the optical wave amplitude and phase change significantly during the FEL interaction. The expansions (27) and (31) are invalid, but the fundamental gain mechanism is still due to electron bunching in phase space [54,122-124,127-129]. Further analysis of high current effects can be found in the chapters by Sprangle-Tang-Roberson, T. Scharlemann, and T. Marshall. Table 1 shows that most FELs have operated in the low, or modest, gain regime with $j \sim 1$; the exceptions are the ELF-LLNL ($j \approx 10^4$), Boeing ($j \approx 600$), and possibly the LANL ($j \approx 50$) experiments. The high gain regime is becoming more important as accelerators are specifically designed and optimized for the FEL interaction.

Maximizing j can depend on several factors. Undulator technology appears to dictate that $\lambda_u \sim 5$cm, and $K \sim 1$. In order keep the filling factor near unity, the electron beam size should be comparable to the optical mode size $\sqrt{L_u\lambda/\pi}$, so the dimensionless current depends only on $j \propto IN_u^3\lambda^{1/2}$. At short wavelengths j is smaller, because more relativistic electrons traveling nearer the speed of light are difficult to bunch. The easiest way to increase j is to work at longer wavelengths, but an application generally fixes the wavelength before the design of the FEL begins. The penalty for increasing the undulator length indefinitely is the increased sensitivity to emittance and energy-spread as the gain bandwidth decreases. Similarly, the penalty for increasing the current indefinitely is that the beam quality from the accelerator begins to

[illegible] table 1 that has managed to achieve large j (LLNL, Boeing, and [illegible]) [illegible] degradation due to poor beam quality.

The wave and pendulum equations (21) and (27) are valid in the high gain regime so that we can immediately explore the phase space evolution numerically. In figure 4, electrons start at [illegible] velocity $v_0 = 1.6$ in a weak field $a_0 = \pi$ with high current $j = 100$. The phase velocity [illegible] will lead to maximum gain at this current. As in figure 2, there is a small inconsequential [illegible] spread in phase velocities of width $\sigma_G = 0.2$, while the initial phases are uniform. At the beginning of the undulator $\tau = 0$, there is no optical gain or phase shift as shown on the right. Because the beam is *near resonance, the electrons start bunching near the relative phase* $\zeta + \phi = \pi/2$, and drive the optical field phase ϕ in (21), but not the amplitude $|a|$. When the optical phase grows, it shifts the separatrix in phase space and shifts the relative phase $\zeta + \phi$ towards π where gain begins. The peak-to-peak height of the separatrix, $4|a|^{1/2}$, increases dramatically from about 7 to 20 because of the high gain, $G \approx 80$; the optical phase $\phi(\tau)$ moves the critical points *in the separatrix* to the left by almost $\pi/2$. In the low current case of figure 2, the optical phase change was negligible, but it is crucial here. The gain is exponential from $\tau \approx 0.5$, where bunching first develops, to the end of the undulator. No strong-field saturation is apparent even though the optical field amplitude has reached $|a| = \sqrt{G}\, a_0 \approx 9\pi$. As in the low-current case, strong fields are identified with the over-bunching that complicates and diminishes coherent bunching as some electrons over-take others. In the low-current regime, strong-field saturation begins when $|a| \gtrsim \pi$, but in the high-current regime, saturation is extended. Also, the interaction becomes collective since all electrons interact with each other through the growing optical wave amplitude and phase.

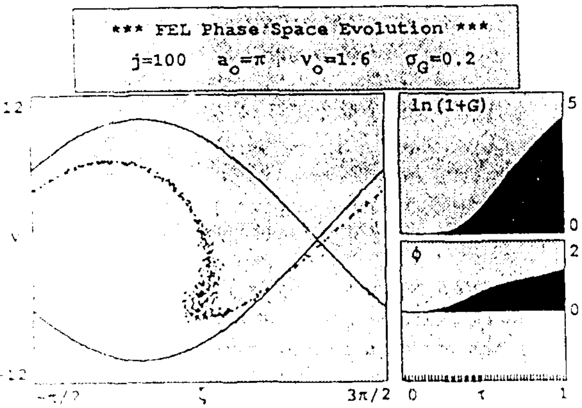

Figure 4. The [illegible] phase space evolution with high current and weak fields.

In weak optical fields, the wave and pendulum equations can [illegible] with high current $j \gg 1$. In weak fields, $|a(\tau)| \ll \pi$, the phase of the i^{th} [illegible] can be expanded as $\zeta = \zeta_0 + v_0\tau + \zeta^{(1)}$ where $\zeta^{(1)}$ is the first order perturbation [illegible]. [illegible] performed in (27), the τ-integrals are not integrated because of the [illegible] changes in the field $a(\tau)$. Combining the expanded pendulum and wave equations, and integrating over all initial phases $\int d\zeta_0$, we obtain an integro-differential equation governing the evolution of the optical field [128,129]

$$\overset{\circ}{a}(\tau) = \frac{ij}{2}\int_0^{\tau} d\tau'\, \tau' F(\tau')\, e^{[illegible]}\, a(\tau - \tau') \quad , \qquad (32)$$

where $F(\tau') = \int dq\, f(q) e^{-iq\tau'}$ is the characteristic function of the distribution $f(q)$. $f(q)$ is the distribution of initial electron phase velocities $v_i = v_0 + q$ about v_0, and $\int dq\, f(q) = 1$. Reference to all electron phases has been removed, but there remains an average over the distribution of initial electron phase velocities. Note that $F(\tau')$ and $f(q)$ only depend on the electron beam's initial conditions with subsequent dynamics described exactly. The integral equation (32) is not only valid for high current and low current, but also includes an arbitrary electron distribution function in phase velocities $f(q)$; we have only assumed weak fields. Some important results can be obtained from (32) analytically, as is done below, but it can also be solved numerically on a small computer. In the limit of weak optical fields, the integral equation has a distinct *advantage over a simulation that must follow the evolution of many sample electrons.*

We can recover the low-current results derived earlier by taking the distribution function in (32) to represent a perfect beam, $f(q) = \delta(q)$. In the low current case, the optical field growth is small so that $a(\tau - \tau') \approx a_0$, and the field can be extracted from the integrand in (32). The resulting integrals are easily solved to obtain the usual low-current gain and phase formulas (31).

In order to solve (32) with $a(\tau)$ treated self-consistently inside the integral, consider an FEL with perfect electron beam quality, $F(\tau') = 1$, and starting on resonance, $v_0 = 0$. The differential form of (32) can be found by taking successive derivatives, $\dddot{a}(\tau) = ij\,a(\tau)/2$. The general solution has three roots of the form $a_n \exp(\alpha_n \tau)$. The exponents α_n are the three complex roots of the cubic equation $\alpha_n^3 - ij/2 = 0$, while the coefficients a_n are determined by the initial conditions $a(0) = a_0$ and $\dot{a}(0) = \ddot{a}(0) = 0$. The solution for $a(\tau)$ is the sum of all the roots,

$$a(\tau) = \frac{a_0}{3}\left[e^{(j/2)^{1/3}(i+\sqrt{3})\tau/2} + [illegible] \right] \qquad (33)$$

For small times $\tau \ll 1$, (33) reduces to $a(\tau) \approx a_0(1 + ij\tau^3/12 + \ldots)$ [illegible] optical amplitude $|a| \approx a_0 + \ldots$ [illegible] order, and therefore [illegible] increases slowly in proportion to τ^3 as found earlier. There [illegible] the [illegible] bunching time, $\tau \approx \tau_B \approx (2/j)^{1/3}$, that [illegible] experiment [illegible]

bunching forms, the high current immediately causes exponential field growth and high gain.

In the high-current limit $j \gg 1$, only the fastest growing root dominates and describes exponential growth in τ. Then, complex field and gain are

$$|a(\tau)| = \frac{a_0}{3} e^{(j/2)^{1/3}\sqrt{3}\tau/2} \quad , \quad \phi(\tau) = (j/2)^{1/3}\tau/2 \quad , \quad \text{and} \quad G(\tau) = \frac{1}{9} e^{(j/2)^{1/3}\sqrt{3}\tau} \quad . \qquad (34)$$

The growth rate of the optical field amplitude, $(j/2)^{1/3}\sqrt{3}/2$, is a simple function of the dimensionless current density j. The ELF FEL in table 1 has $j \sim 10^4$, so that the weak-field gain can be enormous $G \sim 10^{12}$. The large accompanying optical phase shift, $\phi(\tau) = (j/2)^{1/3}\tau/2 \sim 3\pi$ for ELF, is the significant feature of the high gain regime.

In order to solve (32) self-consistently for a non-zero phase velocity v_0 and a perfect beam, use the substitution $b = a\, e^{iv_0\tau}$. Successive derivatives then lead to the differential form $\dddot{b} - iv_0\ddot{b} - ijb/2 = 0$. Three solutions of the form $b_n \exp(\alpha_n \tau)$ have roots α_n that satisfy the cubic equation $\alpha_n^3 - iv_0\alpha_n^2 - ij/2 = 0$. The solution is lengthy, and some limiting results are more useful. In the limit of high current, the exponential growth rate, $G = \exp((j/2)^{1/3}\sqrt{3}(1-(v_0\tau_B/3)^2))/9$, is reduced by a factor proportional to v_0^2, and the bunching time is $\tau_B = (2/j)^{1/3}$. As $j \to \infty$, the non-zero phase velocity becomes inconsequential, and the gain spectrum is center about resonance $v_0 = 0$. For finite $j \gg 1$, the gain spectrum bandwidth in the high-current regime is wider compared the to gain spectrum bandwidth in the low-current regime. If the gain bandwidth is defined by the range of phase velocities over which the gain is reduced by 1/e, then we have $\Delta v_0 = 4j^{1/6}$. It might be more appropriate to identify the gain bandwidth as the range of phase velocities over which the exponential growth rate is reduced by 10%; then we have $\Delta v_0 = 2\tau_B^{-1} = 2j^{1/3}$.

Figure 5 shows the gain spectrum $G(v_0)$ at $\tau = 1$, for $j = 100$ in weak optical fields calculated from the integral equation (32) with perfect beam quality $f(q) = \delta(q)$. The high-current gain spectrum is nearly symmetric compared the low-current case of figure 3. At higher currents, the gain spectrum develops a long tail to the left of peak gain. The peak gain of $G = 81$ (alternatively, $G(\text{dB}) = 10\log(G-1) = 19\text{dB}$ of gain) is now at $v_0 \approx 1.6$, closer to resonance than the low-current case. The gain spectrum bandwidth for this large current, $\Delta v_0 = 4j^{1/6} \approx 2\pi$, is about twice as wide as in figure 3. Below the gain spectrum is the corresponding phase shift $\phi(v_0)$. At the phase velocity for maximum gain $v_0 \approx 1.6$, the phase shift is only $\Delta\phi \approx \pi/3$ over the length of the undulator.

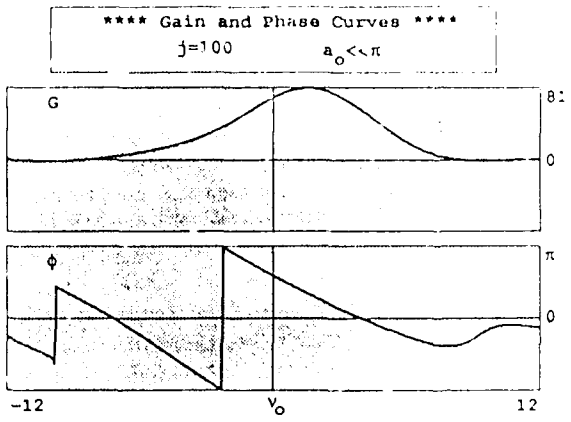

Figure 5. The weak-field gain spectrum $G(v_0)$ and optical phase shift $\phi(v_0)$ for high current.

A high current, electron bunching can be affected by inter-electron Coulomb forces [54,60,69,1[illegible]3.123]. The Coulomb force on one sample electron due to the periodic density variation from the other electrons in the bunched beam can be calculated using Poisson's equation. The resulting pendulum equation has an additional term that depends on the averaged phases of the electrons in the beam,

$$\dot{\zeta} = \dot{v} = |a|\cos(\zeta+\phi) + \frac{j}{4N_u\xi}\left(\sin(\zeta)\langle\cos(\zeta)\rangle - \cos(\zeta)\langle\sin(\zeta)\rangle\right) \quad . \qquad (35)$$

where $\xi = K^2/2(1+K^2)$. The factor weighing the Coulomb force contains the relativistic plasma frequency $j/4N_u\xi = \pi\omega_p^2(1+K^2)$, where $\omega_p = (4\pi e^2 n_e/\gamma^3 m)^{1/2}(L_u/c)$ is the "relativistic plasma frequency" times the "FEL interaction time" L_u/c. In a uniform, unbunched beam, the Coulomb term is zero, but plasma oscillations could grow from any noise source and alter the resonance condition. In order to get one plasma oscillation during the FEL interaction, the current needed is $j \geq 2(2\pi)^2 N_u \sim 10^4$ for $K \approx 1$. Coulomb forces are negligible except for a value of j that would result in extremely high gain; in this case, there would already be much more dramatic collective effects due to the high gain itself. Other macroscopic effects can come from the distortion of a short electron pulse while traveling through the undulator [130], but these are usually minor as well.

9. FEL coupling to higher frequency harmonics

Gain and spontaneous emission in the higher harmonics of an FEL has already been observed and measured [77,131-134]. Coupling to harmonics can extend the FEL tunable range to shorter wavelengths, and induce simultaneous lasing at multiple wavelengths. The fundamental cause of harmonics is the fast motion of the narrow, relativistic radiation cone around the direction of observation. The calculation of the coupling factors [69,108,111] uses the same averaging method as was used to eliminate the fast motion found for the linear undulator in (10). The laser field has the selected frequency $h\omega = hkc$, where $h = 1,2,3,....$ is the harmonic number, $h = 1$ is the fundamental wavelength, and the field envelope is taken to be slowly varying.

In the linear undulator, an electron that is perfectly injected has the fast z motion found in (10). If the electron is injected at a slight angle with components $\theta_x = \beta_x/\beta_z = \theta\cos(\Phi)$ and $\theta_y = \beta_y/\beta_z = \theta\sin(\Phi)$, the motion is more complicated. Projecting out the electron's fast z motion, it is found that $k\Delta z = -\xi\sin(2k_w z) + \sqrt{2}\chi\cos(\Phi)\sin(k_w z)$, where $\xi = K^2/2(1+K^2+\gamma^2\theta^2)$, and $\chi = 2K\gamma\theta/(1+K^2+\gamma^2\theta^2)$. For $K = 1$ and $\gamma\theta\cos(\Phi) = 1$, the fast z motion can be important. Averaging the fast z motion over an undulator period introduces Bessel functions that express the reduced coupling as a factor multiplying the undulator constant K. The product of the undulator constant and the Bessel functions is

$$K_{L,h}^2 = hK^2\left[\sum_{k=-\infty}^{\infty} J_k(h\xi)\left(J_{2k+h+1}(hZ)+J_{2k+h-1}(hZ)\right)\right]^2 , \qquad (36)$$

where $Z = \sqrt{2}\chi\cos(\Phi)$. The form of the wave and pendulum equations, (21) and (26), or the integral equation (32) are the same with the replacement $K^2 \rightarrow K_{L,h}^2$ in the dimensionless field a and the current density j. The new coupling is expressed in the Bessel functions of these variables, and the formulas of derived for the low-current and high-current regimes remain the same. On axis, only the odd harmonics emit spontaneously and have gain; off axis, all the harmonics have gain. The angles θ and Φ can result from the misalignment of the electron beam or the light wave with respect to the undulator. It is assumed that the betatron focusing in the undulator is weak so that the angle θ is constant.

In the helical undulator, there is no fast z motion unless the electron is injected at a slight angle θ. Then, the fast z motion is given by $k\Delta z = \chi\sin(k_w z)$. When $\gamma\theta$ and K are comparable to unity, the amplitude of $k\Delta z$ is large enough to cause emission and gain into higher harmonics and reduce the coupling to the fundamental. The modified coupling multiplies the undulator constant K to define

$$K_{H,h}^2 = hK^2 J_{h-1}^2(h\chi) \quad . \qquad (37)$$

This modified undulator constant can be used in the wave, pendulum, and integral equations as discussed above.

The practical possibility of extending FEL operation to higher harmonics by means of off-axis tuning is limited by the solid angle of a coherent optical mode, $\theta_c = 1/\gamma N_w^{1/2}$. Any misalignment that leaves the electron beam inside the optical mode has reduced coupling to higher harmonics.

10. Gain degradation due to electron beam quality

Optimizing an FEL experiment often leads to a design trade-off between high beam current and poor beam quality as defined by the accelerator. A given application usually fixes the optical wavelength λ so that the dimensionless current, $j \propto IN_w^3\lambda^{1/2}$, must be maximized with the current I and the number of undulator periods N_w. But, increasing I tends to decrease beam quality from the accelerator, while increasing N_w increases the FEL sensitivity to the beam quality by narrowing the gain spectrum bandwidth. To confuse the issue further, recall that figure 5 showed how the gain spectrum bandwidth is wider if we do manage to increase j to the high-current regime. In the "warm-beam" regime there is some, but not too much, gain degradation resulting from the effort to maximize both I and N_w [54,128,129]. The integral equation (32) is valid for an arbitrary electron distribution of phase velocities, but assumes weak optical fields. In strong optical fields, $|a| \geq \pi$, the FEL interaction induces an phase velocity spread that makes the initial spread relatively less important. Accurately describing electron beams with poor beam quality is difficult with simulations, but comparatively easy with the integral equation.

Poor electron beam quality reduces FEL performance by degrading bunching. Two electrons starting at the same phase, but having phase velocities differing by $\Delta v_0 = q = \pi$ will drift apart by half an optical wavelength, $\Delta\zeta \approx q\,\Delta\tau \approx \pi$, over the length of the undulator, $\Delta\tau = 1$. One example is a Gaussian spread in initial electron energies that are all perfectly injected. The result is a Gaussian distribution in phase velocity $f_G(q) = \exp[-q^2/2\sigma_G^2]/\sqrt{2\pi}\sigma_G$ about v_0 where $\sigma_G = 4\pi N_w\overline{\Delta\gamma}/\gamma$ is the standard deviation. A random spread of width $\sigma_G \approx \pi$ causes a random phase spread $\approx \pi$ and impairs bunching.

A monoenergetic beam can have a random spread in initial positions and angles consistent with the emittance of the beam as discussed in section 3. Because of the quadratic dependence of the phase velocity on entrance angle and position shown in (12), the phase velocity distribution $f(q)$ is not the same distribution as is the spread in angle or position. A Gaussian spread in angles, symmetric in x and y, gives the exponential distribution $f_\theta(q) = \exp(q/\sigma_\theta)/\sigma_\theta$ for $q \leq 0$; and $f_\theta(q) = 0$ for $q > 0$, where $\sigma_\theta = 4\pi N_w\gamma^2\bar{\theta}^2/(1+K^2)$ and $\bar{\theta}$ is the rms angle away from the z axis. A Gaussian spread in initial positions would also give the exponential distribution, and a beam with matched contributions from positions and angles, $\gamma\bar{\theta}_y = Kk_w\bar{y}_0$ with betatron focusing, gives the exponential distribution [135]. Just as for the Gaussian distribution, a random spread of

width $\sigma_\theta = \pi$ causes a random phase spread = π and impairs bunching.

The characteristic function $F(\tau)$ must be found from $f(q)$ to evaluate the integral equation (32). In summary, we have

- Gaussian: $f_G(q) = \dfrac{\exp[-q^2/2\sigma_G^2]}{\sqrt{2\pi}\,\sigma_G}$ => $F_G(\tau) = \exp[-\sigma_G^2\tau^2/2]$, (38)

- Exponential: $f_\theta(q) = \dfrac{\exp[q/\sigma_\theta]}{\sigma_\theta}$ for $q<0$, => $F_\theta(\tau) = (1 - i\,\sigma_\theta\tau)^{-1}$.

The Gaussian and exponential distributions are two important examples of characteristic shapes found in practice. In a realistic FEL, the correct shape is generally not known precisely, and is determined by several complicating factors. In any case, if the beam quality is perfect so that $\sigma_G = 0$, or $\sigma_\theta = 0$, then $F(\tau) = 1$. As the optical field $a(\tau)$ in (32) starts to grow, the field in the integrand $a(\tau')$ increases the growth rate; this is the normal FEL feedback mechanism that gives exponential gain. However, when the beam is not perfect, the characteristic function $|F(\tau')|$ decays within a time $\approx \sigma_G^{-1}$, or $\approx \sigma_\theta^{-1}$, so that the feedback mechanism deteriorates. $F(\tau)$ depends on the shape of $f(q)$, and diminishes the FEL's ability to bunch electrons in a different way for each shape. It can be easily shown that if $f(q)$ is symmetric, then $F(\tau)$ is real, and if $f(q)$ is asymmetric, then $F(\tau)$ is complex.

As an example of the FEL interaction with poor beam quality, figure 6 shows the final (ζ,v) phase space distribution of a beam with an initial spread of $\sigma_\theta = \pi$ in an exponential distribution.

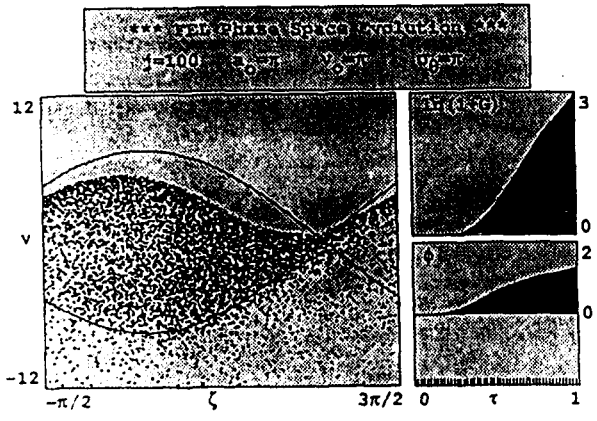

Figure 6. Phase space evolution with high current and poor beam quality.

The electron beam current is $j = 100$ in an initial optical field of $a_0 = \pi$. The initial phase velocity, or resonance condition, is at the value $v_0 = \pi$ for optimum gain under these conditions. The sharp edge along the top of the distribution results from the sharp edge in the initial exponential distribution at v_0. The FEL interaction has resulted in visible bunching near the phase $\pi/2$, but the bunch is diffuse compared to the similar example in figure 4. The final gain in figure 6 is only $G = 19$ compared to $G = 81$ for the same FEL as in figure 4; the only difference is beam quality. The phase shift in figure 6 is slightly larger than in figure 4.

Figure 7 follows the deterioration of the gain spectrum $G(v_0)$ as the beam spread σ_θ is increased for the exponential distribution. The current density is $j = 1$. The perfect beam, $\sigma_\theta = 0$, gives the usual anti-symmetric gain spectrum with a peak at phase velocity $v_0 = 2.6$ just as in figure 3. As the beam spread is increased, the maximum available gain decreases while the phase velocity for peak gain increases away from resonance. The gain spectrum curve also becomes broader in v_0 around its maximum. At the maximum spread explored, $\sigma_\theta = 8$, there is a factor of = 5 loss in gain.

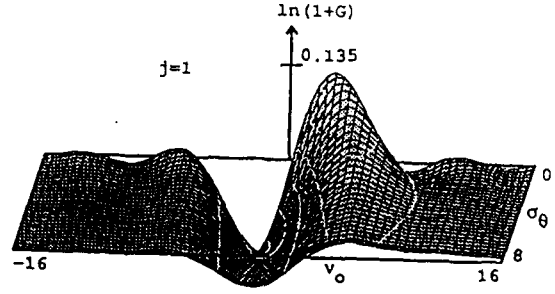

Figure 7. The weak-field gain spectrum, $G(v_0)$, for low current with an increasing angular spread σ_θ.

Figure 8 shows the degradation of the gain spectrum with higher current $j = 100$. The spread of the exponential distribution is increased to $\sigma_\theta = 16$ where the loss of gain is substantial.

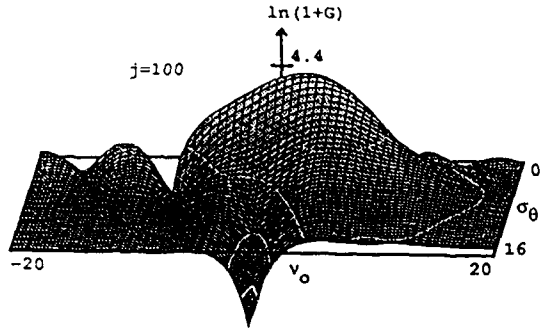

Figure 8. The weak-field gain spectrum $G(v_0)$ for high current with an increasing angular spread σ_θ.

As spread of any beam distribution is increased, the general features shown in figures 7 and 8 remain: the peak gain decreases steadily, the phase velocity at peak gain increases away from resonance, and the gain spectrum width becomes broader. These qualitative features are common to several other distributions, but the details of the degradation can be dramatically different. When the current density is large, $j \gg 1$, and the beam quality is poor, the FEL gain can be dangerously difficult to predict. A slight change in the distribution shape can alter the gain by orders of magnitude [129].

While the amount of gain reduction depends strongly on the distribution function shape, the FEL also becomes more resistant to gain degradation when there is exponential growth in the field $a(\tau)$. The integrand of the integral equation is only significantly modified when the characteristic function's rate of decay, the decay of the beam's ability to bunch, is comparable to the optical field's growth rate $(j/2)^{1/3}\sqrt{3}/2$ in the high-current limit. With this consideration the characteristic spread is $\sigma_j = j^{1/3}$ instead of $\sigma_\theta = \pi$, or $\sigma_\theta = \pi$. The high-current characteristic spread does not depend on the undulator length, but on a comparison of growth rates along τ. For $j \sim 10^4$, the increase in the critical spread $\sigma_j = 20 \gg \pi$ can be significant. Furthermore, for large j there can be large FEL gain even if there is also a large amount of gain degradation.

When an electron enters an undulator, even with perfect initial injection, the electron trajectories can be altered by errors in the undulator field [109,136]. Random field errors in each undulator period will deflect the electron in the transverse direction as it enters the next period. In a typical period of the undulator, describe the field by $\vec{B}^* = (0, B_w \sin(k_w z) + \Delta B_w, 0)$ with a small error ΔB_w. The deflection after that period is $\Delta x = \sqrt{2}\pi\Delta K \lambda_w / \gamma$ where $\Delta K = e\Delta B_w \lambda_w / 2\sqrt{2}\pi mc^2$. The size of the deflection is typically $\Delta x = 0.01$mm when the undulator field has a 1% tolerance from period to period. While traveling over many periods, the electron performs a random walk in x with varying step size and direction. Assuming constant step size, a typical deflection after N_w periods is $\overline{\Delta x} = \sqrt{N_w}\Delta x = 0.1$mm. The angular deflection caused by the random path is $\overline{\Delta\theta} = \overline{\Delta x} / N_w \lambda_w$. In order that the transverse excursions not take the electron out of the optical mode, the field error must only satisfy $\overline{\Delta\theta} \le \theta_c = 1/\gamma N_w^{1/2}$; this reduces to only $\Delta K \le 1/\sqrt{2}\pi$. In order that the reduced z velocity caused by the transverse excursions not remove the electron from the gain spectrum bandwidth, the field must satisfy the same requirement. Typically, $\Delta K/K \approx 10^{-2}$, so that random errors are not the worst problem for building an undulator in the low current FEL. However, systematic errors over many undulator periods can be more damaging.

In the high current FEL, the optical mode size can be smaller over a longer distance than in free space, or in the low current FEL, since the FEL interaction continually distorts a rapidly growing mode. In this case, the deflection of the electron beam caused by random undulator errors can upset the delicate "guiding" of the optical wave, and can even send the guided optical beam into the FEL vacuum pipe. See the chapter by T. Scharlemann for more discussion.

11. Strong optical fields and saturation

The wave and pendulum equations, (21) and (26), are valid for strong optical fields. Several physical variables determine the dimensionless field strength $|a| \propto KN_w^2 E/\gamma^2$ which measures the electron's bunching rate through the pendulum equation. Strong fields begin when $|a| \gtrsim \pi$, and cause the electrons to be trapped in the closed orbit region of phase space. The fraction of the electron beam energy converted to light, the FEL's efficiency, is larger in strong fields, but gain decreases indicating the onset of saturation. Typically, the complete saturation of an FEL amplifier, or the FEL oscillator, occurs at a field strength beyond the onset of saturation, and are well into the strong field regime. The strong fields cause over-bunching in the electron beam so that some electrons can overtake, or fall behind, other electrons in the beam. This begins to complicate the phase distribution $f(\zeta)$ from its simple sinusoidal form in (30) [137]. The electron bunch is moved too far along the phase axis in phase space for optimum gain. Looking at the pendulum equation (26), we see that a bunch, once formed, at the proper relative phase for gain, $\zeta + \phi = \pi$, would soon evolve by $\Delta\zeta(\tau) = -|a| \approx -\pi$ to the relative phase for absorption, $\zeta + \phi = 0$.

When a bunch is formed at the relative phase $\zeta + \phi = \pi$ it is on a downward path in phase space and loses energy to the optical wave. The energy that can be lost by the bunch is

determined by the height of the separatrix path $4|a|^{1/2}$ from peak-to-peak. The change in the phase velocity is $\Delta v(\tau) = 4|a|^{1/2} = 2\pi$ when $|a| = \pi$ at saturation, and corresponds to a change in the bunch's energy by $\Delta v = 4\pi N_u \Delta\gamma/\gamma = 2\pi$. This change in phase velocity is large enough to move the electron bunch across the gain bandwidth. The fraction of the beam energy that is extracted by the optical wave as saturation begins is the "natural" FEL efficiency, $\eta^* = 1/2N_u$. In a longer undulator, $N_u \gg 1$, there is the opportunity for larger gain, since $j \propto N_u^3$, but the natural efficiency is reduced. The actual efficiency of either an FEL amplifier or oscillator can be much larger than the natural efficiency, since η^* describes just the onset of saturation.

Figure 9 shows the result of solving the pendulum and wave equations numerically with 10^4 sample electrons in a strong optical field $a_0 = 20$ and for low current $j = 1$. The electrons are started with a random Gaussian spread corresponding to $\sigma_G = 1$ about the phase velocity $v_0 = 5$. This phase velocity gives nearly maximum gain at this field strength. The final phase-space positions of the electrons are drawn in (ζ, v). The gain and phase, given on the right, begin to grow rapidly near the beginning of the undulator because of the strong fields and the rapid rate of bunching. The best bunching is formed part of the way through the undulator at about $\tau = 1/2$, then the bunch evolves further, past the optimum relative phase $\zeta + \phi = \pi$ for gain, around to $\zeta + \phi = 0$ causing absorption. The gain is seen to first peak, and then decrease as the over-bunched electron beam drives the optical wave, and continues to evolve so that energy flows back into the electron beam. The final gain, $G = 0.03j$, is significantly reduced from the theoretically possible, $G = 0.135j$, in weak optical fields as shown in figure 1.

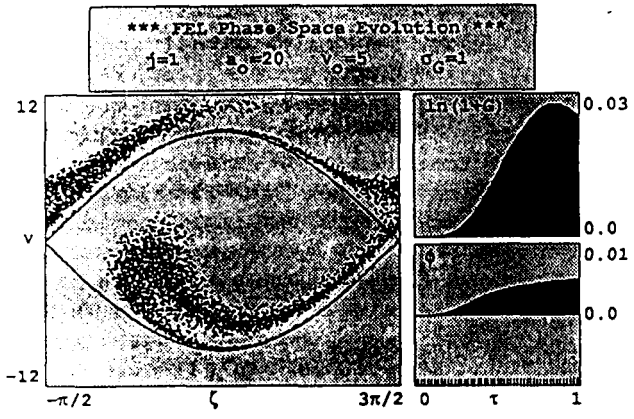

Figure 9. The strong-field phase space evolution with low current.

Figure 10 shows the phase space evolution in a strong field, $a_0 = 20$, with high current $j = 100$ and spread $\sigma_G = 1$. The initial phase velocity is $v_0 = 2$ for maximum gain. The features of the high-current FEL and strong field saturation are combined together in this example. The optical phase shift is significant as indicated by the shift of the separatrix. The strong optical fields still cause a decrease in the FEL gain as shown on the right; compare to figure 4. Over-bunching is the saturation mechanism just as in the low-current case, but for high current, there is the superimposed optical phase shift. Note that since the instantaneous separatrix shifts in phase, it cannot be interpreted as separating the open and closed orbits; electrons are steadily passing through the separatrix as it evolves.

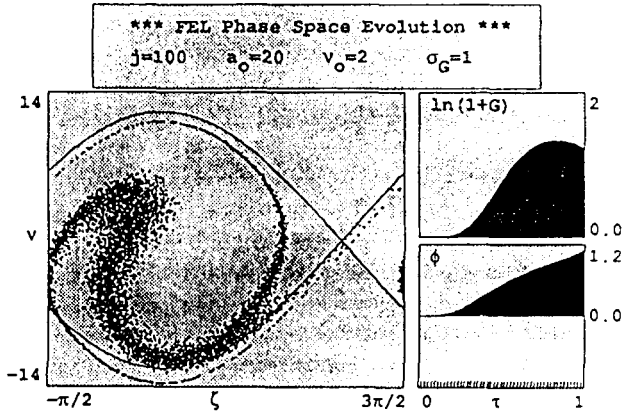

Figure 10. The strong-field phase space evolution with high current.

The gain spectrum $G(v_0)$ changes its shape in strong optical fields. Figure 11 shows the behavior of the FEL gain spectrum $G(v_0)$ as the initial field strength a_0 is increased. The gain is calculated numerically at each point (v_0, a_0) with low current $j = 1$. In weak fields $a_0 \leq \pi$, the gain spectrum is anti-symmetric about resonance, $v_0 = 0$, with a peak value $G = 0.135j$ at the phase velocity $v_0 = 2.6$. The peak absorption, or loss, is $G = -0.135j$ at the phase velocity $v_0 = -2.6$. The gain bandwidth in weak fields is roughly $\Delta v_0 \approx \pi$. As the initial field strength increases to $a_0 \approx 40$, the peak gain decreases to about 5% of the weak-field value. The phase velocity that gives peak gain increases away from resonance as the field strength a_0 increases. As the gain spectrum decreases and distorts, it also becomes broader in v_0. The spectral width,

from peak gain to peak absorption, roughly follows the full width of the separatrix, $4|a|^{1/2}$, as can be seen in figure 11.

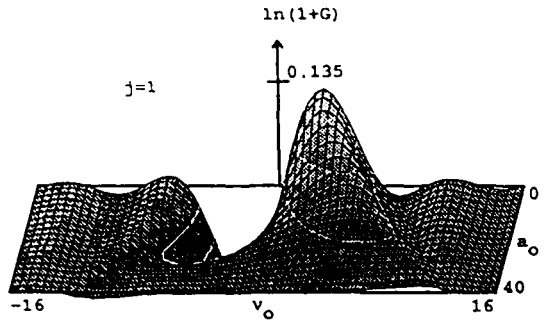

Figure 11. The gain spectrum $G(v_0)$ for low current with increasing optical field strength a_0.

This gives another explanation for the onset of the saturation process. When the separatrix height, $2|a|^{1/2}$, becomes greater than the phase velocity for peak gain in weak fields, $v_0 = 2.6$, then an increasingly larger fraction of the beam becomes trapped in the closed orbit region of phase space. The field strength for the onset of particle trapping in strong fields is roughly $a_0 \sim \pi$ as found before. The gain bandwidth roughly increases with the height of the separatrix above resonance, and is given by $\Delta v_0 \approx 2|a|^{1/2}$ in the strong field regime. The general features of diminishing gain due to beam quality shown in figure 7 are similar to those due to saturation in figure 11. This occurs because the strong field interaction induces a spread in phase velocities about equal to the height of the separatrix, $2|a|^{1/2}$. If we were to plot the gain surface shown in figure 11 as a function of the induced spread, $2|a|^{1/2}$, figures 7 and 11 would almost be identical.

After each pass in the FEL oscillator, the optical field becomes a little stronger, and the gain describing the interaction is a little further along the a_0-axis in figure 11. We expect a relatively narrow optical spectrum to evolve over many passes, and follow the peak gain in figure 11 as the power grows [138]. Typically, an FEL oscillator will require several hundred passes to evolve from the weak-field regime to the strong-field regime near saturation. As it does so, the optical wavelength is observed to shift to longer wavelengths, corresponding to a larger initial phase velocity, just as shown in figure 11 [70,74].

For low current, the electron pendulum equation (26) is expanded to lowest order in the field a_0 in (27). This form was used to calculate the phase distribution (30), and is accurate up to field strengths of order $a_0 \lesssim \pi$. In order to follow the onset of saturation, the electron phase can be inserted into the wave equation (21) to describe the evolution of the driving current and phase average <...>. After integrating over the initially uniform electron phases ζ_0, and expanding self-consistently, the wave equation becomes [68]

$$a(\tau) = a_0 + a_0 j\, \alpha(v_0\tau) - a_0^2\, j\, \beta(v_0\tau) + \dots \quad , \tag{39}$$

where $\alpha(u) = (2 - iu - (2+iu)e^{-iu})/2v_0^3$ and $\beta(u)$ are complex functions of $u = v_0\tau$ with magnitudes of order unity. The function $\alpha(u)$ is given also in the expansion (31). The real part of $\alpha(u)$ is anti-symmetric and is the gain spectrum, while the imaginary part is symmetric about resonance as shown in figure 3. The lengthy function $\beta(u)$ is not presented here, but its real part is also anti-symmetric with a symmetric imaginary part. Conventional lasers often discuss saturation and oscillator evolution with an expansion of the form in (39), but in the FEL, we will see that the strong field regime cannot be adequately described by a finite order expansion in a_0. The value of the expansion is more conceptual than accurate.

In weak optical fields, mode competition in the FEL oscillator will establish an optical wavelength near maximum gain at $v_0 = 2.6$. At the end of each pass, there is some loss to the optical field amplitude described by the resonator Q. The optical field amplitude measured at the end of many passes $s(n) = |a(n)|$ is given by

$$\frac{ds}{dn} = \left\{ j\,|\,\alpha(v_0)\,| - \frac{1}{2Q} \right\} s(n) - j\,|\,\beta(v_0)\,|\, s^2(n) + \dots \quad , \tag{40}$$

where n is the pass number. In the absence of current ($j = 0$), the optical power decays as $e^{-n/Q}$. For all the wavelengths such that $2|\alpha(v_0)| > Q^{-1}$, the FEL is said to be above "threshold", and the optical field grows on each pass in proportion to the current j. In the early stages of evolution, the field grows exponentially, and the saturation term, $\propto |\beta(v_0)|$, is negligible. At the peak gain, $v_0 = 2.6$, the magnitude of the saturation function is positive so that the growth of the field magnitude $s(n)$ decreases in stronger fields. When the field strength increases so that terms in (40) cancel, $ds(n)/dn = 0$, and the FEL operates in steady-state. While the conceptual role of the expansion (40) is valuable, care must taken when modes other than $v_0 = 2.6$ are considered, or when the resonator Q is large. If $Q \gg 1$, then the optical power may be large enough so that the expansions in (39) and (40) are inadequate. More importantly, at the wavelengths corresponding to other values of v_0, the amplitude of $\beta(v_0)$ may be negative, or zero, and cannot describe saturation. At these wavelengths, higher order terms in the expansions are needed even if saturation occurs at a relatively modest field strength.

In the case of low Q, (40) can be described as the overdamped motion of the coordinate $s = |a|$ in the generalized potential $V(s)$. Then,

$$V(s) = -\frac{1}{2}\alpha_0 s^2 + \frac{1}{4}\beta_0 s^4 \quad , \tag{41}$$

where $\alpha_0 = j\,|\alpha(\nu_0)| - 1/2Q$ and $\beta_0 = j\,|\beta(\nu_0)|$ are evaluated at $\nu_0 = 2.6$. The behavior of $s = |a(n)|$ depends critically on the sign of α_0. If $\alpha_0 < 0$, the losses of the FEL system exceed the gain, and the steady-state amplitude of the field is zero. As the dimensionless electron current density j is increased from a low value where $\alpha_0 < 0$, there is no change in the only stable point of the system: $s = 0$. At the critical value of the current where $\alpha_0 > 0$, the $s = 0$ solution becomes an unstable operating point, and fluctuations will drive the system to a new steady-state at $s = (2\alpha_0/\beta_0)^{1/2}$. A continuous change in the current density results in a discontinuous change in the final state of the FEL, analogous to a phase transition. The generalized potential $V(s)$ has the same form as the thermodynamic potentials which describe ferroelectricity, ferromagnetism (in the Ginzburg-Landau formulation), superconductivity, and the laser action of atomic lasers. The "order parameter" of the FEL is the optical field amplitude $s = |a|$ which is analogous to the magnetization in a ferromagnet. When the optical field is small, there are only a few photons in the resonator and the laser's phase ϕ is disordered. When the optical field is large at saturation, because $\alpha_0 > 0$, the optical wave becomes ordered and coherent.

The onset of saturation in the high-current regime, $j \gg 1$, begins at a different field strength than in the low-current case, but the essential physics of saturation is the same. For high current, the optical field magnitude grows as $|a(\tau)| = a_0 \exp[(j/2)^{1/3}\sqrt{3}\tau/2]/3$. The pendulum equation (26) shows that the field magnitude $a_j = 2(j/2)^{2/3}$ causes the electron phases to be shifted by as much as $\Delta\zeta(\tau) \approx \pi$ at the onset of saturation. For $j \sim 10^4$, the saturation field magnitude $a_j = 200\pi$ can be significantly larger then the low current case as has been observed [86]. The efficiency in the high-current limit is also greater than in the low-current case. The saturation field a_j causes the trapped electrons to change their phase velocity by $\Delta v_j = \pi(j/2)^{1/3}$, and corresponds to a change in energy through $\Delta v = 4\pi N_u \Delta\gamma/\gamma$. The natural efficiency in the high-current limit is therefore $\eta_j = (j/2)^{1/3}/8N_u$ when half of the electrons are trapped. For $j \sim 10^4$ and $N_u \sim 10^2$, the efficiency is typically $\eta_j = 0.02$. For the LLNL ELF experiment described in Table 1, $\eta_j = 0.07$, close to the observed value. Figure 12 shows the change in the gain spectrum $G(\nu_0)$ as a function of the initial field strength a_0 for the case of high current. The qualitative features are the same as in the low-current case, but details of the decay are different.

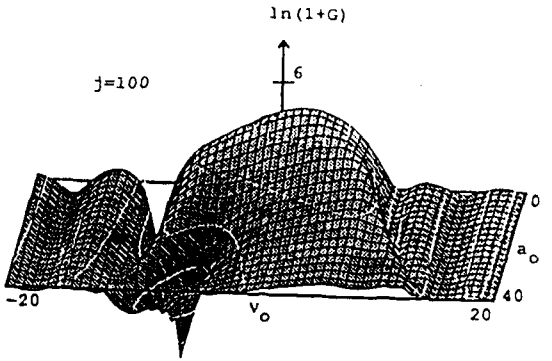

Figure 12. The gain spectrum $G(\nu_0)$ for high current with increasing optical field strength a_0.

12. The FEL klystron and tapered undulator designs

The characteristics of the FEL interaction can be changed by altering the undulator properties along its length. Special undulator designs can enhance certain FEL characteristics for special applications [1]. The undulator polarization [139,140], wavelength, or field strength, can be varied continuously, or discontinuously, along the undulator axis to alter detailed interaction properties. The analogy in a conventional atomic laser would be to change the properties of the electron binding-potential during the radiative emission time $L_u/c \approx 10^{-8}$s. This aspect of the FELs design flexibility is one of its most attractive advantages. In this section, the two-stage FEL klystron undulator and the tapered undulator are described. These two examples serve to show how the gain spectrum, and interaction can be significantly altered. The klystron increases gain in weak optical fields, but at the expense of low-power saturation; in contrast, the tapered undulator increases the saturation limit, but at the expense of weak-field gain. Both designs can be studied using simple modifications to the pendulum equation. The goal is to present a clear, simple picture while remaining conceptually accurate. More general designs are possible, and will be the subject of continuing research in the future. Addition discussion of the tapered undulator can be found in the chapters by Sprangle-Tang-Roberson, T. Scharlemann, and T. Marshall. The klystron undulator is also described in the chapter by Deacon-Ortega.

At normal saturation, the electrons lose enough energy to drop out of the gain spectrum bandwidth. As the energy of the beam decreases and shifts across the gain bandwidth, the corresponding change in the beam's phase velocity is $\Delta v = 4\pi N_u \Delta\gamma/\gamma = -2\pi$. If the electrons are accelerated to replace their lost energy, resonance would be restored, and the interaction could presumably continue to higher optical powers [65,66]. This could be accomplished with an accelerating electric field $-E_z$ directed along the undulator axis. The increase in electron energy is $\dot{\gamma} = eE_z/mc$, and the electron phase changes by $\dot{\zeta} = \delta \approx eE_z k(1+K^2)L_u^2/\gamma^3 mc^3$. The same phase acceleration, $\dot{\zeta} = \delta$, can also be achieved by decreasing the undulator wavelength λ_u along z, or decreasing the undulator field strength B along z, or both. Each method of tapering the undulator is conceptually equivalent. In weak optical fields, the electron's equation of motion is of the form $v = \delta\tau + \ldots$ where δ is the artificial acceleration given by $\delta \approx -2\pi N_u \Delta\lambda_u/\lambda_u$ when the undulator wavelength is decreased, or by $\delta \approx -4\pi N_u K^2 \Delta B_u/B_u(1+K^2)$ when the undulator field strength is decreased. With tapering included, the pendulum and wave equations have the form

$$\dot{\zeta} = \dot{v} = \delta + |a| \cos(\zeta+\phi) , \qquad \dot{a} = -j\langle e^{-i\zeta}\rangle , \quad \text{where} \quad \zeta = \int_0^\tau k_u(\tau')d\tau' + kz - \omega t . \tag{42}$$

The simple pendulum equation now includes an additional constant torque due to δ, and the wave equation remains the same. The new electron phase definition follows its usual meaning while accounting for the changing undulator wavenumber $k_u(\tau) = 2\pi/\lambda_u(\tau)$ along the undulator length. The self-consistent equations (42) are again valid in weak and strong optical fields with either high or low gain, but are not valid when the efficiency is expected to be large ($\gtrsim$ 10%). When high efficiency is anticipated, so that the electron energy and undulator properties change significantly, the more accurate equations of motion (20) and (25) can be used. In the limit of $N_u \gg 1$, the phase acceleration can be significant with only a small change in the undulator properties. Then, the dimensionless optical field and current densities are to be evaluated with the untapered values of K, λ_u, and L_u. A simple case tapers both λ_u and the undulator field strength B_u so that K remains constant. Then, the magnitude of the transverse electron velocity oscillations remains constant along the undulator. We assume here that the tapering is such that $\delta = L_u^2 dk_u(z)/dz$ is constant along the undulator.

In the tapered undulator defined by (42), the instantaneous phase space paths are given by $v(\zeta) = (S_0 + 2\zeta\delta + 2|a|\sin(\zeta+\phi))^{1/2}$ where $S_0 = v_0^2 + 2\zeta_0\delta - 2|a|\sin(\zeta_0+\phi)$. When the taper rate is too large, so that $\delta > |a|$, the electron phase space has no closed orbits. In a sufficiently strong optical field, $|a| > \delta$, some electrons can be "trapped" in the closed orbits of the pendulum phase space centered near the relative phase $\zeta+\phi \approx \cos^{-1}(-\delta/|a|)$. In stronger fields $|a| \gg \delta$, a large fraction of the electrons can be trapped near resonance around $\zeta \approx \pi$ and continue to lose energy to the optical field. When $\delta < |a|$, and there are closed orbits, there are two "critical fixed points" where the electron phase and phase velocity remain constant in time in the low-current limit $j \ll 1$. The stable fixed point is at $(\zeta, v) = (\cos^{-1}(-\delta/|a|) - \phi, 0)$, while the unstable fixed point is at $(\zeta, v) = (2\pi - \cos^{-1}(-\delta/|a|) - \phi, 0)$. With tapering, the stable and unstable fixed points are separated by less than π, and, unlike the conventional untapered FEL, the tapered design can have zero closed-orbit area at a finite field strength. The separatrix passing though the unstable fixed point, and surrounding the closed orbits, is given by $v_s^2 = 2\delta(\zeta_s - \zeta_0) + 2|a|(\sin(\zeta_s+\phi) - \sin(\zeta_0+\phi))$ where $\zeta_0 = 2\pi - \cos^{-1}(-\delta/|a|) - \phi$. For $\delta > |a|$, the arccosine has no solution, and there is no separatrix. For $\delta = 0$, we recover the expression for the separatrix in a conventional untapered undulator.

Tapering represents an advantage over the untapered design when the artificial acceleration δ exceeds the deceleration that can be obtained without taper in strong optical fields. The maximum untapered deceleration is estimated from the height of the separatrix in the untapered phase space, so that there is an advantage to tapering when $\delta \gtrsim 4|a|^{1/2}$. The natural deceleration of electrons without taper occurs when the electron bunch is decelerated across the gain spectrum bandwidth from gain to absorption, so that there is an advantage to tapering when $\delta \gtrsim 2\pi$. Combining the necessary and desirable criteria for tapering, we have

$$|a| > \delta \gtrsim 4|a|^{1/2} \gtrsim 2\pi . \tag{43}$$

On the left is the condition for trapping electrons in the tapered phase space; in the middle is the condition that the tapered acceleration exceed the natural untapered deceleration; and on the right is the condition that the tapered FEL work in the strong field regime.

Electrons starting near the phase $\zeta_0 = 0$ are accelerated by both the torque δ and the strong optical field $|a|$, while the electrons starting near $\zeta_0 = \pi$ see the torques δ and $|a|$ roughly cancel leaving them trapped in closed orbits. Those that are accelerated away from resonance eventually contribute less to the interaction. In this view, tapering is effective because electrons near the phase for gain $\zeta \approx \pi$ are trapped, while electrons near the phase for absorption $\zeta \approx 0$ are taken away from resonance and eventually stop interacting; the imbalance leads to net gain.

The tapered undulator is more efficient in strong optical fields, but has smaller gain than the untapered undulator in weak fields. For moderate tapers the gain reduction in weak fields is small and simply shifts the position of peak gain to $v_0 \approx 2.6 - \delta/2$; larger tapers decrease the gain more significantly and distort the gain spectrum [113]. A typical value of $\delta = 20\pi$ is given by an undulator with 10% taper in wavelength over $N_u = 100$ periods. If 50% of the electrons remained trapped, the efficiency is estimated at $\eta_\delta \approx \delta/8\pi N_u \approx 3\%$, and is increased by 5 over the natural efficiency $\eta^* = 1/2N_u$. The limit on η_δ is determined by the maximum taper rate, δ, that can maintain trapping over the lowest number of periods, N_u. When δ is too large for the FEL field strength or the growth rate, electrons will not remain trapped and η_δ is reduced. When the current is large, $j \gg 1$, we have already seen that the saturation field strength is increased and

grows exponentially. As a result, the fraction of the beam trapped can exceed 50%; an impressive efficiency of 40% has already been observed [87]. Some examples of tapered undulators and their approximate values of δ are given in Table 1.

Figure 13 shows the final phase space distribution of 10^4 electrons that started at $v_0 = 0$ with a Gaussian spread of $\sigma_G = 1$. The initial strong field $a_0 = 40$ is amplified by current $j = 1$ in a tapered undulator with phase acceleration $\delta = 10\pi$ satisfying the conditions in (43). The separatrix identifying the closed orbits in figure 13 surrounds a smaller area than the untapered case of figure 9 where there is even a stronger optical field. The untrapped electrons have final phase velocities around $v = 40$ and are spread along the ζ-phase axis, whereas trapped electrons tend to remain inside the separatrix. Near the unstable fixed point on the right side of the separatrix electrons are seen "leaking" out of the trapped orbits. This occurs because the optical field evolves with a growth in amplitude $|a|$ and a shifting phase ϕ during the interaction. Oscillations in the evolution of the gain $G(\tau)$ and the optical phase $\phi(\tau)$ shown at the right are caused by the oscillations of the electron bunch in the harmonic closed orbits around the stable fixed point inside the separatrix. The separation in phase velocity between the trapped and untrapped electrons is $\Delta v = 40$ in figure 13, and roughly 50% of the electrons are trapped. Using $\Delta v = 4\pi N_u \Delta\gamma/\gamma$, the efficiency in an undulator with $N_u = 100$ periods is $\eta_\delta \approx 3/2N_u \approx 1.5\%$, or about 3 times the natural efficiency without taper.

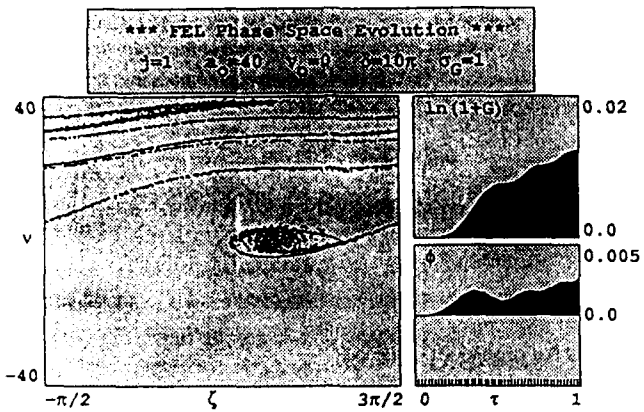

Figure 13. Phase evolution in a tapered undulator with low current.

In the case of high current, the tapered undulator can have much more gain and a larger trapping fraction than with low current. Figure 14 shows the same tapered FEL as in figure 13, but with the current increased to $j = 100$. The optical phase shift is not large because of the diminished interaction strength in strong fields and with taper. The separatrix has grown larger than trapped bunch.

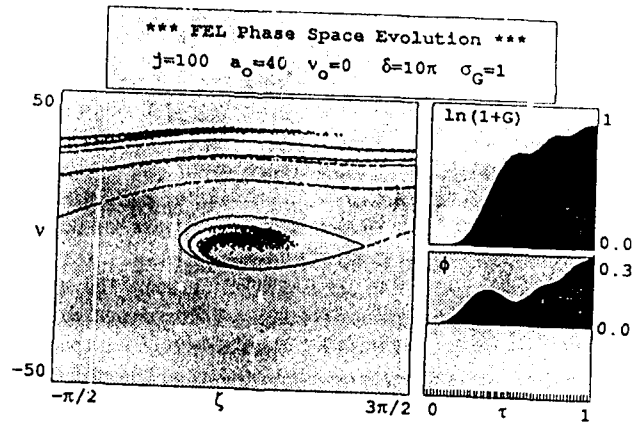

Figure 14. Phase evolution in a tapered undulator with high current.

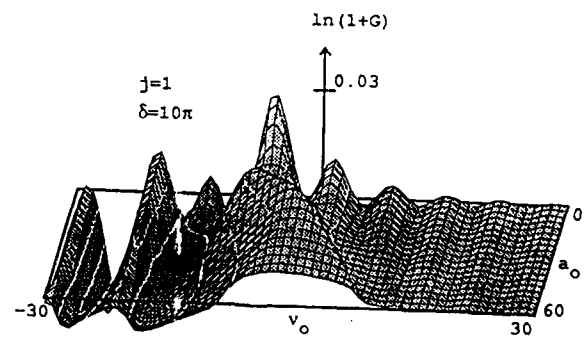

Figure 15. The gain spectrum $G(v_0)$ for the tapered undulator with increasing optical field strength a_0.

Figure 15 shows the gain spectrum $G(v_0)$ as a function of initial optical field strength a_0 for a tapered undulator with $\delta = 10\pi$. The low current $j = 1$ results in peak gain of 3% below resonance in weak optical fields. The phase acceleration δ interferes with the gain development and produces many oscillations in $G(v_0)$ when $a_0 \ll \pi$. In stronger fields $a_0 \geq \delta = 10\pi$, trapping begins so that optimum gain is at resonance $v_0 = 0$. The gain spectrum bandwidth in strong fields is given by the height of the separatrix $v_s(\zeta_s)$.

The klystron undulator

The two-stage optical "klystron" is designed to improve FEL gain in weak optical fields [141-145], just as the tapered undulator is designed to improve FEL performance in strong optical fields. Such an improvement may be useful when the weak-field gain of a conventional undulator would be unacceptably low for start-up of the FEL oscillator. The FEL klystron consists of two undulator sections separated by a drift, or dispersive section. The drift and dispersive mechanisms are the same mathematically, but practically, it is the dispersive section that gives a substantial increase in the FEL gain for a given interaction length. The optical fields in the first undulator section , the "modulator", prepare electrons to bunch as they go through the dispersive section, and then to radiate coherently in the second undulator section, the "radiator". In the dispersive section, the electron-optical interaction is effectively turned off because the electrons are far from resonance. The net change in ζ is proportional to the modulated value of v exiting the first klystron section, $\Delta\zeta = vD$, where D is the dimensionless time of the drift, or is a measure of the strength of the dispersive section [145]. The self-consistent equations describing the FEL klystron can be written compactly as

$$\overset{\circ\circ}{\zeta} = \overset{\circ}{v} = |a| \cos(\zeta + \phi) \quad , \quad \overset{\circ}{a} = -j\langle e^{-i\zeta} \rangle \quad , \quad \text{for } 0 \leq \tau < 0.5 \text{ , and } 0.5 < \tau \leq 1 \quad , \qquad (44)$$

$$\text{and} \quad \Delta\zeta = vD \quad , \quad \Delta v = 0 \quad , \quad \text{at} \quad \tau = 0.5 \quad .$$

The dispersive interaction is applied instantaneously at $\tau = 0.5$ since we know the analytic solution resulting from the drift. Again, the combined equations (44) are valid in weak and strong optical fields with both high and low current.

In weak optical fields with low gain, (44) can be linearized and solved analytically to give the final gain at $\tau = 1$,

$$G(v_0) = -\frac{j}{v_0^3}\,[2\cos(x) + x\sin(x)]\left[\, 2\,|_0^{v_0/2} + |_{v_0(D+1/2)}^{v_0(D+1)} - |_{v_0 D}^{v_0(D+1/2)} \right] \quad , \qquad (45)$$

$$\phi(v_0) = \frac{j}{2v_0^3}\,[2\sin(x) - x(1+\cos(x))]\left[\, 2\,|_0^{v_0/2} + |_{v_0(D+1/2)}^{v_0(D+1)} - |_{v_0 D}^{v_0(D+1/2)} \right] \quad ,$$

where $f(x)|_a^b = f(b) - f(a)$. The gain and phase expressions for the standard FEL are recovered when $D = 0$, and the limits in the brackets reduce to $|_0^{v_0}$. The result (45) is only valid for $jD \leq 1$, when there is no significant optical phase shift, and the FEL mechanism is not collective.

Figure 16 shows the gain spectrum for a klystron with a dispersive strength $D = 2$ in weak optical fields $a_0 \ll \pi$ and low current $j = 0.1$. Several peaks occur within the range $|v_0| \leq 2\pi$, because of the interference between the two undulators. The peak gain is increased to $G = 0.63j$ at $v_0 = 0.5$ as compared to $G = 0.135j$ at $v_0 = 2.6$ in the conventional undulator.

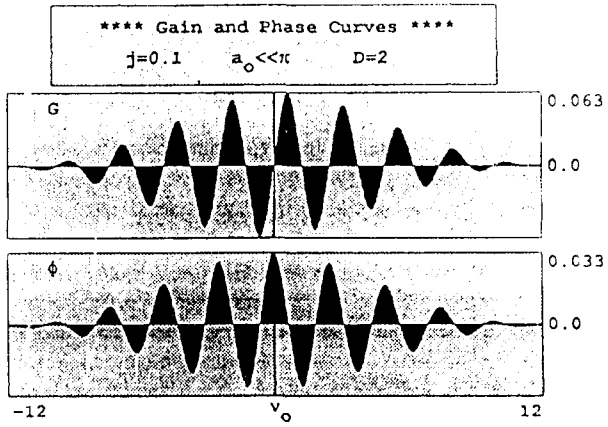

Figure 16. The gain spectrum $G(v_0)$ and optical phase shift $\phi(v_0)$ for the klystron undulator.

In the limit of $D \to \infty$ and $v_0 \to 0$ with the product Dv_0 fixed, the gain and optical phase shift are given by the simpler expressions

$$G(v_0) = \frac{jD}{4}\sin(v_0 D) \quad , \quad \text{and} \quad \phi(v_0) = \frac{jD}{8}\cos(v_0 D) \quad . \qquad (46)$$

The peak gain available in the FEL klystron is $jD/4$ at phase velocity $v_0 = \pi/2D$. Typical dispersive sections are designed to give $D = 4$ as seen in table 1. When the dimensionless current density is low, say $j = 0.1$, the FEL klystron design can give $G = jD/4 = 10\%$ gain just as in the normal undulator. As can be seen in (46), the electron-beam quality (energy spread, emittance, etc.) should be good enough to ensure that the spread in the initial phase velocities is $\Delta v_0 \leq \pi/D$. In the conventional FEL, the limit on electron-beam quality is only $\Delta v_0 \leq \pi$, showing

that the klystron configuration is more sensitive to electron-beam quality. This limitation can become severe when the klystron is strong and D is large.

The electron phase distribution function $f_D(\zeta,\tau)$ for the FEL klystron is

$$f_D(\zeta,\tau) = \frac{n_e}{2\pi}\left[\,1 + \frac{a_0}{v_0^2}\left[\sin(\zeta - x) + x\cos(\zeta - x)\right] R(v_0,\tau) + \ldots\right] , \tag{47}$$

$$\text{where} \quad R(v_0,\tau) = \theta(1/2-\tau)\,\Big|_0^{v_0\tau} + \theta(\tau-1/2)\left[\,\Big|_0^{v_0(\tau-1/2)} + \Big|_{v_0(\tau+D-1/2)}^{v_0(\tau+D)}\right] .$$

For a strong FEL klystron, the limit of $D \to \infty$ and $v_0 \to 0$ gives the final electron phase distribution

$$f_D(\zeta) = \frac{n_e}{2\pi}\left[\,1 + \frac{a_0 D}{2}\sin(\zeta - v_0 D) + \ldots\right] . \tag{48}$$

The amplitude of the modulation increases with $a_0 D$, and the phase bunches at $(\pi/2 + v_0 D) = \pi$ when gain is maximum at $v_0 = \pi/2D$. For stronger fields, the klystron mechanism does not work well and saturation occurs. The qualitative features of saturation are similar to the ordinary FEL design.

We have assumed a value of the current j that is low enough so that the resultant klystron gain is low, and the quantity jD is small. When there is high gain, owing to either large j or large D, the optical-phase shift can be significant and can modify the results (45-48). The shifting of the optical phase during the interaction alters the interaction so that the areas of absorption in figure 16 decrease with respect to the areas of gain. Eventually, the gain spectrum becomes more symmetric just as in the conventional undulator.

13. FEL Lagrangians and Hamiltonians

As a mathematical development, it is useful to display the Lagrangian describing the wave and pendulum equations for each undulator design [138]. The FEL Lagrangians and Hamiltonians can be used to find constants of motion for each of the FEL undulators and have a broad range of validity.

The conventional periodic undulator has the Lagrangian

$$L = -\frac{1}{2}|a|^2\dot{\phi} + \frac{1}{2}j\langle\dot{\zeta}^2\rangle + j\,|a|\,\langle\sin(\zeta+\phi)\rangle \quad . \tag{49}$$

The three terms in (49) are, respectively, the optical kinetic energy (which is not the same as the total energy of the optical field), the electron "kinetic energy" (in terms of the coordinate ζ), and the electron-optical-field interaction energy, or ponderomotive potential. A nonzero value of $\dot{\phi}$ corresponds to a change in the optical frequency ω, and therefore a change in the energy of

optical photons. The equations of motion recovered from (49) are the Euler-Lagrange equations describing the coordinates $|a|$, ϕ, and ζ for each electron in the average $\langle\ldots\rangle$.

From (49) we find two constants of motion. Since the optical phase ϕ appears in the Lagrangian only in the combination $\zeta + \phi$, we can transform to the variable $\chi = \zeta + \phi$ so that L is cyclic in ϕ. The corresponding canonical momentum p is a conserved quantity,

$$p = \frac{1}{2}|a|^2 + j\langle v\rangle = \text{constant}. \tag{50}$$

The electron phase velocity averaged over all sample electrons $\langle v\rangle$ must decrease if the field strength $|a|$ is to grow from its initial value a_0. The term $|a|^2/2$ is proportional to the number of photons and gives the optical field momentum.

Since the Lagrangian (49) is explicitly independent of the time τ, the corresponding Hamiltonian is conserved,

$$H = \frac{1}{2}j\langle\dot{\zeta}^2\rangle - j\,|a|\,\langle\sin(\zeta+\phi)\rangle = \frac{1}{2}j\langle\dot{\zeta}^2\rangle - |a|^2\dot{\phi} = \text{constant}. \tag{51}$$

The Hamiltonian H is recognized as the energy since it is quadratic in the generalized velocity $\dot{\zeta}$. An increase in the mean-square electron velocity $\langle\dot{\zeta}^2\rangle$ results in a phase advance of the optical field.

The Lagrangian for the tapered undulator design includes the additional acceleration, or torque δ,

$$L_\delta = -\frac{1}{2}|a|^2\dot{\phi} + \frac{1}{2}j\langle\dot{\zeta}^2\rangle + j\,|a|\,\langle\sin(\zeta+\phi)\rangle + j\delta\langle\zeta\rangle \quad . \tag{52}$$

The periodic ponderomotive potential now has an upward tilt increasing the electron phases ζ. The final term in (52) breaks the cyclicity of L_δ in ϕ, so that the corresponding canonical momentum is no longer conserved but rather increases linearly with time,

$$p_\delta = \frac{1}{2}|a|^2 + j\langle v\rangle = \frac{1}{2}a_0^2 + jv_0 + j\,\delta\tau \quad . \tag{53}$$

This is simply a consequence of the uniform acceleration applied to the electrons. If all electrons were untrapped in weak optical fields, then $\langle v\rangle = v_0 + \delta\tau + \ldots$ and $|a|^2 = a_0^2 + \ldots$ so that there would be little energy exchange between the electrons and light. The trapping of electrons decreases $\langle v\rangle$ from its weak-field value, allowing $|a|^2$ and efficiency to increase. The Hamiltonian is again conserved since L_δ remains explicitly time independent,

$$H_\delta = \frac{1}{2}j\langle\dot{\zeta}^2\rangle - |a|^2\dot{\phi} - j\delta\langle\zeta\rangle = \text{constant}. \tag{54}$$

The additional electron acceleration δ acts to retard the advance $\dot{\phi}$ of the optical phase.

The two-stage FEL klystron undulator with a dispersive section of strength D is mathematically equivalent to using a drift space of physical length DL_u. In the drift space, the FEL interaction is turned off since $j \propto K^2 \to 0$. The interaction is on for $0 \le \tau < 0.5$, off for the drift space, and then turned on again for $0.5+D < \tau \le 1+D$, while traversing the second undulator section. Represented in this way, the Lagrangian for the FEL klystron design becomes

$$L_D = -\frac{1}{2}\,|a|^2\dot{\phi} + \frac{1}{2}\,j\,\varepsilon(\tau)\,\langle\dot{\zeta}^2\rangle + j\,\varepsilon(\tau)\,|a|\,\langle\sin(\zeta+\phi)\rangle \quad , \tag{55}$$

where $\varepsilon(\tau) = \theta(0.5-\tau) + \theta(\tau-0.5-D)$, and $\theta(\tau) = 1$ for $\tau > 0$, and $\theta(\tau) = 0$ for $\tau < 0$. The function $\varepsilon(\tau)$ simply turns off the undulator $K \to 0$ for a time $\tau = D$ in the middle of the undulator. As in the conventional undulator, the canonical ϕ-momentum is conserved, so that the constant of motion (50) also applies to the optical klystron,

$$p_D = \frac{1}{2}\,|a|^2 + j\langle v\rangle = \text{constant}. \tag{56}$$

The klystron Hamiltonian corresponding to the klystron Lagrangian (55) is not conserved, since it is explicitly time dependent,

$$H_D = \frac{1}{2}\,j\langle\dot{\zeta}^2\rangle - j\,\varepsilon(\tau)\,|a|\,\langle\sin(\zeta+\phi)\rangle \quad . \tag{57}$$

This mathematical description of the FEL klystron appears to violate energy conservation. In fact, the transitions out of and back into the undulator sections happen at the same z positions instead of at the same time τ for all electrons, and if the physical variables involving z were used, H_D would not depend explicitly on time. We cannot make such a representation, however, having transformed to the electron phase coordinate $\zeta(\tau)$. For our purposes the equations of motion are adequate to describe the physical processes in the optical klystron.

14. Mode competition and coherence development

In the limit of low current and low gain, the modes of the FEL oscillator evolve independently. Since we have the expression for the weak-field gain in each mode over a single pass, we can simply follow the development of the modes over many passes n though the undulator. Because of the relativistic nature of the FEL interaction, modal decompositions in the transverse and longitudinal directions along the beam have different characteristic scale lengths. The natural scale in the longitudinal dimension is determined by the gain bandwidth, and corresponds to the electron-optical slippage distance $N_u\lambda$; this is the distance that light passes over electrons as the electrons travel through the undulator. At resonance, exactly one wavelength of light passes over an electron as the electron passes through an undulator

wavelength; over the whole undulator, N_u wavelengths of light pass over the resonant electron. The slippage distance, $N_u\lambda$, is the characteristic length over which electrons and light can exchange information during one pass. In the low-gain FEL oscillator, the optical signal develops from spontaneous emission with an initial coherence length of $N_u\lambda$. Over many passes in the resonator, mode competition can narrow the spectrum significantly and increase the coherence length. In the transverse dimension, the important scale is roughly the radius of the optical beam, $(L_u\lambda/\pi)^{1/2}$, that will double in area due to natural diffraction as it passes through the undulator length. The boundary conditions at metal, or dielectric, mirrors beyond the ends of the undulator define a minimum intermode spacing roughly given by $\Delta k \sim L_u^{-1}$. The minimum mode spacing is then estimated as $\Delta v(k) \sim \gamma^{-2}$. For the relativistic FEL, there is, in effect, a continuum of modes across the gain spectrum bandwidth $\Delta v = \pi$.

Following the evolution of independent optical modes in the longitudinal direction shows how coherence develops from spontaneous emission. In the low-gain oscillator, the modes evolve independently, and can be followed with the theory developed already. Each longitudinal mode, or wavelength $\lambda = 2\pi/k$, is identified by a phase velocity $v(k) = L_u[(k+k_u)\beta_z - k]$. The undulator wavelength and initial electron beam energy from the accelerator are fixed during the evolution over many passes. The FEL gain spectrum, $G(v)$, with its anti-symmetric shape peaking at $v = 2.6$ is determined by the undulator. The spontaneous emission lineshape $s(v) \propto (\sin(v/2)/(v/2))^2$ is symmetric in shape with a width $\Delta v = 2\pi$. Typically, the spontaneous power emitted each pass is $\sim 10^{-8}$ below the optical power level in strong fields. At the bottom of figure 17 the shapes of the gain and spontaneous emission spectra are displayed for the range of phase velocities $\Delta v(k) = \pm 6$ around resonance. On each pass, the power in each mode changes due to the spontaneous emission, the gain, and the loss or output coupling at the resonator mirrors. On the n^{th} pass, the change in the optical power, $P_n = |a(n)|^2$, is

$$\Delta P_n(v) = s(v) + P_n(v)\,[\,G(v) - 1/Q\,] \tag{58}$$

where $P_n(v)$ is the optical power in mode $v(k)$, $s(v)$ is the spontaneous emission into mode $v(k)$ on each pass, $G(v)$ is the gain spectrum, and $-1/Q$ determines the loss on each pass for all modes independent of v. Only the optical power spectrum $P_n(v)$ evolves on each pass, because we are in the weak field limit.

The contour-intensity plot in figure 17 shows how the normalized spectrum $P(v,n)/P_{max}$ evolves from spontaneous emission into a narrower spectrum over $n = 0 \to 500$ passes. The peak gain is $G = 13\%$ with $j = 1$, and the loss is determined by $Q = 100$. The level of loss is shown as a horizontal line in the gain spectrum, $G(v)$. The final spectrum is centered around the phase velocity $v = 2.6$ at peak gain, and has about 4 times the coherence length of the spontaneous spectrum. As the spectrum continues to narrow, the development of each mode can be expressed as a function of the second derivative of the gain spectrum expanded in a

Taylor series about its maximum. A simple expression gives the FEL optical spectrum width after n passes with current j,

$$\Delta\nu = 2\pi (nj)^{-1/2} \tag{59}$$

The physical width of the spectrum is $\Delta\lambda/\lambda = 1/N_u(nj)^{1/2}$. Eventually, at long evolution times, the spectral width is limited by practical noise sources like vibrating optical components, or the short electron pulse from an RF linac.

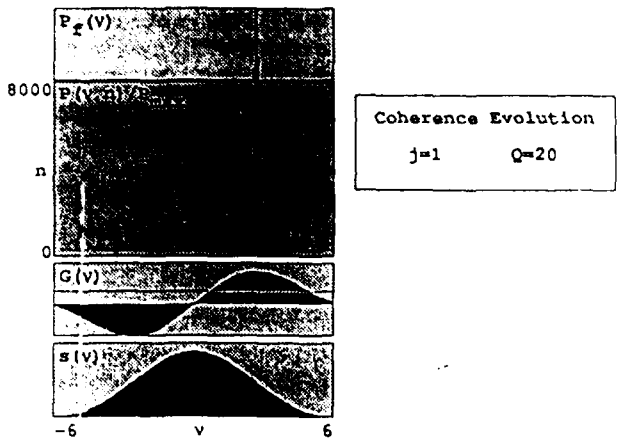

Figure 17. Mode competition and coherence development in the low current oscillator.

Mode competition in an optical klystron with $D = 2$ is shown in figure 18. The dimensionless current is $j = 0.1$ with losses determined by $Q = 40$. The spontaneous emission spectrum is altered in the FEL klystron because radiation from the two undulator sections interferes, and $s_D(\nu) \propto (1-\cos(\nu/2))(1+\cos(\nu/2+\nu D))/(\nu/2)^2$. The are now several gain peaks with similar gain, and they compete over several hundred passes. Only the highest gain mode has significant power at the end of $n = 800$ passes.

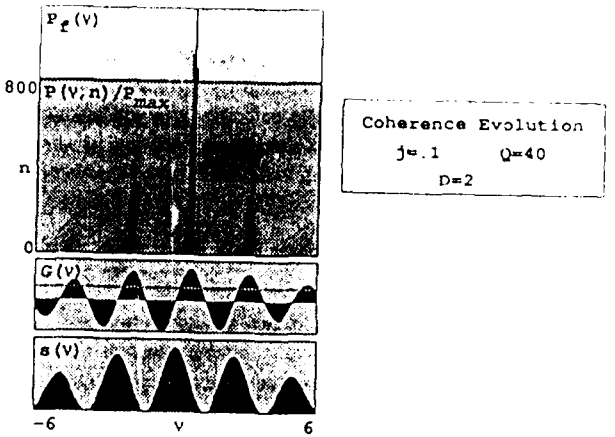

Figure 18. Mode competition and coherence development in the low current oscillator with a klystron undulator.

One of the distinguishing features of a conventional laser as a light source is its narrow optical spectrum. Coherence lengths, extending over thousands, or more, optical wavelengths are established through the process of mode competition, and not because of selected atomic states or cavity modes. The general concept of mode competition should be expected to apply in much the same manner in the case of the FEL. Each FEL configuration has a well-known gain spectrum shape that can be calculated to show that there is a wavelength with the peak, maximum gain surrounded by wavelengths with less gain.

15. Longitudinal multimode theory

FEL optical modes can be coupled by strong fields, short pulses, or high gain, and generally require a more complete approach than used in the last section [55,56,68,92,124,125,146-155] Following multiple sites along the complex wave envelope, $a(z)$, generalizes the optical field in the longitudinal direction. The extension to spatial modes $a \rightarrow a(z)$ is complete'y equivalent to an extension in longitudinal wavenumbers $a \rightarrow a(k)$. The natural scale-length in the z dimension is the slippage distance, $N_u\lambda$, as given by the gain spectrum bandwidth, or by the distance over which information is exchanged during the FEL interaction. A site in the electron beam amplifies N_u optical wavelengths, while a site in the optical wave passes over a section of the beam $N_u\lambda$ long. The slippage distance between electrons and light develops over the interaction time L_u/c.

because of the difference between the electron speed $c\bar{\beta}_z$ and the speed of light c, $(c - c\bar{\beta}_z)(L_w/c) = N_u\lambda$.

All longitudinal distances are normalized to this slippage distance so that $z/N_u\lambda \to z$. The full extension of the theory uses $a \to a(z)$, $v \to v(z)$, and $\zeta \to \zeta(z)$ over a number of sites N_W. The value of N_W needed in a particular problem is determined by the amount of detail to be followed in the optical spectrum. The optical field sites span a window of width, W, that is an integral number of slippage distances long. Modes that are properly represented in the window are given by

$$\nu_l = \nu_0 - \left[\frac{\pi}{W}\right](2l - N_W) \quad \text{where} \quad l = 0, 1, 2, \ldots, N_W - 1 \quad , \tag{60}$$

where l is an integer, $W = N_W\Delta z$, and Δz is the dimensionless spacing between sites. Consistent with the slowly varying optical envelope and the possible distortion of the envelope, the site spacing must be selected to satisfy $N_u^{-1} \ll \Delta z \ll 1$. The mode spacing is given by $\Delta\nu = 2\pi/W$, where the window W is typically only a few, to several, slippage distances long. In most cases, $W = 1 \to 4$ is adequate to characterize FEL phenomena.

When the electron and optical pulses are much longer than the slippage distance, $N_u\lambda$, periodic boundary conditions can be imposed at the ends of the window, W, in order to restrict the number of modes and sites followed [152-155]. The end effects of the periodic boundary conditions are considered non-physical and inconsequential. The boundary condition is

$$\zeta(z - W/2) = \zeta(z + W/2) \quad ; \quad \nu(z - W/2) = \nu(z + W/2) \quad ; \quad \text{and} \quad a(z - W/2) = a(z + W/2) \tag{61}$$

The periodic boundary conditions are not used in short pulse problems where the electron pulse, and consequently the optical pulse, are about one slippage distance long. For short pulses, the window width W is slightly longer than the extent of either the light or electron pulses. The generalized equations for electrons and light are

$$\overset{\circ\circ}{\zeta}_{i,\tau} = |a_z| \cos(\zeta_{i,\tau} + \phi_i) \quad , \quad \overset{\circ}{a}_z = -j_{z,\tau} < \exp(-i\zeta_{i,\tau}) >_{i,\tau} \quad , \tag{62}$$

where the longitudinal field sites z refer to a position in the optical field envelope. The light, traveling at speed c, remains fixed in z, while the slower electrons slip back to site $z-\tau$. The dimensionless current density, $j_{z,\tau}$, is a macroscopic variable, and does not distort due to the microscopic bunching on a much smaller scale. When the electrons pass through the undulator, those at a site z interact with a range of sites in the optical wave envelope; in this way, the electron beam and light wave exchange information, and the electrons pass information from one optical field site to its neighbor.

The site spacing Δz can be made equal to the integration time step $\Delta\tau$, so that electrons slip one site each time step. In weak optical fields with low gain, the step size can be large, $\Delta\tau = \Delta z = 0.1$, but in strong optical fields or high gain, $\Delta\tau = \Delta z = 0.01$ or smaller, is sometimes necessary. A number of electrons must be followed at each site z as well; the electron phase and phase velocity must be calculated each time step at each site. In weak fields as few as 20 sample electrons at each site is adequate, but in strong fields, a few hundred may be necessary. If there is an initial energy or angular spread due to emittance, then many more electrons may be required. This is the worst situation for a simulation to accurately handle. In the case of high current, the weak-field gain can be large enough so that there is large growth in the bunching field a. Details of the interaction are not "remembered" for more than the characteristic growth time, so that it is usually possible to use $W \le 1$ in high-current simulations. Viewed another way, the gain spectrum for a high current FEL is wider so that only a short sampling distance is necessary.

16. The FEL trapped-particle instability

One of the important effects to describe using the longitudinal multimode analysis is the FEL trapped-particle instability [152-157]. In strong optical fields electrons can become trapped in deep potential wells in phase space. The oscillation of the beam current that is trapped in these wells can drive the carrier wave unstable, and cause sideband frequencies to grow from noise. When either the FEL amplifier or oscillator evolves to power levels beyond the onset of saturation, the FEL may well encounter the trapped-particle instability. The coherence that is established in weak optical fields can then be modified or destroyed by the trapped-particle instability. The effect is well-known in storage-rings as the Robinson instability, and originates from the same kind of longitudinal electron oscillations in an RF trapping potential. In the FEL, the instability was first predicted for high-power tapered undulators with many synchrotron periods. It has now been shown that the FEL trapped-particle instability can be exhibited in a wide range of undulator designs operating in strong fields.

As the FEL reaches high-power saturation, the height of the separatrix is large, and many electrons are trapped in the closed orbits of phase-space. The instability starts with the motion of those trapped electrons. The electrons trapped near the stable fixed-point, $\zeta_0 = \pi/2 - \phi$, are seen to execute a part of a synchrotron oscillation in figures 9 and 10. In the tapered FEL, the stable fixed-point is at $\zeta_0 = \cos^{-1}(-\delta/|a|) - \phi$, and moves to $\zeta_0 = \pi/2 - \phi$ as the taper rate decreases, $\delta \to 0$. Motion of the trapped electrons near phase ζ_0 is described by

$$\zeta(\tau) = \zeta_0 + \frac{\nu_0}{\nu_S}\sin(\nu_S\tau) \quad , \tag{63}$$

for the initial position (ζ_0, ν_0), with the synchrotron, or trapped-particle oscillation frequency given by $\nu_S = (|a|^2 - \delta^2)^{1/4}$. In the untapered FEL, the synchrotron frequency is $\nu_S = |a|^{1/2}$. In the tapered FEL, where the condition $|a| > \delta$ is necessary to trap electrons, the synchrotron

frequency is only slightly reduced from the untapered value, $\nu_s = |a|^{1/2}(1-\delta^2/4|a|^2+....)$. In either case, sidebands can appear around the fundamental at $\nu_0 \pm \nu_s$, and are shifted away from the fundamental wavelength by $\Delta\lambda/\lambda = \nu_s/2\pi N_u$. The fractional shift is simply the ratio of the "number of synchrotron oscillations" to the "number of undulator periods". The field strength required to cause one synchrotron oscillation is $|a| = 4\pi^2 \approx 40$, and corresponds to a peak-to-peak separatrix height of $4|a|^{1/2} = 25$. Because of the relatively large separatrix height, most beam quality effects are minimized.

Figure 19 shows the result of a simulation with periodic boundary conditions in a window of width $W = 2$, corresponding to two slippage distances along the beam. The long electron beam is described by current $j = 8$ at all points in the window, and interacts with the optical field for $n = 500$ passes. Each pass, the electrons start almost uniformly spread in phase at each site along z; a small random phase displacement with rms spread $\delta\zeta = 10^{-4}$ is added to each electron phase to represent shot noise. Without some source of noise, every site z would evolve identically, and no spectral features could develop. The resulting steady-state solution is insensitive to the noise source; many alternate noise sources have been tried, with the same final result. The resonator loss on each pass is determined by $Q = 8$.

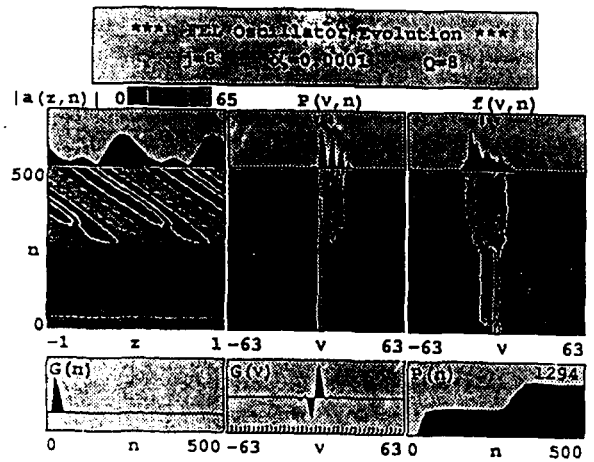

Figure 19. The trapped-particle instability in a low-current FEL oscillator.

During the first $n \approx 12$ passes, the FEL in figure 19 shows only small gain at the end of each pass, $G(n)$ (shown at the bottom-left), because the initial field determined by shot noise has a broad spectrum. Equation (59), with $j = 8$, estimates that in $n = 12$ passes the spectrum would narrow by ×10 to width $\Delta\nu = 2\pi \rightarrow 0.2\pi$ around $\nu_0 = 2.6$. The narrower spectrum would have net

gain $G = 0.135j - 1/Q = 95\%$. At $n = 25$ passes, the gain peaks and then decreases as the FEL reaches normal, single-mode saturation. The dimensionless optical power at the end of each pass, $P(n)$ (shown at the bottom-right), becomes constant for several hundred passes. The power $P(n)$ is the average value of $|a_z|^2$ for all sites in the window. From $n = 0 \rightarrow 25$ passes, the field strength, $|a|$, has increased by many orders of magnitude until reaching single-mode saturation at $|a| = 25$. After single-mode saturation, the optical field amplitude at the end of each pass, $|a(z,n)|$ (shown at the middle-left), remains substantially constant but for a small growing modulation over each slippage distance, $\Delta z = 1$. The grey scale above $|a(z,n)|$ shows the peak field amplitude, $|a(z,n)| = 65$, in white, and zero field in black with two contours. Note that there is only a fraction of a synchrotron oscillation at single-mode saturation, $\nu_s/2\pi = 0.8$ when $|a| = 25$. The synchrotron frequency is imposed on the optical wave over many hundreds of passes so that a fraction of an oscillation each pass is sufficient to establish the information transfer. The onset of the trapped-particle instability begins when the optical power is sufficient to cause approximately one synchrotron oscillation each pass, but there need not be exactly one oscillation.

As the electrons slip back past the optical field sites and execute synchrotron oscillations, they continually modulate the wave envelope. The modulation can be clearly seen in the amplitude evolution of $|a(z,n)|$ after $n \approx 300$ passes. The power $P(n)$ increases dramatically as sidebands appear in the power spectrum, $P(\nu,n)$ (shown at the middle-center). For reference the weak-field gain spectrum, $G(\nu)$, is plotted below the power spectrum on the same scale. When the final peak power is reached after $n \approx 300$ passes, and a dynamic steady-state is achieved. The modulation structure continues to move back in the window at a steady rate over many passes, but the total power and power spectrum remain constant. The steady-state average field strength is $|a| = 36$ so that there is one full synchrotron oscillation of the trapped electrons. Note that an approximate 20% change in the synchrotron frequency ν_s corresponds to an approximate 100% increase in the optical power, since $P \propto \nu_s^4$. The evolution of the electron's phase-velocity distribution at the end of each pass, $f(\nu,n)$ (shown at the middle-right), increases in spread as the stronger optical fields extract more energy from the beam. The peak-to-peak height of the closed-orbit region of phase space, $4|a|^{1/2} = 4\nu_s$, gives an estimate of the induced spread. In normal, single-mode saturation the electron spread is $4\nu_s = 20$. After the trapped-particle instability occurs, the peak field, $|a| = 65$, increases the spread to $4\nu_s = 32$.

The final field shape, $|a(z)|$ (shown at the top-left), is nearly 100% modulated at the slippage distance length, $\Delta z = 1$, with a peak value of $|a| = 65$ and an average value corresponding to $\nu_s = 2\pi$. The final power spectrum, $P(\nu)$ (shown at the top-center), has two prominent sidebands spaced at $\Delta\nu = \nu_s = 2\pi$ away from the fundamental. Optical power in the sidebands is comparable to the fundamental, and accounts for the 100% field modulation. The pointed tick-mark at the top of the final power spectrum indicates the central wavelength of the

optical radiation at resonance. The rectangular tick-mark indicates the center of the final power spectrum. With or without the trapped-particle instability, the FEL oscillator spectrum generally moves to larger values of $\nu(k)$ at higher power levels. The final phase-velocity spectrum of the electrons in the beam, $f(\nu,n)$ (shown at the top-right), is spread by the trapping of electrons in strong optical fields. The pointed tick-mark at the top of the electron spectrum indicates the electron beam's initial phase-velocity at resonance. The rectangular tick-mark indicates the final value of the beam's averaged phase-velocities, and shows a loss of energy corresponding to $<\Delta\nu> = -10$. Note that this change in the beam's phase-velocity almost exactly equals the shift in the optical spectrum, showing how bunched electrons at reduced energy will drive a longer wavelength.

If the resonator Q in figure 19 is reduced to $Q = 6$, the simulation would find only one sideband with a final average field value $|a| \approx 22$, and a peak field value of $|a| \approx 46$. If the Q is further reduced to $Q = 5$, the FEL operates in a single-mode with final field $|a| \approx 21$. If the Q is increased to $Q = 20$, the FEL optical field and power spectrum become chaotic and there is no steady-state; the power $P(n)$ increases and continues to fluctuate erratically over many passes. The optical field structure $|a(z)|$ evolves into intricate patterns showing modulation at many frequencies. The power spectrum has many lines to the right of resonance that grow and decay as the spectrum continually changes shape. Similar trends occur when the current j is altered by similar amounts.

The general features of trapped particle instability in the FEL oscillator depend only on the dimensionless current j and the loss factor Q. For sufficiently low values of j and Q, the trapped-particle instability does not occur, and the FEL operates in a steady-state single mode. Increasing either j or Q can result in the trapped-particle instability. When the instability is near threshold, there are only one or two sidebands and the optical power is near $|a| \approx 4\pi^2$ causing about one synchrotron oscillation. As illustrated in figure 19, the instability can occur with $\nu_s \leq 2\pi$. Over many passes, the optical wave "sees" many repeated synchrotron oscillations, and the sidebands grow to saturation. Most normal values of j and Q give rise to the instability. Values in the range of $j = 5$ and $Q = 50$ actually produce several sidebands at multiples of ν_s away from the fundamental, as has been observed experimentally in the LANL FEL of table 1. As these frequency mix again, a chaotic spectrum with many lines develops. The chaotic spectrum does not reach a steady-state, and is several times wider than the normal gain bandwidth. Numerically, some source of noise is essential for the development of the trapped-particle instability, but the details are not important.

The trapped-particle instability in the FEL has mixed benefits. Often, the experimenter would like a high-power laser that has a narrow spectrum and no sidebands. But, the presence of sidebands means that high power has been obtained, and the FEL is operating well. In fact, as more sidebands develop, even more power and higher efficiency is attained. Decreasing the sideband power can be realized by degrading the FEL performance. The resonator Q, or the current j, may be decreased so that the FEL saturates at a more moderate field strength, thereby decreasing the synchrotron frequency. In an FEL driven by an RF linac, it will be shown later that a slight change in the position of the resonator mirrors can remove sidebands, but again, reduces power. More constructive methods for suppressing sideband growth use selective resonators that increase the losses, lowering Q, in the frequency range of the sidebands, but this method restricts the FELs tuning range. Tapering the undulator of the FEL oscillator significantly reduces sidebands, and can reach high power with a narrow spectrum. The sideband frequency is nearly the same as in the untapered case, as shown above, but the sideband gain is reduced because fewer electrons are trapped in phase-space. The efficiency of the tapered FEL oscillator without sidebands tends to be comparable to the efficiency of the untapered case, because of its extra power in the sidebands.

The FEL amplifier with high current density, $j \gg 1$, can reach high power in a single pass. The growth rates are large enough that electrons can be trapped early in the undulator, and begin executing synchrotron oscillations. There can be several to tens of synchrotron oscillations along the undulator, but these are the only oscillations experienced by the optical field. Even with far fewer synchrotron cycles than in the oscillator case, the large current density j can give significant sideband gain once trapping occurs. The sources of noise are much more important in the FEL amplifier than in the FEL oscillator. Suppression of input noise at the sideband frequency could be an important method for avoiding the trapped-particle instability in amplifiers.

Figure 20 shows an FEL with high current $j = 5\times10^4$, no taper $\delta = 0$, an initial field $a_0 = 10$ starting at resonance $\nu_0 = 0$. A small amount of shot noise is introduced over a wide range of frequencies using the random electron phase displacement $\delta\zeta = 2\times10^{-4}$. A high-current beam with electrons trapped by strong fields will provide a source for the sideband field, and the small fluctuations from shot noise lead to a significant noise contribution. The arrangement of figure 20 is similar to figure 19, except that evolution is followed over a single pass, $\tau = 0 \rightarrow 1$, instead of many passes, $n = 0 \rightarrow 500$. The gain spectrum in weak optical fields, $G(\nu)$, is nearly symmetric about resonance, and the power spectrum evolution, $P(\nu,\tau)$, shows that the fundamental line grows fastest at resonance.

The optical field in figure 20 grows rapidly from noise to the onset of saturation at field strength $|a| \approx 2(j/2)^{1/3} = 1700$. A short time later, the field reaches single-mode saturation with field strength $|a| \approx 2\times10^3$ at $\tau = 0.25$ along the undulator length. The gain and power decrease, and begin to oscillate as the trapped electrons oscillate in the closed orbits of phase space. The gain evolution $\ln(1+G(\tau))$, power evolution $P(\tau)$, optical evolution $|a(z,\tau)|$, and electron spectrum $f(\nu,\tau)$, all show the results of approximately four synchrotron oscillations. Note that the oscillations are not exactly sinusoidal, since the peaks are sharper than the troughs. This occurs because the power, $P(\tau) \propto \nu_s^4$, varies by nearly 100% so that the synchrotron frequency varies by about 20% over each synchrotron period. On the average, the synchrotron frequency is estimated at $\nu_s \approx 11\pi$ corresponding to an average trapping field of $|a| = \nu_s^2 = 1200$. The field

evolution, $|a(z,\tau)|$, shows all z sites oscillating together in τ for the first two synchrotron periods. On the third and fourth oscillations, the temporal τ-oscillations are converted to spatial z-oscillations as the trapped-particle instability modulates the wave envelope. As the modulation appears, the sideband in the power spectrum, $P(\nu,\tau)$, also appears. The final power spectrum shows a prominent sideband spaced at about ν_s to the right of the fundamental.

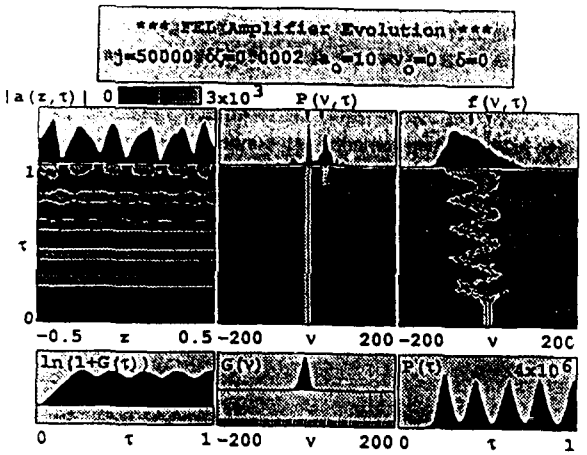

Figure 20. The trapped-particle instability in a high-current FEL amplifier.

The details of the evolution of the electron spectrum, $f(\nu,\tau)$, are especially interesting. For the first few synchrotron oscillations, the electron spectrum appears tightly bunched in energy; the large oscillations in $P(\tau)$ indicate that the phase spectrum is bunched as well. A large fraction of initial beam is following a small range of phase-space orbits that oscillate about the stable fixed-point $\zeta_0 = \pi/2 - \phi$. The maximum peak-to-peak height of the instantaneous separatrix is $4|a|^{1/2} = 180$, but decreases by about 20% in each synchrotron period. The bunched electrons remain well inside the separatrix, and only undergo excursions of $\Delta\nu = \pm 120$. The bunch remains tight until the sidebands become significant on the fourth synchrotron oscillation to change the phase-space dynamics. Then, the bunch disperses to fill the full height of the separatrix, and is no longer tightly bunched. The final electron spectrum, $f(\nu)$, is spread to $\Delta\nu = 200$.

Figure 21 shows the same high-current FEL as in figure 20, but with taper rate $\delta = 60\pi$. The current is $j = 5\times10^4$ with an initial field of $a_0 = 10$ starting at resonance $\nu_0 = 0$. The initial weak-field gain spectrum, $G(\nu)$, is peaked near $\nu = -\delta = -60\pi$, because the phase acceleration, δ, alters the FEL resonance. But, the FEL is started at resonance where there is maximum gain and efficiency in the anticipated strong fields; recall figure 15. The FEL power, $P(\tau)$, and gain, $\ln(1+G(\tau))$, saturate at $\tau = 0.3$, then execute synchrotron oscillations. The oscillations are less severe than in the untapered case, because fewer electrons are trapped, those that are trapped contribute more of their energy to the optical field. The power increases to about five times the power of the untapered FEL in figure 20, and shows a correspondingly higher synchrotron frequency in the stronger optical fields. Sidebands appear in the power spectrum, $P(\nu,\tau)$, spaced at $\Delta\nu = \pm\nu_s = \pm 20\pi$ on both sides of the fundamental; the synchrotron frequency, ν_s, is roughly given by the fourth root of the final power. The spatial modulation in the optical field, $|a(z,\tau)|$, becomes significant near the third synchrotron oscillation, but over the next few periods, the wave does not develop the full modulation seen in figure 20. The electron spectrum, $f(\nu,\tau)$ becomes steadily broader as untrapped electrons are accelerated to larger phase velocities, and trapped electrons are decreased in energy. Untrapped electrons form a second peak on the right of the final electron spectrum, but most electrons remain trapped and decelerate.

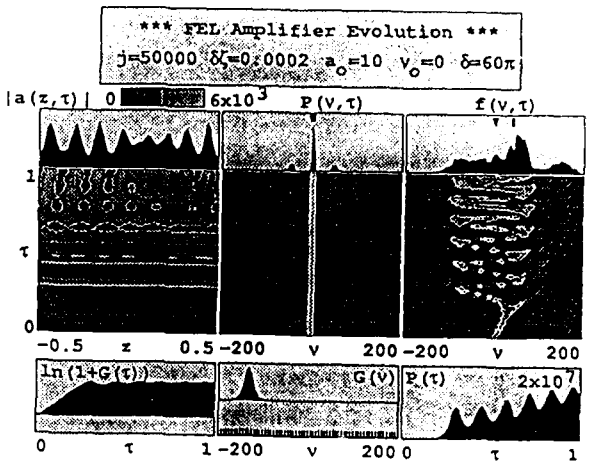

Figure 21. The trapped-particle instability in a high-current FEL amplifier with a tapered undulator.

The general characteristics of the trapped-particle instability in the FEL amplifier differ in several ways from the FEL oscillator. As in the oscillator, large j makes the trapped-particle instability more severe. However, in the amplifier, it is only the largest values of j that have a possibility of developing a significant sideband in a single pass. The optical field at the onset of high-current saturation is given by $a_j \approx j^{2/3}$. In terms of the associated synchrotron frequency, $a_j = \nu_s^2$, the current needed to establish the trapping potential is $j_s = \nu_s^3$. There must be at least a few synchrotron oscillations (say about four) for the optical wave to pick up the synchrotron

frequency. Then, the threshold value of the current for the trapped particle instability in the FEL amplifier is

$$j_s = 2 \times 10^4 \qquad (64)$$

The value of the initial field, a_0, does not significantly alter this estimate, because the weak-field gain for such a current is $\sim 10^{15}$; any small, practical field leads to saturation early in the undulator. The threshold current density, j_s, is needed before sidebands can significantly alter the final FEL amplifier spectrum. Currents below j_s are not as susceptible to the trapped-particle instability. No FEL amplifier has observed the trapped-particle instability, and no FEL in table 1 has reached the dimensionless threshold current j_s in (64). When the FEL is tapered, the instability is less severe, because less current is trapped and the synchrotron oscillations have smaller amplitude. Suppression of input noise at the sideband frequency may be an important method for avoiding the trapped-particle instability in the FEL amplifier.

17. Short optical pulses in FEL oscillators

Many FEL oscillators are driven by short, picosecond long, electron pulses from an RF accelerator. The resulting short optical pulses may find scientific applications using the picosecond time-scale as an advantage. When the electron pulse length is comparable to the slippage distance, $N_u\lambda \approx 1$mm, the modal structure of the pulse current is comparable to the gain bandwidth, and short-pulse effects dominate the FEL interaction [146-151]. If the electron pulse length is much longer than the slippage distance, the pulse is considered long, and each part of the pulse experiences gain proportional to the local density. Short-pulse behavior is intimately tied to the time development of gain along the undulator. At present, only the FEL oscillator uses short pulses, while high-current amplifiers use long pulses. Exotic short-pulse aspects of the FEL have been experimentally and theoretically explored almost as early as the fundamental theory. The agreement between theory and experiments with short-pulses is probably the best confirmation of our understanding of the FEL. The same multimode analysis used for the trapped-particle instability can be used to examine FELs with short current pulses.

As a series of short electron pulses enter the FEL oscillator, short optical pulses start from spontaneous emission, and bounce between the resonator mirrors separated by a distance $S > L_u$. The rebounding optical pulse arrives at the beginning of the undulator, $\tau = 0$, at time intervals, $2S/c$, where the series of electron pulses from the RF accelerator must be synchronized to arrive at $\tau = 0$ coincident with the light. Define d, the "desynchronism", as the displacement between the electron and optical pulses at $\tau = 0$ on each pass; d is normalized to the slippage distance, as usual, and when $d = 0$, exact synchronism, the electron pulse time interval is exactly $2S/c$. In practice, d is adjusted by actually moving one the resonator mirrors a small distance.

In Figure 22, the arrival time of the electron pulse is synchronized precisely with the bounce time of the light pulse, so $d = 0$. The calculational window is three slippage distances long, $W = 3$, and travels with the light wave at speed c; the slower electron pulse slips back through one third of the window width each pass. The position of the short electron pulse, $j(z-\tau)$ (shown at the lower-left), is indicated in dark grey at the beginning of the undulator, $\tau = 0$, and is light grey at the end of the undulator, $\tau = 1$. The pulse shape is parabolic with the form $j(z) = j(1-2z^2/\sigma_z^2)$ for $j(z) > 0$, and zero otherwise. The pulse length is $\sigma_z = 1$, and the peak current is $j = 5$. The weak-field gain spectrum, $G(v)$, is shown for reference, and is calculated separately for $j = 5$ with no pulses. The resonator loss is determined by $Q = 20$. A small random phase $\delta\zeta \approx 10^{-4}$ is added to each of the sample electron phases to represent shot noise, and to start the optical pulse growth. During the simulation over $n = 600$ passes, the optical field is free to evolve, subject only to amplification by the electron pulse and uniform loss from Q.

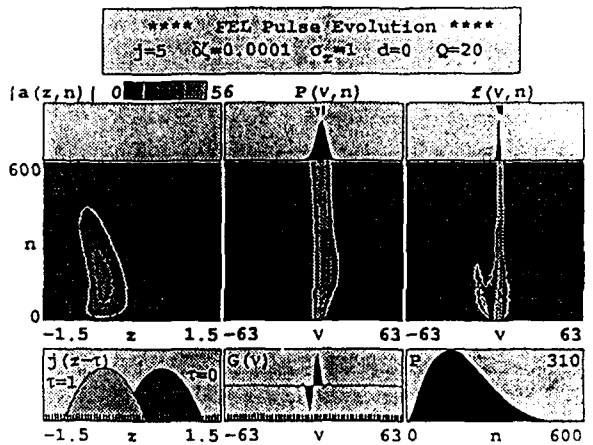

Figure 22. Short pulse evolution in the FEL oscillator at exact synchronism.

On each pass, the unbunched electron pulse starts at $\tau = 0$ (dark grey) and slips back to $\tau = 1$ (light grey) as bunching develops. The shot noise contributes a small amount of spontaneous emission to form a broad-spectrum optical pulse with a length that is roughly the sum of the electron pulse length and the slippage distance, $\approx \sigma_z + 1$. As the optical spectrum narrows around peak gain, the power P grows. But, the gain along the optical pulse length is not uniform. At $\tau = 0$, the optical wave is not driven by the electron pulse, because there is no bunching, and the electron phases average to zero $\langle .. \rangle = 0$. As τ increases, the electron phases pass through the local radiation field $a(z)$, bunching occurs, and $\langle .. \rangle$ becomes non-zero. Recall

that the single-mode gain in weak fields is described by $G(\tau) = j\,\nu_0\,\tau^4/12$ for small τ, so that there is no gain at the beginning of the interaction. This delay in the gain medium is sometimes called "lethargy" [59]. At later times $\tau \lesssim 1$, the electron pulse is bunched, and drives the trailing edge of the light pulse with its maximum local gain. The light pulse is distorted on each pass, because gain is preferentially deposited on the trailing edge of the pulse. Consequently, the centroid of the light pulse is traveling slower than c, as can be seen in the contour plot of $|a(z,n)|$, even though it is in vacuum. Each pass, the gain starts farther back on the front edge of the optical pulse until the pulse finally begins to move away from the driving medium, the bunched electron pulse. The power begins to decay around $n \approx 200$ passes, and continues on to $n = 600$ passes.

At exact synchronism, the light pulse drifts away from the electron pulse over many passes so that the steady-state FEL power is zero. To compensate for the slower speed of the light pulse, the path S must be reduced so that $d = -2\Delta S/N_w\lambda \approx 10^{-3} \rightarrow 10^{-1}$. When d is too large, the compensation is too severe; the electron and optical pulses do not overlap over a sufficient number of passes, and the FEL is below threshold coupling. In the range where short-pulse gain is above threshold, the desynchronism, d, is important to the characteristics of pulse evolution and final saturation.

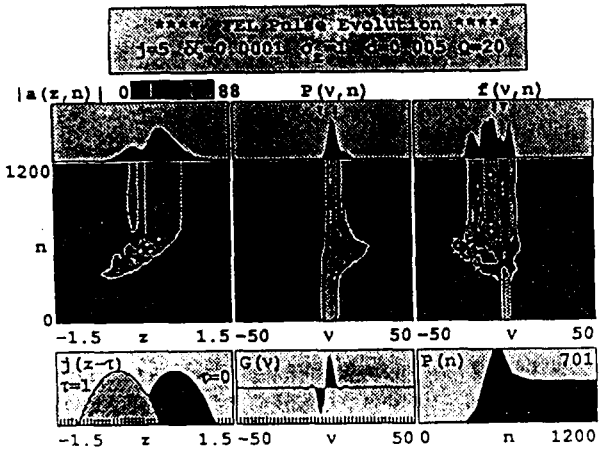

Figure 23. Short pulse evolution in the FEL oscillator at small desynchronism.

In Figure 23, the desynchronism is $d = 0.005$ with the same FEL as in figure 22. The peak current is $j = 5$ in a parabolic electron pulse of width $\sigma_z = 1$ with shot noise represented by $\delta\zeta = 10^{-4}$, and the resonator losses are determined by $Q = 20$. The optical pulse survives in this case, and reaches a steady-state after $n \approx 800$ passes where the optical power, $P(n)$, and the pulse shape, $|a(z,n)|$, are approximately constant in n. The peak power and peak field strength, $|a| \approx 88$, are reached somewhere between $n = 500$ and 600 passes. This is not easily explained, but is often observed in simulations at small values of d, and more importantly, is also observed in experiments. While the gain and resonator loss combine to reshape the optical pulse until steady-state is achieved, the pulse evolution is still subject to the initial conditions determined by spontaneous emission. The optical pulse in figure 23 is partially modulated, and the power spectrum, $P(\nu,n)$, has a small sideband due to the trapped-particle instability. The power spectrum width is limited to $\Delta\nu \approx 2\pi$ by the short optical pulse length, $\Delta z = 1$, and is centered at the peak gain in strong fields. The spread in the electron spectrum, $f(\nu,n)$, is roughly given by the peak-to-peak height of the separatrix with final field $|a| = 60$.

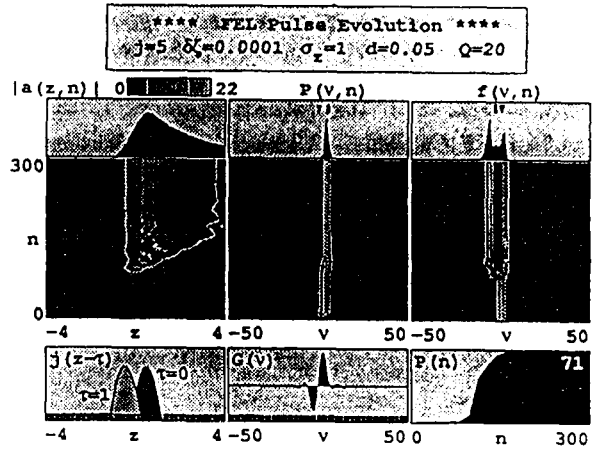

Figure 24. Short pulse evolution in the FEL oscillator at large desynchronism.

At larger values of the desynchronism, the operating characteristics of the FEL change considerably. Figure 24 shows the same FEL as in figures 22 and 23, but with desynchronism $d \approx 0.05$. Steady state is achieved after $n \approx 200$ passes, and the optical power, $P(n)$, and optical pulse shape, $|a(z,n)|$ do not appear to evolve further. The final power is significantly reduced by $\times 10$ compared to the smaller desynchronism case of figure 23. The peak field is only $|a| \approx 22$, and is not sufficient for the trapped-particle instability. On each pass, the short electron pulse is only amplifying the trailing edge of a much longer optical pulse, while the large desynchronism is artificially advancing the front edge of the optical pulse well ahead of the electrons. The calculational window is now $W = 8$, because the optical pulse has significant power spread over more than four slippage distances. Much of the optical pulse remains in front

of the electron pulse, and is decoupled from electrons. In front of $j(z)$, the optical pulse decays, because of resonator losses, and can be described analytically by $|a(z)| \propto \exp(-z/4Qd)$. The long pulse is coherent and has a narrow spectrum, $P(\nu, n)$. There are no sidebands in the weak fields, and the resulting electron spectrum, $f(\nu, n)$, is narrow. In fact, the electron spectrum is smaller than expected for this field strength, because electrons start near the trailing edge of the optical pulse, and drop back out of the bunching field before the end of the undulator.

The general features of short-pulse behavior have now been observed in many simulations and several experiments. At small desynchronism, $d \geq 0$, the power is often large enough to cause the trapped-particle instability, a broad optical spectrum, and a broad electron spectrum. The optical pulse shape is short, and centered on the electron pulse; it can be modulated with sharp spikes due to the trapped-particle instability. Since a small change in d can make a large difference in the steady-state power, the FEL tends to be unstable at small values of desynchronism. For larger d in the operating range, the FEL becomes more stable. At large desynchronism, the steady-state power is smaller due to the reduced coupling, and the trapped-particle instability usually does not occur. The final optical pulse can be much longer than the electron pulse so that the power spectrum is narrow. The electron spectrum is narrow in the weaker optical fields, and the center of the optical pulse may actually be well ahead of the electron pulse. The FEL's operating range in d is typically $\Delta d \approx 0.1$, so that the resonator length must be adjusted within a surprisingly small range $\Delta S \approx -5\mu m$ for $N_u = 10^2$ and $\lambda = 1\mu m$. If the trapped-particle instability is undesirable in an FEL application with short pulses, it may be easily removed by increasing d, and decreasing power.

Another feature predicted by short-pulse theory is limit cycle behavior in the optical pulse structure and power. The power oscillates periodically over several hundred passes as does the optical pulse shape and spectrum. Limit cycle behavior occurs at moderate values of d where a stable configuration does not occur. The moderate field strengths produce about one synchrotron oscillation, and the optical pulse continually changes from one shape to another. The subpulse structure initiates on the trailing edge of the optical pulse, and is "pushed" through the pulse envelope over many passes by the desynchronism mechanism.

18. FELs using waveguides

After the longitudinal multimode extension, and studying the trapped-particle instability and short pulses, the transverse mode extension is now examined. Some aspects of transverse modes must be evaluated in terms of their effect on the longitudinal modes. When an FEL uses a waveguide to confine the radiation along the undulator, there can be several changes to the simple FEL interaction [158-16]. Typically, the goal of the design is to make these changes as small as possible while confining the wave around the co-propagating electron beam.

When the FEL optical wavelength is long, free-space diffraction can spread the optical wavefront away from the co-propagating electron beam, and reduce coupling. The natural distance for a light beam expand is the Rayleigh length, $\pi w_0^2/\lambda$. Comparing this length to the undulator length L_u defines the dimensionless Rayleigh length $z_0 = \pi w_0^2/L_u\lambda$. Using the resonance condition, the Rayleigh length becomes $z_0 = 2\pi w_0^2\gamma^2/(1+K^2)N_u\lambda_u^2$, and expresses how an FEL with a low energy electron beam gives a short Rayleigh length.

A design attempting to compensate for low γ by expanding the optical beam size w_0 would suffer reduced coupling because of a small filling factor $F = \pi r_b^2/\pi w_0^2$ where r_b is the electron beam radius. When natural diffraction spreads the optical wave away from the electron beam, the filling factor is reduced further. Assuming the light remains in the lowest order Gaussian mode with its waist at the center of the undulator, the average filling factor over the undulator length is $\bar{F} = \sigma_x^2/(z_0+(12z_0)^{-1})$ where $\sigma_x = r_b(\pi/L_u\lambda)^{1/2}$ is the dimensionless electron beam radius. Typically, $\sigma_x \leq 1$ in an FEL, but the following arguments are independent of that value, and only depend on the Rayleigh length z_0. For $z_0 \to 0$, $\bar{F} \to 0$ and FEL coupling $\to 0$, because the optical wave spreads away from the electron beam at the two ends of the undulator. For $z_0 \to \infty$, $\bar{F} \to 0$ and FEL coupling $\to 0$ again, because the wavefront is always too large compared to the electron beam. The maximum filling factor, $\bar{F}_{max} \approx \sqrt{3}\sigma_x^2$, occurs at $z_0^{max} = 1/2\sqrt{3} = 0.3$. The maximum is relatively broad in z_0, and $\bar{F}_{max}$ drops to half of its peak value at $z_0 = 0.11$ and 0.75.

The filling factor could be increased for an optical wavefront of any size, if the electron beam size is increased. But, as the electrons move off of the undulator axis, (12) gives the change in the electron phase velocity in a matched beam, $\Delta\bar{v}_\beta = 4\pi N_u(Kk_u r_b)^2/(1+K^2)$. Gain degradation begins when the beam radius is large enough to cause $\Delta\bar{v}_\beta \approx \pi$. The limit on the beam radius for good coupling is then $r_b \leq (1+K^2)^{1/2}\lambda_u/4\pi K N_u^{1/2}$. Generally, the electron beam radius is restricted to a small fraction of the undulator wavelength. For $N_u \approx 10^2$ and $K = 1$, we have $r_b \leq 0.01\lambda_u$, or for $K \ll 1$, we have $r_b \leq 0.01\lambda_u/K$.

The restriction on the beam radius, and a good filling factor give a restriction on the Rayleigh length in terms of γ, K, and N_u. To relate r_b and w_0, assume that the filling factor is not too small, say $F \geq 0.1$, so that $w_0 \leq 3r_b$. Then, the dimensionless Rayleigh length is limited by $z_0 \leq \gamma^2/\pi K^2 N_u^2$. Either a low energy beam or a long undulator can limit z_0 to a small value, and decrease the filling factor. Gain degradation begins when the filling factor, $\bar{F}_{max}$, decreases to less than half its value as the limit above reaches $z_0 \leq 0.1$. Therefore, an FEL design requires

$$\gamma \geq KN_u/2 \tag{65}$$

so that natural diffraction does not significantly decrease the interaction strength. An FEL with low electron beam energy and a long, strong undulator, requires a waveguide for good coupling strength.

When a waveguide is used to confine the radiation near the co-propagating electron beam,

there is a change in the FEL resonance condition. In a single waveguide mode, the cross-section of the mode can be used in the filling factor to estimate coupling to the mode. The electron beam size should be close to, but smaller than, the radiation cross-section for best coupling. Assuming the electron beam is on-axis, the mode should have a transverse electric field on-axis as well. Higher order modes will average to smaller coupling if the electron beam size is not much smaller than the mode.

The time dependence of the waveguide fields is taken to be $\propto e^{-i\omega t}$ with longitudinal dependence $\propto e^{\pm ikz}$. The waveguide cross-section and boundary conditions specify an eigenvalue problem with a number of eigenvalues Λ_{pq}, where $p,q = 0,1,2,3,\ldots$. For a given frequency, the wave equation determines the longitudinal wavenumber, $k_{pq}^2 = \omega^2/c^2 - \Lambda_{pq}^2$. When the frequency is below cut-off, $\omega/c \le \Lambda_{pq}$, the wavenumber k_{pq} is zero, or imaginary, and the mode does not propagate; $\omega_{pq}^C = c\Lambda_{pq}$ is called the cut-off frequency of the waveguide. The backward propagating wave results in an FEL interaction at long wavelengths, and is not discussed here. The phase velocity for the forward wave is then $v_{pq} = L_u[(k_u + k_{pq})\beta_z - \omega/c]$. The eigenvalue Λ_{pq} depends on the waveguide dimension and shape. For the rectangular waveguide, Λ_{pq}^R, with sides X and Y, and the circular waveguide, Λ_{nm}^C, with radius R, the eigenvalues are

$$\Lambda_{pq}^R = \pi\left[\frac{p^2}{X^2} + \frac{q^2}{Y^2}\right]^{1/2}, \quad \text{and} \quad \Lambda_{pq}^C = \frac{x_{pq}}{R}, \tag{66}$$

where $p,q = 0,1,2,3,\ldots$, but not both $p = q = 0$, and x_{pq} is the qth root of $J_p'(x_{pq}) = 0$. The first few roots are roughly given by $x_{pq} \approx \pi q$, so that with $R = 1.5$cm, a typical cut-off frequency is $\omega^C \approx 10$GHz. The resonant FEL frequency is given by $\omega = c(k_u + k_{pq})\beta_z$ where $k_{pq} = (\omega^2/c^2 - \Lambda_{pq}^2)^{1/2}$; this expression can solved for ω in terms of k_u, β_z, and the waveguide eigenvalues.

An FEL using a waveguide must operate above cut-off, and when far above cut-off, the expression for the electron phase velocity can be expanded in Λ_{pq}. This gives the shift in phase velocity, and clarifies the effect of the waveguide on the FEL operation. Expanding in Λ_{pq} gives the form of the phase velocity $v = v^{(0)} + \Delta v_{pq} + \ldots$ where $v^{(0)}$ is the unperturbed phase velocity without waveguide corrections, and Δv_{pq} is the first-order waveguide correction in Λ_{pq}. A relativistic FEL, near resonance, has its phase velocity shifted by

$$\Delta v_{pq} = -\frac{N_u \lambda_u^2 \Lambda_{pq}^2 (1+K^2)}{8\pi f^2}, \tag{67}$$

where Λ_{pq} is taken from (66). The shift in resonance is negative, and diminishes when $\gamma \to \infty$. As an example, consider the LLNL ELF experiment where $\gamma = 7$, $\lambda_u = 10$cm, $N_u = 30$, $K = 2.4$, and the smallest rectangular waveguide dimension is $Y = 3$cm. The waveguide shift is then $\Delta v_{0p}^{ELF} \approx -6\pi p^2$, or $\Delta v_{01}^{ELF} \approx -6\pi$ for the lowest-order mode. The gain spectrum bandwidth for ELF, $4j^{1/6} \approx 4\pi$, is comparable so that the resonant frequency is affected by the waveguide, but the FEL mechanism is not dramatically altered.

19. FELs using a Gaussian optical mode

When the FEL's relativistic Doppler shift is used to obtain short optical wavelengths, $\gamma \gg 1$, a waveguide becomes unnecessary and even impractical, since the waveguide dimension would be comparable to the optical wavelength. Just as the extension of the atomic maser to laser wavelengths necessitated the invention of the open Gaussian resonator [4], the extension of electron microwave tubes to the FEL necessitated the use of the open resonator [1].

In the low gain FEL oscillator configuration, the optical mode is primarily determined by the resonator mirrors and diffraction. The radius of curvature, R_c, of the resonator mirrors that are separated by distance S gives a dimensionless Rayleigh length $z_0 = (2SR_c - S^2)^{1/2}/2L_u$ [162]; typically, R_c is comparable to the undulator length, L_u, so that $z_0 \le 1$. A solution to the free-space wave equation is called a "Gaussian" beam after its shape in the transverse dimension,

$$a_G(r,\tau) = \frac{a_0}{w(\tau)} \exp[-r^2/w^2(\tau)z_0] \exp[i\phi_G(\tau)], \quad \phi_G(\tau) = -\tan^{-1}[(\tau-\tau_w)/z_0] + \frac{r^2(\tau-\tau_w)}{z_0^2 + (\tau-\tau_w)^2}, \tag{68}$$

where the radial coordinate $r = (x^2+y^2)^{1/2}$ is normalized to $(L_u\lambda/\pi)^{1/2}$, $w^2(\tau) = 1 + (\tau-\tau_w)^2/z_0^2$, and $a_0 = 4\pi N_u e K L_u E/\gamma^2 mc^2$ is the dimensionless optical wave amplitude at the center ($r=0$) of the mode's waist positioned at τ_w. As $z_0 \to \infty$, so that $w \to 1$, $\phi_G \to 0$, (68) describes plane waves of infinite extent. The dimensionless radius of the wavefront is $z_0^{1/2}$ at the mode waist $\tau = \tau_w$, and spreads by diffraction as τ moves away from τ_w; the area of the beam doubles as it propagates a distance $\Delta\tau = z_0$.

In the combined FEL undulator field and the Gaussian optical mode, the electron equation of motion still has the form of the pendulum equation,

$$\overset{\circ\circ}{\zeta} = \overset{\circ}{v} = |a_G(\tau)| \cos(\zeta + \phi_G(\tau)) . \tag{69}$$

The electron coordinates (ζ, v) follow the pendulum phase-space paths with parametrically changing amplitude, $|a_G(\tau)|$, and phase, $\phi_G(\tau)$. When $z_0 \to \infty$, the pendulum equation for plane waves is recovered. To illustrate some of the effects of the Gaussian mode, consider $z_0 \gg 1$ so that $w(\tau) = 1 + \ldots$ and $\phi_G = -z_0^{-1}(\tau - \tau_w) + \ldots$. To simplify the pendulum equation, consider weak optical fields, $a_0 \ll \pi$, so that the lowest-order solution is $\zeta^{(0)} = \zeta_0 + v_0\tau$ and $v^{(0)} = v_0$. To first order in a_0, the pendulum equation becomes

$$\overset{\circ\circ}{\zeta} = \overset{\circ}{v} = a_0 \exp(-z_0^{-1}r^2) \cos[\zeta_0 + z_0^{-1}\tau_w + (v_0 - z_0^{-1})\tau] . \tag{70}$$

The changes caused by the non-planar Gaussian beam now become quite clear. The field optical amplitude becomes $a_0 \to a_0 \exp(-z_0^{-1} r^2)$, and decreases off-axis as electrons move to the mode waist, $r \to z_0^{1/2}$. The electron initial phase becomes $\zeta_0 \to \zeta_0 + z_0^{-1}\tau_w$, but since the beam is uniformly spread, the new phase is inconsequential. An important modification is the shifted phase velocity, $v_0 \to v_0 - z_0^{-1}$, which causes a measurable change in the operation of the FEL. Gain is maximum at $v_0^{max} = 2.6 + z_0^{-1}$, and is shifted to a larger phase velocity by the Gaussian mode. The shift away from exact resonance is $\Delta v = z_0^{-1}$, and the resonant FEL wavelength is shifted by $\Delta\lambda/\lambda = 1/2\pi N_w z_0$; the reason is the phase evolution $\phi(\tau) = -z_0^{-1}\tau$.

For smaller values of z_0, the Gaussian beam, $a_G(\tau)$, cannot be expanded in z_0^{-1}. But the pendulum equation can still be expanded in weak fields, $a_0 \ll \pi$, integrated, and phase averaged, to get the final FEL gain using energy conservation as in (29). The result is

$$G(v_0, z_0) = \frac{j\,\sigma_x^2}{a_0^2 z_0} \int_0^1 d\tau \int_0^\tau d\tau' \int_0^{\tau'} d\tau'' \; |a_G(\tau)|\,|a_G(\tau')| \sin[\, v_0(\tau-\tau'') + \phi_G(\tau) + \phi_G(\tau'')\,] \quad . \qquad (71)$$

where $\sigma_x^2 = \pi r_b^2 / L_w \lambda$. As $z_0 \to \infty$, the coefficient of the triple integral $\to 0$, and $G(v_0, z_0) \to 0$, because the optical mode is much larger than the electron beam. Also, as $z_0 \to 0$, the triple integral $\to 0$, and $G(v_0, z_0) \to 0$ again, because the FEL is shifted far off-resonance by $\phi_G = -z_0^{-1}\tau$. So, there must be an optimum value of z_0 where gain is maximum. The expression (71) is difficult to integrate analytically, but easy to integrate numerically to find the gain spectrum, $G(v_0)$, as a function of the Rayleigh length z_0. The result shows that the optimum resonator for the low-gain FEL oscillator has $z_0 = 0.3$ [163]. This is consistent with the simpler estimate made by maximizing $\bar{F}$ in the last section.

The prescription for generalizing (71) to include a tapered undulator is $v_0\tau \to v_0\tau + \delta\tau^2/2$. Numerical integration then finds that the optimum Rayleigh length for the tapered undulator is $z_0 = 0.4$ with $\delta = 5\pi$ [163]. A similarly simple generalization can be made for the FEL klystron to find an optimum value of $z_0 = 0.25$ with $D = 2$ [163]. Surprisingly, the optimum value of the Rayleigh length for these different FEL interactions are all near $z_0 = 0.3$. In each case, the range of Rayleigh lengths where the gain is within 50% of its peak value is $\Delta z_0 = 1$.

20. General transverse mode theory and diffraction

The FEL theory can be extended further to include many transverse modes self-consistently. When the three dimensional parabolic wave equation is coupled to the electron Lorentz force equation, the method is general enough to include arbitrary undulator designs, optical mirror arrangements, and driving currents. For sufficient FEL oscillator gain, the electron beam can distort the optical mode into a combination of resonator modes [164-170]. In the FEL amplifier, there can be more significant distortion of the optical wavefronts called "optical guiding"

[171-180]. When the transverse and longitudinal extensions are combined, the optical field is given spatial dependence in all directions, $a(x,y,z,t)$, instead of using a modal decomposition [164].

The complex optical field envelope is taken to be slowly varying in z and t, so that when the optical vector potential is inserted into the wave equation, the result is the well-known parabolic wave equation. The derivation closely follows the earlier derivation of the wave equation without diffraction in section 5. The difference in the result is just the $\nabla_\perp^2$ term in (72) below. The transverse coordinates are normalized to the characteristic mode size, so that $x(\pi/L_w\lambda)^{1/2} \to x$ and $y(\pi/L_w\lambda)^{1/2} \to y$, and the longitudinal coordinate is normalized to the slippage distance so that $(z - ct)/N_w\lambda \to z$, and $\tau = ct/L_w$. The parabolic wave equation can then be written as

$$\left[-\frac{i}{4}\nabla_\perp^2 + \frac{\partial}{\partial\tau} \right] a(x,y,z,\tau) = -\,< j e^{-i\zeta} >_{(x,y,z-\tau,\tau)} \quad . \qquad (72)$$

where $\nabla_\perp^2 = \partial_x^2 + \partial_y^2$. Equation (72) governs the dynamics of the optical wave over many optical wavelengths in the longitudinal z dimension, and the $\nabla_\perp^2$ operator properly describes the diffraction of the optical wave in the transverse (x,y) directions. To order $j\Delta\tau^2$ the solution to (72) over distance $\Delta\tau$ is

$$a(x,y,z,\tau+\Delta\tau) = \exp\left[\frac{i\,\Delta\tau}{4}\nabla_\perp^2 \right] a(x,y,z,\tau) - \Delta\tau < j e^{-i\zeta} >_{(x,y,z-\tau,\tau)} + \ldots \quad . \qquad (73)$$

The solution (73) is exact for any $\Delta\tau$ when there is no current, but when $j > 0$, a small time step, $\Delta\tau \ll 1$, is required to accurately integrate the driving term, and the accompanying pendulum equation. In Fourier space, the diffraction operator, $\exp(i\Delta\tau\nabla_\perp^2/4)$, is diagonal, and may be efficiently implemented numerically. The optical wavefronts, $a(x,y)$, can now be correctly propagated forward in time, and the beam current will amplify the wave where $j(x,y)$ is non-zero. When the transverse size of the electron beam and the wavefronts are much larger than $(L_w\lambda/\pi)^{1/2}$, the operator $\exp(i\Delta\tau\nabla_\perp^2/4) \approx 1$ over the propagation distance $\Delta\tau = 1$, and diffraction can be neglected.

The self-consistent evolution of the electron current is governed by the Lorentz force equation for each electron in the beam. The pendulum equation has the same form as before with the generalizations $\zeta \to \zeta(x,y,z-\tau,\tau)$ and $v \to v(x,y,z-\tau,\tau)$.

$$\dot{v}(x,y,z-\tau,\tau) = \ddot{\zeta}(x,y,z-\tau,\tau) = |\,a(x,y,z,\tau)\,| \cos[\,\zeta(x,y,z-\tau,\tau) + \phi(x,y,z,\tau)\,] \quad . \qquad (74)$$

The theory is now fully self-consistent in 4 dimensions (x,y,z,τ), and a simulation introduces arrays of sites in (x,y) at each longitudinal site z in (74). The 3D electron array moves backwards along z with respect to the 3D optical array at every τ-step because of slippage. When the electron pulse is long compared to the slippage distance, and there is long range

coherence in the z direction, the coupled equations (73)-(74) become z invariant so that only one z point need be considered. As an example of a transverse diffractive effect without the complication of the longitudinal multimode problem described earlier, the coupled equations are used to determine the stable resonator modes in the FEL oscillator.

The eigenvalues of the optical resonator with the amplifying electron beam are determined by propagating an optical wavefront from mirror to mirror over many passes n until steady state is achieved [181]. The FEL schematic with an actual resonator mode is shown in Figure 1. Each time the wavefront reaches a mirror, the optical field is set equal to zero beyond the edges of the mirror. Upon reaching the curved mirror surface, the wavefront experiences a phase shift given by $\delta\phi(x,y) = -2r^2/r_c$ where $r^2 = x^2 + y^2$ and $r_c = R_c/L_u$ is the normalized radius of curvature of the mirror. Free propagation continues until the wave overlaps freshly injected electrons traveling through the undulator from $\tau = 0 \rightarrow 1$. The shape of the electron beam density has the form $j(r) = j(1-r^2/2\sigma_x^2)$ for $r < \sqrt{2}\sigma_x$, and $j = 0$ elsewhere. The peak current is j, and the beam radius is σ_x. After the end of the undulator at $\tau = 1$, the wave is propagated freely again until reaching the output coupling mirror. The fractional power lost through this mirror is $e^{-1/Q}$ each pass. Finally, the free return trip back to the perfectly reflecting mirror is made, and the calculation is repeated. Bouncing the light between the mirrors is continued until a steady-state mode is attained. When the optical fields become strong, the gain per pass decreases, and steady state occurs as the reduced gain balances the resonator losses. The phase velocity for the electrons is $v_0 = 2\pi$ for nearly optimum gain in strong fields. The final mode structure depends on the combined properties of the electron beam and resonator.

Figure 25 shows a steady-state resonator mode after $n = 100$ passes with $Q = 66$. The mirrors have radius of curvature $r_c = 1.4$, and radius $r_m = 3.0$ normalized to $(L_u\lambda/\pi)^{1/2}$ with the mirror separation $\tau_s = 2.4$ normalized to the undulator length L_u. The peak current density is $j = 60$ in a beam of radius $\sigma_x = 0.25$. When the beam current, $j(r)$, is centered on the resonator axis, the resulting steady-state mode is close to the fundamental Gaussian mode determined by the mirror separation, τ_s, and curvature, r_c. The peak field, $|a(x,y)| \approx 24$, is in the strong field regime, and reduces the gain to equal the loss. In order to see more interesting mode structure, the electron beam is made to travel parallel to, but off of the mode axis by an amount $\Delta y = 1.2 = 4.8\sigma_x$. The resultant multimode structure is shown in figure 25. The wavefront energy, $P(n) = \int dxdy\,|a(x,y)|^2$ (inset curve), grows over $n = 100$ passes until reaching strong optical fields, and the gain per pass (inset dots) decreases to match the resonator losses. The structure of the steady-state wavefront, $|a(x,y)|$, resembles the TEM_{30} mode with only a small coupling to the lowest-order mode.

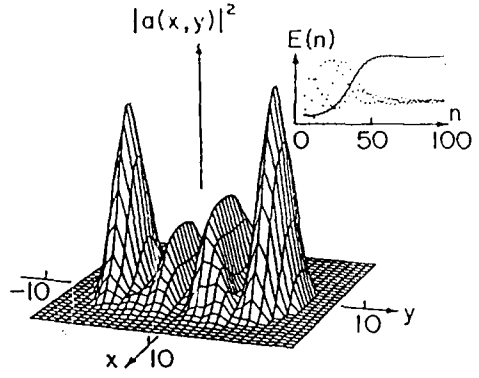

Figure 25. Distorted resonator mode in the FEL oscillator.

Another example of transverse mode distortion is "optical guiding". In the case of large current, $j \gg 1$, the transverse optical mode can be continuously distorted by the electron beam. The large optical phase shift associated with the high-current regime actually focuses the light back into the electron beam. This is an important practical advantage for the high-gain amplifier configuration where natural diffraction would provide a limitation to a long undulator length. The FEL interaction can distort the optical field amplitude, "gain guiding", as well as distort the optical field phase, "phase guiding". Gain guiding is not surprising, but phase guiding is not necessarily common to all gain media. FEL phase guiding is true focusing and does not require FEL gain; it can occur after strong field saturation where there is little or no gain.

Consider a small electron beam in the middle of a co-propagating optical wave. In free space, the optical phase at the center of a wavefront evolves as $\Delta\phi = -\Delta\tau/z_0$ for a small step $\Delta\tau$. The FEL interaction also modifies the wavefront. If the parabolic wave equation is averaged over the transverse Gaussian mode area, πz_0, for a small step $\Delta\tau$, the simple form of the wave equation (21) is recovered with the new dimensionless current $j \rightarrow jF$ where the "filling factor" is $F = \pi\sigma_x^2/\pi z_0$. The quantity $jF \propto n_e F$ does not depend on the electron beam area, but only on the current within the optical mode area. In the high-current, $jF \gg 1$, weak-field, $|a| \ll a_j \approx 2(jF/2)^{2/3}$, regime, the optical phase evolves as $\Delta\phi = (jF/2)^{1/3}\Delta\tau/2$. In the high-current, strong-field, $|a| \approx 2a_j \approx 4(jF/2)^{2/3}$, regime, electrons are bunched near $\zeta \approx \pi/2 - \phi$ so that

the optical phase evolves as $\dot{\phi} = j/a_0$, or $\Delta\phi = (jF/2)^{1/3}\Delta\tau/2$ again. Remarkably, within these approximations, the optical phase evolution in the high current regime is roughly the same in both strong and weak optical fields. In either strong or weak fields, the FEL interaction induces a phase shift that is opposite to that of natural diffraction, and therefore focuses the light back into the beam along τ.

When the FEL has large enough current for optical guiding to persist, the FEL interaction must continually compensate for the phase shift associated with free-space diffraction at each step $\Delta\tau$; that is $(jF/2)^{1/3}/2 \geq z_0^{-1}$. The critical current density needed for optical guiding is then given by $j_G \approx 16 z_0^{-2}\sigma_x^{-2}$. An FEL utilizing a small electron beam and a small optical wavefront (with a correspondingly short Rayleigh length), requires a larger current density for guicing. When the initial optical wavefront is focused onto the electron beam, we would expect that the filling factor F is not too small; we use $\sigma_x^2 = z_0/2$ to write a simpler relation estimating the critical current density needed for optical guiding,

$$j_G \approx 32\, z_0^{-3} \quad . \tag{75}$$

If the normalized Rayleigh length is small, say $z_0 = \pi w_0^2/L_u\lambda = 0.2$, natural diffraction would spread the light over a large transverse area after the interaction length $\Delta\tau = 1$. Optical guiding can compensate in a typical high-current case where $j = 10^4 > j_G = 4\times10^3$. Note that the relations, $j_G \approx 16 z_0^{-2}\sigma_x^{-2}$ and $j_G = 32\, z_0^{-3}$, do not depend on the length of the undulator L_u, but express a comparison between the rates of natural diffraction and FEL focusing along τ.

Figure 25 shows a simulation that solves the parabolic wave equation, together with the pendulum equation, numerically to illustrate guiding. The electron pulse is long, so that no z dependence is followed; in the transverse dimension, the electron beam is symmetric in x-y with the parabolic shape of width $\sigma_x = 0.2$. The peak density is $j = 5\times10^4$, and the initial phase velocity of the beam is $v_0 = 0$ for maximum gain in the high-current case. A Gaussian optical mode is focused at the beginning of the undulator with a Rayleigh length $z_0 = 0.1$, and an initial field strength $a_0 = 10$ at the center of the mode. The field amplitude, $|a(x,\tau)|$, grows along τ, and reaches a peak value $|a| = 2300$ shown in white; points of zero field amplitude are shown as black. The scale at the top-right indicates the field amplitudes plotted in grey, and two contours following points of constant amplitude are superimposed. Without the FEL interaction, the mode radius would spread to several times the width of the window shown. But, the contours show how the wavefront is focused back into the electron beam, and maintains nearly the same area even after reaching strong optical fields.

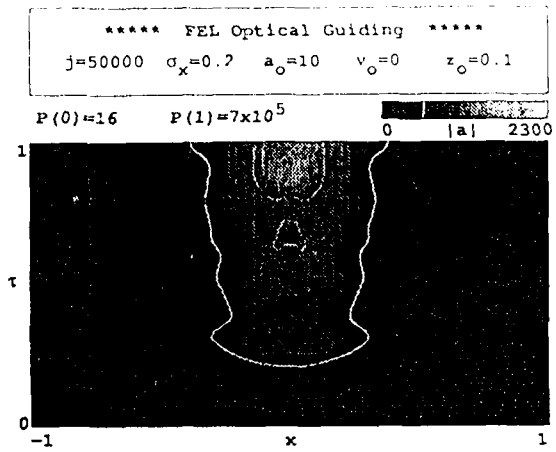

Figure 26. Optical guiding in a high-current FEL amplifier.

21. Acknowledgments

The author is grateful for support of this work by the Lawrence Livermore National Laboratory, and the U.S. Office of Naval Research.

22. References

[1] J. M. J. Madey, J. Appl. Phys. 42, 1906 (1971); J. M. J. Madey, *Stimulated Emission of Radiation in Periodically Deflected Electron Beam*, U.S. Patent 3,822,410 (1974).

[2] L. R. Elias, W. M. Fairbank, J. M. J. Madey, H. A. Schwettman, T. I. Smith, Phys. Rev. Lett. 36, 717 (1976).

[3] D. A. G. Deacon, L. R. Elias, J. M. J. Madey, G. J. Ramian, H. A. Schwettman and T. I. Smith, Phys. Rev. Lett. 38, 892 (1977).

[4] A. L. Schawlow and C. H. Townes, Phys. Rev. 112, 1940 (1958).

[5] Proceedings of the First Free Electron Laser Conference, Telluride, CO, eds. S. F. Jacobs, M. Sargent, III, and M. O. Scully, *Physics of Quantum Electronics*, Vol. 5 (Addison-Wesley, 1978).

[6] Proceedings of the Second International Free Electron Laser Conference, Telluride, CO, eds. S. F. Jacobs, H. S. Pilloff, M. Sargent, III, M. O. Scully, and R. Spitzer, *Physics of Quantum Electronics*, Vol. 7 (Addison-Wesley, 1980).

[7] Proceedings of the Third International Free Electron Laser Conference, Sun Valley, ID, eds. S. F. Jacobs, H. S. Pilloff, M. Sargent, III, M. O. Scully, and R. Spitzer, *Physics of Quantum Electronics*, Vol. 8 & 9 (Addison-Wesley, 1982).

[8] Proceedings of the Fourth International Free Electron Laser Conference, Bendor Island, France, eds. M. Billardon and D. A. G. Deacon, *Bendor Free Electron Laser Conference*, Journal de Physique, Colloque C1-44 (Feb. 1983).

[9] Proceedings of the Fifth International Free Electron Laser Conference, Orcas Island WA, eds. C. A. Brau, S. F. Jacobs, and M. O. Scully, *Free Electron Generators of Coherent Radiation*, SPIE (Int. Soc. Opt. Eng.) 453 (1984).

[10] Proceedings of the Sixth International Free Electron Laser Conference, Castelgondolfo, Italy, eds. J. M. J. Madey and A. Renieri, *Free Electron Lasers*, Nucl. Instr. & Methods in Phys. Res. A237 (North-Holland Publishing, Amsterdam, 1985).

[11] Proceedings of the Seventh International Free Electron Laser Conference, Tahoe City, CA, eds. E. T. Scharlemann and D. Prosnitz, *Free Electron Lasers*, Nucl. Instr. & Methods in Phys. Res. A250 (North-Holland Publishing, Amsterdam, 1986).

[12] Proceedings of the Eighth International Free Electron Laser Conference, Glasgow UK, ed. M. Poole, *Free Electron Lasers*, Nucl. Instr. & Methods in Phys. Res. A259 (North-Holland Publishing, Amsterdam, 1987).

[13] Proceedings of the Ninth International Free Electron Laser Conference, Williamsburg, VA, eds. P. Sprangle et. al., *Free Electron Lasers*, Nucl. Instr. & Methods in Phys. Res. A272 (North-Holland Publishing, Amsterdam, 1988).

[14] International Conference on LASERS '79, Orlando, FL (Dec. 1979).

[15] International Conference on LASERS '80, New Orleans, LA (Dec. 1980).

[16] International Conference on LASERS '81, New Orleans, LA (Dec. 1981).

[17] International Conference on LASERS '82, New Orleans, LA (Dec. 1982).

[18] International Conference on LASERS '83, San Francisco, CA (Dec. 1983).

[19] International Conference on LASERS '84, San Francisco, CA, (Nov. 1984).

[20] International Conference on LASERS '85, Las Vegas, NV (Dec. 1985).

[21] International Conference on LASERS '86, Orlando, FL (Nov. 1986).

[22] International Conference on LASERS '87, Lake Tahoe, NV (Dec. 1987).

[23] Special Issue of IEEE Journal of Quantum Electronics, QE-17, No. 8 (Aug. 1981).

[24] Special Issue of IEEE Journal of Quantum Electronics, QE-19, No. 3 (Mar. 1983).

[25] Special Issue of IEEE Journal of Quantum Electronics, QE-21, No. 7 (Jul. 1985).

[26] Special Issue of IEEE Journal of Quantum Electronics, QE-23, No. 9 (Sept. 1987).

[27] *Free Electron Lasers*, Ettore Majorana International Science Series, Series Editor: Antonino Zichichi, Physical Sciences, vol. 18, Eds. S. Martellucci and Arthur N. Chester (Plenum Press, New York, 1983).

[28] Nucl. Instr. & Methods in Phys. Res., eds. R. Bonifacio, F. Casagrande, C. Pellegrini, A239, (North-Holland Publishing, Amsterdam, 1985).

[29] *Free Electron Generation of Extreme Ultraviolet Coherent Radiation*, eds. J. M. J. Madey and C. Pollegrini, AIP Conference Proceedings, New York (1984).

[30] Proceedings of the Workshop on Applications of Free Electron Lasers, eds. D. A. G. Deacon and A. De Angelis, Applications of Free Electron Lasers (North-Holland, Amsterdam, 1985).

[31] W. B. Colson, Nucl. Instr. & Methods in Phys. Res. A237, 1 (1985); W. B. Colson, Ph.D. Thesis, Stanford University, 1977.

[32] *Short Wavelength Coherent Radiation: Generation and Applications*, eds. D. T. Attwood, J. Bokor, Optical Science and Engineering Series 7, AIP Conference Proceedings No. 147, New York (1986).

[33] *Free Electron Lasers: Critical Review of Technology*, editor B. E. Newnam, Proc. SPIE 738 (1988).

[34] C. A. Brau, "Free Electron Lasers", *Science*, vol. 239, p. 1115 (March 4, 1988).

[35] H. Motz, Contemporary Physics 20, 547 (1979).

[36] D. Prosnitz, "Free electron lasers." CRC Handbook of Laser Science and Technology 1, ed. M. J. Weber, p. 425, Boca Raton (CRC Press, 1982).

[37] P. Sprangle and T. Coffey, Physics Today, 44 (1984).

[38] W. B. Colson and A. M. Sessler, Annual Review Nuclear & Particle Science 35,25 (1985).

[39] G. Dattoli, A. Renieri, Experimental and Theoretical Aspects of the Free Electron Laser, in Laser Handbook 4, ed. M. L. Stitch and M. S. Bass (North-Holland, Amsterdam, 1985).

[40] A. M. Sessler and D. Vaughan, American Scientist, 75, 35 (1987).

[41] T. C. Marshall, *Free Electron Lasers* (MacMillan, New York, 1985).

[42] W. B. Colson, Phys. Lett. A59, 187 (1976).

[43] P. Bosco, W. B. Colson, and Roger A. Freedman, IEEE Journal of Quantum Electronics, QE-19, 272 (1983).

[44] W. Becker, Phys. Lett. 65A, 317 (1978).

[45] G. Dattoli, Lett. Nuovo Cimento 27, 247 (1980).

[46] R. Bonifacio, F. Casagrande, and L.A. Lugiato, Optics Comm. 36, 159 (1981).

[47] M. V. Fedorov, IEEE J. Quantum Electron. QE-17, 1359 (1981).

[48] W. Becker and J.K. McIver, Phys. Rev. **A27**, 1030 (1983).

[49] F. A. Hopf, P. Meystre, M. O. Scully, W. H. Louisell, Phys Rev. Lett. 37, 1342 (1976).

[50] W. B. Colson, Phys. Lett. **64A**, 190 (1977).

[51] W. B. Colson and S. K. Ride, Phys. Lett. **76A**, 379 (1980).

[52] A. Bambini, A. Renieri, and S. Stenholm, Phys. Rev., **19A**, 2013 (1979).

[53] V. N. Baier and A. I. Milstein, Phys. Lett., **65A**, 310 (1978).

[54] N. M. Kroll and W. A. McMullin, Phys. Rev., **17A**, 300 (1978).

[55] H. Al-Abawi, F. A. Hopf, G. T. Moore, and M. O. Scully, Optics Commun. 30, 235 (1979).

[56] F. A. Hopf, T. G. Kuper, G. T. Moore and M. O. Scully, *Physics of Quantum Electronics*, Vol. 7, 31 (Addison-Wesley, 1980).

[57] R. Bonifacio, P. Meystre, G. T. Moore and M. O. Scully, Phys. Rev. **A21**, 2009 (1980).

[58] N. Al-Abawi, G.T. Moore and M.O. Scully, Phys. Rev. **A24**, 3143 (1981).

[59] H. Al-Abawi, J. K. McIver, G. T. Moore and M. O. Scully, *Physics of Quantum Electronics*, Vol. 9, 415 (Addison-Wesley, 1982).

[60] P. Sprangle, C. Tang, and W. Manheimer, Phys. Rev. Lett., **43**, 1932 (1979).

[61] D. B. McDermott and T. C. Marshall, *Physics of Quantum Electronics*, Vol. 7, 509 (Addison-Wesley, 1980).

[62] A. Gover, *Physics of Quantum Electronics*, Vol. 7, 701 (Addison-Wesley, 1980).

[63] T. Kwan, J. M. Dawson, and A. T. Lin, Phys. Fluids, **20**, 581 (1977).

[64] A. T. Lin and J. M. Dawson, Phys. Rev. Lett., **42**, 1670 (1979).

[65] N. M. Kroll, P. L. Morton, and M. N. Rosenbluth, *Physics of Quantum Electronics*, Vol. 7, 89 (1980).

[66] N. M. Kroll, P. L. Morton, and M. N. Rosenbluth, Journal of Quantum Electronics QE-17, 1436 (1981).

[67] W. B. Colson, *Physics of Quantum Electronics*, Vol. 5, 157 (1980).

[68] W. B. Colson and S. K. Ride, *Physics of Quantum Electronics*, Vol. 7, 377 (1980).

[69] W. B. Colson, IEEE Journal of Quantum Electronics **QE-17**, 1417 (1981).

[70] J. N. Eckstein, J. M. J. Madey, K. Robinson, T. I. Smith, S. Benson, D. Deacon, R. Taber, and A. Gaupp, *Physics of Quantum Electronics* **8**, 49 (1982).

[71] M. Billardon, P. Elleaume, J. M. Ortega, C. Bazin, M. Bergher, M. Velghe, Y. Petroff, D. A. G. Deacon, K. E. Robinson, and J. M. J. Madey, Physical Review Letters **51**, 1652 (1983).

[72] R. W. Warren, B. E. Newnam, J. G. Winston, W. E. Stein, L. M. Young, and C. A. Brau, IEEE Journal of Quantum Electronics **QE-19**, 391 (1983).

[73] J. M. Slater, J. L. Adamski, D. C. Quimby, T. L. Churchill, L. Y. Nelson, and R. E. Center, IEEE Journal of Quantum Electronics **QE-19**, 374 (1983).

[74] J. A. Edighoffer, H. Boehmer, M. Z. Caponi, S. Fornaca, J. Munch, G. R. Neil, B. Saur, and C. Shih IEEE Journal of Quantum Electronics, **QE-19**, 316 (1983).

[75] B. E. Newnam, R. W. Warren, R. L. Sheffield, J. C. Goldstein, and C. A. Brau, Nucl. Instr. & Methods in Phys. Res. **A237**, 187 (1985).

[76] J. A. Edighoffer, G. R. Neil, C. E. Hess, T. I. Smith, S. W. Fornaca, and H. A. Schwettman Phys. Rev. Lett., **52**, 344 (1984).

[77] G. A. Kornyukhin, G. N. Kullpanov, V. N. Litvinenko, N. A. Mesentsev, A. N. Skrinsky, N. A Vinokurov and P. D. Voblyi, Nucl. Instr. & Methods in Phys. Res. **A237**, 281 (1985).

[78] U. Bizzarri, F. Ciocci, G. Dattoli, A. De Angelis, G. P. Gallerano, I. Giabbai, G. Giordano, T. Letardi, G. Messina, A. Mola, L. Picardi, A. Renieri, E. Sabia, A. Vignati, E. Fiorentino, and A. Marino, Nucl. Instr. & Methods in Phys. Res. **A250**, 254 (1986).

[79] M. Billardon, P. Elleaume, Y. Laplerre, J. M. Ortega, C. Bazin, M. Berghor, J. Marilleau, and Y. Petroff, Nucl. Instr. & Methods in Phys. Res. **A250**, 26 (1986).

[80] L. R. Elias, J. Hu and G. Ramaln, Nucl. Instr. & Methods in Phys. Res. **A237**, 203 (1985).

[81] R. Ba ..li, G. Vignola, S. Trillo, R. Boni, S. DeSimone, S. Faini, S. Guiducci, M. Preger, M. Serio, B. Spataro, S. Tazzari, F. Tazzioli, M. Vescovi, A. Cattoni, C. Sanelli, M. Castellano, N. Cavallo, F. Cevenini, M. R. Masullo, P. Patteri, R. Rinzivillo, S. Solimeno, and A. Cutolo, Journal de Physique, **44**, C1-1 (1985).

[82] T. J. Orzechowski, B. Anderson, W. M. Fawley, D. Prosnitz, E. T. Scharlemann, S. Yarema, D. Hopkins, A. C. Paul, A. M. Sessler, and J. Wurtele, Phys. Rev. Lett. 54, 889 (1985).

[83] R. W. Warren, D. W. Feldman, B. E. Newnam, S. C. Bender, W. E. Stein, A. H. Lumpkin, R. A. Lohsen, J. C. Goldstein, B. D. McVey, and K. C. D. Chan, Nucl. Instr. & Methods in Phys. Res. **A259**, 8 (1987).

[84] S. V. Benson, J. M. J. Madey, J. Schultz, M. Marc, W. Wadensweiler, G. A. Westenskow, and M. Velghe, Nucl. Instr. & Methods in Phys. Res. **A250**, 39 (1986).

[85] T. J. Orzechowski, B. R. Anderson, W. M. Fawley, D. Prosnitz, E. T. Scharlemann, S. M. Yarema, A. M. Sessler, D. B. Hopkins, A. C. Paul, and J. S. Wurtele, Nucl. Instr. & Methods in Phys. Res. **A250**, 144 (1986).

[86] T. J. Orzechowski, B. R. Anderson, J. C. Clark, W. M. Fawley, A. C. Paul, D. Prosnitz, E. T. Scharlemann, and S. M. Yarema, Phys. Rev. Lett., **57**, 2172 (1986).

[87] A. L. Throop, T. J. Orzechowski, B. R. Anderson, F. W. Chambers, J. C. Clark, W. M. Fawley, R. A. Jong, A. C. Paul, D. Prosnitz, E. T. Scharlemann, R. D. Stever, G. A. Westenskow, and S. M. Yarema, "Experimental Characteristics of a High-Gain Free-Electron Laser Amplifier Operating at 8 mm and 2 mm Wavelengths," presented at AIAA 19th Fluid Dynamics & Lasers Conf., Honolulu, HA, June 8, 1987.

[88] K. E. Robinson, T. L. Churchill, D. C. Quimby, D. M. Shemwell, J. M. Slater, A. S. Valla, A. A. Vetter, J. Adamski, T. Doering, W. Gallagher, R. Kennedy, B. Robinson, D. Shoffstall, E. Tyson, A. Vetter, and A. Yeremian, Nucl. Instr. & Methods in Phys. Res. **A259**, 49 (1987).

[92] A. Brownell, M. S. Curtin, W. A. McMullin, S. V. Benson, J. M. J. Madey, B. A. Richman, and L. Vintro, "First Operation of the Rocketdyne-Stanford FEL", Williamsburg FEL Conf. 1988.

[93] F. W. van Amersfoort, R. W. B. Best, C. A. J. van der Geer, W. J. Mastop, B. J. F. Meddens, A. F. G. van der Meer, D. Oepts, The Felix Project, status report April 1988, FOM-report # 04886.

[94] A. Luccio, C. Pellegrini, A. van Steenbergen, and L. H. Yu, Proc. Int. Conf. LASERS '82, 138 (1982).

[95] J. C. Goldstein and B. D. McVey, Nucl. Instr. & Methods in Phys. Res. A259, 203 (1987); B. E. Newnam, J. C. Goldstein, J. S. Fraser, R. K. Cooper, "A Linac-Driven XUV Free-Electron Laser," Los Alamos National Laboratory Report, Los Alamos, NM.

[96] J. E. LaSala, D. A. G. Deacon, and J. M. J. Madey, Nucl. Instr. & Methods in Phys. Res. A250, 252 (1986).

[97] K. K. Maruyama, S. Penner, C. M. Tang, and P. Sprangle, Nucl. Instr. & Methods in Phys. Res. **A259**, 259 (1987).

[98] Xie Jialin, Director, Institute of High Energy Physics, Beijing PRC, private communication.

[99] K. Halbach, *Bendor Free Electron Laser Conference*, eds. M. Billardon and D. A. G. Deacon, Journal de Physique, Colloque **C1-44**, p. 211 (1983).

[100] J. P. Blewett, and R. Chasman, J. Appl. Phys. **48**, 2692 (1977).

[101] L. R. Elias, and J. M. J. Madey, *Rev. Sci. Instrum.* **50**, 1339 (1979).

[102] E. T. Scharlemann, J. Appl. Phys. **58**, 2154 (1985).

[103] J. D. Jackson, *Classical Electrodynamics*, (Wiley, New York, 1975).

[104] H. Winick, Physics Today, May (1981); H. Winick, Physics Today, November (1987).

[105] L. R. Elias and J. C. Gallardo, Phys. Rev. **A24**, 3276 (1981).

[106] L. R. Elias and J. C. Gallardo, *Physics of Quantum Electronics*, Vol. 9, 603 (Addison-Wesley, 1982).

[107] W. B. Colson, *Free Electron Generators of Extreme Ultraviolet: Coherent Radiation*, AIP Conf. Proc. No. **118**, p. 260, eds. Madey and Pellegrini, Brookhaven National Lab, Upton NY (1984).

[108] G. A. Schott, *Electromagnetic Radiation*, (Cambridge University, London, 1912).

[109] D. Alferov, Y. Bashmakov, and E. Bessonov, Proc. of P.N. Lebedev Phys. Inst. **80**, 97 (1976).

[110] B. M. Kincaid, J. Appl. Phys. **48**, 2684 (1977).

[111] W. B. Colson, Phys. Rev. **A24**, 639 (1981).

[112] R. Colson, IEEE Journal of Quantum Electronics **QE-17**, 1109 (1981).

[113] M.V. Fedorov and S. Stenholm, Optics Communications **49**, 385 (1984).

[114] W. B. Colson, G. Dattoli, and F. Ciocci, Phys. Rev. A31, 828 (1985).

[115] B. M. Kincaid, Nucl. Instr. & Methods in Phys. Res. A246, 135 (1986).

[116] P. Bosco and W. B. Colson, Phys. Rev. A28, 811 (1983).

[117] M. Sargent III, M. O. Scully and W. E. Lamb, Jr., *Laser Physics*, (Addison-Wesley, 1974).

[118] M. Borenstein and W. E. Lamb, Jr., Phys. Rev. A5, 1298 (1972).

[119] P. Sprangle, C. M. Tang, and W. M. Manheimer, Phys. Rev. A21, 301 (1980).

[120] D. Prosnitz and A. M. Sessler, *Physics of Quantum Electronics*, Vol. 9, 651 (1982).

[121] E. T. Scharlemann, W. M. Fawley, B. R. Anderson and T. J. Orzechowski, Nucl. Instr. & Methods in Phys. Res. **A250**, 150 (1986).

[122] J. S. Wurtele, E. T. Scharlemann and A. M. Sessler, Nucl. Instr. & Methods in Phys. Res. **A250**, 176 (1986).

[123] B. D. McVey, Nucl. Instr. & Methods in Phys. Res. A250, 449 (1986).

[124] D. C. Quimby, Nucl. Instr. & Methods in Phys. Res. A250, 456 (1986).

[125] T. J. Orzechowski, E. T. Scharlemann and D. B. Hopkins, Phys. Rev. **B35**, 2184 (1987).

[126] C.-C. Shih and A. Yariv, IEEE Journal of Quantum Electronics **QE-17**, 1387 (1981).

[127] G. Dattoli, A. Marino, A. Renieri and F. Romanelli, IEEE Journal of Quantum Electronics, **QE-17**, 1371 (1981).

[128] W. B. Colson, *Free Electron Laser Wave and Particle Dynamics*, in the International Summer School of Quantum Electronics, A. Renieri and S. Martellucci, Eds. New York, Plenum (1981).

[129] W. B. Colson, *Physics of Quantum Electronics*, Vol. 8, 457 (1982).

[130] C.-M. Tang, and P. Sprangle, J. Appl. Phys. **53**, 831 (1982).

[131] R. Bonifacio, C. Pellegrini, and L. M. Narducci, Optics Communication 50, 373 (1984).

[132] W. B. Colson, J. C. Gallardo, and P. M. Bosco, Phys. Rev. A34, 4837 (1986).

[133] W. B. Colson and J. Blau, Nucl. Instr. & Methods in Phys. Res. A259, 198 (1987).

[134] C. M. Tang, H. Freund, P. Sprangle and W. B. Colson, *Physics of Quantum Electronics* 8 503 (Addison-Wesley, 1982).

[135] M. Billardon, P. Elleaume, J. M. Ortega, C. Bazin, M. Bergher, M. Velghe, Y. Petroff, D. A. G. Deacon, K. E. Robinson, and J. M. J. Madey, Phys. Rev. Lett. **51**, 1652 (1983).

[136] R. W. Warren, B. E. Newnam, W. E. Stein, J. G. Winston, R. L. Sheffield, M. T. Lynch, J. C. Goldstein, M. C. Whitehead, O. R. Norris, G. Luedemann, T. O. Gibson, and G. M. Humphrey, Proceedings of the Sixth International Conference on Lasers and Applications, San Francisco (Dec. 12-16, 1983).

[137] M. Biagini, R. Boni, S. De Simone, S. Guiducci, M. Preger, M. Serio, S. Tazzari, F. Tazzioli, S. Trillo, M. Vescovi, M. Ambrosio, G. C. Barbarino, M. Castellano, N. Cavallo, F. Cevenini, M. R. Masullo, P. Patteri, R. Rinzivillo, and S. Solimeno, Proc. Soc Photo-Opt. Instr. Eng. SPIE 453, 275 (1984).

[134] S. Benson and J. M. J. Madey, International Conference on LASERS '88, Lake Tahoe, NV (Dec. 1988).

[135] W. B. Colson, *Free Electron Lasers: Critical Review of Technology*, Proc. SPIE 738, 2-27 (1988).

[136] K. E. Robinson, D. C. Quimby, and J. M. Slater, IEEE Journal of Quantum Electronics, QE-23, 1497 (1987).

[137] W. H. Louisell, J. Lam, D. A. Copeland, and W. B. Colson, Phys. Rev. **A19**, 188 (1979).

[138] W. B. Colson and R. A. Freedman, Phys. Rev. **A27**, 1399 (1983).

[139] D. Attwood, K. Halbach, K.J. Kim, Science **228**, 1265-1272 (1985).

[140] K.J. Kim, Nucl. Instr. & Methods in Phys. Res. **219**, 425-429 (1984).

[141] N.A. Vinokurov and A.N. Skrinsky, Novosibirsk preprint INP77-59 (1977); N.A. Vinokurov, Proc. 10th Int. Conf. on High Energy Particle Accelerators **2**, 454 (Serpukhov, 1977).

[142] I. Boscolo and V. Stagno, Nuovo Cimento **B58**, 267 (1980).

[143] P. Elleaume, *Physics of Quantum Electronics*, Vol. **8**, 119 (1982).

[144] P. Elleaume, Journal de Physique, **44**, Colloque C1, 333 (1983).

[145] W. B. Colson and I. Boscolo, Phys. Rev. **A31**, 2353 (1985).

[146] J. C. Goldstein and W. B. Colson, International Conference on LASERS '81, p. 93, ed. C.B. Collins (STS Press, McLean, VA, 1981).

[147] G. Dattoli, A. Marino, and A. Renieri, *Physics of Quantum Electronics*, Vol. **8**, 515 (1982).

[148] J. C. Goldstein and W. B. Colson, International Conference on LASERS '82, p. 218, ed R. C. Powell, (STS Press, McLean, VA, 1982).

[149] S. Benson and J. M. Madey, *Free Electron Generators of Coherent Radiation*, eds. C. A Brau, S. F. Jacobs and M. O. Scully, SPIE **453**, 55 (1983).

[150] M. N. Rosenbluth, H. V. Wong, B. N. Moore, *Free Electron Generators of Coherent Radiation*, eds. C. A. Brau, S. F. Jacobs and M. O. Scully, SPIE **453**, 25 (1983).

[151] W. B. Colson and A. Renieri, Journal de Physique, Colloque **C1-44**, 11 (1983).

[152] W. B. Colson and Roger A. Freedman, Optics Communication **46**, 37 (1983).

[153] Roger A. Freedman and W. B. Colson, Optics Communication **52**, 409 (1985).

[154] W. B. Colson, *Free Electron Generators of Coherent Radiation*, SPIE **453**, 289, eds. Brau Jacobs, Scully (1984).

[155] D. C. Quimby, J. M. Slater, and J. P. Wilcoxon, IEEE Journal of Quantum Electron QE-21, 979 (1985).

[156] N. M. Kroll and M. N. Rosenbluth, *Physics of Quantum Electronics*, Vol. 7, 147 (1980).

[157] W. B. Colson, Nucl. Instr. & Methods in Phys. Res. A250, 168 (1986).

[158] J.S. Wurtele, E.T. Scharlemann and A.M. Sessler, Nucl. Instr. & Methods in Phys. Res. A250, 176, (1986).

[159] J. Gallardo and L. Elias, Nucl. Instr. & Methods in Phys. Res. A250, 436, (1986).

[160] E. Sternbach, Nucl. Instr. & Methods in Phys. Res. A272, 323, (1988).

[161] J.A. Byers and R.H. Cohen, Nucl. Instr. & Methods in Phys. Res. A272, 595, (1988).

[162] A. Yariv, *Quantum Electronics*, Chapter 6, (Wiley, 1975).

[163] W. B. Colson and P. Elleaume, Appl. Phys. **B29**, 101 (1982).

[164] W. B. Colson and J. L. Richardson, Phys. Rev. Lett. 50, 1050 (1983).

[165] A. Amir and Y. Greenzweig, Nucl. Instr. & Methods in Phys. Res. A250, 404, (1986).

[166] G.T. Moore, Nucl. Instr. & Methods in Phys. Res. A250, 418, (1986).

[167] R.W. Warren and B.D. McVey, Nucl. Instr. & Methods in Phys. Res. A259, 154, (1987).

[168] B.D. McVey and R.W. Warren, Nucl. Instr. & Methods in Phys. Res. A259, 158, (1987).

[169] D.C. Quimby, Nucl. Instr. & Methods in Phys. Res. A237, 10, (1985).

[170] S. Solimeno and A. Torre, Nucl. Instr. & Methods in Phys. Res. A237, 404, (1985).

[171] G. T. Moore, Optics Communication 52, 46 (1984).

[172] E. T. Scharlemann, A. M. Sessler, and J. S. Wurtele, Phys. Rev. Lett. 54, 1925 (1985).

[173] C. M. Tang and P. A. Sprangle, IEEE Journal of Quantum Electronics QE-21, 970 (1985).

[174] G.T. Moore, Nucl. Instr. & Methods in Phys. Res. A250, 381, (1986).

[175] P. Luchini and S. Solimeno, Nucl. Instr. & Methods in Phys. Res. A250, 389, (1986).

[176] P.Sprangle, A. Ting and C.M. Tang, Nucl. Instr. & Methods in Phys. Res. A259, 136, (1987).

[177] T.M. Antonsen, Jr. and B. Levush, Nucl. Instr. & Methods in Phys. Res. A272, 476, (1988).

[178] Y.-J. Chen, S. Solimeno and L. Carlomusto, Nucl. Instr. & Methods in Phys. Res. A272, 490, (1988).

[179] M. Xie, D. A. G. Deacon and J. M. J. Madey, Nucl. Instr. & Methods in Phys. Res. A272, 528, (1988).

[180] P. Sprangle, A. Ting, B. Hafizi and C. M. Tang, Nucl. Instr. & Methods in Phys. Res. A272, 536, (1988).

[181] A. G. Fox and T. Li, Bell System Tech. Journal 40, 453 (1961).